286

ELASTO-PLASTIC DYNAMIC ANALYSIS OF COUPLED SHEAR WALLS

ELASTO-PLASTIC DYNAMIC ANALYSIS

OF

COUPLED SHEAR WALLS

By

OSAMA M. EL-SHAFEE

B.Sc. (Hon.), Alexandria, Egypt

A Thesis

Submitted to the School of Graduate Studies

in Partial Fulfilment of the Requirements

for the Degree

Master of Engineering

McMaster University

Hamilton, Ontario

1976

MASTER OF ENGINEERING (1976)
(Civil Engineering)

McMaster University
Hamilton, Ontario

TITLE: Elasto-Plastic Dynamic Analysis of Coupled Shear Walls

AUTHOR: Osama M. El-Shafee, B.Sc. (Alexandria University)

SUPERVISOR: Dr. W.K. Tso

NUMBER OF PAGES: (xiv), 199

ABSTRACT

A method for the dynamic analysis of planar coupled shear walls subjected to ground motions is developed herein. The method is capable of application to nonuniform coupled shear walls resting on flexible foundations. The possibility of development of yield hinges at the ends of the connecting beams is included in the analysis. Also P-Δ Effect is incorporated in the stiffness of the structure.

The method is based on the transfer matrix technique in combination with the continuum method. A step-by-step integration approach is used in solving the equation of motion. The response to a number of earthquake records are obtained. The effect of the rotational ductility factor of connecting beams is studied.

ACKNOWLEDGEMENTS

The author would like to express his sincere appreciation to Dr. W.K. Tso for his consistent guidance and encouragement during the course of this investigation. His valuable suggestions and advice are gratefully acknowledged.

The author thanks McMaster University for financial support during this research.

TABLE OF CONTENTS

LIST OF FIGURES

LIST OF TABLES

LIST OF SYMBOLS

A_{i1}, A_{i2} cross-sectional area of left and right walls of segment i.

A_i equivalent cross-sectional area of the coupled shear walls, such that $\frac{1}{A_i} = \frac{1}{A_{i1}} + \frac{1}{A_{i2}}$.

A_{bi}^* effective shear cross-sectional area of connecting beam.

a_i distance between centroidal axes of left and right walls of segment i.

a_n ground acceleration at time t_n.

c_i clear span length of the connecting medium within segment i.

{D} damping forces vector at time t_n.

E elastic modulus.

G shear modulus.

H_i height of segment i.

HT total height of the structure.

HTT_i the height from the ith mass to the top, such that $HTT_i = HT - \sum_{k=1}^{i} H_k$

h_i storey height within segment i.

I_{i1}, I_{i2} second moment of area of left and right walls, respectively.

I_i $I_{i1} + I_{i2}$

I_{bi}	second moment of area of connecting beam within segment i
$K_{\delta 1}$, $K_{\delta 2}$	vertical displacement stiffness of foundation under left and right walls, respectively.
K_{δ}	equivalent vertical displacement stiffness of the foundation, such that $\frac{1}{K_{\delta}} = \frac{1}{K_{\delta 1}} + \frac{1}{K_{\delta 2}}$
$K_{\theta 1}$, $K_{\theta 2}$	rotational stiffness of foundation under left and right walls, respectively.
K_{θ}	equivalent rotational stiffness of foundation, such that $K_{\theta} = K_{\theta 1} + K_{\theta 2}$
$M_i(x)$	walls bending moment at a distance x from the bottom of segment i.
$M_i^e(x)$	cantilever moment at a distance x from the bottom of segment i due to external loads only.
M_{iA}, M_{iB}	walls bending moment at the upper and lower surfaces, respectively, of station i.
$M^e_{f_{iB}}$	factious cantilever moment at top of the ith plastic hinged segment, such that $M^e_{f_{iB}} = M^e_{iB} + q_{pi}\ a_i\ H_i$.
NSEG	number of segments within the wall.
P_i	concentrated lateral load at station i.
$\{P\}$	applied loads vector at time t_n.
$q_i(x)$	shear distribution per unit height along the connecting medium in segment i.

$\{R\}_n$	resisting forces vector at time t_n.
T_i	period of the ith mode.
$T_i(x)$	axial force in the piers within segment i.
T_o	axial force at base of walls.
u_{i1}, u_{i2}	axial deformation in the left and right walls, respectively, in segment i.
u_i	$u_{i1} + u_{i2}$
$\{u\}_n$	displacement vector at time t_n.
$\{\dot{u}\}_n$	velocity vector at time t_n.
$\{\ddot{u}\}_n$	acceleration vector at time t_n.
V_{iA}, V_{iB}	inter-storey shear on upper and lower surfaces, respectively, of station i.
V^*_{iA}, V^*_{iB}	wall shear on upper and lower surfaces, respectively, of station i.
$\{W\}_t$	inertia load acting on the structure at time t.
$y_i(x)$	lateral deflection at a distance x from the bottom of segment i.
$y_i^n(x)$	nth derivative of $y_i(x)$

Suffices iA and iB refer to the upper and lower surfaces, respectively, of station i.

α_i^2	$\frac{a_i \mu_i^2}{E I_i} (1+I_i/A_i a_i^2)$
βi^2	$1 + \frac{12E I_{bi}}{GA^*_{bi} c_i^2}$

γ_i^2	$\dfrac{\mu_i^2}{E^2 A_i I_i a_i}$,
Δ	relative displacement of the foundation due to axial force at base.
Δt	time interval for the numerial integration of the equations of motion.
Δ_{yi}	yield deflection of the ith segment's laminae.
Δ_{ui}	ultimate deflection of the ith segment's laminae.
δt	time interval for calculating the straining actions due to the inertia load.
θ_o	rotation of foundation.
$\{\lambda\}_j$	the jth eigenvector.
μ_i^2	$\dfrac{12EI_{bi}a_i}{h_i c_i^3 \beta_i^2}$.
μ	ductility factor of connecting beams.
ζ_i	critical damping ratio for mode i.
$[\Phi]$	modal matric
$\{\Phi\}_{iA}$, $\{\Phi\}_{iB}$	state vectors at the upper and lower surfaces, respectively, of station i.
$\{\phi\}_j$	the jth normalized eigenvector.
ω_i	the ith natural frequency in radians per second.

CHAPTER 1

INTRODUCTION

1.1. General

In high-rise buildings, the design consideration due to lateral loads becomes particularly important. It is necessary to provide adequate lateral strength and stiffness to the structure. One alternative in design is the use of reinforced concrete shear walls. The high stiffness of the shear walls in their planes is employed to resist the lateral loads. Usually, these walls extending the entire height of the building. In order to have windows, doors and service ducts, openings must be provided in the shear walls, and the resulting structure often consists of two or more smaller walls coupled together by a system of horizontal spandrel beams or connecting slabs. Usually, the exterior walls have spandrel beams, which are short and relatively deep, while the interior walls have connecting slabs which are less stiff.

When the shear walls are arranged in a symmetric manner in the plan of the building, wind and seismic loads will cause translational displacements only. In such a case, the behaviour of the whole building can be studied from the two-dimensional behaviour of a typical pair of shear walls. The shear walls may be coupled either through the floor slabs or floor beams. This class of problem is generally known as the plane coupled shear walls problem.

Coupled shear walls can be analysed as equivalent frames using standard matrix structural analysis techniques. The finite width of the shear wall is accounted for by assuming sets of infinitely rigid beams connected to the column of the equivalent frame. The length of the rigid beam is taken from the center line of the wall to the inner edge of the shear wall. This approach has the advantage of being versatile. Coupled shear walls can also be analysed using the continuous approach which replaces the connecting beams between the walls by a continuous distribution of laminae of equivalent stiffness. This approach has the advantage of being relatively simple and explicit solutions can be obtained for a wide range of coupled shear wall geometries.

In countries where wind load is the only source of lateral load on a high-rise building, the elastic analysis of shear walls is extremely useful in assessing the behaviour of the structure. On the other hand, in seismic areas where the structure may be exposed to moderate or severe earthquake, the lateral load may be sufficiently large to cause plastic deformations in some elements of the structure.

In coupled shear walls of ordinary proportion, the most valuable areas are the ends of the connecting beams between the shear walls. It is expected that even under a moderate intensity earthquake, plastic hinges will develop at the ends of some, if not all, the connecting beams. The behaviour of a coupled shear wall building during a moderate earthquake will therefore depend on the extent plastic hinges are formed. When subjected to a strong earthquake, the rotation demand at the plastic hinges may even exceed the member's rotational capacity, causing the connecting beams to fail. Therefore, the behaviour of a coupled shear wall building subjected to a strong earthquake will depend not only the extent the formation of the plastic hinges, but also the extent the proportions of connecting beams that have failed completely.

Therefore, in order to study the behaviour of a coupled shear wall structure subjected to strong earthquakes, it is necessary to perform a dynamic analysis to the structure, allowing the possibility of plastic hinges or real hinges formed at the ends of the connecting beams. An understanding of the dynamic behaviour is an essential step to design coupled shear wall structure in seismic areas.

1.2 Review of Past Works

It is useful to review the existing knowledge of coupled shear walls by citing some of the studies carried out by different authors. One can divide the works into three general categories: static elastic studies, static inelastic studies and dynamic elastic studies. Unfortunately, there does not appear any studies on the dynamic inelastic analysis of coupled shear walls.

Based on the continuous approach, set of design curves for uniformly distributed lateral load, triangularly distributed lateral load or a point load at the top are presented by Coull and Choudhury [5,6]. The effect of the flexibility of foundation on the coupled shear walls is studied by Tso and Chan [20]. In that study, closed form solutions are obtained for the stresses and deformations under the same loading considered by Coull and Choudhury. Based on the transfer matrix technique coupled with the continuous approach, a general method is presented for the static analysis of planar nonuniform coupled shear walls by Tso and Chan [18]. The arbitrary lateral loading can be approximated by concentrated loads acting at a number of discrete stations along the height of the wall. The effect of the flexibility of foundation can be incorporated in this general method.

Based on the equivalent frame approach, a modified beam equivalent structure method is presented by Smith [16]. In this method, the finite width of shear wall is accounted for by assuming sets of rigid arms connected to the columns of the equivalent frame. The modified beam method presented by Smith is valid only for symmetrical coupled shear walls.

Based on the continuous approach, the elasto-plastic static analysis of uniform plane coupled shear wall has been presented by Gluck [8], Paulay [13] and Winokur and Gluck [23]. Graphs are presented, assuming an upper triangle lateral load pattern for various design characteristics by Gluck [8]. These graphs may be used directly for practical design including the ultimate load for a given rotational ductility factor. Gluck [8] concluded that "Full plastification with height of the laminae is very rarely possible, due to the limitations on the rotational ductility factor". Winokur and Gluck [23] proposed a design method based on a collapse mechanism consisting of plastic hinges at the ends of the connecting beams and the base of the shear walls. By means of an example building, Paulay [13] showed that large rotations would have occurred at the plastic hinges at the ends of the connecting beams when the ultimate strength of the structure is attained. Experimental work has been carried out by Paulay [14], in which the spandrel beams are studied under simulated seismic loading. The post elastic behaviour of the spandrel beams is studied, and improvement in the beams ductility and capacity is achieved using a new method for the arrangement of the reinforcing steel.

The dynamic properties of planar, coupled shear walls are studied by Jennings and Skattum [9]. For elastic planar coupled shear walls the natural frequencies and mode shapes are studied, both with and without the inclusion of the inertia of vertical motion. The results affirm the necessity of including vertical displacement of the shear walls in the analysis of such systems, and suggest the inertia of vertical motion also must be considered in the analysis for certain ranges of the parameters.

The planar coupled shear walls are analysed dynamically by Tso and Chan [19] to study the dynamic characteristics of such structures both analytically and experimentally. The natural frequency is to be found via a trial and error procedure. Also, no assumption is made that the midpoints of the connecting beams are points of contraflexure. In other words, the formulation by Tso and Chan [19] is a generalization of the continuous method of coupled shear walls.

The dynamic analysis mentioned above is elastic analysis, and due to the plastic deformations which are associated with the seismic loading in most cases especially in the coupling system for coupled shear walls, it is necessary to carry out dynamic analysis include the plastic deformations happened during the application of the ground motion.

1.3 Aim of Present Investigation

The purpose of the present analysis is to develope a method for a complete time-history analysis for nonuniform planar coupled shear walls, taking into account the plastic deformations in the connecting beams and the P-Δ Effect. The proposed method may enable us to obtain more realistic time-history response of planar coupled shear walls. With this proposed method, it is possible to study the effect of connecting beam ductility on the seismic response of coupled shear walls.

1.4 Scope

An elasto-plastic dynamic analysis for planar nonuniform coupled shear wall is presented in this research work. The method used for the dynamic elastic analysis including the P-Δ Effect is presented in Chapter 2. The modification to the proposed method for dynamic elasto-plastic analysis is presented in Chapter 3. To examine the safety of the shear walls building designed according to the NBCC [10], the coupled shear walls designed according to NBCC is subjected to a variety of ground excitations. The responses of these walls are presented in Chapter 4. The design calculation for exterior and interior planar coupled shear walls is presented in Appendix A.

It is hoped that the present work will provide some insight to the inelastic dynamic behaviour of planar coupled shear walls under seismic loading.

CHAPTER 2

ELASTIC DYNAMIC ANALYSIS

2.1 Introduction

The present chapter describes a study on the seismic analysis of an elastic coupled shear walls. A complete dynamic response analysis is used to estimate the design load due to earthquakes. The analysis is based on the transfer matrix technique of the structure after replacing the connecting beams by an equivalent continuous medium capable of transmitting actions of the same type as the discrete spandrels.

A study of the natural frequencies and mode shapes is presented. It takes into account the effect of axial deformations of the walls. Also, the P-Δ Effect is included in computing the stiffness matrix of the system.

Numerial integration methods are used in the integration of the equations of motion of the system. The choice of the proper method for the step-by-step integration is governed by the stability of the integration and the accuracy of the resulting accelerations, velocities and displacements.

The purpose of the chapter is to give an idea about the main concept adopted in the work and to clarify the transfer matrix technique used in the analysis.

2.2 Appraisal of Existing Approaches

Generally, coupled shear walls can be studied by one of two methods. These methods are the equivalent frame method and the continuum method. In the first method, the coupled shear wall is treated as a single bay frame. The columns and beams are located at the center lines of the piers and spandrels as shown in Figure (2-1a). The finite width of the walls are represented by rigid arms as shown in Figure (2-1b). In the second method, the discrete system of the spandrel beams is replaced by an equivalent continuous medium capable of transmitting actions of the same type as the discrete spandrels.

The continuum method model, Figure (2-1c) is assumed to have uniform connecting beams distribution and wall stiffness throughout the wall height. Therefore, it lacks the flexibility to be adopted to analyse buildings where the floor height, connecting beam stiffness and wall stiffnesses may change along the height of the structure.

To overcome the difficulty of applying the continuum method for nonuniform coupled shear walls, a method of analysis using the continuum approach is presented by Tso and Chan [18]. This method is based on the transfer matrix technique. The continuum approach with the transfer matrix technique produce a simple method to apply and in the same time very flexible, so that it can be used to analyse a wide variety of wall configurations, foundation conditions and loading conditions. The technique is to divide the wall into a number of segments, and each segment can be considered as a uniform coupled shear wall. The continuum method of analysis can therefore apply to each segment to relate the parameters of interest from one end of the segment to the other end. The solution of the problem is then obtained by relating the boundary conditions at the base to those at top by means of the segments transfer

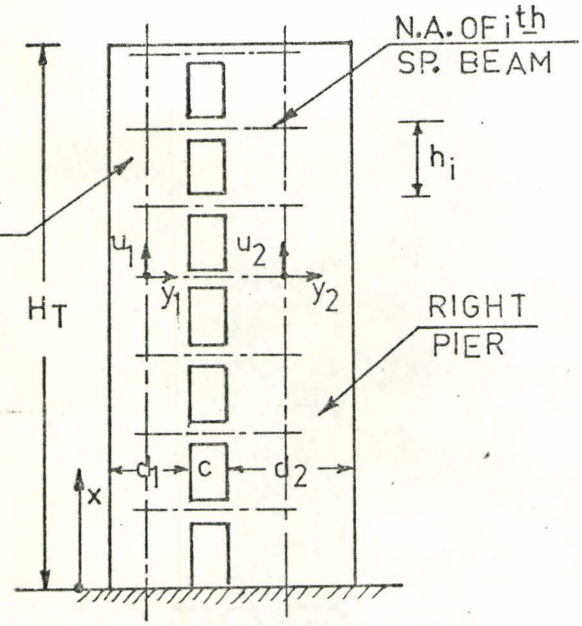

(a)

WIDE COLUMN FRAME

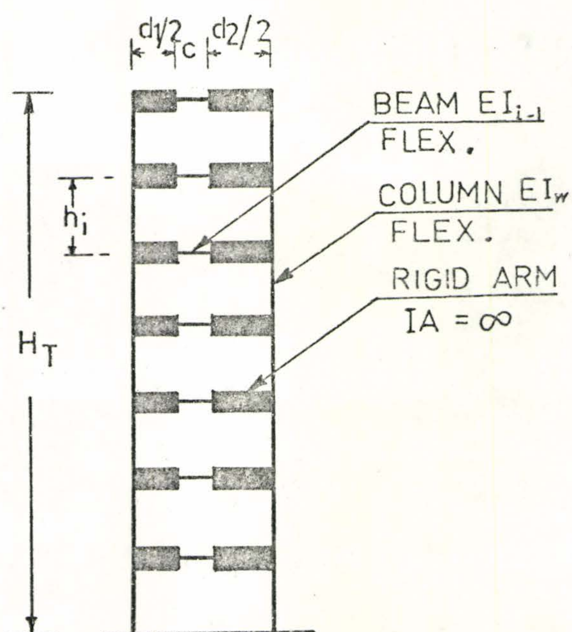

(b)

EQUIVALENT WIDE COLUMN FRAME (d1 & d2 must be equal)

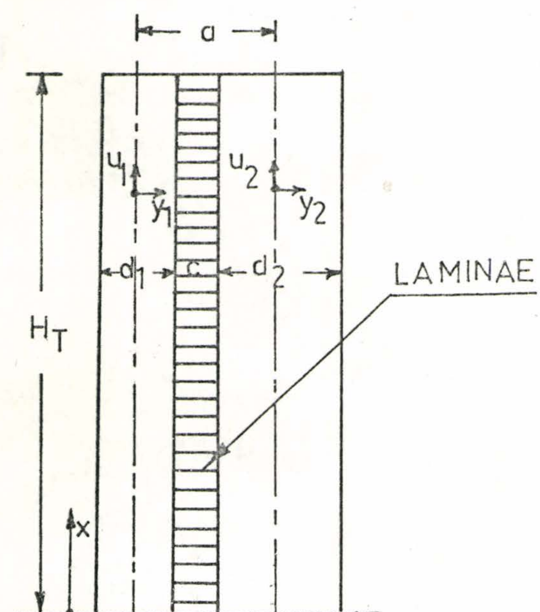

(c)

CONTINUUM METHOD MODEL

FIG. 2-1 SHEAR WALLS MODELS

matrices. In addition, the transfer matrix technique can be used even with computers of limited memory capacity. Because of the above advantages, the transfer matrix technique together with the continuum method of analysis is used in the present analysis.

2.3 Outlines of the Transfer Matrix Technique

For completeness, the main feature of using the transfer matrix technique to solve a nonuniform coupled shear wall is outlined below.

Figure (2-2) shows a nonuniform coupled shear wall on flexible foundation. The cross-sectional properties of the coupled wall change at a number of discrete stations along the height of the wall and concentrated lateral loads are acting at these stations. So, the station is defined as the section at which the wall cross-section properties changed or when there is a lateral concentrated load acting. The base is taken to be station zero, and the top is taken to be station n, where n is the number of segments into which the wall is divided. Between the base and the top the stations are numbered from 1 to n-1. Between each pair of stations, the cross-section is uniform and will be referred to as a segment of the wall. The ith segment lies between the $(i-1)^{th}$ station and the ith station. A complete solution of the problem is obtained by determining the state vectors $\{\phi\}_{iA}$ and $\{\phi\}_{iB}$ above and below the ith station respectively. The state vectors are defined by:

$$\begin{aligned} \{\phi\}_{iA} &= \text{Column } \{y, y', y'', y''', M^e, V\}_{iA} \\ \{\phi\}_{iB} &= \text{Column } \{y, y', y'', y''', M^e, V\}_{iB} \end{aligned} \qquad (2\text{-}1)$$

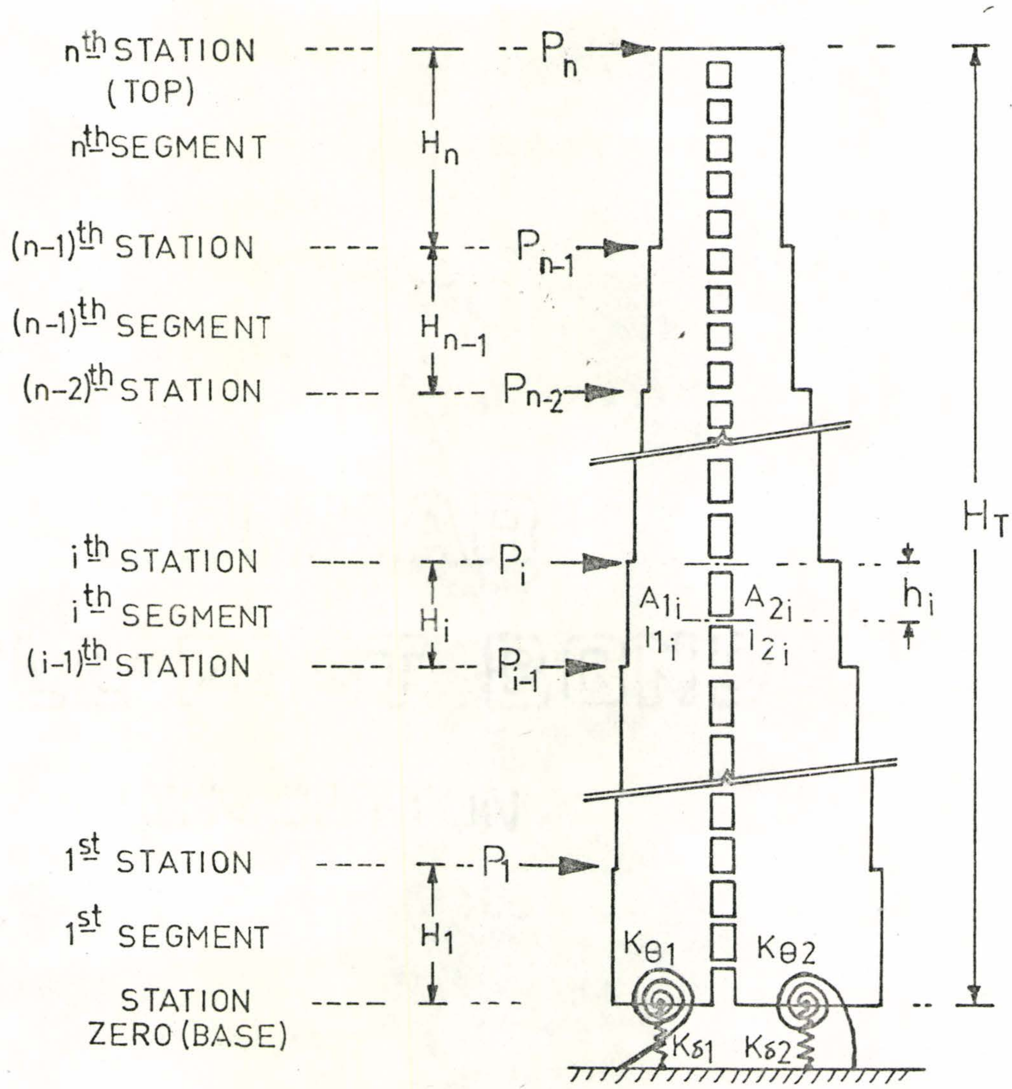

FIG. 2_2 STEPPED COUPLED SHEAR WALL ON FLEXIBLE FOUNDATION

Where $\{\phi\}_{iA}$ refers to the side where station i and the $(i+1)^{th}$ segment join together, and $\{\phi\}_{iB}$ refers to the side where station i and the ith segment join together. The prime denotes differentiation with respect to x, Figure (2-3b).

Station zero has one state vector $\{\phi\}_o$ only, and also station n has one state vector $\{\phi\}_{nB}$. These state vectors contain the boundary conditions of the coupled shear wall problem. By relating the state vector $\{\phi\}_o$ to the state vector $\{\phi\}_{nB}$ by means of the segment transfer matrices, $\{\phi\}_o$ and $\{\phi\}_{nB}$ can be determined. Then by back-substitution using the transfer matrices of the segments, other state vectors can be found. The transfer matrices necessary for the solution of the problem are defined as follows:

a - Field Transfer Matrix $[F]_i$

The matrix $[F]_i$ is the ith field matrix which relates the state vector at one end of the segment, $\{\phi\}_{(i-1)A}$, to the state vector at the other end of the segment, $\{\phi\}_{iB}$.

$$\{\phi\}_{(i-1)A} = [F]_i \{\phi\}_{iB} \qquad (2\text{-}2)$$

b - Station Transfer Matrix $[S]_i$ and the Load Vector $\{L\}_i$

The matrix $[S]_i$ represents the station transfer matrix of the ith station, it relates the state vector at one side of the station to the state vector at the other side. The externally applied concentrated load P_i is included in the load vector $\{L\}_i$. The state vector $\{\phi\}_{iB}$ is

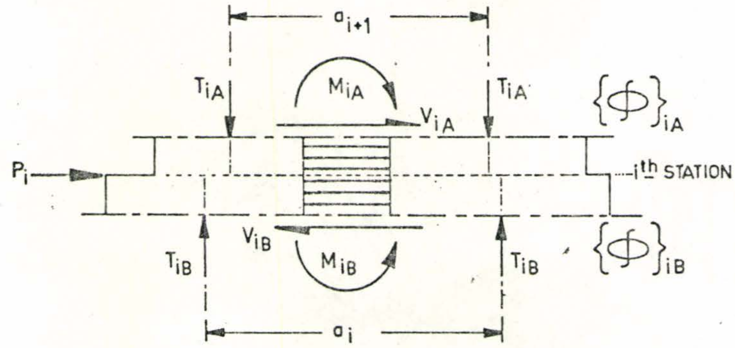

FIG. 2_3a FORCE COMPONENTS ACTING ON THE i^{th} STATION

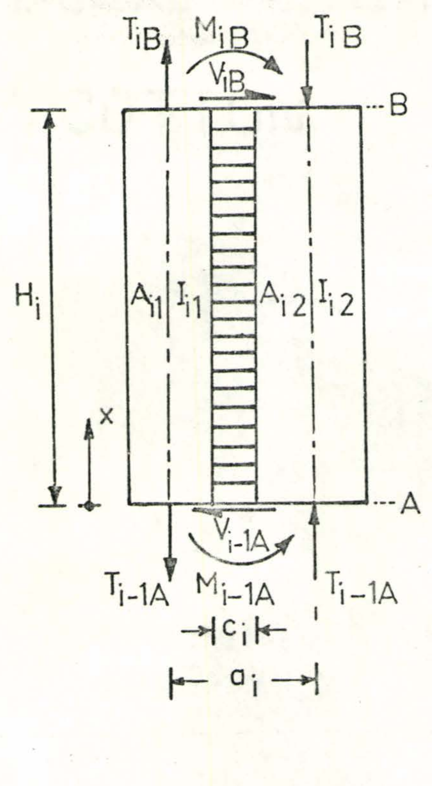

FIG. 2_3b FORCE COMPONENTS ACTING ON THE i^{th} SEGMENT

related to the state vector $\{\phi\}_{iA}$ by the following equation.

$$\{\phi\}_{iB} = [S]_i \{\phi\}_{iA} + \{L\}_i \qquad (2\text{-}3)$$

c - Total Transfer Matrix of the Structure $[\bar{F}]$

The matrix $[\bar{F}]$ is the product of all the field and station matrices of the segments. The $[\bar{F}]$ matrix relates the state vectors at the base, $\{\phi\}_o$, to the state vector at the top, $\{\phi\}_{nB}$, $[\bar{F}]$ is given by the following equation [18].

$$[\bar{F}] = (\prod_{i=1}^{n} [F]_i [S]_i) \qquad (2\text{-}4)$$

with $[S]_n = [I] =$ identity matrix

d - Total Load Vector for the Structure $\{\bar{L}\}$

The externally applied concentrated loads are included in the total load vector for the structure $\{\bar{L}\}$. This load vector is formed by the following equation [18].

$$\{\bar{L}\} = [F]_1 \{L\}_1 + \sum_{i=2}^{n-1} [\prod_{k=1}^{i-1} [F]_k [S]_k] [F]_i \{L\}_i \qquad (2\text{-}5)$$

From equations (2-4) and (2-5), the necessary transfer matrices for relating the state vector $\{\phi\}_o$ to the state vector $\{\phi\}_{nB}$ can be obtained. The following equation gives this relation.

$$\{\phi\}_o = [\bar{F}]\ \{\phi\}_{nB} + \{\bar{L}\} \tag{2-6}$$

There are six elements in each of the state vectors $\{\phi\}_o$ and $\{\phi\}_{nB}$. Out of these twelve elements, six of them are known as given by the boundary conditions at the top and bottom of the structure. These remain six are unknowns and equation (2-6) is a set of six equations for the solutions of these six unknowns. Once equation (2-6) is solved, then every element in the state vectors $\{\phi\}_o$ and $\{\phi\}_{nB}$ will be known.

By means of the transfer matrices of the segments other state vectors can be determined for all segments starting from the top and going down until segment 1.

The stress state of the structure, the wall moment $M_{i(x)}$, the wall axial force $T_{i(x)}$ and the distributed shear $q_{i(x)}$ can be determined from the following equations.

$$M_{i(x)} = E\ I_i\ y''_{i(x)} \tag{2-7}$$

$$T_{i(x)} = [M_{iB}+V_{iB}(H_i-x)-M_{i(x)}]/a_i \tag{2-8}$$

$$q_{i(x)} = (E\ I_i\ y'''_{i(x)}+V_{iB})/a_i \tag{2-9}$$

2.4 Assumptions

Various assumptions are used for the present analysis. The assumptions which are listed below can be divided into two main groups, the first one is the general assumptions which have been verified by most investigators, and the second group of assumptions concerns the present problem specifically.

2.4.1 General Assumptions

These assumptions are dealing with the stress-strain relationship and compatability conditions.

1. Moment-Rotation relationship is considered linear up to the plastic moment followed by a horizontal plastic plateau.
2. Plane section perpendicular to the axis of the member before loading remains plane after application of the load.
3. Shear deformation is neglected for the piers and axial deformation is neglected for connecting beams.
4. The midpoints of the connecting beams are points of contraflexure.

2.4.2 Special Assumptions

These assumptions are made in order to simplify the analysis and to make it compatible with the approach used. These assumptions are dealing with the modeling of the structure.

1. Wall remains elastic throughout the analysis.
2. Uncracked section for the wall is used in the calculation of wall stiffness.
3. The connecting beams are taken as a double reinforced

concrete section and the cracked section is used for stiffness determination of the connecting beams.

4. The masses are to be lumped at discrete points along the height of the walls. Therefore, the inertia forces of the building are approximated by concentrated loads acting at different heights of the building.

2.5 Dynamic Modelling

The lumped-mass approach is used in the dynamic analysis. The masses of each segment are lumped at discrete points along the height of the wall. The location of the masses are taken as the stations in the problem. Therefore, the number of degrees of freedom will be equal to the number of segments of the wall. The mass matrix, stiffness matrix and damping matrix in the equations of motion for the system are as follows:

2.5.1 Mass Matrix [M]

It is a diagonal matrix with the mass of the ith segment to be the element $m_{(i,i)}$ on the main diagonal.

2.5.2 Stiffness Matrix [K*]

For stepped coupled shear wall on flexible foundation, Figure (2-2), the static analysis of it is already done. The transfer matrix method by Tso and Chan [18], which is described in subsection (2.3), can be used to determine the flexibility matrix $[F']$. This flexibility matrix is n by n where n is the number of segments. The jth column is to be formed by calculating the lateral deflection y_i of the ith mass due to unit load acting at the jth mass, (i=1, n).

P-Δ Effect can be introduced in this stage, i.e. before inverting the flexibility matrix $[F']$ to obtain the stiffness matrix. If P-Δ Effect is to be neglected the inversion of $[F']$ will give the stiffness matrix [K], which does not include the geometric stiffness. The combined stiffness matrix $[K^*]$, which includes the geometric stiffness, can be obtained by inverting the combined flexibility matrix $[F^*]$. The combined flexibility matrix $[F^*]$ includes the P-Δ Effect.

To introduce the P-Δ Effect, the following iterative procedure is to be carried out:

1. From the resulting flexibility matrix $[F']$, the lumped weights at the stations will cause additional bending moment due to the eccentricity from the axis of the wall, Figure (2-4).
2. The additional lateral deflection Δf_i is calculated at each station i and added to the flexibility coefficient f_i to get a modified coefficient f_i^*.
3. Step (1) is to be repeated using f_i^* and from which a new Δf_i can be calculated. This new Δf_i is to be added to the flexibility coefficient f_i to obtain a new f_i^{**}. Comparison is to be made between the resulting f_i^{**} and f_i^*. If the difference between two cycles is within certain allowable error, the resulting modified flexibility coefficient f_i^* is taken to be correct. Otherwise steps (1) to (3) have to

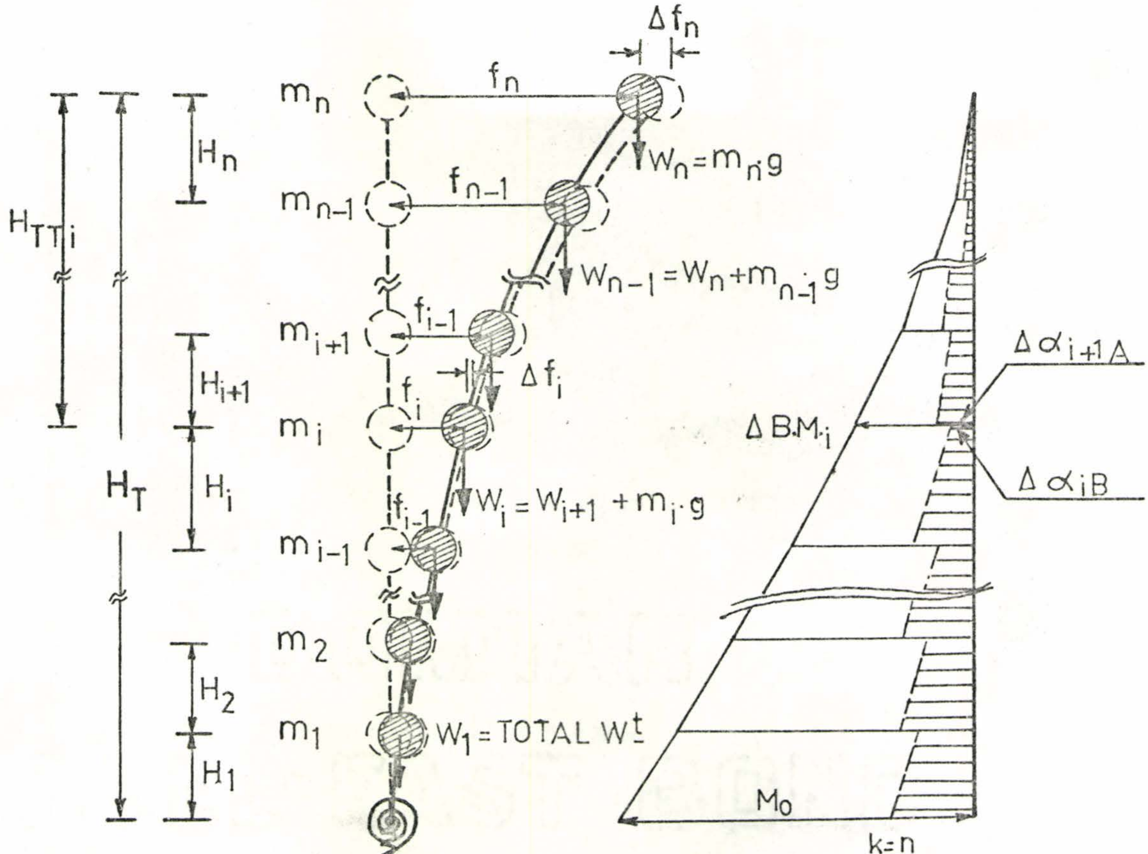

$$\Delta\ B.M._i = \sum_{k=i-1}^{k=n} W_k (f_k - f_{k-1}) \quad \text{------} \quad (2\_10)$$

- H_T = TOTAL HEIGHT
- $H_{TTi} = H_T - \sum_{k=1}^{k=i} H_k$

$$\Delta\alpha_{i+1A} = \Delta B.M._i / E I_{i+1}$$

$$\Delta\alpha_{iB} = \Delta B.M_i / E I_i$$

$$W_i 1 = \alpha_{iB} H_i$$

$$W_i 2 = (\alpha_{iA} - \alpha_{iB}) H_i / 2$$

(MODE j)

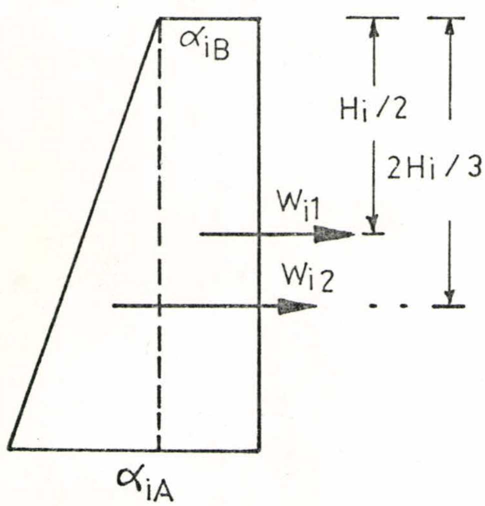

FIG. 2_4

(P-Δ EFFECT)

be repeated again with f_i^{**} as f_i^*.

Figure (2-4) shows the eccentricities f_i for the lumped weights w_i, (i=1, n), and the method of calculating the additional bending moment due to these eccentricities. Also the method of calculating the elastic weights α_i is shown in the same figure. The additional Δf_i can be calculated from the following equation:

$$\Delta f_i = \sum_{K=1}^{K=i} \{W_{i1}[(HTT_K - HTT_i) + H_K/2] + W_{i2}[(HTT_K - HTT_i) + \frac{2}{3}H_K]\} + \Delta\theta_i \tag{2-11}$$

where $\Delta\theta_i$ is the additional deflection due to the additional rotation of the foundation, which can be calculated from the following equation:

$$\Delta\theta_i = \frac{M_o}{K_\theta}(HT - HTT_i) \tag{2-12}$$

It should be noted that in the above method the coupled action is neglected in calculating Δ_f and the coupled shear wall is considered as cantilever with equivalent moment of inertia $I_i = I_{i1} + I_{i2}$.

By applying the above method for all the columns in the flexibility matrix (j=1, n), a modified flexibility matrix $[F^*]$ is obtained. This matrix includes the gravity load effect, i.e. the combined flexibility matrix.

The combined stiffness matrix $[K^*]$ is to be determined by inverting the flexibility matrix $[F^*]$.

$$[K^*] = [F^*]^{-1} \tag{2-13}$$

2.5.3 Damping Matrix [C]

For the numerical integration the damping matrix must be introduced to the equations of motion with its original form. It is assumed that the damping matrix [C] will be diagonalized by the same transformation that diagonalize the [M] and $[K^*]$ matrices. In other words,

$$[\Phi]^T [C] [\Phi] = \begin{bmatrix} \ddots & & 0 \\ & 2\xi_i \omega_i & \\ 0 & & \ddots \end{bmatrix} \qquad (2\text{-}14)$$

where $[\Phi]$ is the modal matrix,

ξ_i is the ith percentage damping ratio, and

ω_i is the ith natural frequency in radians per second.

Therefore, to form [C] it is necessary to calculate the eigenvalues and the eigenvectors of the system. The periods and the normalized unit vectors can be determined from the eigenvalues and eigenvectors respectively.

$$T_i = 2\pi \;/\; \omega_i \qquad (2\text{-}15)$$

$$\{\phi\}_j = \sqrt{\frac{1}{\sum_{i=1}^{n} m_{ii} \; \lambda^2_{ij}}} \;\; \{\lambda\}_j \qquad (2\text{-}16)$$

If the percentage damping ratios $\xi_1, \xi_2, \ldots, \xi_i, \ldots, \xi_n$ are to be assigned, the damping matrix [C] can be determined from equation (2-14),

$$[C] = [\Phi^T]^{-1} \left[\diagdown \; 2\xi_i\omega_i \; \diagdown \right] [\Phi]^{-1} \tag{2-17}$$

From the orthogonality condition

$$[\Phi]^T [M] [\Phi] = [I] \tag{2-18}$$

Premultiplying equation (2-18) by $[\Phi^T]^{-1}$ gives

$$[\Phi^T]^{-1} [\Phi]^T [M] [\Phi] = [\Phi^T]^{-1} [I]$$

therefore
$$[\Phi^T]^{-1} = [M] [\Phi] \tag{2-19}$$

Postmultiplying equation (2-18) by $[\Phi]^{-1}$ gives

$$[\Phi]^T [M] [\Phi] [\Phi]^{-1} = [I] [\Phi]^{-1}$$

therefore
$$[\Phi]^{-1} = [\Phi]^T [M] \tag{2-20}$$

Substituting for $[\Phi^T]^{-1}$ and $[\Phi]^{-1}$ from equations (2-19) and (2-20) in equation (2-17) gives

$$[C] = [M] [\Phi] \left[\diagdown \; 2\xi_i\omega_i \; \diagdown \right] [\Phi]^T [M] \tag{2-21}$$

Equation (2-21) gives the damping matrix [C] by knowing the normalized eigenvector matrix [Φ], the frequencies, the mass matrix [M], and after assuming the critical damping ratios ξ_i, $(i=1,n)$, for the different modes.

In the present study, the critical damping ratios for the different modes are taken as

$$\begin{aligned} \xi_1 &= 4\% \rightarrow 5\% \\ \xi_2 &= 5\% \rightarrow 7\% \\ &\vdots \\ \xi_n &= 9\% \rightarrow 12\% \qquad (n \geq 5) \end{aligned}$$

2.6 Numerical Integration

To obtain the seismic responses numerical integration needs to be carried out for any ground acceleration record input. The choice of the proper method for the step-by-step integration is governed by two factors. These are:

a - Stability of the Integration Procedure

The rate of convergence is dependent upon the period of the highest mode of the system. Consequently, the time interval Δt used must be related to the shortest period of vibration, or the period in the highest mode of vibration, for lumped mass system. The method is unconditionally stable if the solution for any initial conditions does not grow without bound for any time step Δt, in particular when $\Delta t/T_{min}$ is large. Unconditionally stable scheme is needed when we have very high frequencies. Alternatively, a numerical scheme can be conditionally stable. A conditionally stable scheme requires an upper limit for $\Delta t/T_{min}$, and is suitable for systems in which T_{min} is relatively large, so that fairly large integration step Δt can be used. Among the different numerical schemes, such as Newmark method [11], Wilson θ method [2] and the direct step-by-step integration method [21], Newmark method is found to be the most stable method as stated by Wilson and Bathe [22].

b - The Accuracy of the Resulting Acceleration, Velocities and Displacements

The accuracy increases by decreasing Δt, for large values of Δt the errors in period are increased and the percentage amplitude decay also is increased. From Wilson and Bathe's analysis [22], Newmark method proved to be the only method which gives no errors either in the period or in amplitude alternation.

From the above discussion it can be seen that Newmark method is the best one to be used in integrating the equation of motion to ensure the stability of the integration. Given below is a summary of Newmark method [11], using "α" = 0.5 and "β" = 0.25.

1. Assume values of the acceleration of each mass at the end of the interval.
2. Compute the velocity and the displacement of each mass at the end of the interval from the following equations:

$$\{\dot{u}\}_{n+1} = \{\dot{u}\}_n + \frac{\Delta t}{2} \left\{ \ddot{u}_{n+1} + \ddot{u}_n \right\} \tag{2-22}$$

and

$$\{u\}_{n+1} = \{u\}_n + \Delta t \; \{\dot{u}\}_n + \frac{(\Delta t)^2}{4} \left\{ \ddot{u}_{n+1} + \ddot{u}_n \right\} \tag{2-23}$$

3. From the computed displacement $\{u\}_{n+1}$, compute the resisting forces $\{R\}$,

$$\{R\}_{n+1} = [K] \; \{u\}_{n+1} \tag{2-24}$$

4. From the computed velocity $\{\dot{u}\}_{n+1}$, compute the damping forces $\{D\}$,

$$\{D\}_{n+1} = [C] \; \{\dot{u}\}_{n+1} \tag{2-25}$$

5. From the resisting forces $\{R\}_{n+1}$, the damping forces $\{D\}_{n+1}$ and the applied loads $\{P\}_{n+1}$, which is given by $-[M]\{1\}a_{n+1}$, and a_{n+1} is the ground acceleration at t_{n+1}, the acceleration can take a new value for each mass at the end of the interval.

$$\{\ddot{u}\}_{n+1} = [M]^{-1}\{P\text{-}R\text{-}D\}_{n+1} \tag{2-26}$$

6. Compare the derived acceleration with the assumed accelerat-ion at the end of the time interval. If these are the same, the calculation is completed and one can proceed to the next time interval. If these are different, repeat the

calculation with the derived value as the new acceleration for the end of the time interval.

2.7 Equivalent Static Load

The output of the numerical integration process is the displacement, the velocity and the acceleration for each mass as a function of time. The product of mass times the corresponding acceleration will give the inertia load acting on the structure.

$$\{W\}_t = -[M]\ \{\ddot{u}\}_t \qquad (2\text{-}27)$$

It should be noted that $\{\ddot{u}\}_t$ is the total acceleration vector at time (t).

Once the inertial loading is known, the stress state of the structure can be determined using the transfer matrix technique as described in subsection (2-3). In this manner, one can obtain a time-history of the parameters of interest. The parameters of interest may be the top deflection, the base wall moment, the connecting beam end moments or the axial force in the walls.

CHAPTER 3

ELASTO-PLASTIC DYNAMIC ANALYSIS

3.1 Introduction

An inelastic dynamic analysis for a planar coupled shear walls is presented in this chapter. The analysis is based on the transfer matrix technique in combination with the continuum method.

The main differencebetween this analysis and the elastic dynamic analysis as described in the previous chapter is that the present analysis takes into account the inelastic behaviour of the connecting beams. Depending on the shear intensity q(x,t) in the connecting beam, the beam may be in one of three states. It may remain elastic when q(x,t) is small. Plastic hinges may form at the ends of the connecting beams if the end moment exceeds the plastic moment of the beams. Finally, if the deformation requirement on the connecting beam is sufficiently large the beam may fail. No shear nor moment will be transmitted by the connecting beam if this happens. Conceptually, one can represents this state as the formation of two real hinges at the ends of the connecting beam. At any given time, the shear intensity q(x,t) varies along the height of the structure. Therefore, part of the connecting beams may be elastic, part of them may have plastic hinges formed at the ends and part of them may have failed and therefore represented by connecting beams with real hinges at the ends. A segment of a coupled shear wall containing only elastic connecting beams is called an elastic segment. Similarly, a segment of the coupled shear wall containing connecting beams with plastic hinges or real hinges are called plastic hinged segment or real hinged segment respectively.

The properties of a plastic hinged segment or real hinged segment will be different from an elastic segment. Hence, if the transfer matrix technique is used in the solution of the problem, it is necessary to derive appropriate field transfer matrices for plastic hinged segments and real hinged segments in addition to elastic segments. Furthermore, the station transfer matrix relating a state vector in an elastic segment to a state vector in a plastic hinged segment is different from one which relates two state vectors both in the elastic segment. Since each segment can take the form of an elastic segment, a plastic hinged segment or a real hinged segment, it is necessary to develop nine station transfer matrices to cover all combination of segment variations as shown in Figure (3-1).

3.2 Scheme of Computation

In this section the segment states are defined and the over-all scheme of analysis is described. The flow chart of the computer program to perform the computation is presented.

3.2.1 Assumptions for the Definition of Segment State

To decide what state a segment is in, the bending moment and the rotation at the ends of the connecting laminae are to be computed

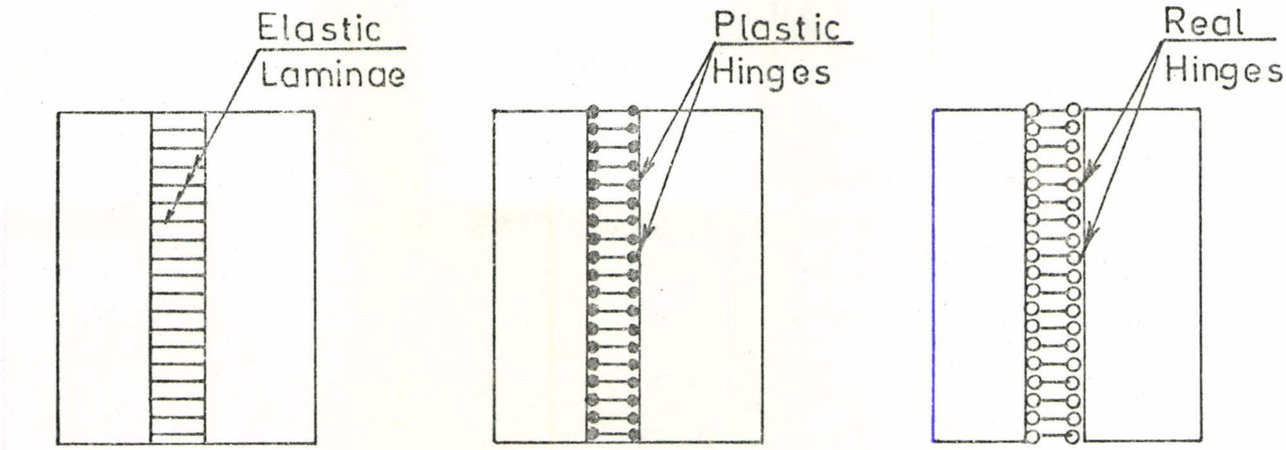

(1) ELASTIC SEG. (2) PLASTIC H. SEG. (3) REAL H. SEG.

FIG. 3.1 (a) SEGMENT STATES

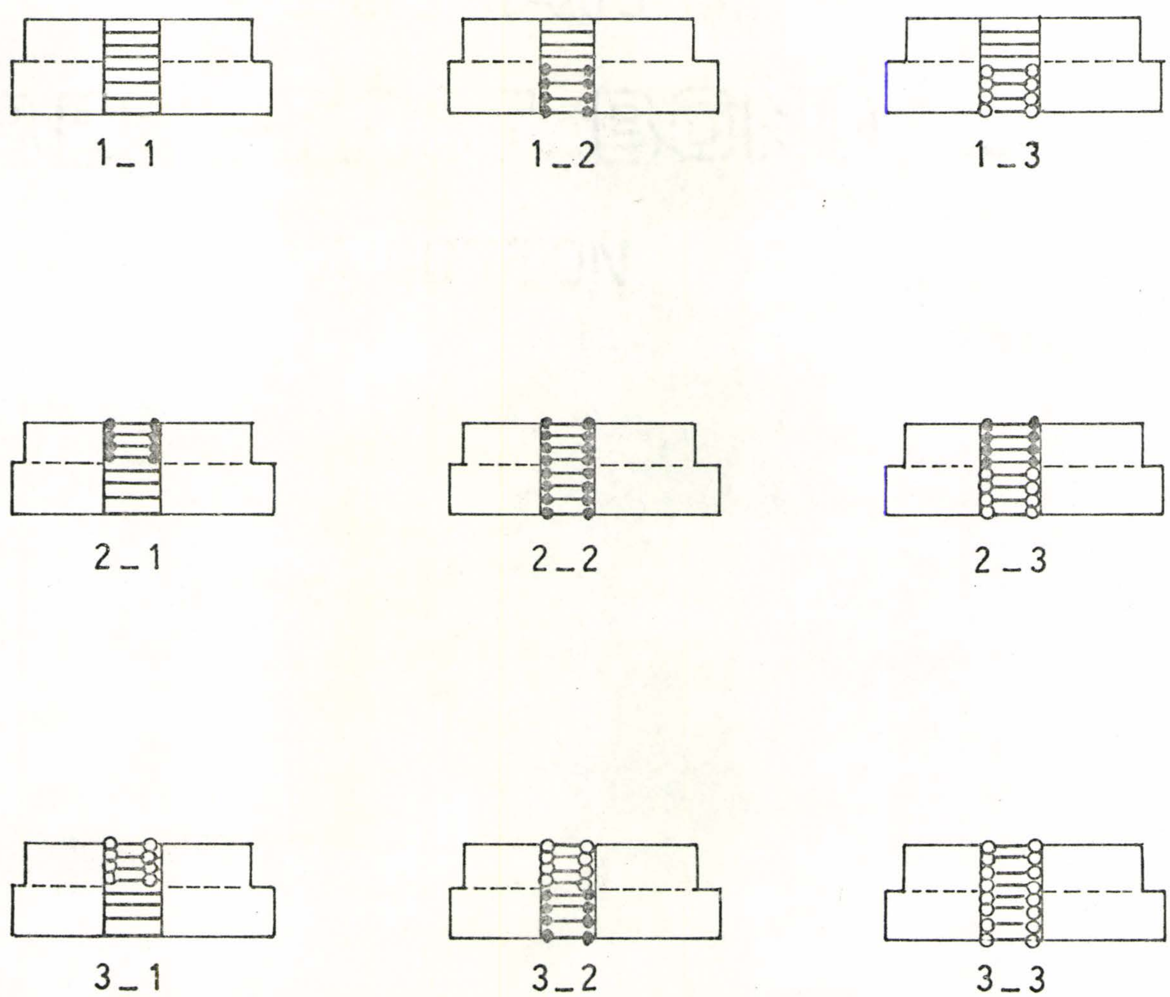

FIG. 3.1 (b) STATION COMBINATIONS

and related to the moment-rotation relationship of the connecting laminae. The relation between the bending moment at ends of the connecting laminae and the shear intensity q_{xi} is as follows:

$$q_{xi} = \frac{2m_{xi}}{c_i} \qquad (3\text{-}1)$$

where

m_{xi} = Bending moment per unit height at distance x from the bottom of the segment (i).

As c_i the length of the connecting laminae within the segment (i) is constant, q_{xi} can be used instead of the end moments to check the conditions of the connecting laminae. Also, the rotation of the lamina can be expressed in terms of the relative end displacements of the laminae Δ.

3.2.1.1 Segment Shearing Force Intensity q_i and Deflection Δ_i

In the present analysis, the shearing force q_i per unit height of the ith segment is taken to be the average value in the ith segment's laminae, q_i can be calculated from the following equation:

$$q_i = \frac{1}{2}\,(q_{io} + q_{iH_i}) \qquad (3\text{-}2)$$

where

q_{io} = Shearing force intensity at the bottom of the ith segment.

and q_{iH_i} = Shearing force intensity at the top of the ith segment.

The deflection Δ_i of the connecting laminae of the ith segment is taken to be one half of the average value of the relative axial deformation between the two walls in the ith segment, Figure (3-2b), Δ_i can be calculated from the following equation.

$$\Delta_i = \frac{1}{2} (\Delta_{io}+\Delta_{iH_i}) \qquad (3\text{-}3)$$

where

$\Delta_{io} = \frac{1}{2}$ the relative axial deformation between the two walls at the bottom of the ith segment.

$\Delta_{iH_i} = \frac{1}{2}$ the relative axial deformation between the two walls at the top of the ith segment.

3.2.1.2 Resistance Function

Instead of using the moment-rotation relationship, the resistance function of the ith segment's laminae will be expressed in terms of q_i and Δ_i defined previously. The resistance function used as shown in Figure (3-2a) is a bilinear hysteretic resistance function. As the deflection Δ_i increases from zero, the resistance q_i increases linearly with a slope of $2u_i^2/a_i$. The linearity continues until the yielding deflection Δy_i is reached. As the deflection Δ_i increased further, the resistance q_i is assumed to remain constant at q_{pi}. The latter value will be maintained until the ductility limit of the member is reached.

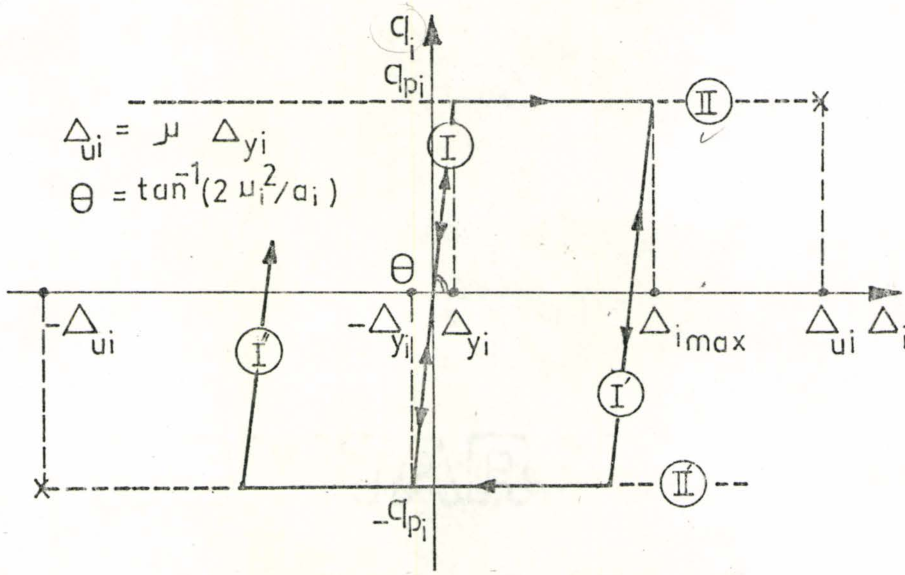

(a)

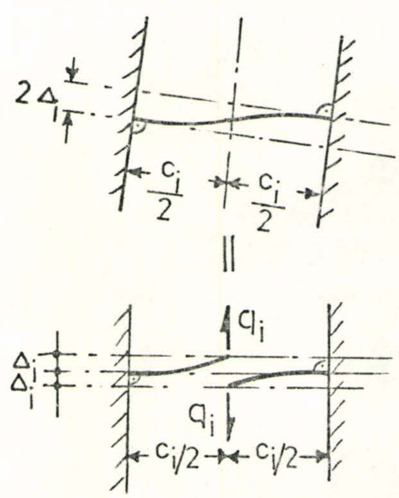

(b)

FIG. 3_2 RESISTANCE FUNCTION

However, if the deflection Δ_i reaches a maximum before the ductility limit and then decreases, the resistance q_i is assumed to decrease along a line parallelled to the initial elastic shape. This decrease will continue with decreasing the deflection Δ_i until a shearing intensity $-q_{p_i}$ is attained.

3.2.1.3 Segment State

Shown in Figure (3-2a) is the resistance function of the connecting laminae in the ith segment. The ductility limit is denoted by Δ_{u_i} which is the product of the yielding deflection Δ_{y_i} and the ductility coefficient μ. Figure (3-2a) contains two sets of lines, namely : Set I and Set II. The segment state can be defined as follows:

- If the average shear intensity q_i in the segment is such that $q_i \geq q_{p_i}$ and average laminae deflection $\Delta_{i_t} \geq \Delta_i(t-\delta t)$, i.e. along line II, or if $q_i \leq -q_{p_i}$ and $\Delta_{i_t} \leq \Delta_i(t-\delta t)$, i.e. along line II$'$ and in both cases, $|\Delta_i| < |\Delta_{u_i}|$, then the segment is in the plastic hinged state.
- If $\Delta_{i_t} < \Delta_i(t-\delta t)$ and $q_i \geq q_{p_i}$ i.e. along line I$'$, or if $\Delta_{i_t} > \Delta_i(t-\delta t)$ and $q_i \leq -q_{p_i}$, i.e. along line I$''$, the segment is in the elastic state. Also, the segment is in the elastic state if $-q_{p_i} < q_i < q_{p_i}$.
- If the laminae deflection exceeds the ductility limit ($|\Delta_i| \geq |\Delta_{u_i}|$), the segment is in the real hinged state.

Once a segment is in the real hinged state, it will remain in the real hinged segment state to the end of the analysis. However, when a segment is in the plastic hinged state, it will return to the elastic segment state upon unloading.

The general procedure for response calculations is as follows: The segments are defined as the wall between the lumped masses and are taken to be elastic initially. Step-by-step integration is performed to obtain the displacement, velocity and acceleration at every time interval Δt. The stress state of the wall is checked not at every time step but at intervals of K_{max} times δt. The value of K_{max} is to be entered as input to the computation, and δt is the time interval of calculating the straining actions of the structure. This arrangement allows the user to obtain a compromise between accuracy of solution and economy in computation time. If any segment changes its state, the overall stiffness matrix of the coupled wall is reevaluated before the next time step integration takes place. This procedure carries on until the end of the earthquake or when the time of integration reaches a prescribed time limit. The time history responses for top deflection, base wall moments, wall axial forces and the shear intensity at the different segments are calculated and plotted out.

If all the segments become real hinged segments before the end of the time integration, all the connecting beams have failed and the coupled wall becomes two independent acting cantilevers. The dynamic properties of this system can then be computed simply based on an equivalent cantilever system as shown in Figure (3-3).

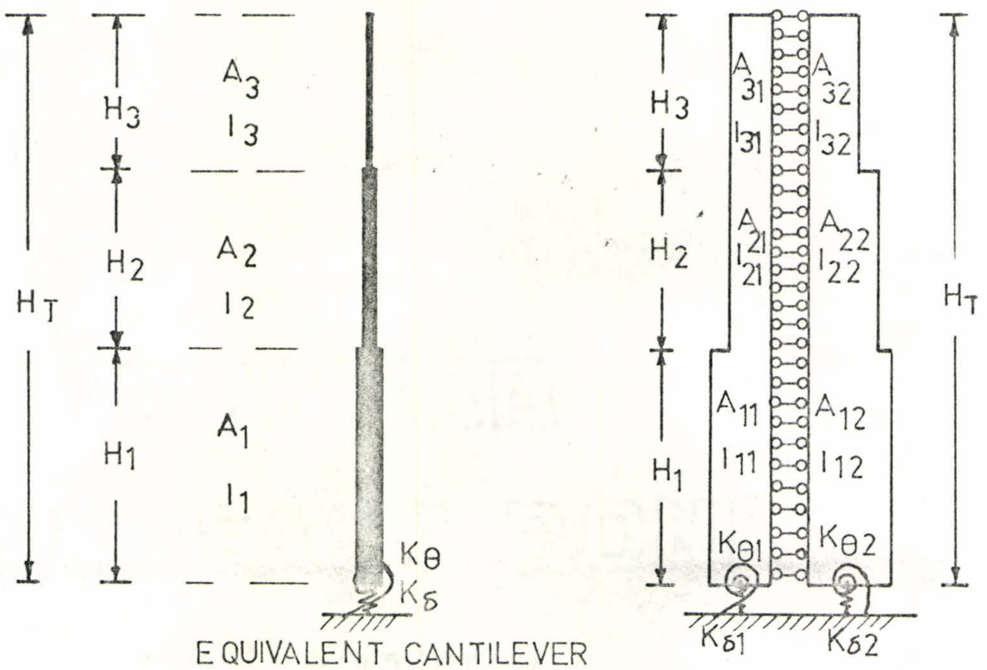

EQUIVALENT CANTILEVER

$1/A_i = 1/A_{i1} + 1/A_{i2} \quad (i = 1, 3)$

$I_i = I_{i1} + I_{i2} \quad (i = 1, 3)$

ALL CONN. BEAMS ARE PENDULUMS

FIG. 3_3 EXAMPLE FOR THE DOUBLE CANTILEVER SYSTEM

3.2.2 Flow Chart for the Elasto-Plastic Dynamic Analysis of Planar Coupled Shear Wall

For the purpose of saving the computer time the following steps are taken in the computer program:

1. The response is printed out at time interval δt=0.1 second, independent of the time interval of the numerical integration Δt. In general, Δt is of the order of 0.01 second. Therefore, the response is printed out once every ten cycles of integration.
2. A factor K_{max} is introduced for the check of segment stress state, so that the segments state is to be checked at time interval = K_{max} δt second, and the segments state is assumed to be constant in the interval between checking.
3. The moment of inertia of the connecting beams, which is assumed as cracked section, is computed manually beforehand in Appendix A, then introduced to the program as input data and kept constant in the analysis.

The flow chart of the computer program is shown in Figure (3-4). Some controlling integer and real parameters are presented in the flow chart to control the operation. These controlling parameters are K_{max}, J, t_{max}, NSEG, q_{p_i}, Δ_{y_i} and Δ_{u_i}. The following definitions may help in understanding the flow chart:

NSEG number of segments for the shear wall.

K_{max} segments state check parameter, i.e. the segments states are to be checked every K_{max} δt, where δt is

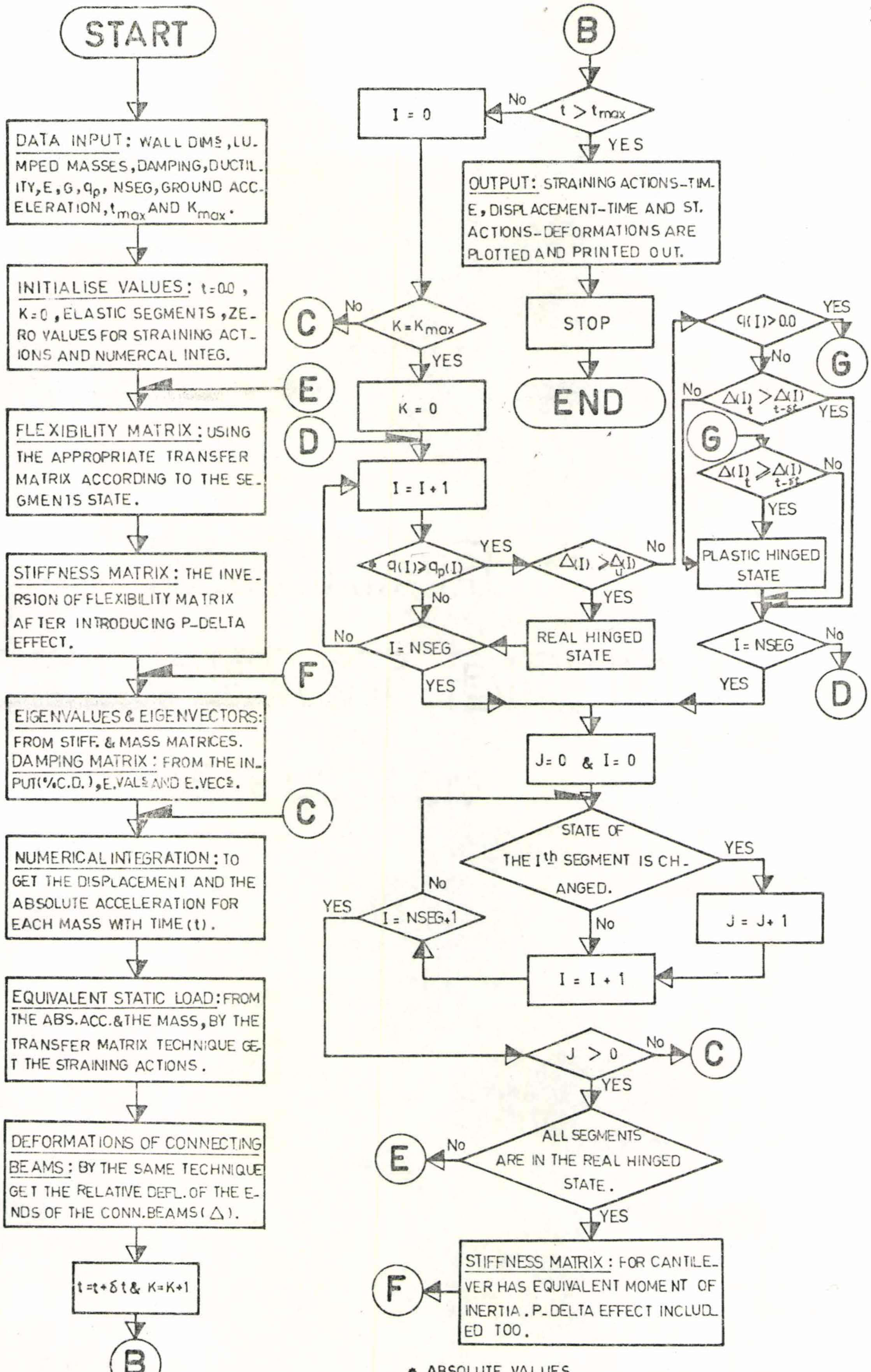

FIG. 3_4 FLOW CHART FOR THE ELASTO_PLASTIC DYNAMIC ANALYSIS OF COUPLED SHEAR WALLS

the time interval for computing the stress state of the structure.

J number of segments which change their states. If $J=0$, no correction of the dynamic properties needs to be made.

t_{max} time limit of the analysis.

q_{p_i} plastic shearing force intensity of the ith segment's laminae.

Δ_{y_i} yield deflection of the ith segment's laminae.

Δ_{u_i} ultimate deflection of the ith segment's laminae. Δ_{u_i} is the product of the yield deflection Δ_{y_i} and the ductility coefficient μ.

3.3 Development of Transfer Matrices

In this section the field transfer matrices for an elastic segment, a plastic hinged segment and a real hinged segment respectively are presented. In addition, nine station transfer matrices are developed to cover all combinations of segment variations.

3.3.1 Field Transfer Matrices

Listed below are the three field transfer matrices with the derivation of the field transfer matrices for aplastic hinged segment, and a real hinged segment. The elastic segment field transfer matrix has been considered by Tso and Chan [18]. Therefore, the final results of the field transfer matrix of an elastic segment is presented without derivation.

3.3.1.1 Field Transfer Matrix for Elastic Segment

By definition, this is the segment in which the connecting beams are in the elastic state [Figure 3-1(1)]. The field transfer matrix for the elastic segment can be written in the following form:

$$[F]_i = [\psi]_i \, [\lambda]_i^{-1} \tag{3-4}$$

where $[F]_i$ is the field transfer matrix for the ith segment shown in figure (3-5).

$$, [\psi]_i = \begin{bmatrix} 1 & 0 & 1 & 0 & 0 & 0 \\ 0 & 1 & 0 & \alpha_i & 0 & 0 \\ 0 & 0 & \alpha_i^2 & 0 & \gamma_i^2/\alpha_i^2 & \dfrac{\gamma_i^2 H_i}{\alpha_i^2} \\ 0 & 0 & 0 & \alpha_i^3 & 0 & -\gamma_i^2/\alpha_i^2 \\ 0 & 0 & 0 & 0 & 1 & H_i \\ 0 & 0 & 0 & 0 & 0 & 1 \end{bmatrix} \tag{3-5}$$

$$
\text{and } [\lambda]_i^{-1} = \begin{bmatrix}
1 & -H_i & -1/\alpha_i^2 & H_i/\alpha_i^2 & \frac{\gamma_i^2}{\alpha_i^2}\left(\frac{1}{2}H_i^2+\frac{1}{\alpha_i^2}\right) & \frac{\gamma_i^2}{\alpha_i^2}H_i\left(\frac{1}{6}H_i^2+\frac{1}{\alpha_i^2}\right) \\
0 & 1 & 0 & -1/\alpha_i^2 & -\gamma_i^2 H_i/\alpha_i^2 & \frac{-\gamma_i^2}{\alpha_i^2}\left(\frac{1}{2}H_i^2+\frac{1}{\alpha_i^2}\right) \\
0 & 0 & \frac{\mathrm{ch}\,\alpha_i H_i}{\alpha_i^2} & \frac{-\mathrm{sh}\,\alpha_i H_i}{\alpha_i^3} & \frac{-\gamma_i^2\,\mathrm{ch}\,\alpha_i H_i}{\alpha_i^4} & \frac{-\gamma_i^2\,\mathrm{sh}\,\alpha_i H_i}{\alpha_i^5} \\
0 & 0 & \frac{-\mathrm{sh}\,\alpha_i H_i}{\alpha_i^2} & \frac{\mathrm{ch}\,\alpha_i H_i}{\alpha_i^3} & \frac{\gamma_i^2\,\mathrm{sh}\,\alpha_i H_i}{\alpha_i^4} & \frac{\gamma_i^2\,\mathrm{ch}\,\alpha_i H_i}{\alpha_i^5} \\
0 & 0 & 0 & 0 & 1 & 0 \\
0 & 0 & 0 & 0 & 0 & 1
\end{bmatrix} \tag{3-6}
$$

where

$$\mathrm{sh}\,\alpha H = \sinh\,\alpha H\ , \quad \mathrm{ch}\,\alpha H = \cosh\,\alpha H$$

and

$$\alpha_i^2 = \frac{a_i\,\mu_i^2}{E\,I_i}\left(1+\frac{I_i}{A_i\,a_i^2}\right)$$

$$\gamma_i^2 = \frac{\mu_i^2}{E^2\,A_i\,I_i\,a_i}$$

$$\mu_i^2 = \frac{12E\,I_{bi}\,a_i}{h_i\,C_i^3\,\beta_i^2}$$

$$\beta_i^{\,2} = 1 = \frac{12E\ I_{bi}}{G\ A_{bi}^{*}\ C_i^{\,2}}$$

$$\frac{1}{A_i} = \frac{1}{A_{i1}} + \frac{1}{A_{i2}}$$

$$I_i = I_{i1} + I_{i2}$$

3.3.1.2 Field Transfer Matrix for Plastic Hinged Segment

A plastic hinged segment has all its connecting beams with plastic hinges formed at their ends. Consider the segment as shown in Figure (3-6) subjected to uniform shearing force per unit height q_{p_i} in the connecting beams.

where

$$q_{p_i} = \frac{2M_{ui}}{c_i\ h_i} \tag{3-7}$$

M_{ui} = Ultimate moment of the connecting beams considered as double reinforced concrete cross section.

and h_i = Storey height in the ith segment.

From axial force equilibrium of an element as shown in Figure (3-7), we have

$$\frac{dT}{dx} = -\ q_p \tag{3-8}$$

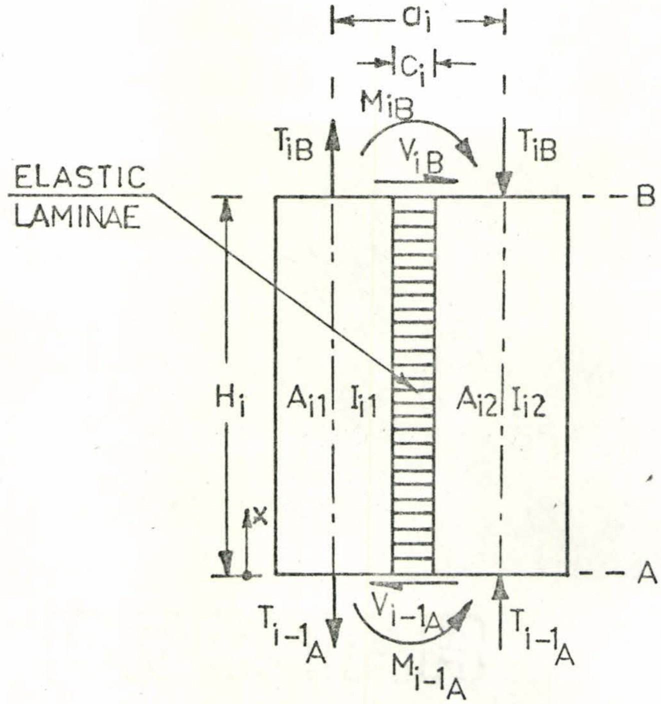

FIG. 3_5 FORCE COMPONENT ACTING ON $i^{\underline{th}}$ SEGMENT (ELASTIC)

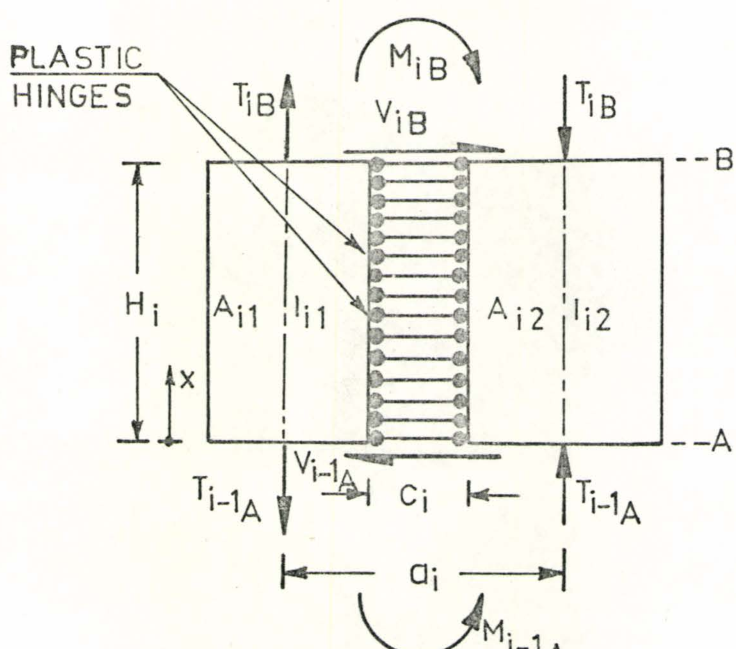

FIG. 3_6 FORCE COMPONENTS ACTING ON $i^{\underline{th}}$ SEGMENT (PLASTIC HINGED)

As q_p is constant along the height of the segment, the change in the axial force T is linear.

And wall moment M is given by the moment equilibrium condition

$$M = M^e - T.a \tag{3-9}$$

where M^e is the overturning moment.

$$\therefore \frac{dM}{dx} = \frac{dM^e}{dx} - \frac{dT}{dx} . a$$

$$\therefore V^* = V - q_p.a \tag{3-10}$$

where V^* = Wall shear

and V = Inter-storey shear

Equations (3-9) and (3-10) provide a relationship between the wall moment and overturning moment; and the wall shear and the inter-storey shear respectively. In a plastic hinged segment, q_p and T are known quantities. Therefore, one can obtain the wall moment and wall shear readily once the overturning moment and inter-storey shear are known. Therefore, for a plastic hinged segment, the problem is statically determinated.

To obtain the field transfer matrix for a plastic hinged segment, it is necessary to obtain relationships between y, y', y'', y''', M^e and V at the top and bottom of the plastic hinged segment. The deflection,slope and curvature relationship can be obtained by

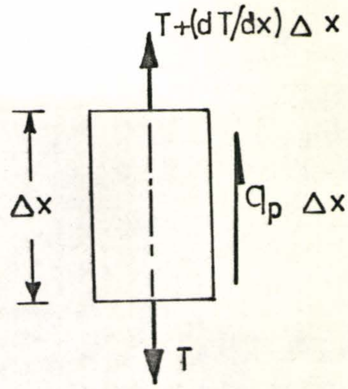

FIG. 3_7 EQUILIBRIUM OF AXIAL FORCES , LEFT WALL

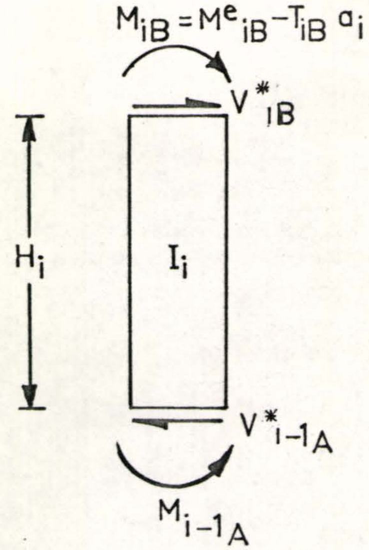

FIG. 3_8 EQUIVALENT WALL

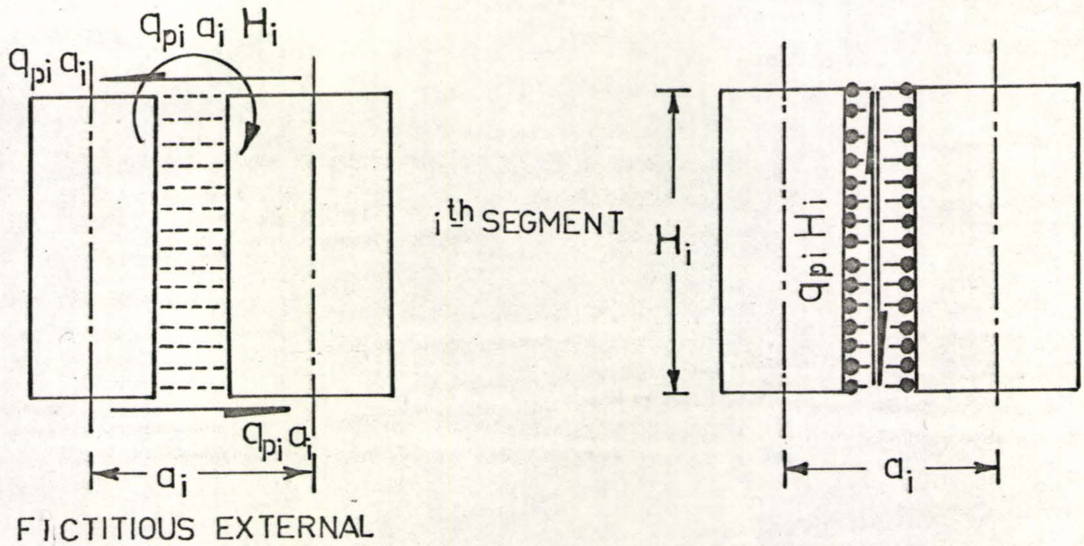

FIG. 3_9 EXTERNAL EFFECT OF THE INTERNAL SHEARING FORCE q_{pi}

considering a plastic hinged segment under overturning moment M^e and inter-storey shear V to be the same as a beam with moment of inertia $I = I_1 + I_2$ under the action of beam moment M and beam shear V^*, Figure (3-8).

Consider a beam of length H_i under the actions of wall moments M_{iB} and wall shears V^*_{ib} at the top of the beam as shown in Figure (3-11), the deflection and slope at the top relative to the base are given by

$$y_{(i-1)A} = y_{iB} - H_i(y'_{iB} - \theta_{iB}) - y^* \tag{3-11}$$

$$y'_{(i-1)A} = y'_{iB} - \theta_{iB} \tag{3-12}$$

To obtain a relation between $(y, y')_{(i-1)A}$ and $(y, y')_{iB}$, it is necessary to express y^* and θ_{iB} in terms of the elements of the state vector $\{\phi\}_{iB}$. This can be achieved by computing the top deflection and slope for the equivalent beam subjected to the wall forces, M_{iB} and V_{iB}^*.

$$y^* = \frac{M_{iB} H_i^2}{2EI_i} + \frac{V_{iB}^* H_i^3}{3EI_i} \tag{3-13}$$

$$\theta_{iB} = \frac{M_{iB} H_i}{EI_i} + \frac{V_{iB}^* H_i^2}{2EI_i} \tag{3-14}$$

Substituting by the above values in equations (3-11) and (3-12) leads to

$$y_{(i-1)A} = y_{iB} - H_i\, y'_{iB} + \frac{H_i^{\,2}}{2}\, y''_{iB} + \frac{H_i^{\,3}}{6EI_i}\, V^*_{iB}$$

(3-15)

$$y'_{(i-1)A} = y'_{iB} - H_i\, y''_{iB} - \frac{H_i^{\,2}}{2EI_i}\, V^*_{iB} \qquad (3\text{-}16)$$

For shear force equilibrium, we have

$$V^*_{(i-1)A} = V^*_{iB} \qquad (3\text{-}17)$$

shear force-bending moment relationship leads to

$$M_{(i-1)A} = M_{iB} + H_i\, V^*_{iB} \qquad (3\text{-}18)$$

$$\therefore\quad y''_{(i-1)A} = y''_{iB} + \frac{H_i}{EI_i}\, V^*_{iB} \qquad (3\text{-}19)$$

Expressing the wall moments in terms of the overturning moments at (i-1)A level and iB level, we have

$$M^e_{(i-1)A} = M^e_{f_{iB}} + H_i\, V^*_{iB} \qquad (3\text{-}20)$$

where $$M^e_{f_{iB}} = M^e_{iB} + q_{pi}\, a_i\, H_i \qquad (3\text{-}21)$$

Equation of shear for the equivalent wall under an applied shearing force V^*_{iB}, as shown in Figure (3-11), can be written as

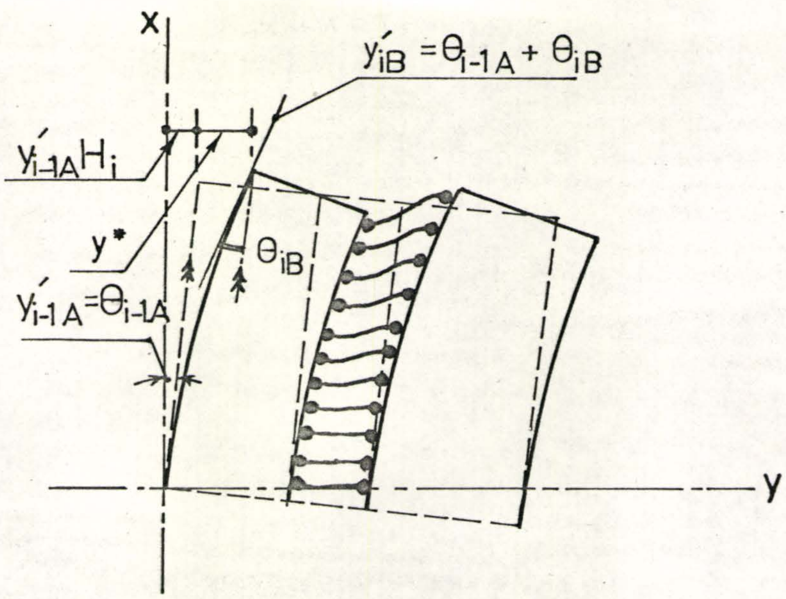

FIG. 3_10 DEFORMED SHAPE OF THE i^{th} SEGMENT

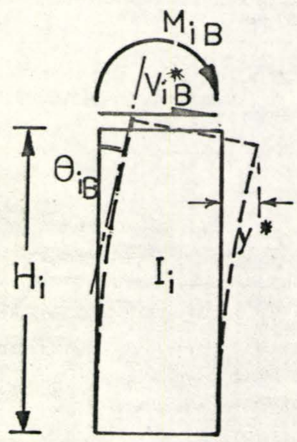

FIG. 3_11 EQUIVALENT WALL WITH RELATIVE DEFORMATIONS BETWEEN THE TOP AND THE BOTTOM

$$EI_i \, y'''_{(i-1)A} = EI_i \, y'''_{iB} + V^*_{iB}$$

$$\therefore \; y'''_{(i-1)A} = y'''_{iB} + \frac{1}{EI_i} V^*_{iB} \qquad (3\text{-}22)$$

Equations (3-15), (3-16), (3-17), (3-19), (3-20) and (3-22) provide the relation between the state vector at (i-1)A level and the state vector at iB level. It should be noted that the state vectors at (i-1)A and iB levels contain the wall shear V^* instead of the inter-storey shear V, also the state vector at iB contains a fictitious parameter $M^e_{f_{iB}}$, which is necessary to keep the equilibrium at the bottom of the segment, i.e. the internal distributed shearing force q_{ip} produces three pseudo elements in the state vectors at top and bottom of the plastic hinged segment; namely V^*_{iB}, $M^e_{f_{iB}}$ and V^*_{iA}. Figure (3-9) shows the external loads necessary to handle the plastic hinged segment by the transfer matrix technique.

The field transfer matrix $[F]_i$ for a plastic hinged segment is given in equation (3-23).

$$\begin{bmatrix} y \\ y' \\ y'' \\ y''' \\ M^e \\ V^* \end{bmatrix}_{(i-1)A} = \begin{bmatrix} 1 & -H_i & \frac{H_i^2}{2} & 0 & 0 & \frac{H_i^3}{6EI_i} \\ 0 & 1 & -H_i & 0 & 0 & \frac{-H_i^2}{2EI_i} \\ 0 & 0 & 1 & 0 & 0 & \frac{H_i}{EI_i} \\ 0 & 0 & 0 & 1 & 0 & \frac{1}{EI_i} \\ 0 & 0 & 0 & 0 & 1 & H_i \\ 0 & 0 & 0 & 0 & 0 & 1 \end{bmatrix} \begin{bmatrix} y \\ y' \\ y'' \\ y''' \\ M^e_f \\ V^* \end{bmatrix}_{iB} \tag{3-23}$$

To use the above equation, two modifications must be done to the station transfer matrices at station (i) and station (i-1). These modifications are necessary to obtain the pseudo vector at iB level, $\{\phi\}'_{iB}$, and to proceed with the inter-storey shear for the (i-1)th segment after computing the pseudo vector at (i-1)A level from equation (3-23). The necessary modifications will be presented in subsection (3.3.2) later.

3.3.1.3 Field Transfer Matrix for a Real Hinged Segment

The field transfer matrix for a real hinged segment can be obtained from the plastic hinged segment assuming the connecting beams have lost their moment transmission capacities, [Figure (3-12)]. i.e., when $q_{pi} = 0$. Therefore, by substituting by the above value of q_{pi} in equations (3-10) and (3-21) leads to

$$V^* = V \tag{3-24}$$

and

$$M^e_{f_{iB}} = M^e_{iB} \tag{3-25}$$

Substituting in V^*_{iB} and $M^e_{f_{iB}}$ by V_{iB} and M^e_{iB} respectively, equation (3-23) gives the field transfer matrix for the real hinged segment $[F]_i$ in the following equation.

$$\begin{bmatrix} y \\ y' \\ y'' \\ y''' \\ M^e \\ V \end{bmatrix}_{(i-1)A} = \begin{bmatrix} 1 & -H_i & \frac{H_i^2}{2} & 0 & 0 & \frac{H_i^3}{6EI_i} \\ 0 & 1 & -H_i & 0 & 0 & \frac{-H_i^2}{2EI_i} \\ 0 & 0 & 1 & 0 & 0 & \frac{H_i}{EI_i} \\ 0 & 0 & 0 & 1 & 0 & \frac{1}{EI_i} \\ 0 & 0 & 0 & 0 & 1 & H_i \\ 0 & 0 & 0 & 0 & 0 & 1 \end{bmatrix} \begin{bmatrix} y \\ y' \\ y'' \\ y''' \\ M^e \\ V \end{bmatrix}_{iB}$$

(3-26)

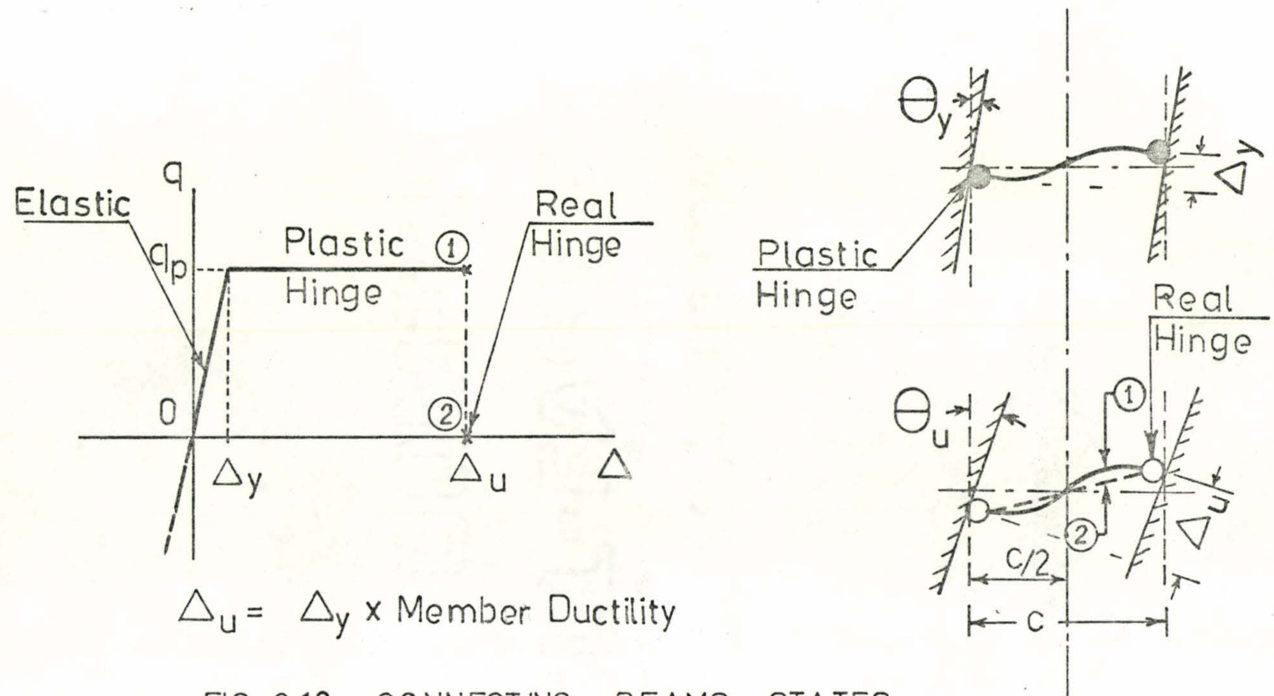

FIG. 3.12 CONNECTING BEAMS STATES

3.3.2 Station Transfer Matrices

Listed below are the nine station transfer matrices necessary to complete the solution of the problem.

3.3.2.1 Station Transfer Matrix Relating a State Vector in Elastic Segment to State Vector in Elastic Segment (Elastic-Elastic Station)

The station transfer matrix for elastic-elastic station as shown in Figure (3-13a) has been formulated by Tso and Chan [18] in the following form:

$$\{\phi\}_{iB} = [S]_i \{\phi\}_{iA} + \{L\}_i \tag{3-27}$$

where $[S]_i$ = Station Transfer Matrix for the ith station.

and $\{L\}_i$ = Load Vector for the ith station.

Equation (3-27) can be written in the following detailed form:

$$\begin{bmatrix} y \\ y' \\ y'' \\ y''' \\ M^e \\ V \end{bmatrix}_{iB} = \begin{bmatrix} 1 & 0 & 0 & 0 & 0 & 0 \\ 0 & 1 & 0 & 0 & 0 & 0 \\ 0 & 0 & \dfrac{I_{i+1}a_i}{I_i a_{i+1}} & 0 & \dfrac{a_{i+1}-a_i}{EI_i a_{i+1}} & 0 \\ 0 & 0 & 0 & \dfrac{I_{i+1}\mu_i^2}{I_i\mu^2_{i+1}} & 0 & \dfrac{\mu_i^2-\mu_{i+1}^2}{EI_i\mu^2_{i+1}} \\ 0 & 0 & 0 & 0 & 1 & 0 \\ 0 & 0 & 0 & 0 & 0 & 1 \end{bmatrix} \begin{bmatrix} y \\ y' \\ y'' \\ y''' \\ M^e \\ V \end{bmatrix}_{iA} + \begin{bmatrix} 0 \\ 0 \\ 0 \\ \dfrac{-P_i}{EI_i} \\ 0 \\ P_i \end{bmatrix} \tag{3-28}$$

where $$\mu_i^2 = \frac{12EI_{bi}\, a_i}{h_i\, c_i^3\, \beta_i^2}$$

and $$\beta_i^2 = 1 + \frac{12EI_{bi}}{G\, A^*_{bi}\, c_i^2}$$

3.3.2.2 Station Transfer Matrix Relating a State Vector in Elastic Segment to State Vector in Plastic Hinged Segment (Plastic-Elastic Station)

From the continuity of the wall, the lateral deflection and the slope above and below the station are equal.

$$\therefore \quad y_{iB} = y_{iA} \tag{3-29}$$

and $$y'_{iB} = y'_{iA} \tag{3-30}$$

The relation between bending moments below and above the station due to wall cross section sudden change is given by

$$EI_i\, y''_{iB} = EI_{i+1}\, y''_{iA} - (a_i - a_{i+1})\, T_{iA}$$

$$\therefore \quad y''_{iB} = \frac{I_{i+1}\, a_i}{I_i\, a_{i+1}}\, y''_{iA} + \frac{a_{i+1} - a_i}{EI_i a_{i+1}}\, M^e_{iA} \tag{3-31}$$

Also due to the sudden change in the cross section of the wall the relation between the shearing force below and above the station is given by

$$-(EI_i\, y'''_{iB} - a_i\, q_{iB}) = (EI_{i+1}\, y'''_{iA} - a_{i+1}\, q_{iA}) + P_i$$

$$\therefore\ EI_i\, y'''_{iB} = EI_{i+1}\, y'''_{iA} + a_i\, q_{iB} - a_{i+1}\, q_{iA} - P_i$$

$$= EI_{i+1}\, y'''_{iA} + \left(\frac{a_{i+1}\, \mu_i^2}{a_i\, \mu_{i+1}^2}\right) q_{i+1P} - a_{i+1}\, q_{i+1P} - P_i$$

$$\therefore\ y'''_{iB} = \frac{I_{i+1}}{I_i}\, y'''_{iA} + \frac{q_{i+1P}\, a_{i+1}}{EI_i}\left(\frac{\mu_i^2}{\mu_{i+1}^2} - 1\right) - \frac{P_i}{EI_i} \qquad (3\text{-}32)$$

For the section just above the station and the section just below it the overturning moment in both sides are equal.

$$\therefore\ M^e_{iB} = M^e_{iA} \qquad (3\text{-}33)$$

As shown in Figure (3-13b) the shearing force at the section just above the station is the fictitious shearing force V^*_{iA} due to the modification done to the state vectors in the plastic hinged segment (i+1), i.e. the external shearing force at this section is reduced by $(q_{p_{i+1}}\ a_{i+1})$.

$$\therefore\ V_{iB} = V^*_{iA} + (q_p\, a)_{i+1} + P_i \qquad (3\text{-}34)$$

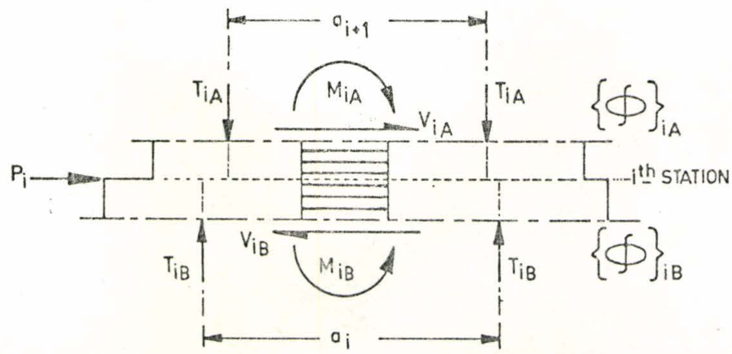

(a) ELASTIC_ELASTIC STATION

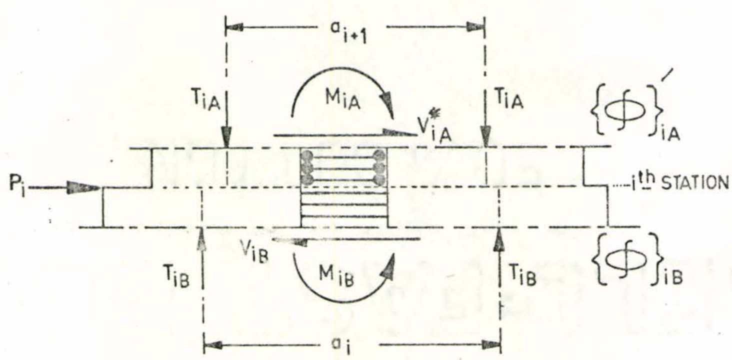

(b) PLASTIC_ELASTIC STATION

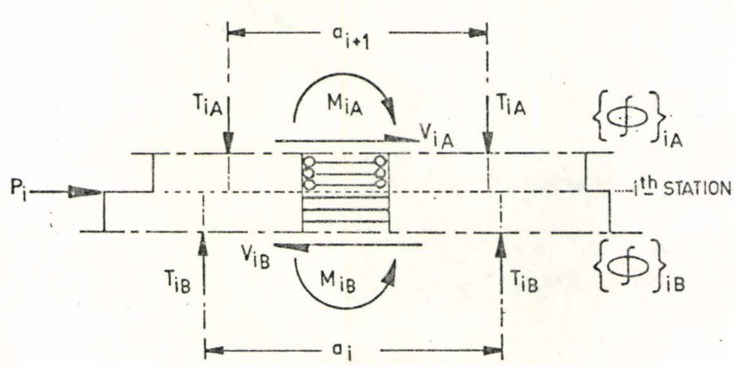

(c) REAL HINGED_ELASTIC STATION

FIG. 3_13 FORCE COMPONENTS ACTING ON THE i^{th} STATION, TRANSFER TO ELASTIC SEGMENT

Equations (3-29), (3-30), (3-31), (3-32), (3-33) and (3-34) give the station transfer matrix for the plastic-elastic station.

$$\begin{bmatrix} y \\ y' \\ y'' \\ y''' \\ M^e \\ V \end{bmatrix}_{iB} = \begin{bmatrix} 1 & 0 & 0 & 0 & 0 & 0 \\ 0 & 1 & 0 & 0 & 0 & 0 \\ 0 & 0 & \frac{a_i I_{i+1}}{a_{i+1} I_i} & 0 & \frac{a_{i+1}-a_i}{EI_i a_{i+1}} & 0 \\ 0 & 0 & 0 & \frac{I_{i+1}}{I_i} & 0 & 0 \\ 0 & 0 & 0 & 0 & 1 & 0 \\ 0 & 0 & 0 & 0 & 0 & 1 \end{bmatrix} \begin{bmatrix} y \\ y' \\ y'' \\ y''' \\ M^e \\ V^* \end{bmatrix}_{iA} + \begin{bmatrix} 0 \\ 0 \\ 0 \\ \frac{-1}{EI_i}\left[P_i + a_{i+1} q_{p_{i+1}} \left(1-\frac{\mu_i^2}{\mu_{i+1}^2}\right)\right] \\ 0 \\ P_i + q_{p_{i+1}} a_{i+1} \end{bmatrix}$$

(3-35)

3.3.2.3 <u>Station Transfer Matrix Relating a State Vector in Elastic Segment to State Vector in Real Hinged Segment (Real Hinged-Elastic Statinn)</u>

This is a special case of the plastic-elastic station. If we substitute in the load vector in equation (3-35) by zero for $q_{p_{i+1}}$, the load vector for the real hinged-elastic station will be obtained. The station transfer matrix $[S]_i$ will be the same as it is independent of the connecting beams shearing force in segment (i+1).

The station transfer matrix in this case can be written as:

$$\begin{bmatrix} y \\ y' \\ y'' \\ y''' \\ M^e \\ V \end{bmatrix}_{iB} = \begin{bmatrix} 1 & 0 & 0 & 0 & 0 & 0 \\ 0 & 1 & 0 & 0 & 0 & 0 \\ 0 & 0 & \frac{a_i \, I_{i+1}}{a_{i+1} \, I_i} & 0 & \frac{a_{i+1}-a_i}{EI_i a_{i+1}} & 0 \\ 0 & 0 & 0 & \frac{I_{i+1}}{I_i} & 0 & 0 \\ 0 & 0 & 0 & 0 & 1 & 0 \\ 0 & 0 & 0 & 0 & 0 & 1 \end{bmatrix} \begin{bmatrix} y \\ y' \\ y'' \\ y''' \\ M^e \\ V \end{bmatrix}_{iA} + \begin{bmatrix} 0 \\ \\ 0 \\ \frac{-P_i}{EI_i} \\ 0 \\ P_i \end{bmatrix}$$

(3-36)

3.3.2.4 <u>Station Transfer Matrix Relating a State Vector in Plastic Hinged Segment to State Vector in Elastic Segment (Elastic-Plastic Station)</u>

Equations (3-29), (3-30) and (3-31) are valid in this case as they are independent of the shearing force intensity in the connecting beams above and below the station.

From the relation between the shearing force above and below the station we get

$$EI_i \, y'''_{iB} = EI_{i+1} \, y'''_{iA} + a_i \, q_{iB} - a_{i+1} \, q_{iA} - P_i$$

But $$q_{iA} = \frac{EI_{i+1}\, y'''_{iA} + V_{iA}}{a_{i+1}} \tag{3-37}$$

and $$q_{iB} = q_{Pi}$$

$$\therefore\ y'''_{iB} = \frac{1}{EI_i}\left[EI_{i+1}\, y'''_{iA} + a_i\, q_{Pi} - EI_{i+1}\, y'''_{iA} - V_{iA} - P_i\right]$$

$$y'''_{iB} = -\frac{1}{EI_i} V_{iA} - \frac{P_i - q_{pi}\, a_i}{EI_i} \tag{3-38}$$

Because of the reduction value $(q_{pi}\ a_i)$ in the shearing force at B which is necessary in forming the field transfer matrix for the plastic hinged segment (i), a modification will be introduced in the load vector (i) in both M^e_{iB} and V_{iB} to get $M^e_{f_{iB}}$ and V^*_{iB} respectively.

$$\therefore\ M^e_{f_{iV}} = M^e_{iA} + q_{pi}\ a_i\ H_i \tag{3-39}$$

And $$V^*_{iB} = V_{iA} + P_i - q_{Pi}\ a_i \tag{3-40}$$

Equations (3-29), (3-30), (3-31), (3-38), (3-39) and (3-40) form the station transfer matrix.

$$\begin{bmatrix} y \\ y' \\ y'' \\ y''' \\ M^e_f \\ V^* \end{bmatrix}_{iB} = \begin{bmatrix} 1 & 0 & 0 & 0 & 0 & 0 \\ 0 & 1 & 0 & 0 & 0 & 0 \\ 0 & 0 & \frac{I_{i+1}\ a_i}{I_i\ a_{i+1}} & 0 & \frac{a_{i+1}-a_i}{EI_i a_{i+1}} & 0 \\ 0 & 0 & 0 & 0 & 0 & \frac{-1}{EI_i} \\ 0 & 0 & 0 & 0 & 1 & 0 \\ 0 & 0 & 0 & 0 & 0 & 1 \end{bmatrix} \begin{bmatrix} y \\ y' \\ y'' \\ y''' \\ M^e \\ V \end{bmatrix}_{iA} + \begin{bmatrix} 0 \\ 0 \\ 0 \\ -(\frac{P_i - q_{Pi} a_i}{EI_i}) \\ q_{Pi}\ a_i\ H_i \\ (P_i - q_{Pi}\ a_i) \end{bmatrix}$$

(3-41)

3.3.2.5 Station Transfer Matrix Relating a State Vector in Plastic Hinged Segment to a State Vector in Plastic Hinged Segment (Plastic-Plastic Station)

As the relations between (y_{iB}, y'_{iB} and y''_{iB}) and (y_{iA}, y'_{iA} and y''_{iA}) are independent of the shearing force in the connecting beams above and below the station, equations (2-39), (3-30) and (3-31) are valid in this case.

The equation of shear is

$$EI_i\ y'''_{iB} = EI_{i+1}\ y'''_{iA} + a_i\ q_{Pi} - a_{i+1}\ q_{P_{i+1}} - P_i\ .$$

$$\therefore y'''_{iB} = \frac{I_{i+1}}{I_i} y'''_{iA} - \left(\frac{P_i - (a_i\, q_{Pi} - a_{i+1}\, q_{P_{i+1}})}{EI_i}\right)$$

(3-42)

As discussed in the previous case a modification will be introduced in the load vector (i) in both M^e_{iB} and V_{iB} to get $M^e_{f_{iB}}$ and V^*_{iB} respectively. In addition, a correction must be done to the reduced shearing force V^*_{iA} to fulfil the external equilibrium of the shearing forces at the station (i).

$$M^e_{f_{iB}} = M^e_{iA} + q_{Pi}\, a_i\, H_i \qquad (3\text{-}43)$$

and

$$V^*_{iB} = V^*_{iA} + P_i + q_{P_{i+1}}\, a_{i+1} - q_{Pi}\, a_i \qquad (3\text{-}44)$$

Equations (3-20), (3-30), (3-31), (3-42), (3-43) and (3-44) form the station transfer matrix. This station transfer matrix is given by equation (3-45). The station matrix $[S]_i$ and the load vector $\{L\}_i$ are different than those for the elastic-plastic station given by equation (3-41).

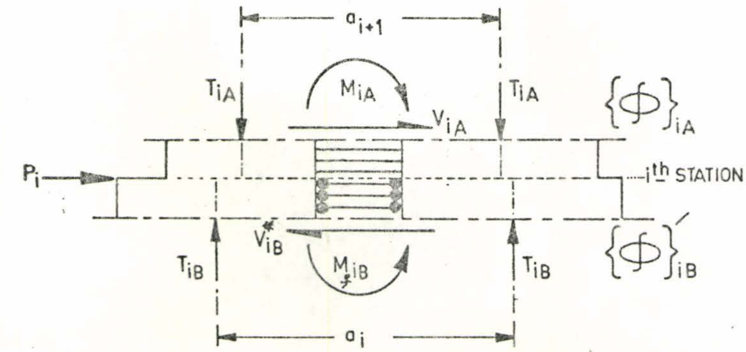

(a) ELASTIC_PLASTIC STATION

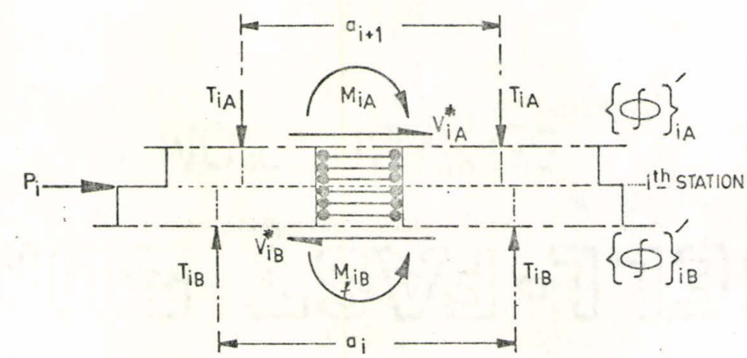

(b) PLASTIC_PLASTIC STATION

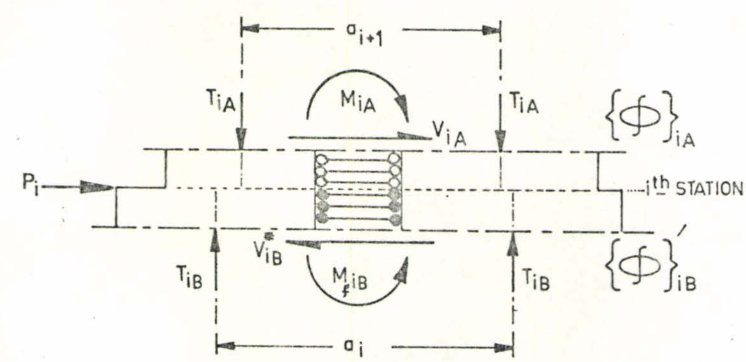

(c) REAL HINGED_PLASTIC STATION

FIG. 3.14 FORCE COMPONENTS ACTING ON THE i^{th} STATION, TRANSFER TO PLASTIC SEGMENT

$$\begin{bmatrix} y \\ y' \\ y'' \\ y''' \\ M^e_f \\ V^* \end{bmatrix}_{iB} = \begin{bmatrix} 1 & 0 & 0 & 0 & 0 & 0 \\ 0 & 1 & 0 & 0 & 0 & 0 \\ 0 & 0 & \dfrac{I_{i+1}\, a_i}{I_i\, a_{i+1}} & 0 & \dfrac{a_{i+1}-a_i}{EI_i a_{i+1}} & 0 \\ 0 & 0 & 0 & \dfrac{I_{i+1}}{I_i} & 0 & 0 \\ 0 & 0 & 0 & 0 & 1 & 0 \\ 0 & 0 & 0 & 0 & 0 & 1 \end{bmatrix} \cdot \begin{bmatrix} y \\ y' \\ y'' \\ y''' \\ M^e \\ V^* \end{bmatrix}_{iA} + \begin{bmatrix} 0 \\ 0 \\ 0 \\ -\left(\dfrac{P_i+q_{Pi+1}a_{i+1}-q_{Pi}a_i}{EI_i}\right) \\ q_{Pi}\ a_i\ H_i \\ (P_i+q_{Pi+1}\ a_{i+1}-q_{Pi}a_i) \end{bmatrix}$$

(3-45)

3.3.2.6 <u>Station Transfer Matrix Relating a State Vector in Plastic Hinged Segment to a State Vector in Real Hinged Segment (Real Hinged-Plastic Station)</u>

By substituting in equations (3-42) and (3-44) for q_{Pi+1} by zero we get

$$y'''_{iB} = \frac{I_{i+1}}{I_i}\, y'''_{iA} - \frac{P_i - a_i\, q_{Pi}}{EI_i} \qquad (3\text{-}46)$$

and

$$V^*_{iB} = V_{iA} + P_i - q_{Pi}\, a_i \qquad (3\text{-}47)$$

Equations (3-29), (3-30), (3-31) and (3-43) are valid.

$$\begin{bmatrix} y \\ y' \\ y'' \\ y''' \\ M^e{}_f \\ V^* \end{bmatrix}_{iB} = \begin{bmatrix} 1 & 0 & 0 & 0 & 0 & 0 \\ 0 & 1 & 0 & 0 & 0 & 0 \\ 0 & 0 & \frac{I_{i+1}\ a_i}{I_i\ a_{i+1}} & 0 & \frac{a_{i+1}-a_i}{EI_i a_{i+1}} & 0 \\ 0 & 0 & 0 & \frac{I_{i+1}}{I_i} & 0 & 0 \\ 0 & 0 & 0 & 0 & 1 & 0 \\ 0 & 0 & 0 & 0 & 0 & 1 \end{bmatrix} \cdot \begin{bmatrix} y \\ y' \\ y'' \\ y''' \\ M^e \\ V \end{bmatrix}_{iA} + \begin{bmatrix} 0 \\ 0 \\ 0 \\ -(\frac{P_i\ q_{Pi}\ a_i}{EI_i}) \\ q_{Pi}\ a_i\ H_i \\ (P_i - q_{Pi}\ a_i) \end{bmatrix}$$

(3-48)

3.3.2.7. Station Transfer Matrix Relating a State Vector in Real-Hinged Segment to a State Vector in Elastic Segment (Elastic-Real Hinged Station)

Equations (3-29), (3-30) and (3-31) are valid in this case. The change will be in the terms concerning the shearing force in the connecting beams above and below the station.

The equation of the shearing force equilibrium above and below the station is

$$EI_i\ y'''_{iB} = EI_{i+1}\ y'''_{iA} + a_i\ q_{iB} - a_{i+1}\ q_{iA} - P_i$$

The second term in the R.H.S. of the last equation will vanish as the shear intensity in the ith segment is equal to zero.

$$\therefore y'''_{iB} = \frac{I_{i+1}}{I_i} y'''_{iA} - \frac{I_{i+1}}{I_i} y'''_{iA} - \frac{V_{iA}}{EI_i} - \frac{P_i}{EI_i}$$

$$y'''_{iB} = -\frac{1}{EI_i} V_{iA} - \frac{1}{EI_i} P_i \qquad (3\text{-}49)$$

From the equilibrium

$$M^e_{iB} = M^e_{iA} \qquad (3\text{-}50)$$

And

$$V_{iB} = V_{iA} + P_i \qquad (3\text{-}51)$$

Equations (3-29), (3-30), (3-31), (3-49), (3-50) and (3-51) form the station transfer matrix as follows:

$$\begin{bmatrix} y \\ y' \\ y'' \\ y''' \\ M^e \\ V \end{bmatrix}_{iB} = \begin{bmatrix} 1 & 0 & 0 & 0 & 0 & 0 \\ 0 & 1 & 0 & 0 & 0 & 0 \\ 0 & 0 & \frac{I_{i+1}\, a_i}{I_i a_{i+1}} & 0 & \frac{a_{i+1} - a_i}{EI_i a_{i+1}} & 0 \\ 0 & 0 & 0 & 0 & 0 & \frac{-1}{EI_i} \\ 0 & 0 & 0 & 0 & 1 & 0 \\ 0 & 0 & 0 & 0 & 0 & 1 \end{bmatrix} \begin{bmatrix} y \\ y' \\ y'' \\ y''' \\ M^e \\ V \end{bmatrix}_{iA} + \begin{bmatrix} 0 \\ 0 \\ 0 \\ \frac{-P_i}{EI_i} \\ 0 \\ P_i \end{bmatrix}$$

(3-52)

3.3.2.8 Station Transfer Matrix Relating a State Vector in Real Hinged Segment to a State Vector in Plastic Hinged Segment (Plastic-Real Hinged Station)

Besides the equations (3-29), (3-30) and (3-31) the following equations can be obtained from station shown in Figure (3-15b)

$$EI_i\, y'''_{iB} = EI_{i+1}\, y'''_{iA} + a_i\, q_{iB} - a_{i+1}\, q_{iA} - P_i$$

$$\therefore\; y'''_{iB} = \frac{I_{i+1}}{I_i}\, y'''_{iA} - \left(\frac{P_i + a_{i+1} q_{Pi+1}}{EI_i}\right) \qquad (3\text{-}53)$$

Equation (3-50) is valid.

Due to the shearing force correction from V^*_{iA} to V_{iA} the shearing force equilibrium will be

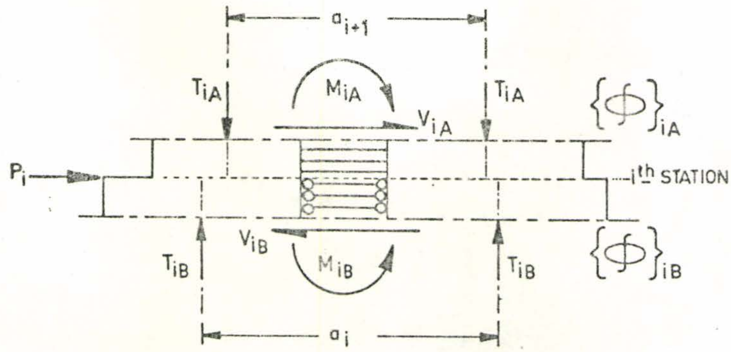

(a) ELASTIC_REAL HINGED STATION

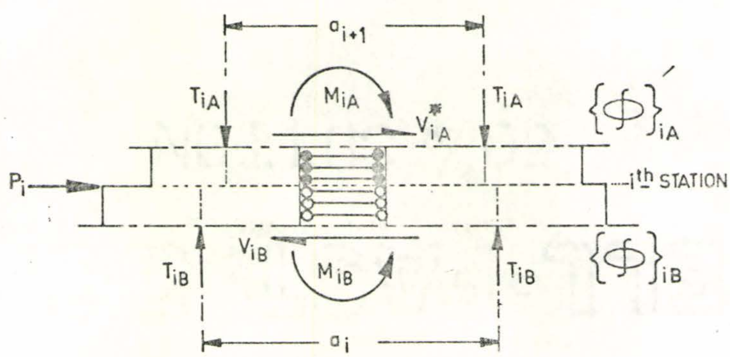

(b) PLASTIC_REAL HINGED STATION

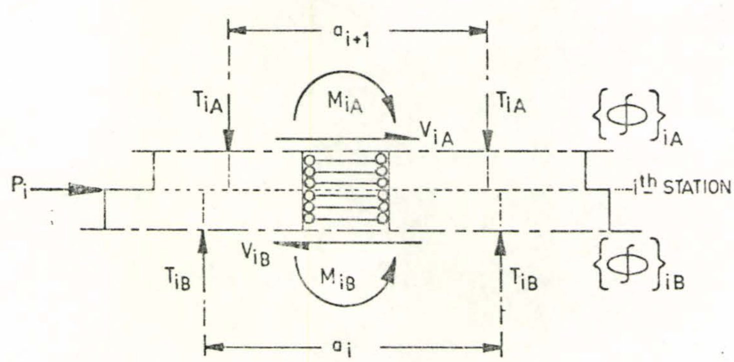

(c) REAL HINGED_REAL HINGED STATION

FIG. 3_15 FORCE COMPONENTS ACTING ON THE i^{th} STATION, TRANSFER TO REAL HINGED SEGMENT

$$V_{iB} = V^*_{iA} + (P_i + q_{p_{i+1}} \; a_{i+1})$$

Therefore, the station transfer matrix will be:

$$\begin{bmatrix} y \\ y' \\ y'' \\ y''' \\ M^e \\ V \end{bmatrix}_{iB} = \begin{bmatrix} 1 & 0 & 0 & 0 & 0 & 0 \\ 0 & 1 & 0 & 0 & 0 & 0 \\ 0 & 0 & \frac{I_{i+1} a_i}{I_i a_{i+1}} & 0 & \frac{a_{i+1} - a_i}{EI_i a_{i+1}} & 0 \\ 0 & 0 & 0 & \frac{I_{i+1}}{I_i} & 0 & 0 \\ 0 & 0 & 0 & 0 & 1 & 0 \\ 0 & 0 & 0 & 0 & 0 & 1 \end{bmatrix} \begin{bmatrix} y \\ y' \\ y'' \\ y''' \\ M^e \\ V^* \end{bmatrix}_{iA} + \begin{bmatrix} 0 \\ 0 \\ 0 \\ -(\frac{P_i + a_{i+1} q_{pi+1}}{EI_i}) \\ 0 \\ (P_i + a_{i+1} q_{p_{i+1}}) \end{bmatrix}$$

(3-54)

3.3.2.9 Station Transfer Matrix Relating a State Vector in Real Hinged Segment to a State Vector in Real Hinged Segment (Real Hinged - Real Hinged Station)

The station shown in Figure (3-15C) is the simplest statinn because of the vanishing of the shearing forces in the connecting beams above and below the station.

Equations (3-29), (3-30) and (3-31) are valid. The equation of shear becomes

$$y'''_{iB} = \frac{I_{i+1}}{I_i} y'''_{iA} - \frac{P_i}{EI_i} \qquad (3-55)$$

Equations (3-50) and (3-51) are valid too. Therefore, the station transfer matrix in this case can be formed from the above equations in the following form:

$$\begin{bmatrix} y \\ y' \\ y'' \\ y''' \\ M^e \\ V \end{bmatrix}_{iB} = \begin{bmatrix} 1 & 0 & 0 & 0 & 0 & 0 \\ 0 & 1 & 0 & 0 & 0 & 0 \\ 0 & 0 & \frac{I_{i+1}a_i}{I_i a_{i+1}} & 0 & \frac{a_{i+1}-a_i}{EI_i a_{i+1}} & 0 \\ 0 & 0 & 0 & \frac{I_{i+1}}{I_i} & 0 & 0 \\ 0 & 0 & 0 & 0 & 1 & 0 \\ 0 & 0 & 0 & 0 & 0 & 1 \end{bmatrix} \begin{bmatrix} y \\ y' \\ y'' \\ y''' \\ M^e \\ V \end{bmatrix}_{iA} + \begin{bmatrix} 0 \\ 0 \\ 0 \\ -\frac{P_i}{EI_i} \\ 0 \\ P_i \end{bmatrix}$$

(3-56)

3.3.3 Summary and Discussion

A development of transfer matrices is presented in this section. Three field transfer matrices are presented. The field transfer matrix for a plastic hinged segment is developed and presented in subsection (3.3.1.2). Although the real hinged segment is a special case of the plastic hinged segment, both of their field transfer matrices are the same, equations (3-23) and (3-26). The field transfer matrix for a plastic hinged segment relates two pseudo state vectors, $\{\phi\}'_{iB}$ and $\{\phi\}'_{(i-1)A}$. While the field transfer matrices for an elastic segment and a real hinged segment relate actual state vectors, $\{\phi\}_{iB}$ and $\{\phi\}_{(i-1)A}$.

where

$$\{\phi\}'_{(i-1)A} = \text{Column } (y, y', y'', y''', M^e, V^*)_{(i-1)A}$$

$$, \quad \{\phi\}'_{iB} = \text{Column } (y, y', y'', y''', M^e{}_f, V^*)_{iB}$$

$$, \quad \{\phi\}_{(i-1)A} = \text{Column } (y, y', y'', y''', M^e, V)_{(i-1)A}$$

$$\text{and} \quad \{\phi\}_{iB} = \text{Column } (y, y', y'', y''', M^e, V)_{iB}$$

$M^e{}_f$ and V^* are given by equations (3-21) and (3-10) respectively.

The position of the pseudo state vectors, $\{\phi\}'_{(i-1)A}$ and $\{\phi\}'_{iB}$, is shown in Figure (3-16) for a plastic hinged segment. The modifications necessary to obtain these state vectors are included in the load vectors of the two stations above and below the segment, they are stations (i) and (i-1) respectively.

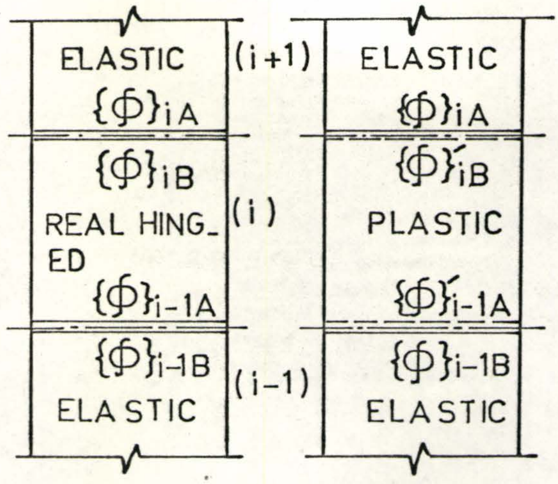

FIG. 3_16 FICTITIOUS STATE VECTORS OF THE PLASTIC HINGED SEGMENT

PLASTIC _ ELASTIC (2_1)

STATION TRANSFER MATRIX IS GIVEN BY EQUATION (3_35)

ELASTIC _ PLASTIC (1_2)

STATION TRANSFER MATRIX IS GIVEN BY EQUATION (3_41)

EQU.(3_35) $\neq$ EQU.(3_41)

FIG.3_17 UNSYMMETRICAL PROPERTY OF THE STATION TRANSFER MATRICES

In addition, nine station transfer matrices are presented in this section. It should be noted that the station transfer matrix relating state vectors from an elastic segment to a vector in a plastic hinged segment is different from that relating a state vector in a plastic hinged segment to a state vector in elastic segment. Figure (3-17) represents an example for this unsymmetrical property.

CHAPTER 4

DYNAMIC ANALYSIS OF SHEAR WALL BUILDINGS

4.1 Coupled Shear Wall Systems

In this chapter, the behaviour of coupled shear wall buildings subjected to earthquake excitation is studied. It is assumed that the buildings considered are symmetrical in plan and consist of a series of planar coupled shear walls. It is assumed that all internal coupled walls are identical and also the two ends coupled walls are the same. In addition, it is assumed that the interior walls are coupled by the floor slabs, while the exterior end walls are coupled by stiff connecting beams.

Two buildings of typical dimensions are considered. The first building is a ten storey coupled shear wall structure. The walls of the structure, the storey height, and the connecting beam stiffness are constant throughout the height. The walls are assumed to rest on a rigid foundation. Figure (4-1) gives the plan and the wall dimensions of the building. The second example building has a similar plan and storey height as the first example building, except the number of stories is increased to twenty. The walls of these buildings are designed according to NBCC [10] and ACI Code [1].

Since the buildings are symmetrical, their overall behaviour can be understood by studying the responses of a typical interior coupled shear walls and a typical external coupled shear walls. For the 10 storey building, the walls are designed to resist a seismic horizontal acceleration of 16% g. Two designs of the walls of the 20 storey building are carried out, one design for a seismic load of 16% g and the other a seismic load of 8% g. Table (4-1) is a summary for the walls dimensions and capacities of the walls of the two buildings.

Wall	20 Storey Building (16% g)					
	Wall Thickness (in)	Conn. beam depth (in)	A_{sb}	A_{sw}	q_p K/ft	$\bar{M}_{uw}$ K.ft
Exterior	12	24	4#10	22#11	20	43400
Interior	12	6*	3#5/ft	18#11	2.68	37700

Wall	10 Storey Building (16% g) & 20 Storey Building (8% g)					
	Wall Thickness (in)	Conn. beam depth (in)	A_{sb}	A_{sw}	q_p K/ft	$\bar{M}_{uw}$ K.ft
Exterior	9	24	4#9	12#10	16	25500
Interior	9	6*	3#5/ft	12#10	2.68	25500

* Effective connecting slab width = 3.5 ft.

Table (4-1) Dimensions, Reinforcement and Capacities of Exterior and Interior Walls of the Example Buildings

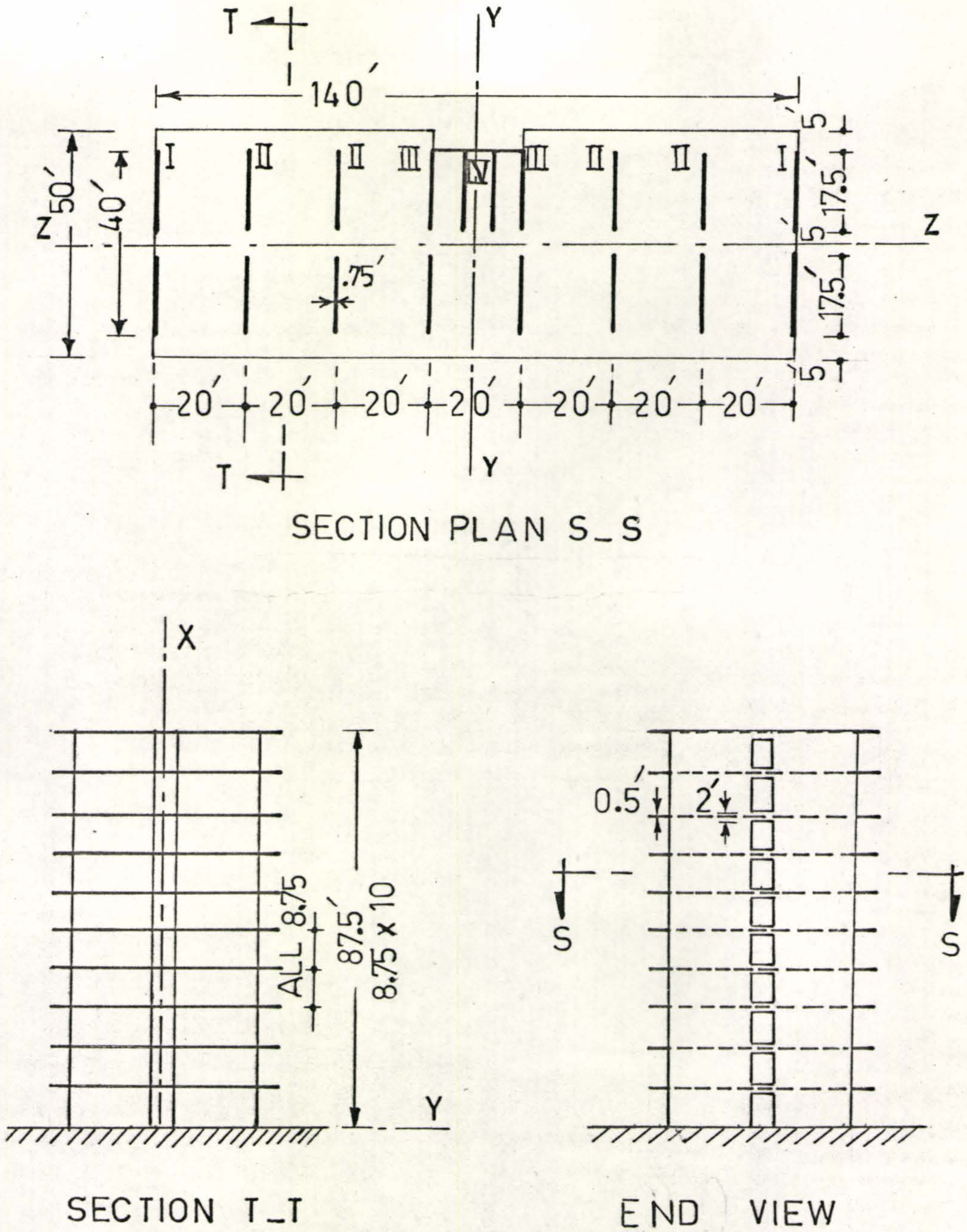

FIG. 4-1 OVERALL DIMENSIONS , 10 STORY BUILDING

The dimensions, reinforcement and capacities presented in Table (4-1) are the final design values.The detailed calculations are presented in Appendix A.

4.2 Dynamic Analysis

The dynamic model for the walls in the 10 storey building is given in Figure (4-2) and for the 20 storey building is given in Figure (4-3).

For buildings with rigid floor diaphragms, the lateral loads caused by the ground acceleration are distributed according to the stiffness of the lateral force resisting elements. To have the building to vibrate as a unit, the mass of the complete structure is also assumed to be distributed proportional to the stiffness of the walls. Table (4-2) gives the periods of the exterior and the interior walls of the 20 storey building. These walls were designed for a lateral seismic load of 16% g maximum ground acceleration. The masses of the building are assumed to be distributed uniformly throughout the height in accordance with the wall stiffnesses in the period calculations.

From Table (4-2), it is seen that the fundamental periods of the walls are the same. However, the periods of the other modes are different. The differance between the corresponding periods increases as the mode number increases. This is because the end walls with stiffer connecting beams behave differently from the interior walls. To obtain identical periods for all modes in the two walls, it becomes necessary to distribute the masses nonuniformly along the height of each wall. For

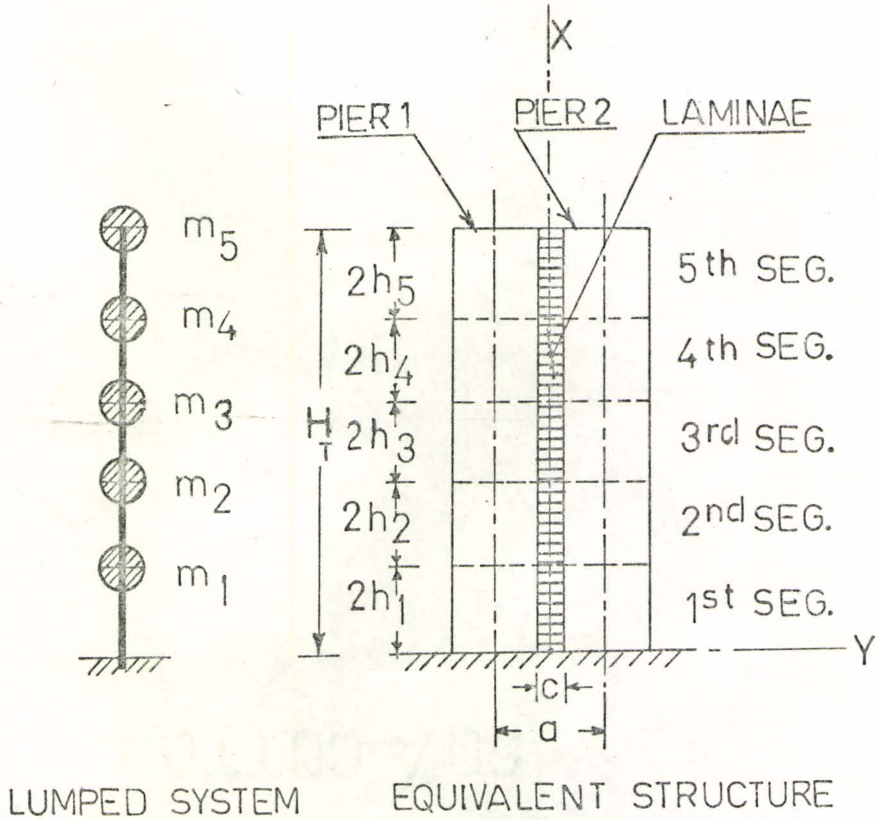

WALL I:

FOR MASS MATRIX $m_1 = m_2 = m_3 = m_4 = m_5 = 20.15 \ \frac{\text{Kip.Sec.}^2}{\text{Feet}}$

FOR P_ Δ EFFECT $m_1 = m_2 = m_3 = m_4 = m_5 = 7.55$ „

$I_b = 0.4575$ Feet^4 & $q_p = 16.0$ Kip/Feet

WALL II:

FOR MASS MATRIX $m_1 = m_2 = m_3 = m_4 = m_5 = 7.19$ „

FOR P_ Δ EFFECT $m_1 = m_2 = m_3 = m_4 = m_5 = 10.78$ „

$I_b = 0.0235$ Feet^4 & $q_p = 2.68$ Kip/Feet

FOR ALL SEGMENTS:

$h = 8.75$ Feet , $c = 5.0$ Feet & $a = 22.5$ Feet

FIG. 4-2 DYNAMIC MODEL, 10 STORY BUILDING

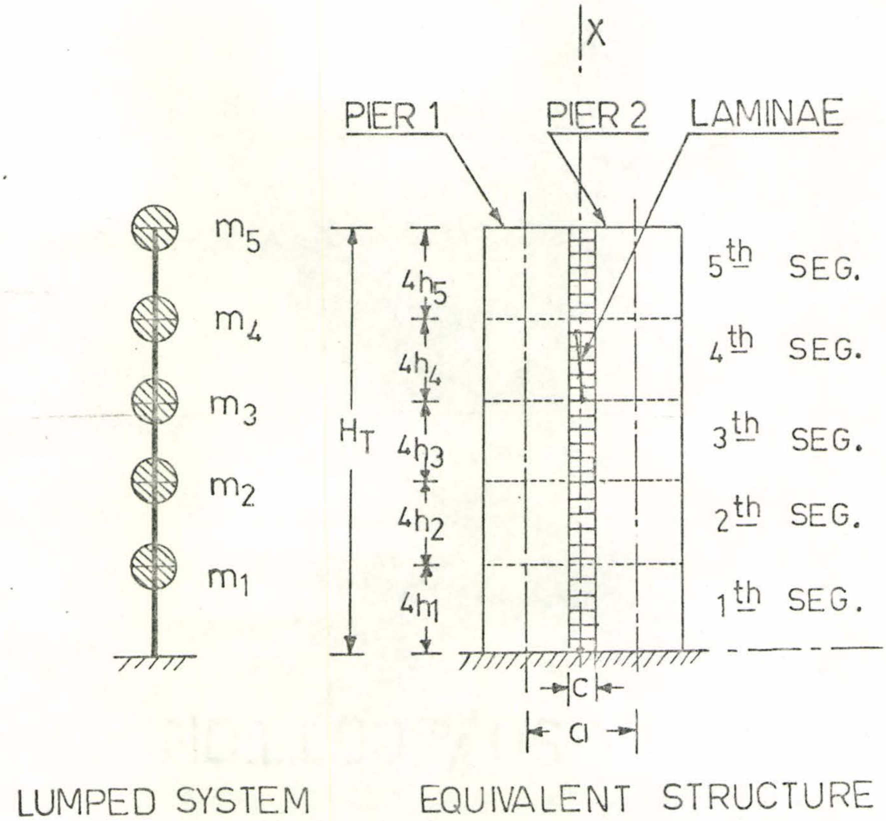

WALL I:

FOR MASS MATRIX $m_1 = m_2 = m_3 = m_4 = m_5 = 42.05 \ \frac{K.Sec^2}{Ft.}$

FOR P_Δ EFFECT $m_1 = m_2 = m_3 = m_4 = m_5 = 17.85$,,

$I_b = 0.560 \ Ft^4$ & $q_p = 20.0$ K/Ft.

WALL II:

FOR MASS MATRIX $m_1 = m_2 = m_3 = m_4 = m_5 = 17.53$,,

FOR P_Δ EFFECT $m_1 = m_2 = m_3 = m_4 = m_5 = 24.55$,,

$I_b = 0.0235 \ Ft^4$ & $q_p = 2.68$ K/Ft.

FOR ALL SEGMENTS:

$h = 8.75$ Ft , $c = 5.0$ Ft & $a = 22.5$ Ft

FIG. 4-3 DYNAMIC MODEL, 20 STORY BLDG (16% g) simplicity, we shall distribute the masses uniformly along the height of the walls in proportion to their stiffness in this study. Therefore, the mass distribution of both the internal and external walls are taken to be uniform in subsequent analyses.

MODE	1	2	3	4	5
(1) Exterior Wall	1.510 sec.	0.292 sec.	0.124 sec.	0.074 sec.	0.054 sec.
(2) Interior Wall	1.510 "	0.309 "	0.116 "	0.061 "	0.041 "
$\frac{(2)}{(1)} \times 100$	100	106	93.5	82.5	76

Table (4-2) Corresponding Periods of the Walls of the 20 Storey Building

4.3 Sinusoidal Excitation

To check the correctness of the computer program, the exterior wall of the 10 storey building is analysed subjected to sinusoidal ground motions. The modal critical damping ratios are taken as: $\zeta_1 = 4\%$, $\zeta_2 = 6\%$, $\zeta_3 = 7.5\%$, $\zeta_4 = 8.5\%$ and $\zeta_5 = 9\%$ in the present and all subsequent studies.

The time interval for calculating the straining actions δt equals 0.1 second. The time interval for checking the segments stress state (K_{max} δt) equals 0.1 seconds. The time limit for the analysis t_{max} is taken to be 20.0 seconds.

The sinusoidal ground acceleration has a maximum amplitude of 20% g and frequency equals 13.37 radian per second. This frequency is exactly equal to the fundamental frequency of the exterior wall when all connecting beams are elastic. However, the wall frequency will be changed slightly if the response is sufficiently large to cause plastic hinges formed at the ends of the connecting beams for a short time during each cycle. To prevent the formation of real hinges at the ends of the connecting beams, the rotational ductility factor for the connecting beams is assumed to be equal to 500. Therefore, the wall will be excited into resonance and its response is predominately that of the first mode. The top deflection response is shown in Figure (4-4).

To check the accuracy of the computer program, the maximum top displacement is calculated by the modal superposition method. Only the first mode will be considered. At resonance the magnification factor α_1 based on elastic analysis can be calculated as

$$\alpha_1 = \frac{1}{2\zeta_1} = \frac{1}{2\text{x}0.04} = 12.5$$

The first eigenvector $\{\lambda\}_1 = \begin{bmatrix} 0.0581 \\ 0.1920 \\ 0.3627 \\ 0.5458 \\ 0.7283 \end{bmatrix}$

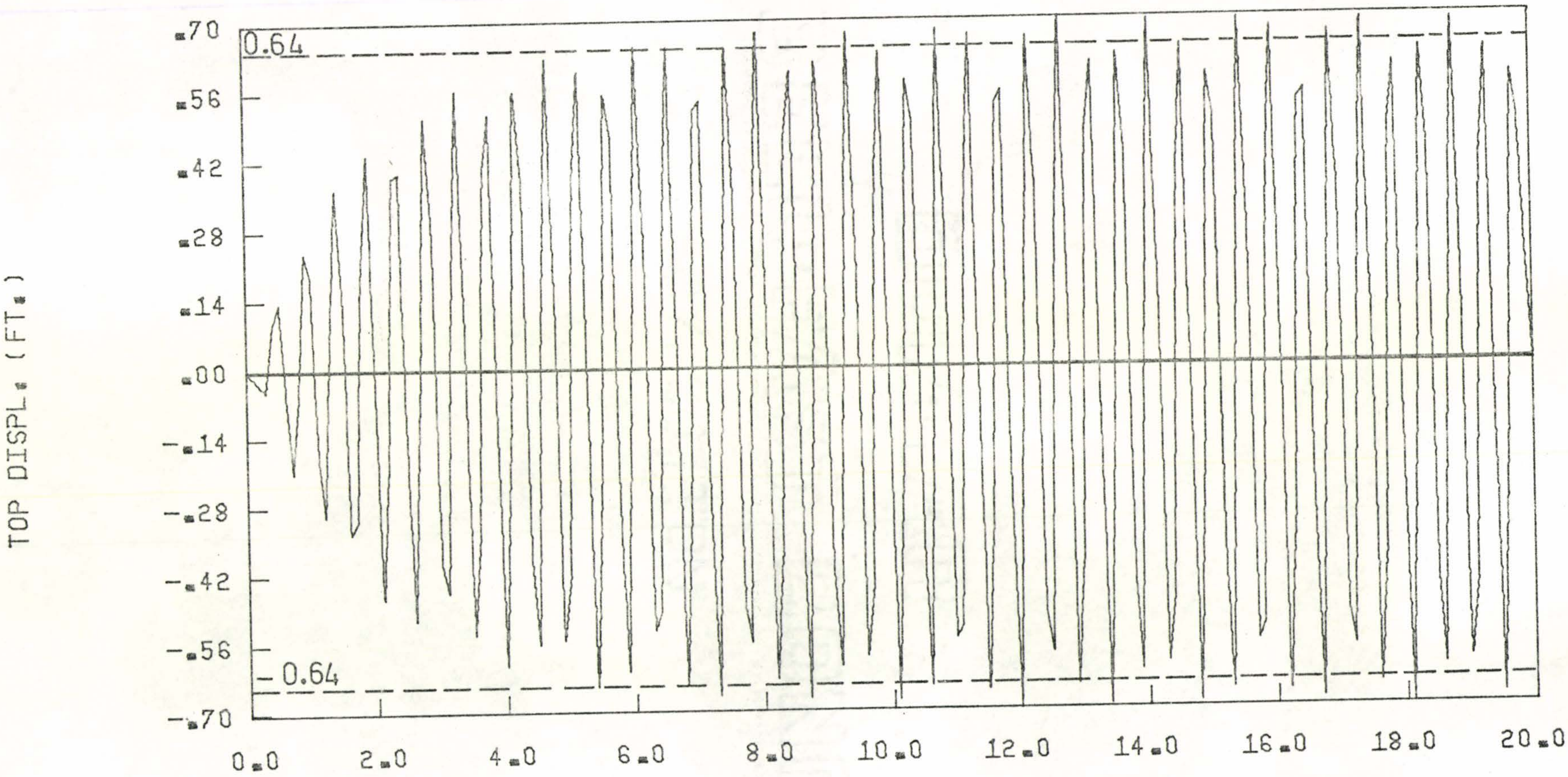

EXTERIOR WALL , 10 STORY BUILDING , $\mu = 500$

SINUSOIDAL GROUND ACC. , $\Omega = \omega_1 = 13.37$ r.p.s. — TOP DISPL. = .64 FT (1st MODE)

FIG. 4-4 COMPARISON BETWEEN THE MODAL SUPER-POSITION SOLUTION AND THE PROPOSED METHOD

The normalized eigenvector $\{\phi\}_1$ can be computed from

$$\{\phi\}_1 = \frac{1}{\sqrt{C_1}} \{\lambda\}_1$$

where

$$C_1 = \sum_{i=1}^{5} m_i \lambda_{i1}^2 = 20.15$$

Therefore

$$\{\phi\}_1 = \begin{bmatrix} 0.0130 \\ 0.0430 \\ 0.0817 \\ 0.1255 \\ 0.1640 \end{bmatrix}$$

The load vector $\{\bar{F}\}$ can be computed from

$$\{\bar{F}\} = -\{m\}\ a_{max}\ g = \begin{bmatrix} 130 \\ 130 \\ 130 \\ 130 \\ 130 \end{bmatrix} \text{Kip}$$

The static displacement for mode (1) can be calculated from

$$A_{1_{st}} = [\sum_{j=1}^{5} \phi_{j1}\ \bar{F}_j]/\omega_1^2 = 0.312 \text{ ft.}$$

The dynamic displacement for mode (1) = $A_{1_{st}} \alpha_1 \doteq 3.9$ ft.
The maximum displacement for mode (1) $\{x\}_{1_{max}}$ can be computed from

$$\{x\}_{1_{max}} = A_{1_{st}} \alpha_1 \{\phi\}_1$$

$$\therefore \quad \{x\}_{1_{max}} = \pm \begin{bmatrix} 0.051 \\ 0.168 \\ 0.318 \\ 0.490 \\ 0.640 \end{bmatrix} \text{ ft.}$$

Therefore, the maximum top displacement = 0.640 ft. ... (1st mode only).

Figure (4-4) indicates that the maximum top displacement calculated from the modal super-position method as a dashed line. Agreement between the step-by-step integration response and the dashed line provides a check on the correctness of the computer program.

4.4 Object of Investigation

The behaviour of a coupled shear walls is affected by the stiffness and rotational ductility of the connecting beams. For architectural reasons, the interior shear walls in a shear wall building are coupled through the floor slabs only. Due to the flexibility of the slabs, the coupling effect is limited. Furthermore, the rotational ductility of the coupling slab is also limited. One may then logically pose the question as to how effective are the slab coupled shear walls with limited ductility in resisting earthquake ground motion. This question will be studied in the present study by comparing the performance of some typical interior coupled shear walls and the performance of uncoupled walls (independently acting Cantilevers) of the same proportion.

For the end walls, one can provide deep connecting beams to increase the coupling effect. Also, by proper reinforcing detailing, it has been shown that very large rotational ductility can be obtained [14]. For the exterior coupled shear walls therefore, it is useful to investigate to what extent the increase in beam ductility will improve the performance of the walls under moderate or strong earthquake excitation. Obviously, the definition of moderate or strong earthquake excitation is relative. In this thesis, if the wall is designed for a seismic load of 16% g and is subjected to ground motion with maximum acceleration of 16% g, we shall define the excitation to this wall as moderate. However, if the wall is designed for an 8% g seismic load and subjected to a ground motion with 16% g peak acceleration, then the excitation to the wall is considered strong.

in a shear wall building are coupled through the floor slabs only. Due to the flexibility of the slabs, the coupling effect is limited. Furthermore, the rotational ductility of the coupling slab is also limited. One may then logically pose the question as to how effective are the slab coupled shear walls with limited ductility in resisting earthquake ground motion. This question will be studied in the present study by comparing the performance of some typical interior coupled shear walls and the performance of uncoupled walls (independently acting Cantilevers) of the same proportion.

For the end walls, one can provide deep connecting beams to increase the coupling effect. Also, by proper reinforcing detailing, it has been shown that very large rotational ductility can be obtained [14]. For the exterior coupled shear walls therefore, it is useful to investigate to what extent the increase in beam ductility will improve the performance of the walls under moderate or strong earthquake excitation. Obviously, the definition of moderate or strong earthquake excitation is relative. In this thesis, if the wall is designed for a seismic load of 16% g and is subjected to ground motion with maximum acceleration of 16% g, we shall define the excitation to this wall as moderate. However, if the wall is designed for an 8% g seismic load and subjected to a ground motion with 16% g peak acceleration, then the excitation to the wall is considered strong.

Before we study the two problems posed above, it is necessary to ensure that the proposed 5 masses dynamic model is an adequate dynamic model for response studies. This investigation is given in the following section.

4.5 Effect of the Number of Lumped Masses

In the present analysis the number of degrees of freedom of the dynamic model equals to the number of segments into which the wall is to be divided. This is because the number of segments equals to the number of lumped masses of the structure as discussed in Chapter 2. To ensure a five masses representation is adequate, a study on the effect of the number of segments used in the dynamic modeling is carried out. The response of the exterior walls of the 20 storey building is computed based on a 5 and a 10 mass representation of the wall. The N.S. component of ElCentro 1940 record normalized to 20% g maximum acceleration is used as input. The parameter of interest are the top displacement, the base moments, and the axial forces at the base of piers.

The output time-history responses of the top displacement, base moments of piers and axial forces at base of the piers for the two models are shown in Figures (4-5) through (4-10). The top-displacement, and the base moment responses have essentially the same shapes with the same peaks for the two models as shown in Figures (4-5), (4-6), (4-7) and (4-8). The axial forces responses shown in Figures

(4-9) and (4-10) have the same peaks. However, there is a minor difference between them in the responses after the main peak response.

Table (4-3) gives the periods of the 5 mass model and the first five periods of the 10 mass model. The periods are found to be sensitive to the number of lumped masses. As the number of masses increases the periods decrease. Table (4-4) gives a summary of the maximum response values for the two models. No significant difference between the two model results is shown in Table (4-4). As an analysis using the five lumped mass system costs about one quarter of the cost of the ten lumped mass system, all subsequent response calculatinns will be carried out using the five mass dynamic model.

MODE	1	2	3	4	5
Period (5 masses) second	1.510	0.292	0.124	0.074	0.054
Period (10masses) second	1.386	0.273	0.115	0.067	0.044

Table (4-3) Effect of the Number of Segments in the Periods, Exterior Wall, 20 Storey Building

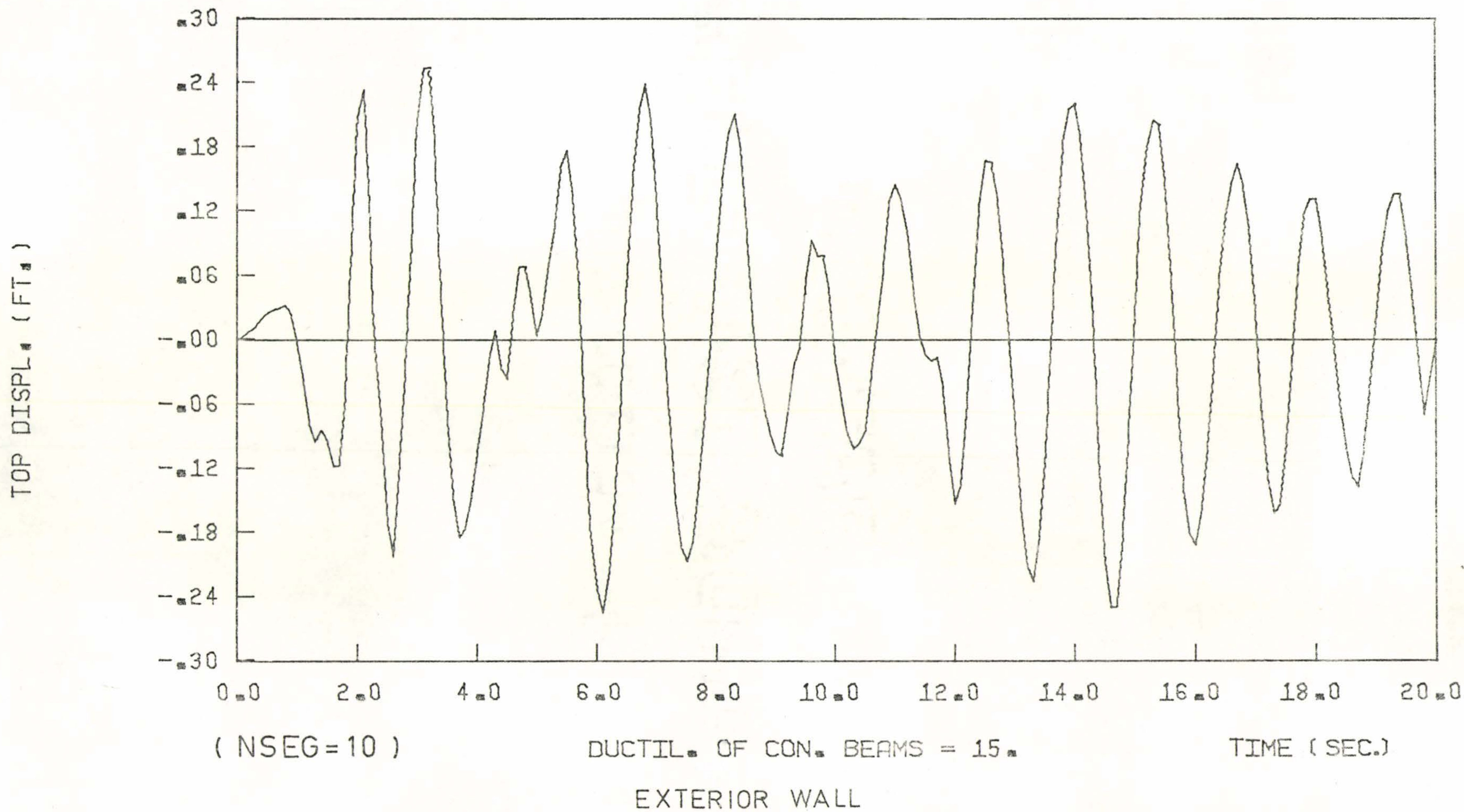

FIG. 4_5 TOP DISPL. , ELCENTRO COMP. NORTH

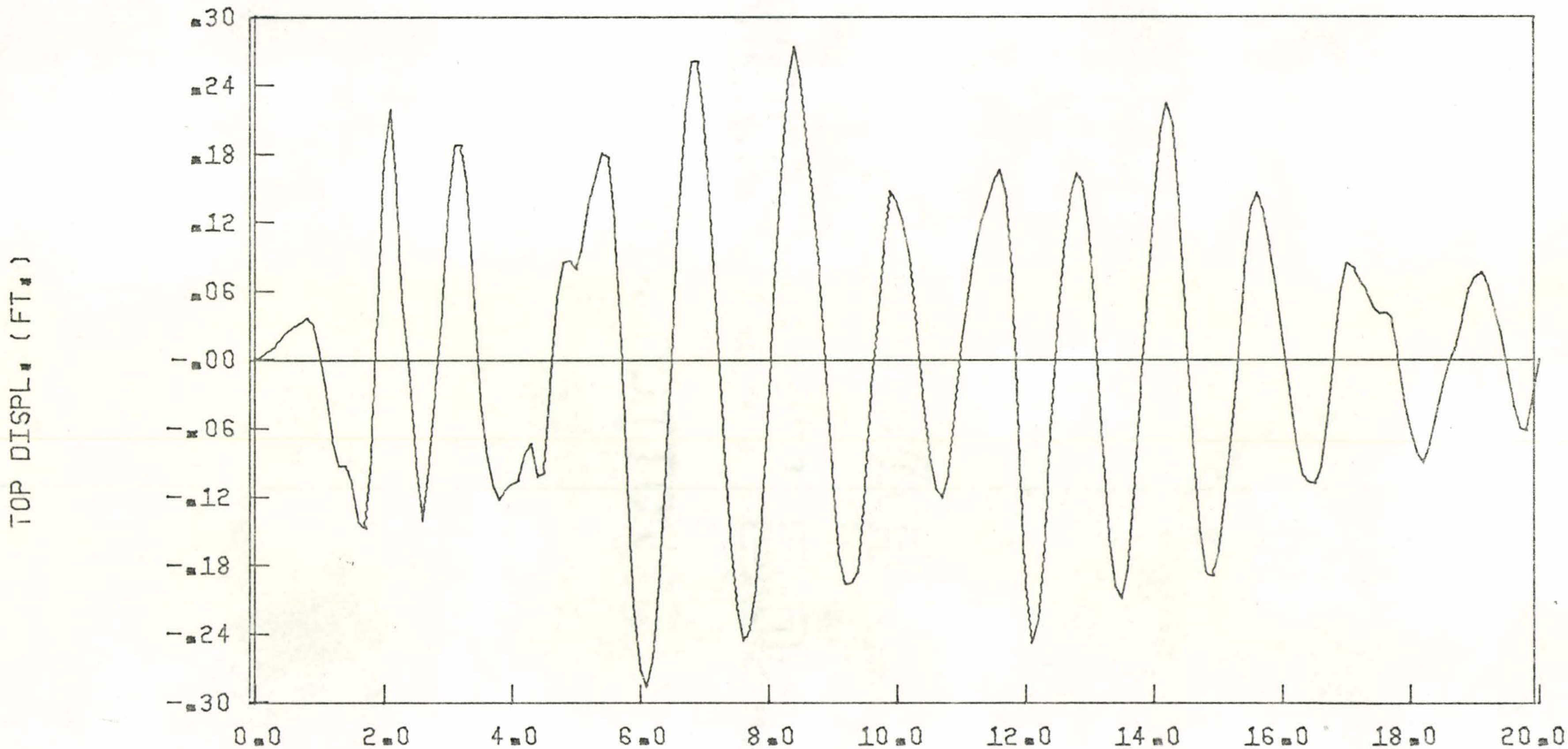

(NSEG = 5)   DUCTIL. OF CON. BEAMS = 15.   TIME (SEC.)

EXTERIOR WALL

FIG. 4-6   TOP DISPL. , ELCENTRO COMP. NORTH

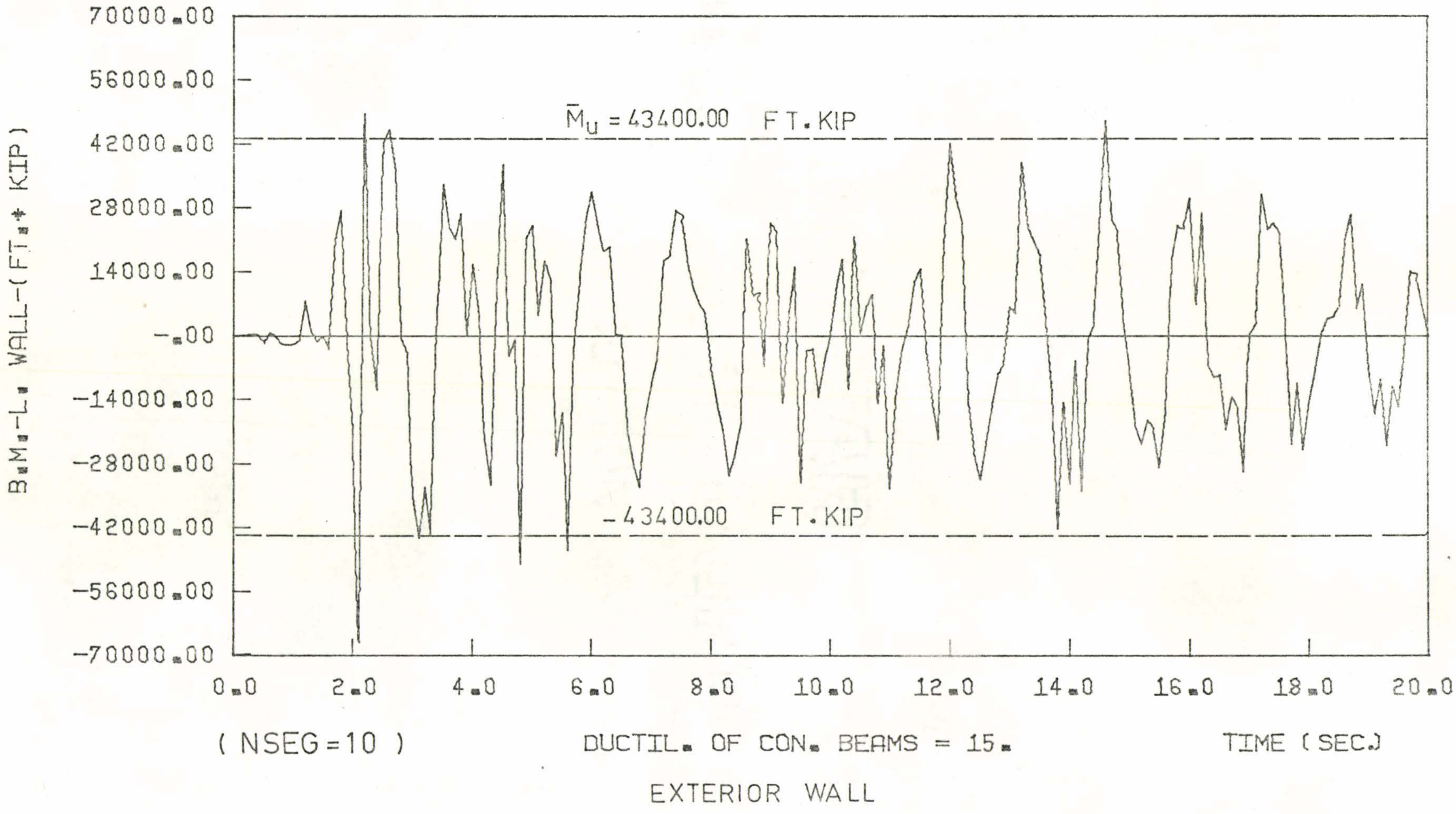

FIG.4_7 B.M.L.WALL , ELCENTRO COMP. NORTH

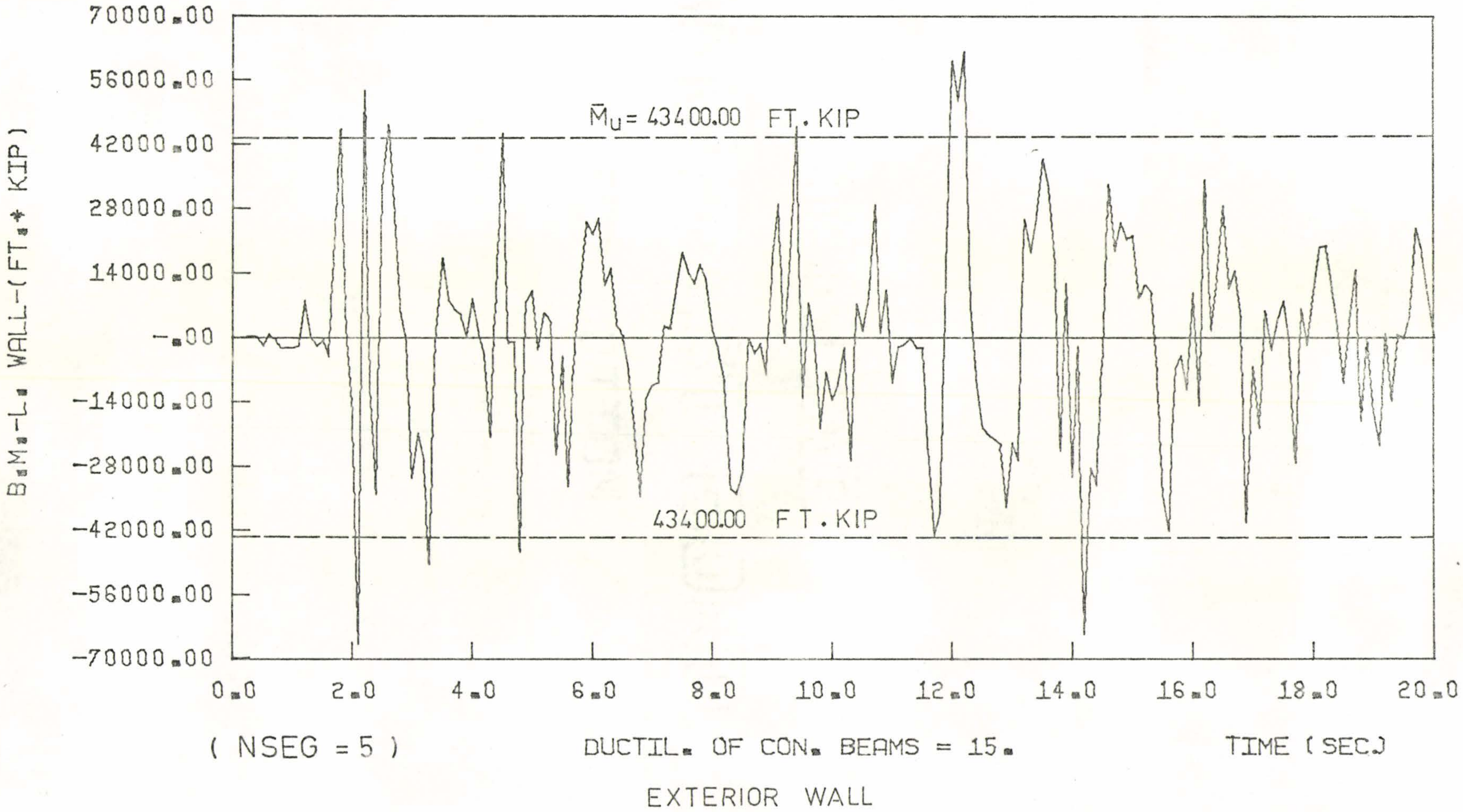

FIG. 4_8 B.M.L. WALL , ELCENTRO COMP. NORTH

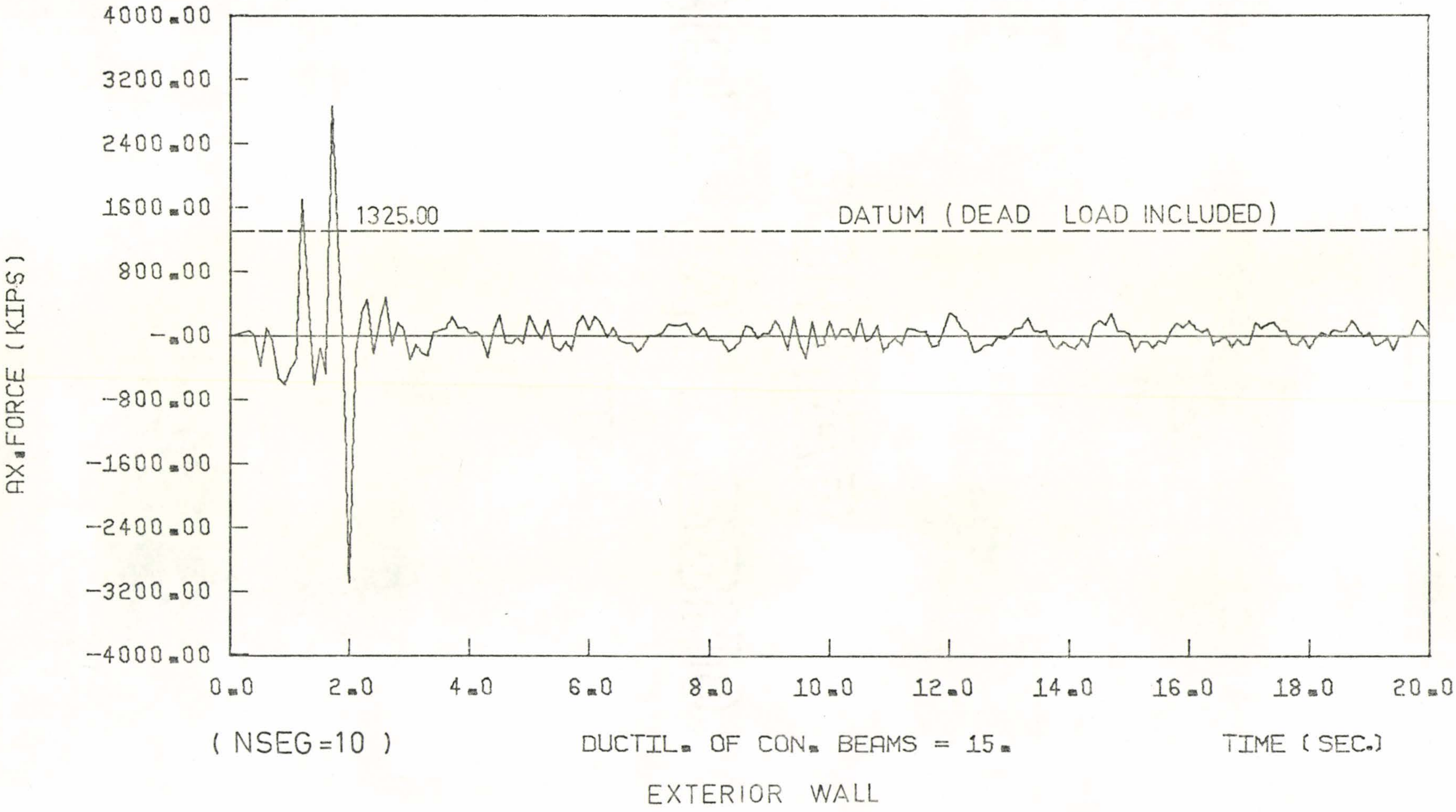

FIG. 4_9 AX. FORCE , ELCENTRO COMP. NORTH

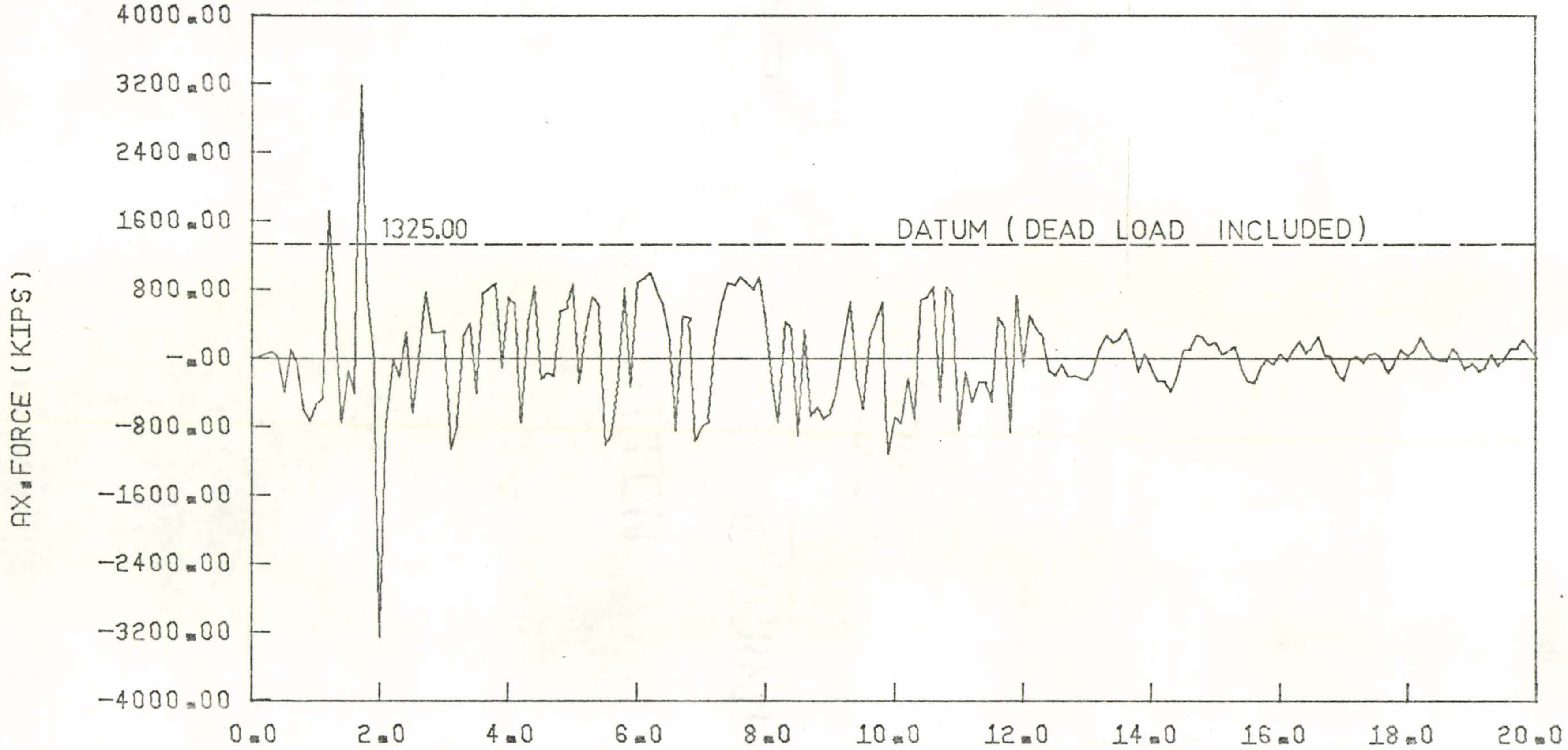

(NSEG = 5)   DUCTIL. OF CON. BEAMS = 15.   TIME (SEC.)

EXTERIOR WALL

FIG. 4_10 AX. FORCE , ELCENTRO COMP. NORTH

MODEL	No. of stor-ies per segment	K/ft q_p	μ	Fund. Period (sec.)	Max. Top Displ. (ft)	Max. Base Moment (1000 K.ft)	Max.Axial Force at Base (K.)	
							Tension	Comp.
5 masses	4	20	15	1.510	0.287	67.04	1950	4600
10 masses	2	20	15	1.386	0.257	67.46	1925	4575

Table (4-4) Effect of the Number of Segments, Exterior Wall, 20 Storey Building (ElCentro N.S.,20%g)

4.6 Method of Excitation

Real earthquake records are used to analyse the 20 storey coupled shear walls. These real earthquake records are normalized to the same maximum horizontal accelerations of 16% g. The duration of the ground accelerations is kept constant throughout the study. Twenty seconds duration is used to allow for large response to be built up.

These ground acceleration records used are shown in Figures (4-11), (4-12) and (4-13). Table (4-5) gives a summary of the earthquake records used in the analysis with each wall of the 20 storey building. In all cases except the case of the double cantilever wall, three runs are made for each case, using three different beam ductility values of 5, 15 and 500. These ductility values are taken as representative of low, moderate and high ductility situations.

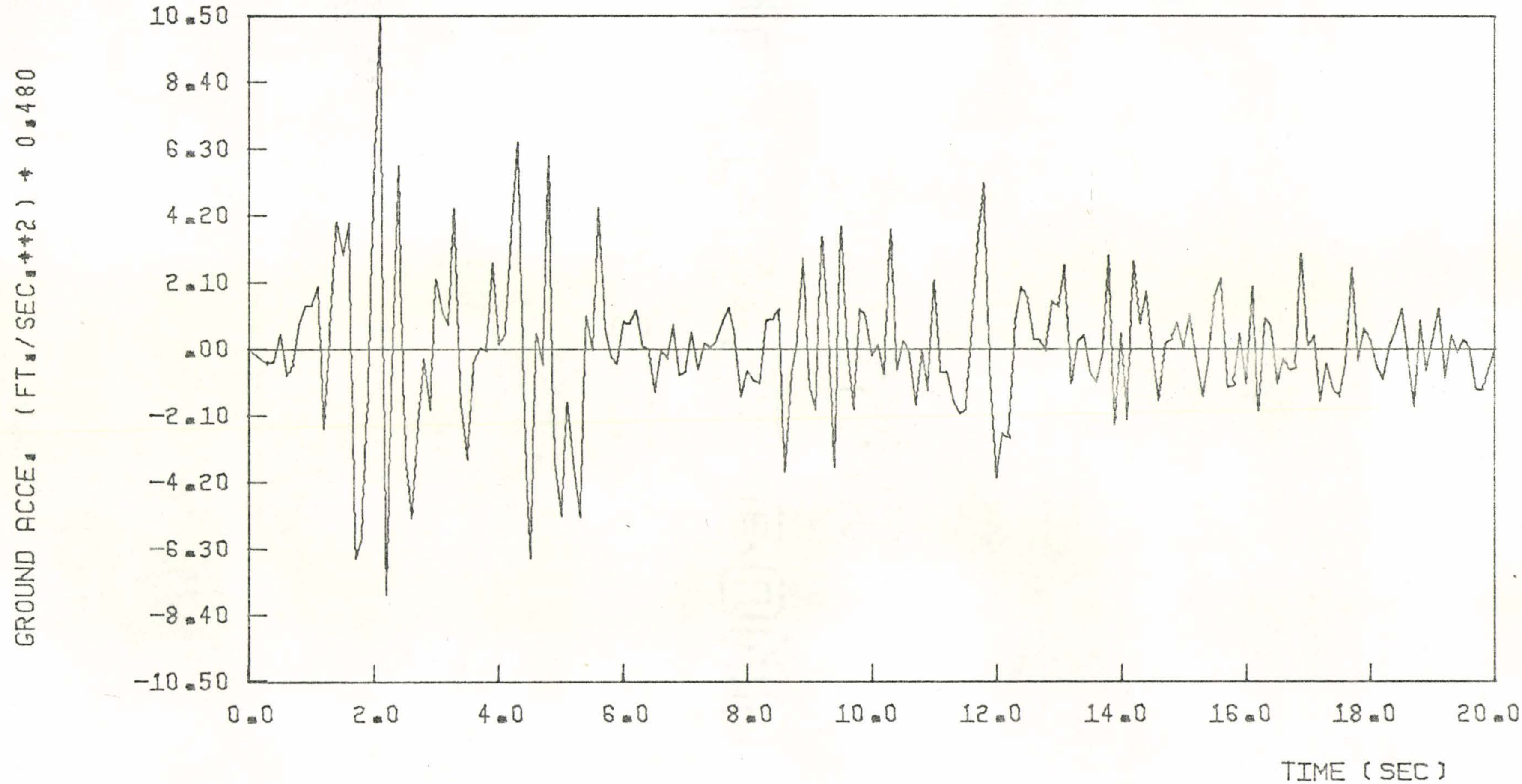

FIG. 4_11 ELCENTRO COMP. NORTH

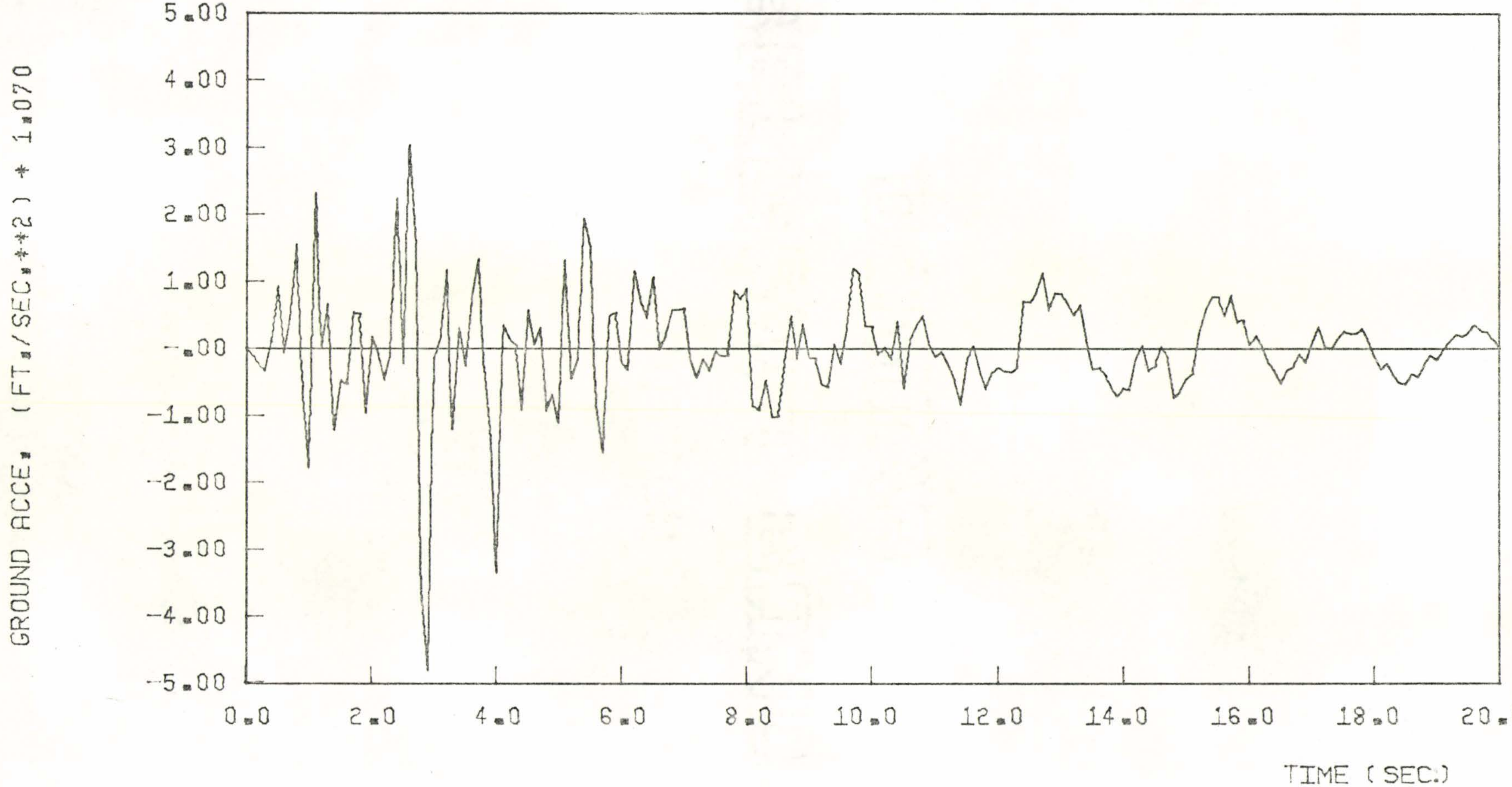

FIG. 4_12 SAN FERNANDO WILSHIRE BLVD. ,BASEMENT, COMP. SOUTH

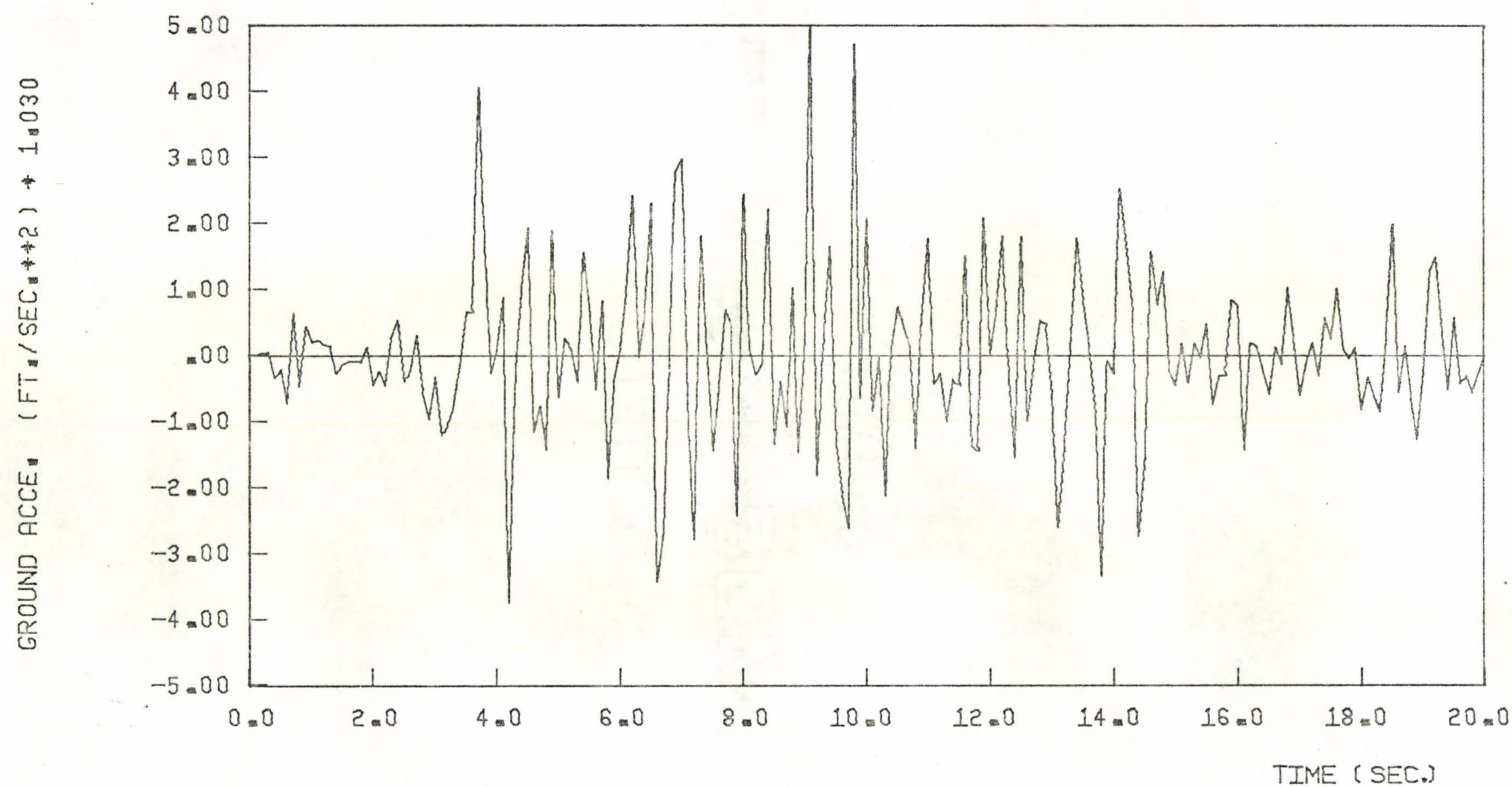

FIG. 4_13 TAFT E.Q. COMP N21E

GROUND ACCELERATION (16% g)	WALL
ELCENTRO, COMP. N.S. (1940)	Exterior Wall (16%g) Exterior Wall (8%g) Interior Wall (16%g) Double Cantilever Wall
SAN FERNANDO, COMP. N.S. Wilshire Blvd., Basement	exterior Wall (16%g) Interior Wall (16%g)
TAFT, COMP. N21E (1952)	Exterior Wall (16%g)

Table (4-5) Input Ground Acceleration

4.7 Seismic Response

In this section the seismic responses of the exterior and interior coupled shear walls of the 20 storey building are presented. The parameters of interest are : (i) the top displacement, (ii) the base moment of the piers, and (iii) the axial forces at the base of piers. These parameters are used to evaluate the performance of the structure under seismic loads. The shearing force intensity in the connecting laminae is also presented to clarify the behaviour, especially when large inelastic deformations occurred in the connecting laminae.

4.7.1 Interior Wall Response

The interior wall is studied using records from the ElCentro and San Fernando earthquakes normalized to 16% g as a maximum horizontal acceleration. In other words, the wall is subjected to ground excitations of the same intensities as it is designed for. The analysis is carried out for the coupled shear wall and also for an equivalent cantilever consisting of the two piers which connected together by beams with hinges at ends. The coupled shear wall is studied with three values of the rotational ductility factors, these are μ=5, 15 and 500 respectively.

4.7.1.1 Coupled Wall

Six computer runs are considered for the interior coupled shear wall to obtain the parameters of interest. Three runs are with the ElCentro record and the other three with San Fernando record. Given below are the seismic responses for the six cases accompanied with the necessary discussions.

a - ELCENTRO COMP. N.S.

Figures (4-14) through (4-22) give the top displacement, base moments, axial force at base of piers and shear intensity of connecting laminae, as time-history responses.

The rotational ductility factor of the coupling slabs μ equals to 5. Figure (4-14) indicates that the top displacement is mainly due to the first mode of vibration. Figures (4-15) and (4-16) are the same as the base moment in the left wall must be identical to that in the right wall, since the two piers have the same moment of inertia. Figures (4-15) and (4-16) indicate that the higher modes also contribute to the bending moment response. Figure (4-17) gives the axial force response at base of the piers. The response in Figure (4-17) is limited to a certain value after about 2.0 seconds. This value is the plastic shear intensity in the connecting laminae times the height of the upper two segments. These two segments remain to be plastic hinged segments, as shown in Figures (4-21) and (4-22), while the lower three segments are changed to real hinged segments after about 2.0 seconds due to the low value of ductility used. The shearing force intensity of the first three segments are given by Figures (4-18), (4-19) and (4-20). The shearing force intensity is dropped to zero when the end rotation of the laminae exceeds the ultimate rotation value and the segment changes to real hinged segment. Also, the contribution of the higher modes is clear in the shearing force intensity responses.

b - SAN FERNANDO EARTHQUATE COMP. N.S., Wilshire Blvd., Basement

Figures (4-23) through (4-30) give the response of

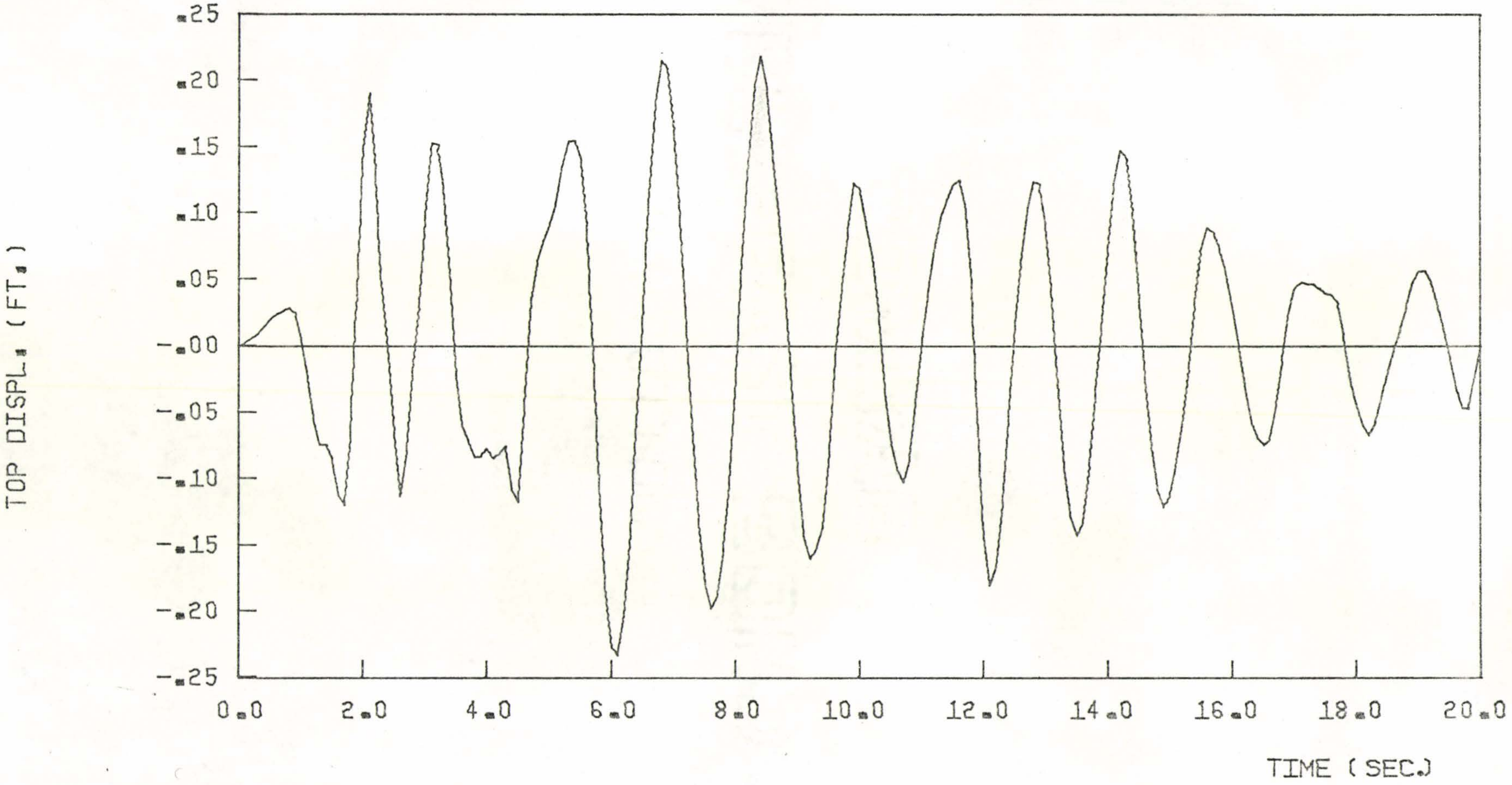

DUCTIL. OF CON. BEAMS = 5. , INTERIOR WALL

FIG. 4_14 TOP DISPL. , ELCENTRO COMP. NORTH

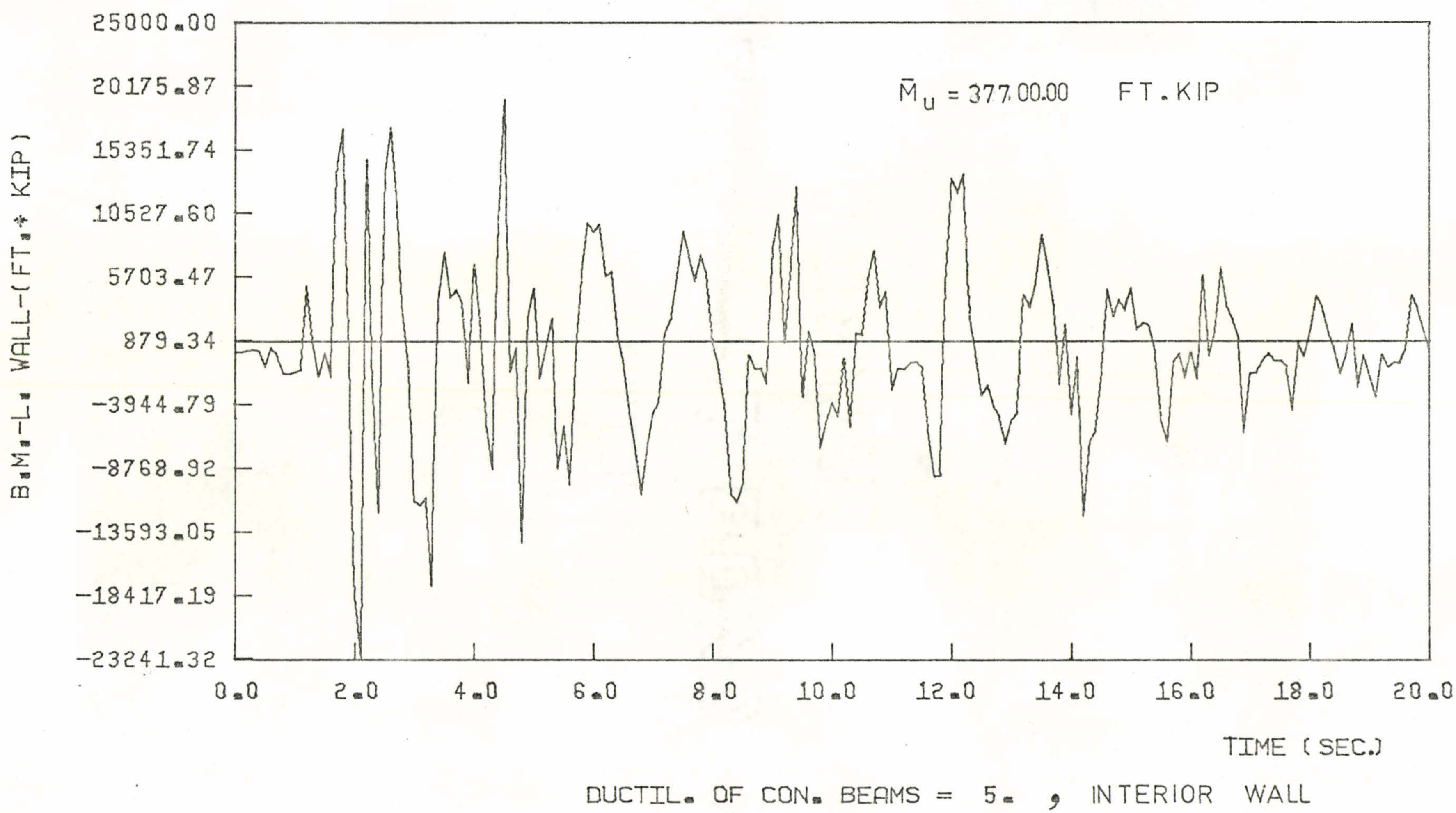

FIG. 4_15 B.M.L.WALL , ELCENTRO COMP. NORTH

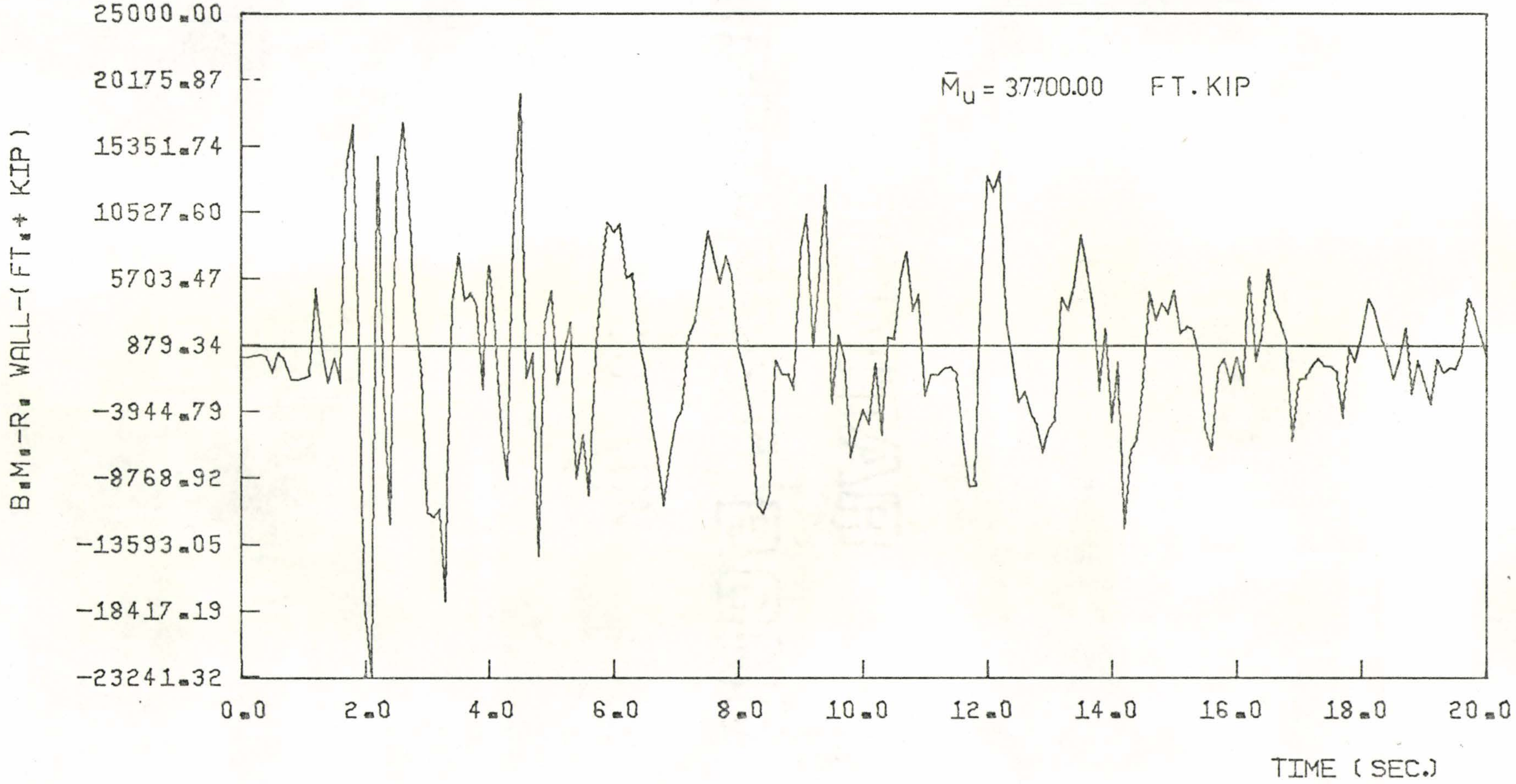

DUCTIL. OF CON. BEAMS = 5. , INTERIOR WALL

FIG. 4_16 B.M.R. WALL , ELCENTRO COMP. NORTH

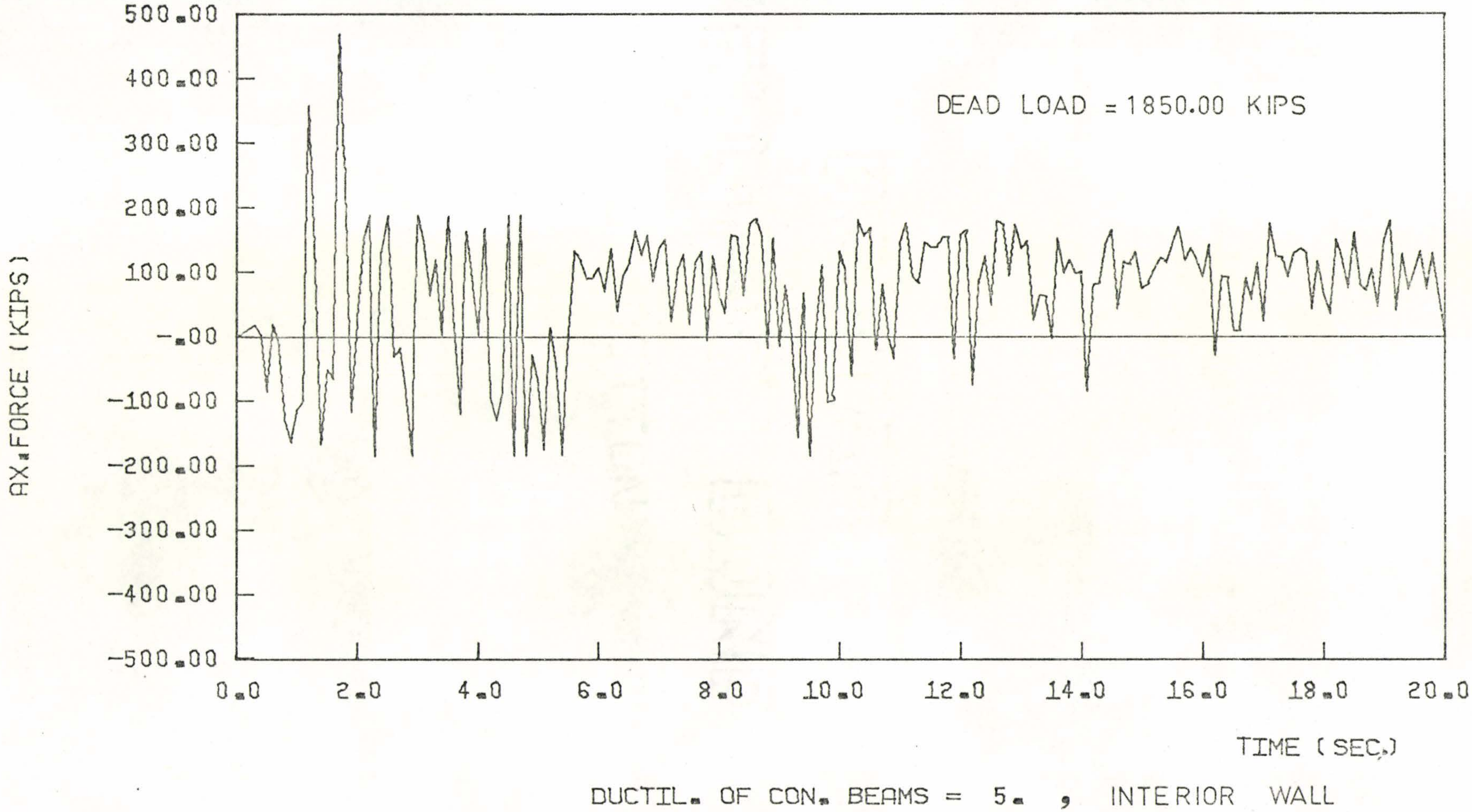

FIG. 4_17 AX. FORCE , ELCENTRO COMP. NORTH

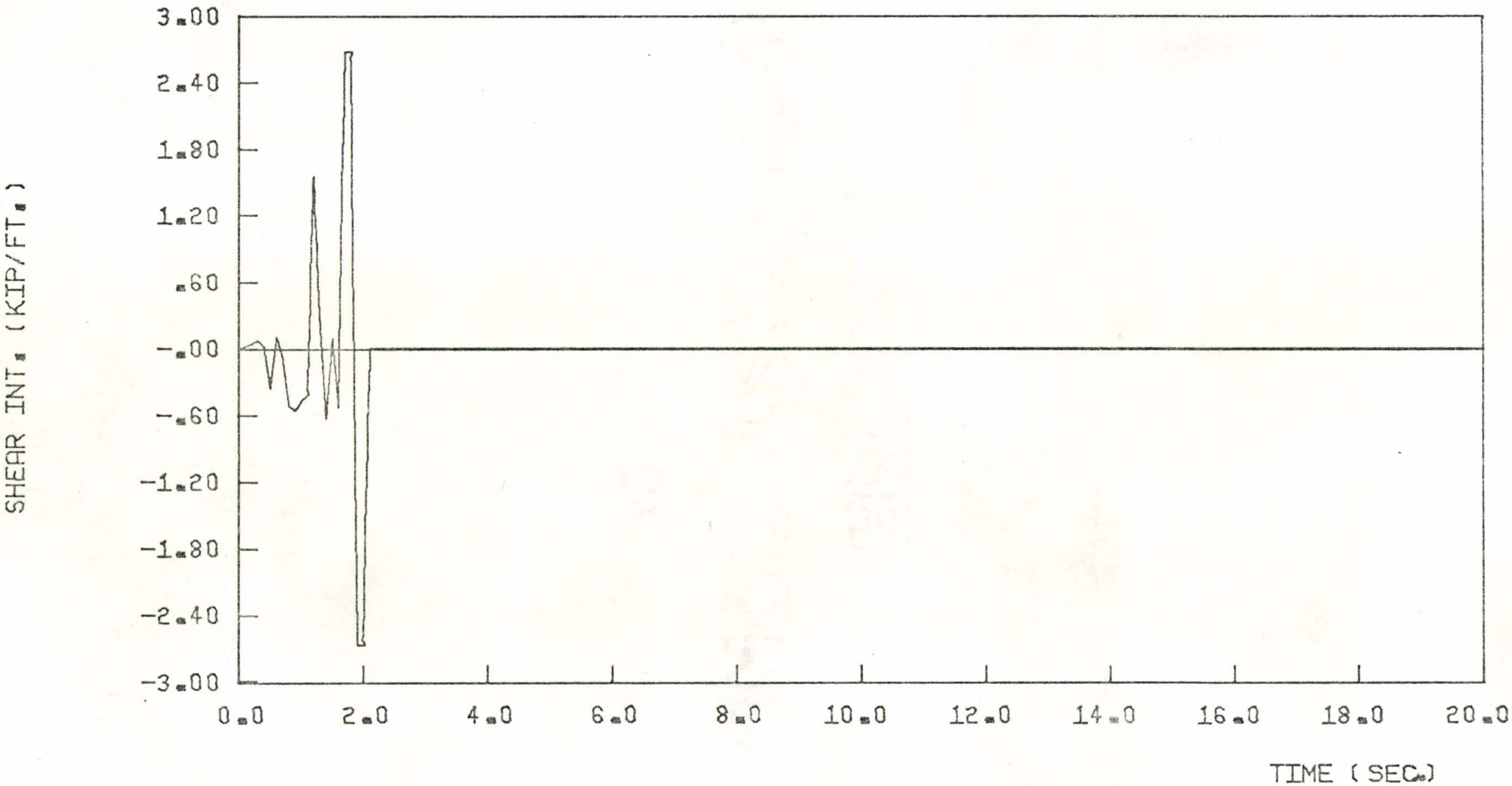

(SEGMENT NO. 1)   DUCTIL. OF CON. BEAMS = 5. , INTERIOR WALL

FIG. 4_18 SHEAR INT. , ELCENTRO COMP. NORTH

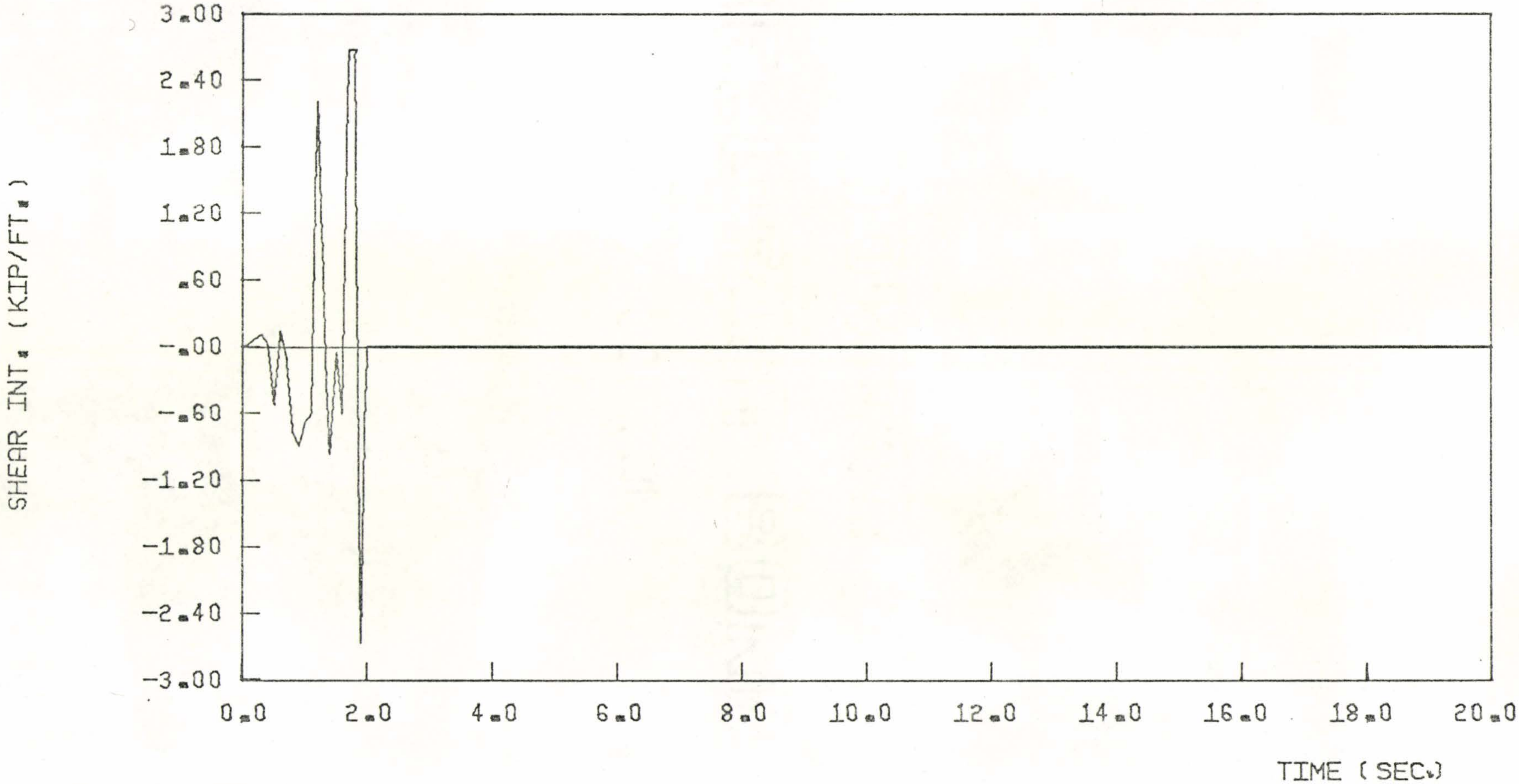

(SEGMENT NO. 2) DUCTIL. OF CON. BEAMS = 5. , INTERIOR WALL

FIG. 4_19 SHEAR INT., ELCENTRO COMP. NORTH

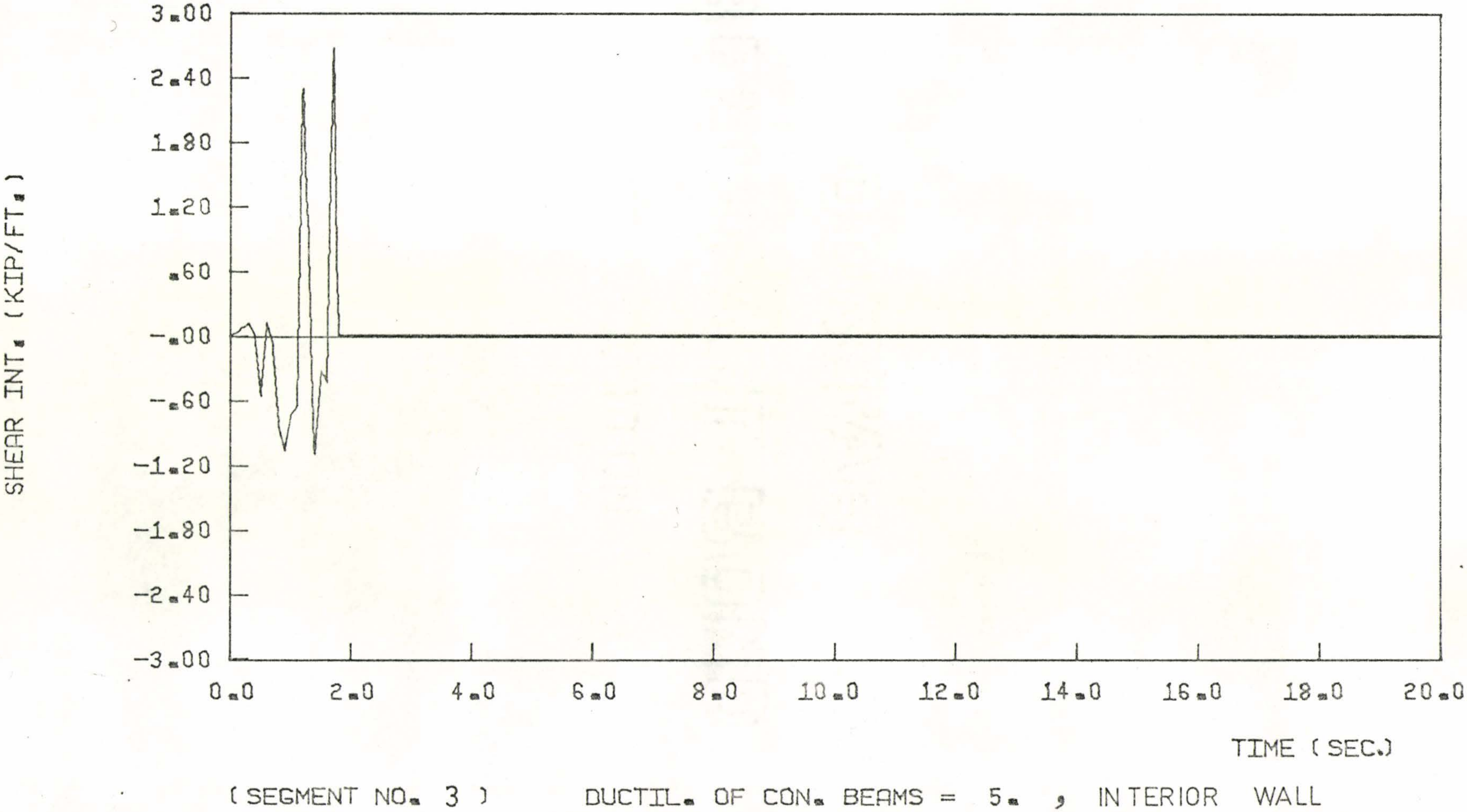

FIG. 4_20 SHEAR INT., ELCENTRO COMP. NORTH

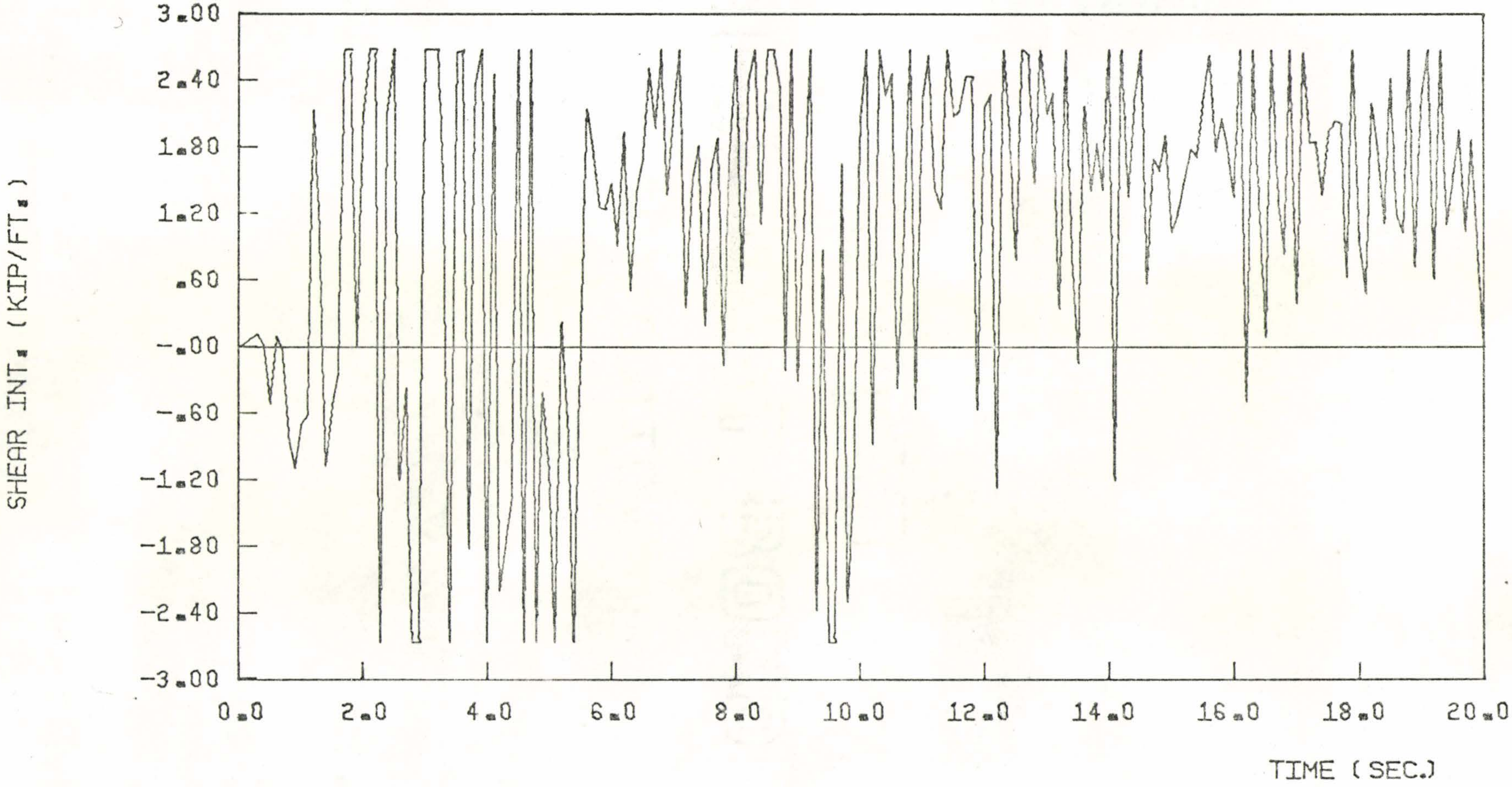

(SEGMENT NO. 4)   DUCTIL. OF CON. BEAMS = 5. , INTERIOR WALL

FIG. 4_21 SHEAR INT., ELCENTRO COMP. NORTH

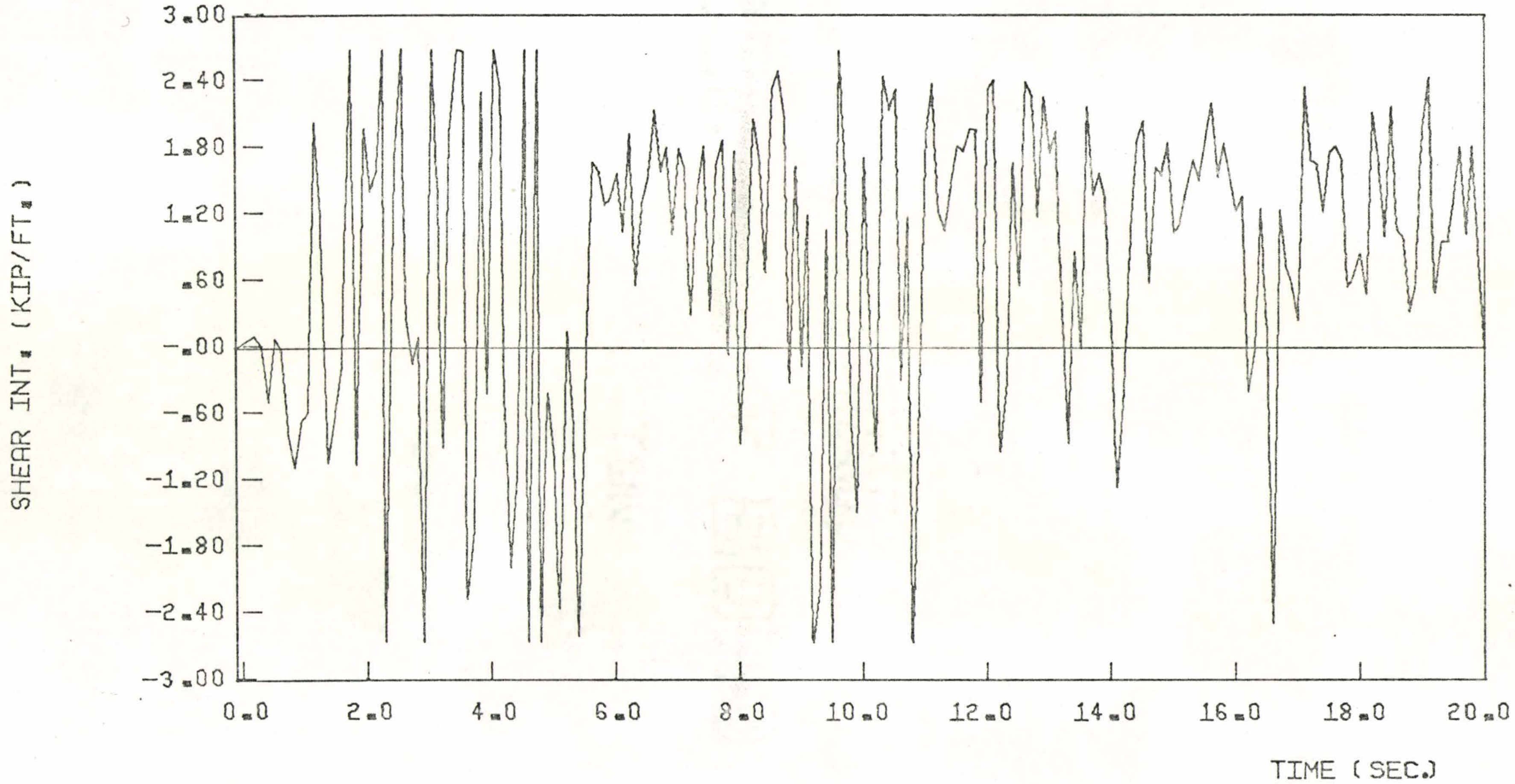

(SEGMENT NO. 5) DUCTIL. OF CON. BEAMS = 5. , INTERIOR WALL

FIG. 4_22 SHEAR INT. , ELCENTRO COMP. NORTH

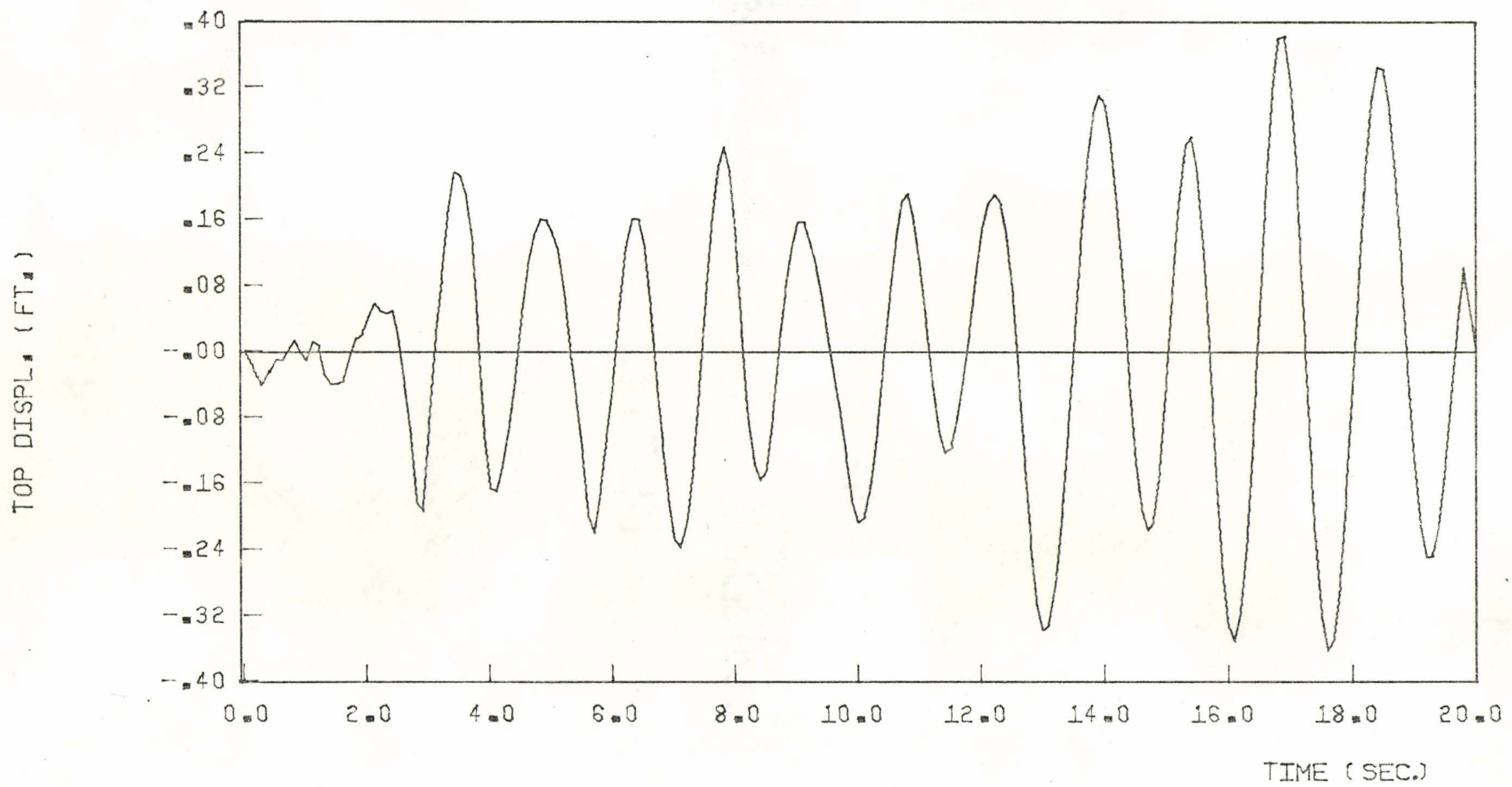

DUCTIL. OF CON. BEAMS = 5. , INTERIOR WALL

FIG. 4_23 TOP DISPL., SAN FERNANDO WILSHIRE BLVD. *BASEMENT* COMP. SOUTH

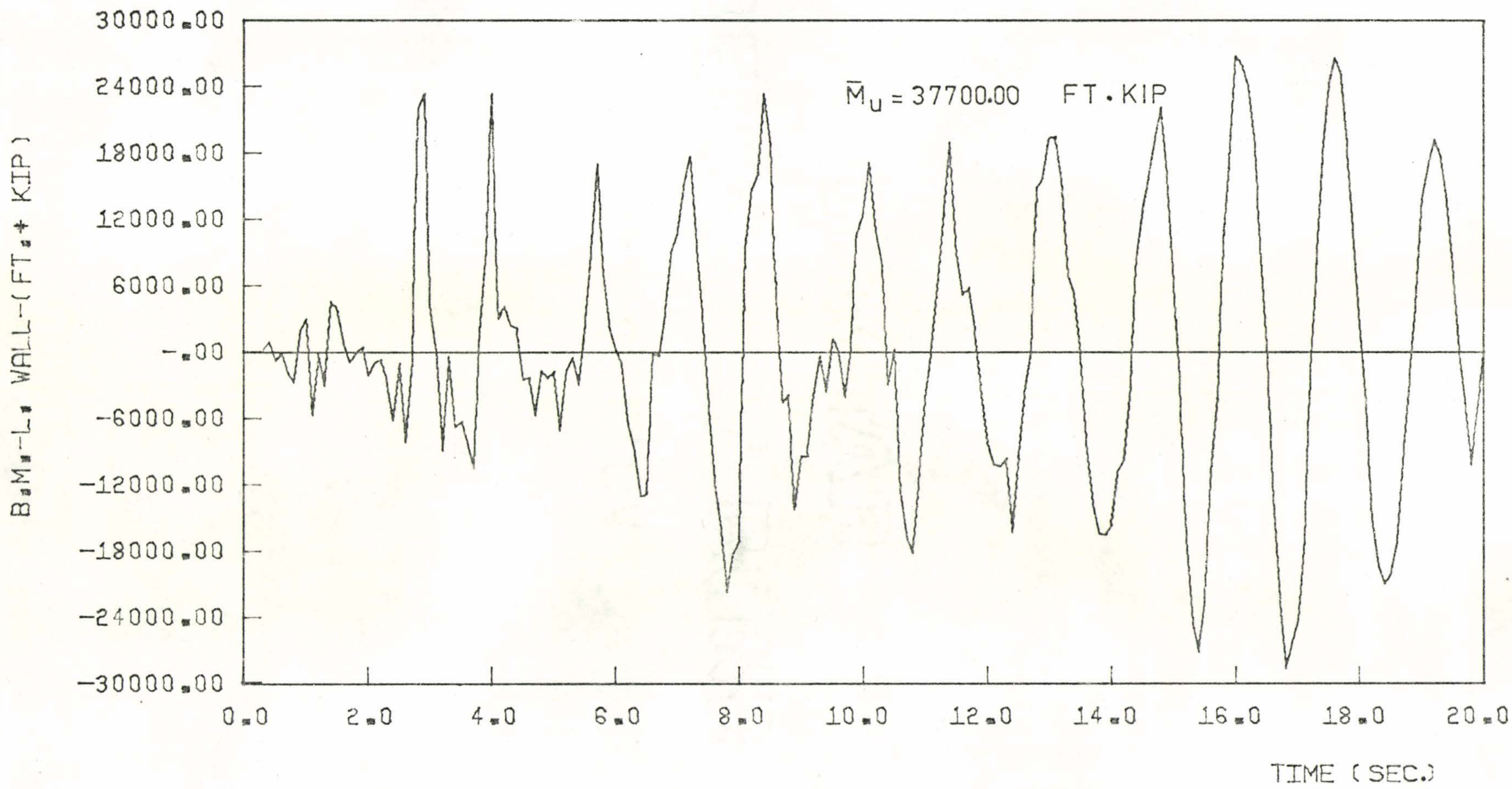

DUCTIL. OF CON. BEAMS = 5. , INTERIOR WALL

FIG. 4.24 B.M.L. WALL, SAN FERNANDO WILSHIRE BLVD. ,BASEMENT, COMP. SOUTH

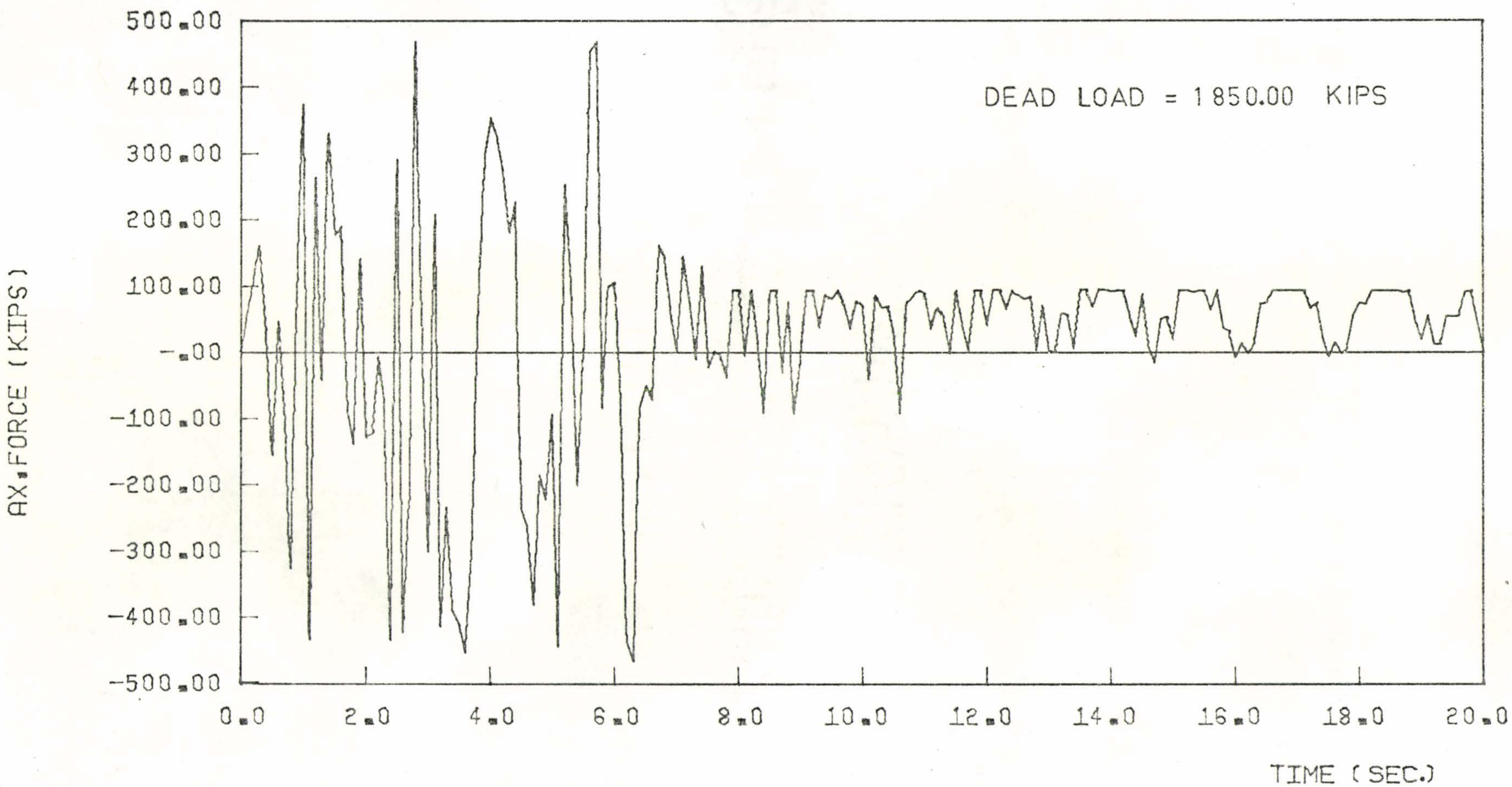

DUCTIL. OF CON. BEAMS = 5. , INTERIOR WALL

FIG.4_25 AX. FORCE , SAN FERNANDO WILSHIRE BLVD. ,BASEMENT, COMP. SOUTH

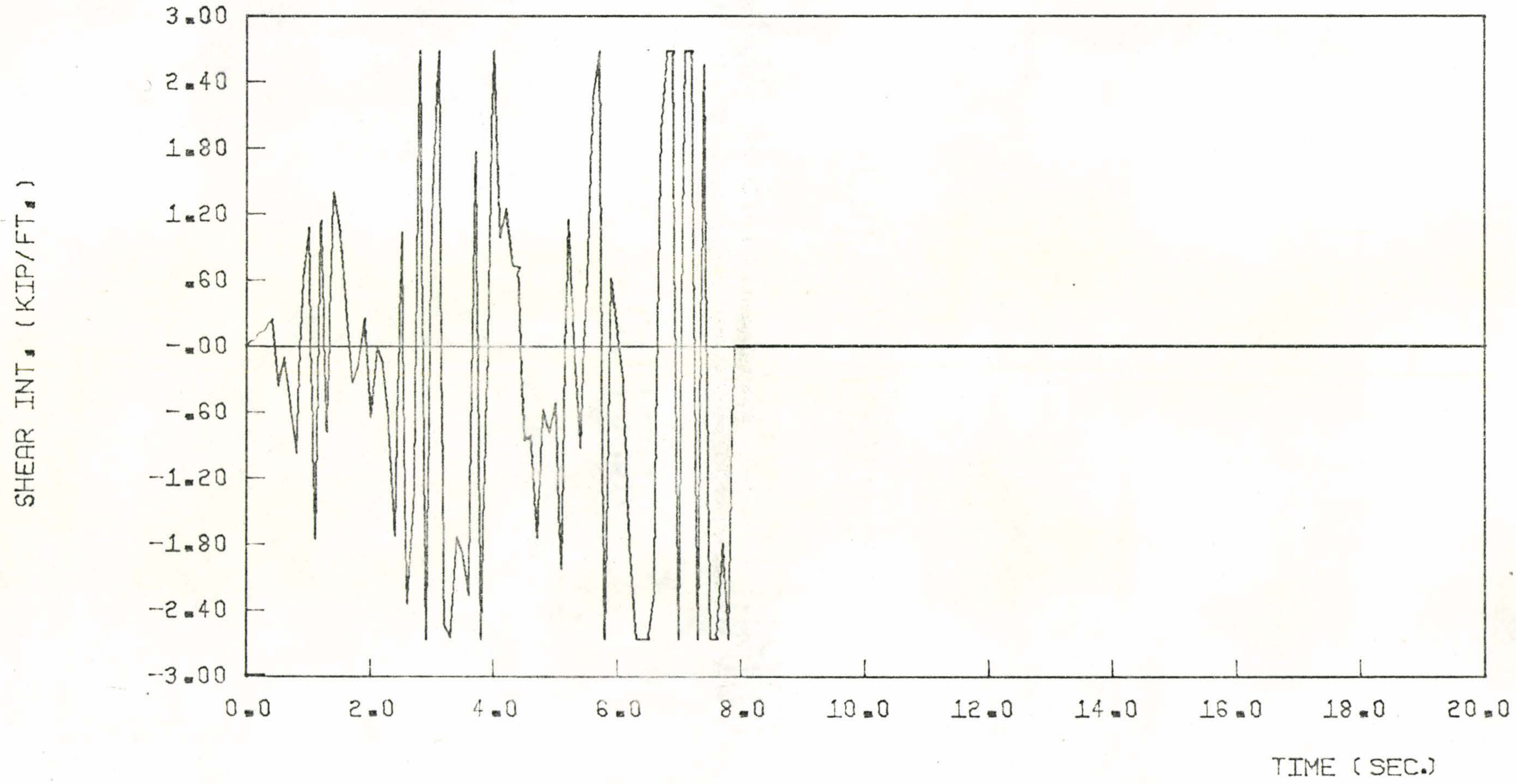

(SEGMENT NO. 1)   DUCTIL. OF CON. BEAMS = 5. , INTERIOR WALL

FIG. 4_26 SHEAR INT. , SAN FERNANDO WILSHIRE BLVD. ,BASEMENT, COMP. SOUTH

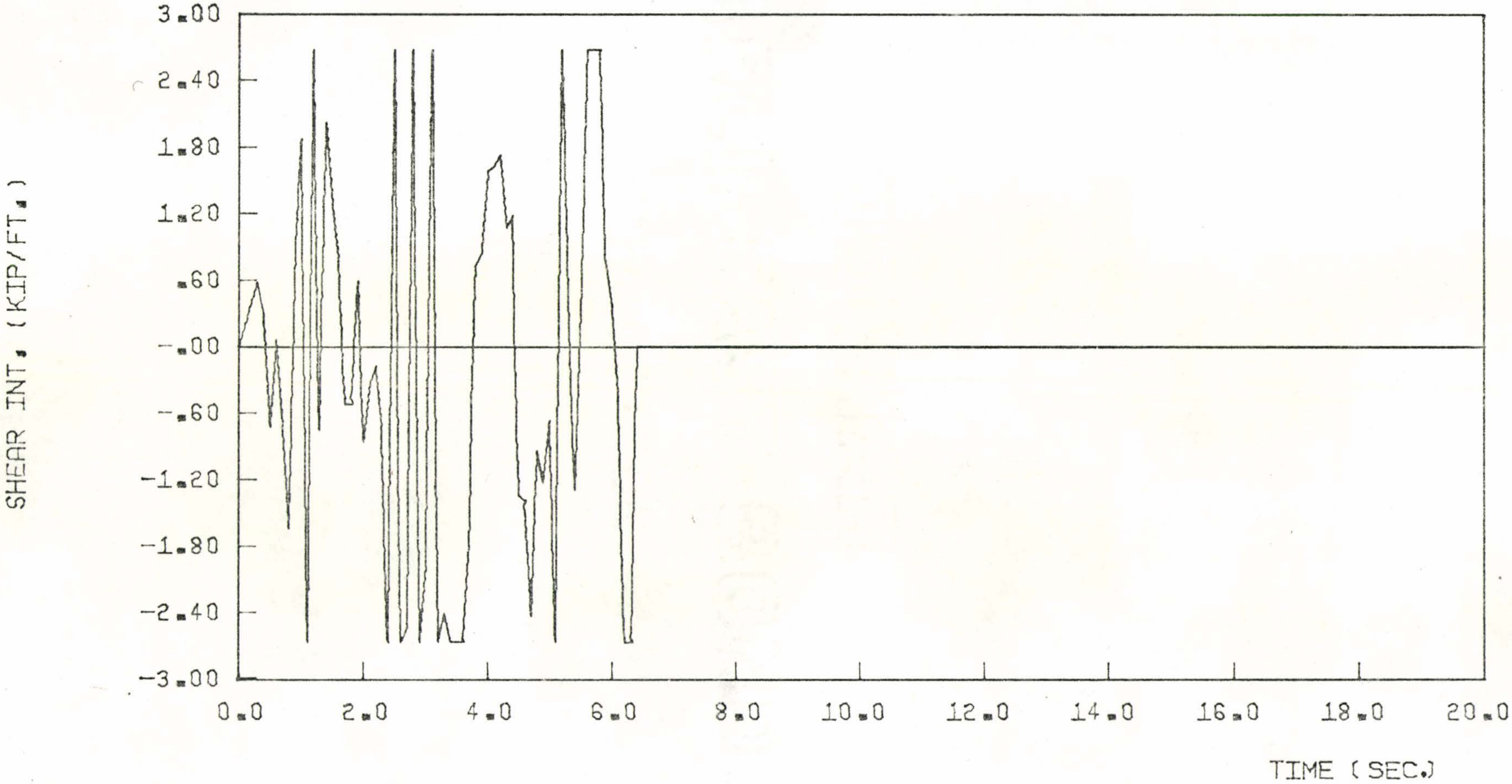

(SEGMENT NO. 2)   DUCTIL. OF CON. BEAMS = 5. , INTERIOR WALL

FIG. 4-27 SHEAR INT. , SAN FERNANDO WILSHIRE BLVD. ,BASEMENT, COMP. SOUTH

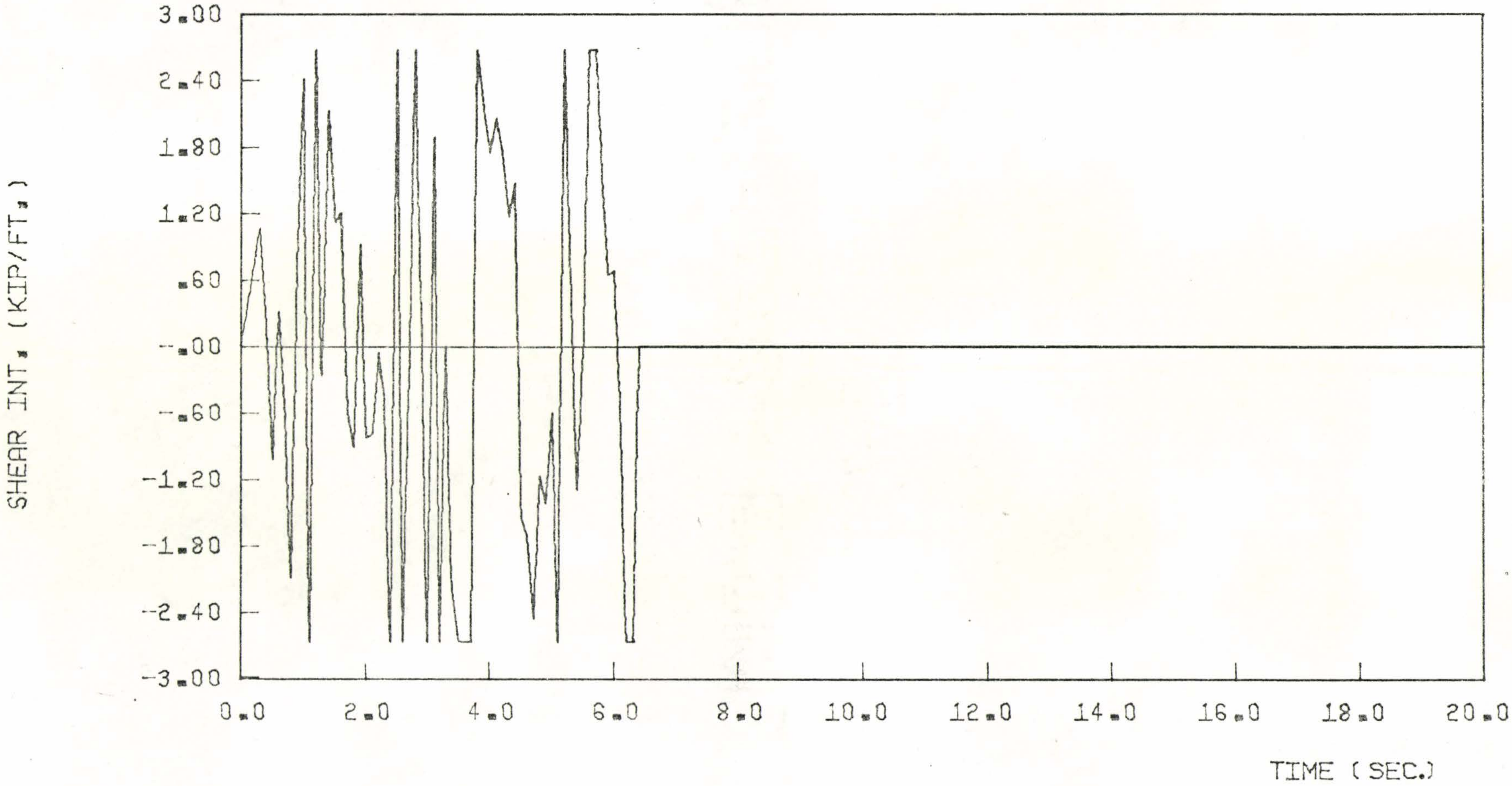

(SEGMENT NO. 3)   DUCTIL. OF CON. BEAMS = 5. , INTERIOR WALL

FIG. 4_28 SHEAR INT.,SAN FERNANDO WILSHIRE BLVD. ,BASEMENT, COMP. SOUTH

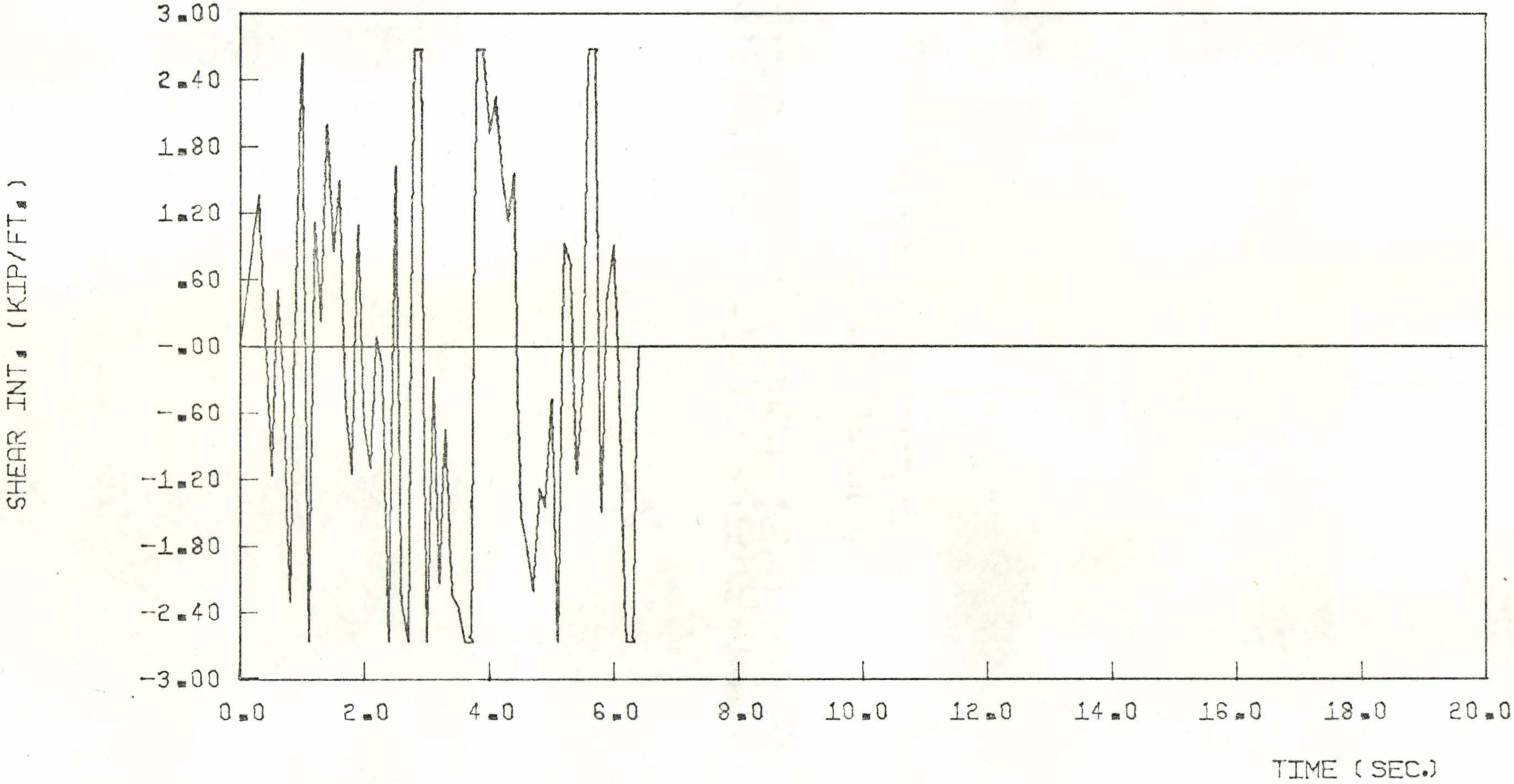

(SEGMENT NO. 4)   DUCTIL. OF CON. BEAMS = 5. , INTERIOR WALL

FIG. 4_29 SHEAR INT. , SAN FERNANDO WILSHIRE BLVD. ,BASEMENT, COMP. SOUTH

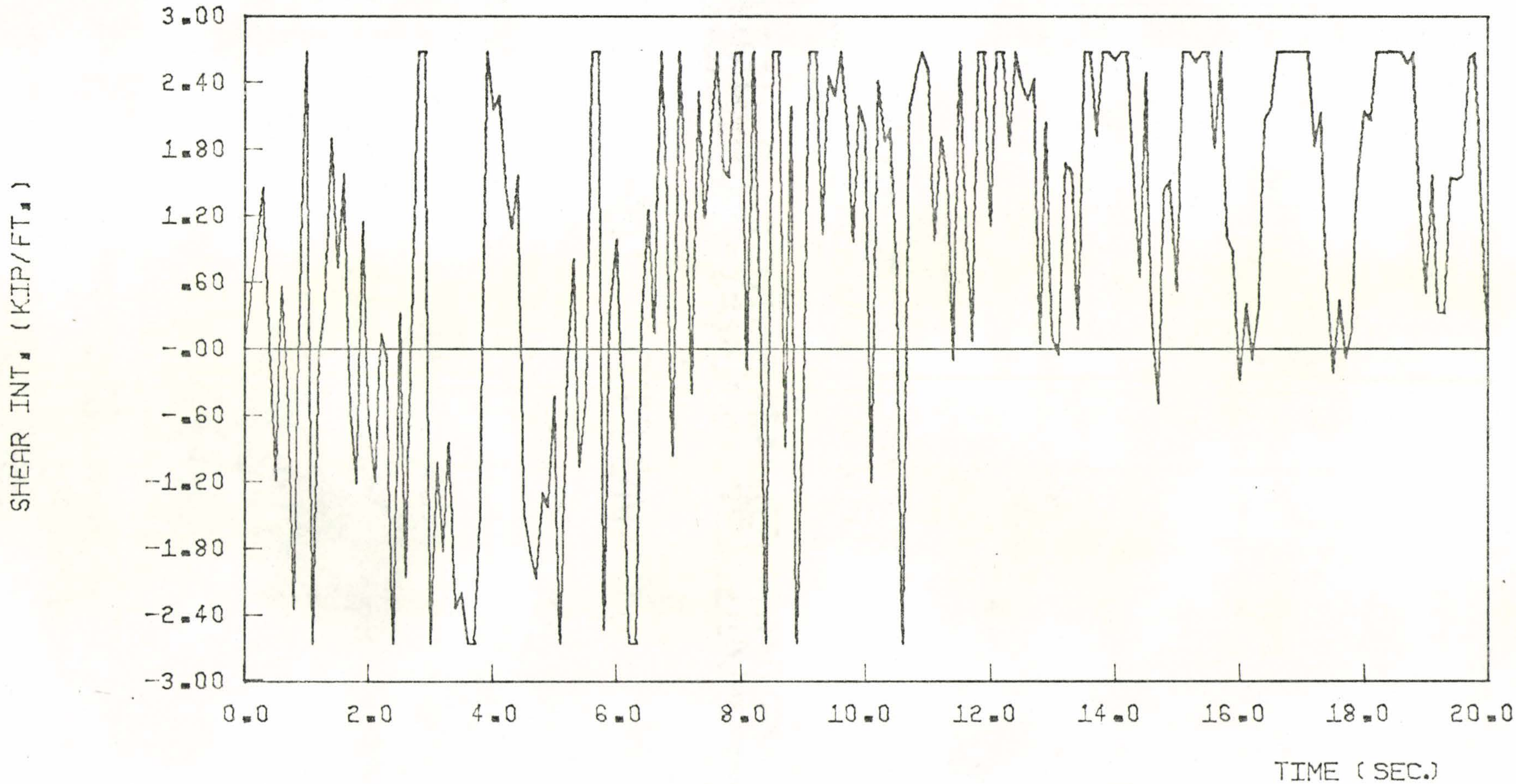

(SEGMENT NO. 5) DUCTIL. OF CON. BEAMS = 5. , INTERIOR WALL

FIG. 4_30 SHEAR INT., SAN FERNANDO WILSHIRE BLVD. ,BASEMENT, COMP. SOUTH the top displacement, base moment in left wall, axial force at base of piers and the shearing force intensity in the connecting laminae, when the wall is subjected to the N.S. component of the Wilshire Blvd., basement record of San Fernando earthquake. The rotational ductility factor of the coupling slabs μ equals to 5 in these calculations. The base moment in the right pier is left out because it is the same as the left pier.

The seismic response of the interior coupled shear wall presented in Figures (4-14) through (4-30) describes the behaviour of the wall under the seismic loads arised from ElCentro and San Fernando earthquakes. Given below is a discussion of the parameters of interest presented based on the calculations made.

(i) Top Displacement

The study of the top displacement is essential for understanding the overall behaviour of the structure. The flexibility of the structure is proportional to the top displacement and the overall ductility of the structure can be calculated from the top displacement.

The time-history response for the top displacement of the interior wall is shown in Figures (4-14) and (4-23). In Figure (4-14) the response increases after the changing of three segments in the structure to real hinged segments. Later, it decreases again due to the absorption of energy due to plastic deformations occurred in the connecting beams of the remaining segments (see Figures (4-18) to (4-22)). In Figure (4-23) the maximum response occurs at toward the last seconds of the analysis. This may be due to the characteristics of the input acceleration. The earthquake produces a high ground velocity in the last eight seconds of the record and this may be the cause of the large response of the structure toward the last eight seconds of computation.

(ii) Base Moment For Piers

The most critical section for the piers is that at the base. The base moments in the left and right piers in combination with the couple arised from the axial force in the piers are responsible for resisting the external overturning moment at the base caused by the seismic loads. The piers of the internal shear walls are identical, so that the bending moment of the left pier will be the same as the bending moment of the right pier. As the base moment in each pier is affected by the axial force in the piers, this moment is sensitive to the condition of the connecting beams. This is because the axial force at the base is the integration of the shearing forces in the connecting beams from the top to the bottom of the wall.

The time-history response for the base moment in the piers of the interior wall of the 20 storey building is shown in Figures (4-15), (4-16) and (4-24). The base moment given in Figure (4-15) has an abrupt increase after two seconds. This abrupt increase is due to the sudden decrease in the axial force at the base as shown in Figure (4-17). The base moment given in Figure (4-24) is different than that discussed above. This is because the ground acceleration given by record shown in Figure (4-12) produce a larger ground velocity in the portion of the record after twelve seconds. The base moment in the last eight seconds of the time-history response, Figure (4-24), shows that not only the magnitude of the ground acceleration has a serious effect on the structural behaviours, but also the ground velocity will affect the response.

(iii) Axial Forces at Base

As the axial force is the integration of the shearing force intensity in the laminae, it is directly affected by the changing of the connecting beams state. When the dead load is included in the axial force, the piers remain under compressive axial forces all the time. This can be seen in Figure (4-17) and (4-25). The high dead load carried by the interior walls arise from the large tributary area of the interior wall as shown in Figure (4-1).

4.7.1.2 Equivalent Cantilever

The behaviour of the double cantilever wall is an elastic one, since the walls are taken to be elastic in the present study. The response of such a case is shown in Figure (4-31) and (4-32) under the ElCentro Comp. N.S. normalized to 16% g maximum horizontal acceleration. The top displacement and the base moment are larger than those for the interior coupled shear walls, presented in Figures (4-14) and (4-15).

Listed below are the maximum values of the parameters of interest discussed above for the interior wall for both of coupled wall and equivalent cantilever wall.

Ground Acceleration (Duration = 20 sec.)	Ductility of Connecting Beams (μ)		
	5	15	500
ELCENTRO, COMP. N.S. (1940)	0.234 Ft	0.238 Ft	0.238 Ft
SAN FERNANDO, Wilshire Blvd., Basement, COMP.N.S.	0.384 Ft	0.281 Ft	0.281 Ft

Table (4-6) Maximum Top Displacement, Interior Coupled Shear Wall

Ground Acceleration (Duration = 20 seconds)	Ductility of Connecting Beams (μ)		
	5	15	500
ElCentro, Comp. N.S. (1940)	$23.2\text{x}10^3$K.ft	$24.4\text{x}10^3$K.ft	$24.4\text{x}10^3$K.ft
San Fernando, Wilshire Blvd., Basement, Comp. N.S.	$27.3\text{x}10^3$ "	$23.4\text{x}10^3$ "	$23.4\text{x}10^3$ "

Table (4-7) Max. Base Wall Moment (Left and Right Piers), Interior Coupled Shear Wall

Ground Acceleration (Duration = 20 seconds)	Ductility of Connecting Beams (μ)					
	5		15		500	
	Tension	Comp.	Tension	Comp.	Tension	Comp.
ElCentro Comp. N.S. (1940)	-	2.32×10^3 K	-	2.32×10^3 K	-	2.32×10^3 K
San Fernando, Wilshire Blvd., Basement, Comp. N.S.	-	2.32×10^3 K	-	2.32×10^3 K	-	2.32×10^3 K

Table (4-8) Max. Axial Force at the Base of Piers, Interior Coupled Shear Wall

Ground Acceleration (Duration = 20 seconds)	Max. Top Displ. Ft	Max. Base Moment Kip. Ft	Max. Axial Force, Kip (Comp.)
ElCentro, Comp. N.S. (1940)	0.626	29.0×10^3	1.85×10^3

Table (4-9) Equivalent Cantilever Wall

Table (4-7) indicates that the maximum top displacement is less than $H_T/450$ while the maximum top displacement for the equivalent cantilever wall (Table (4-9)) is approximately HT/275. This increase in top deflection is due to the lack of couple action in the cantilever wall case. Comparing the maximum base moment for the piers in the equivalent cantilever wall and the coupled wall leads to the conclusion that the coupled shear wall, even with flexible connecting beams,

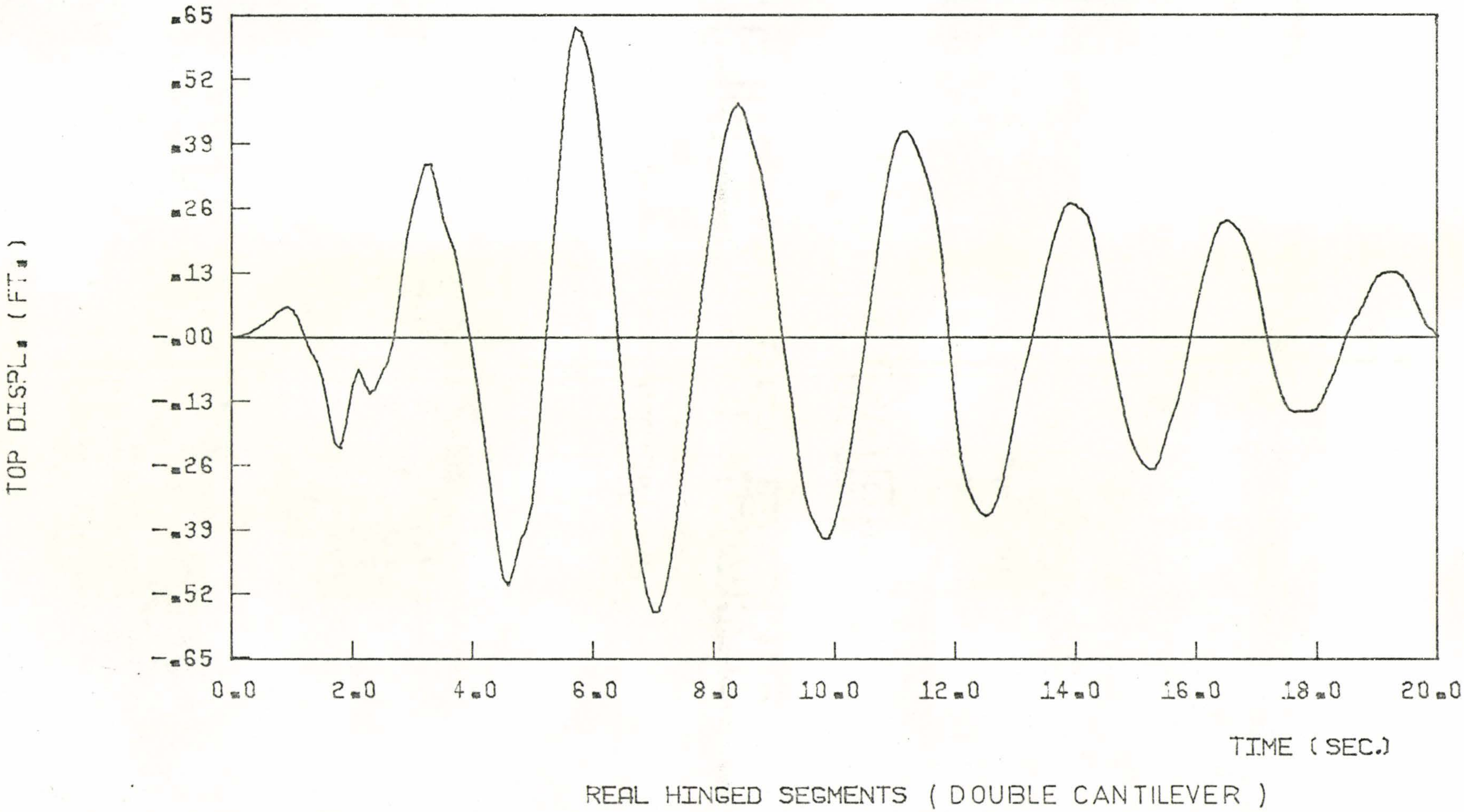

FIG. 4_31 TOP DISPL. , ELCENTRO COMP. NORTH

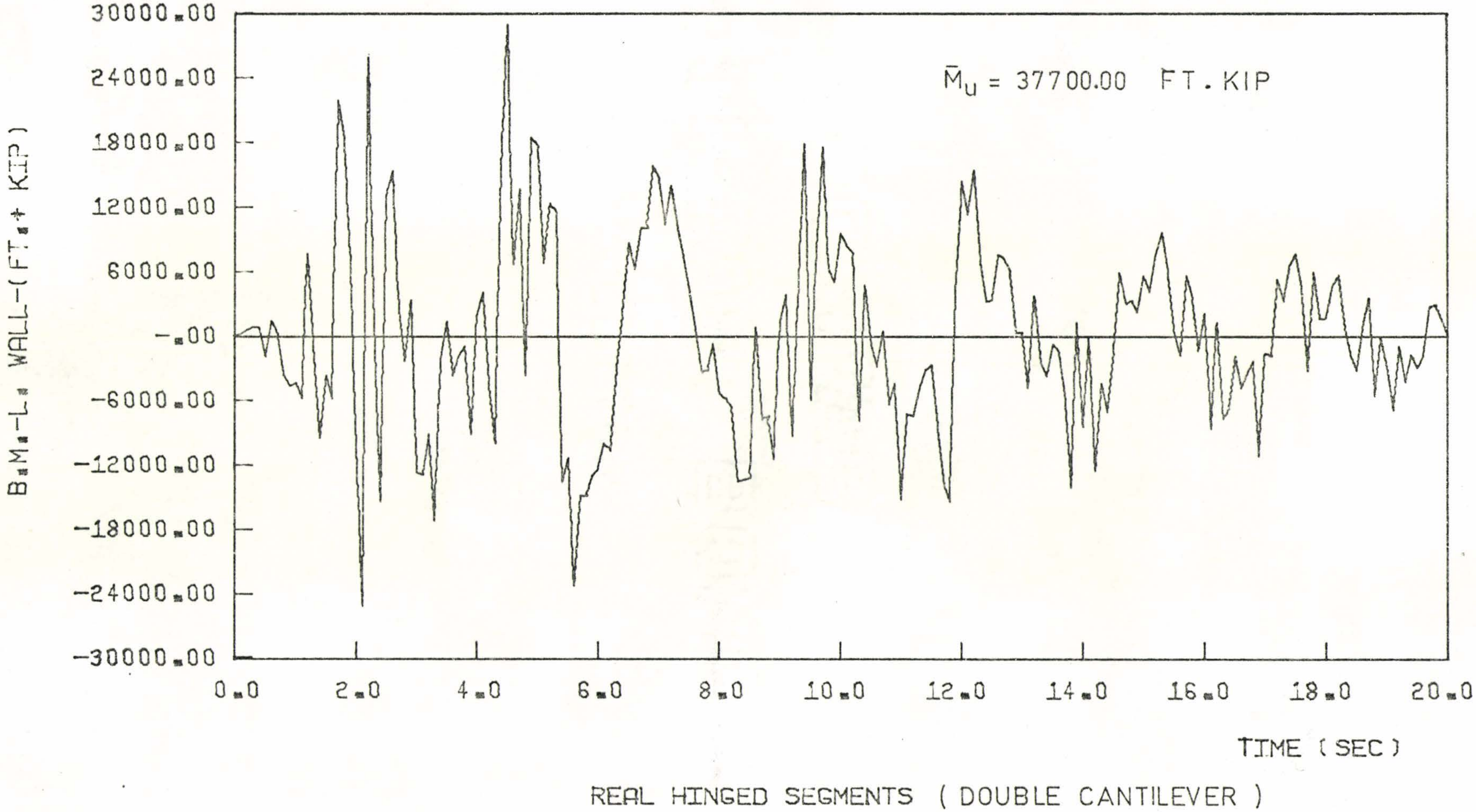

FIG. 4_32 B.M.L.WALL, ELCENTRO COMP. NORTH

behaves better than the equivalent cantilever wall under the same lateral loads.

Due to the small capacity of the connecting slabs in transmitting axial force between the two piers, the axial force in the piers for both type of wallsalways remain compressive as shown in Tables (4-8) and (4-9).

4.7.2 Exterior Wall Response

Two designs are taken for the exterior wall. In one case, the wall designed to resist a maximum horizontal ground acceleration of 16% g. In another case, it designed to resist a maximum horizontal ground acceleration of 8% g. The wall designed for 16% g seismic load is subjected to the ElCentro, San Fernando and Taft earthquake records as an input ground motions. All of the earthquake records are normalized to 16% g maximum horizontal acceleration. The wall designed for 8%g seismic loading is subjected to the ElCentro record only, normalized to 16% g peak acceleration. The main object of this study is to examine the effect of the rotational ductility of the connecting beams when the coupled shear is to be subjected to moderate or strong earthquakes.

The performance of the wall is evaluated through the seismic response of the parameters of interest, namely: the top displacement, the base moment for the piers, and the axial forces at the base. Again, the shearing force intensity in connecting laminae are presented to clarify the behaviour of the walls.

4.7.2.1 Exterior Wall Subjected to Moderate Earthquake Excitation

By moderate earthquake excitation, we consider the peak horizontal acceleration of the earthquakes the same as that the wall is designed for. In the cases studied, this horizontal acceleration is taken to be 16% g.

Given below are the seismic responses for nine cases. There are three earthquake records and for each earthquake record, three values of rotational beam ductility of 5, 15 and 500 are used.

(i) Top Displacement

The time-history response is shown in Figures (4-33), (4-34) and (4-35). In the case of the ElCentro record, the effect of the ductility of the connecting beams is immaterial as the connecting beams remain elastic. The response of the connecting beams are shown in Figures (4-42) to (4-46). For the Wilshire Blvd. record of San Fernando, Figure (4-34) indicates that for ductility greater than fifteen, no improvement for the wall behaviour can be detected. The case of Taft record excitation shows that the connecting beam ductility is of more importance than the previous cases studied under the ElCentro and San Fernando earthquake

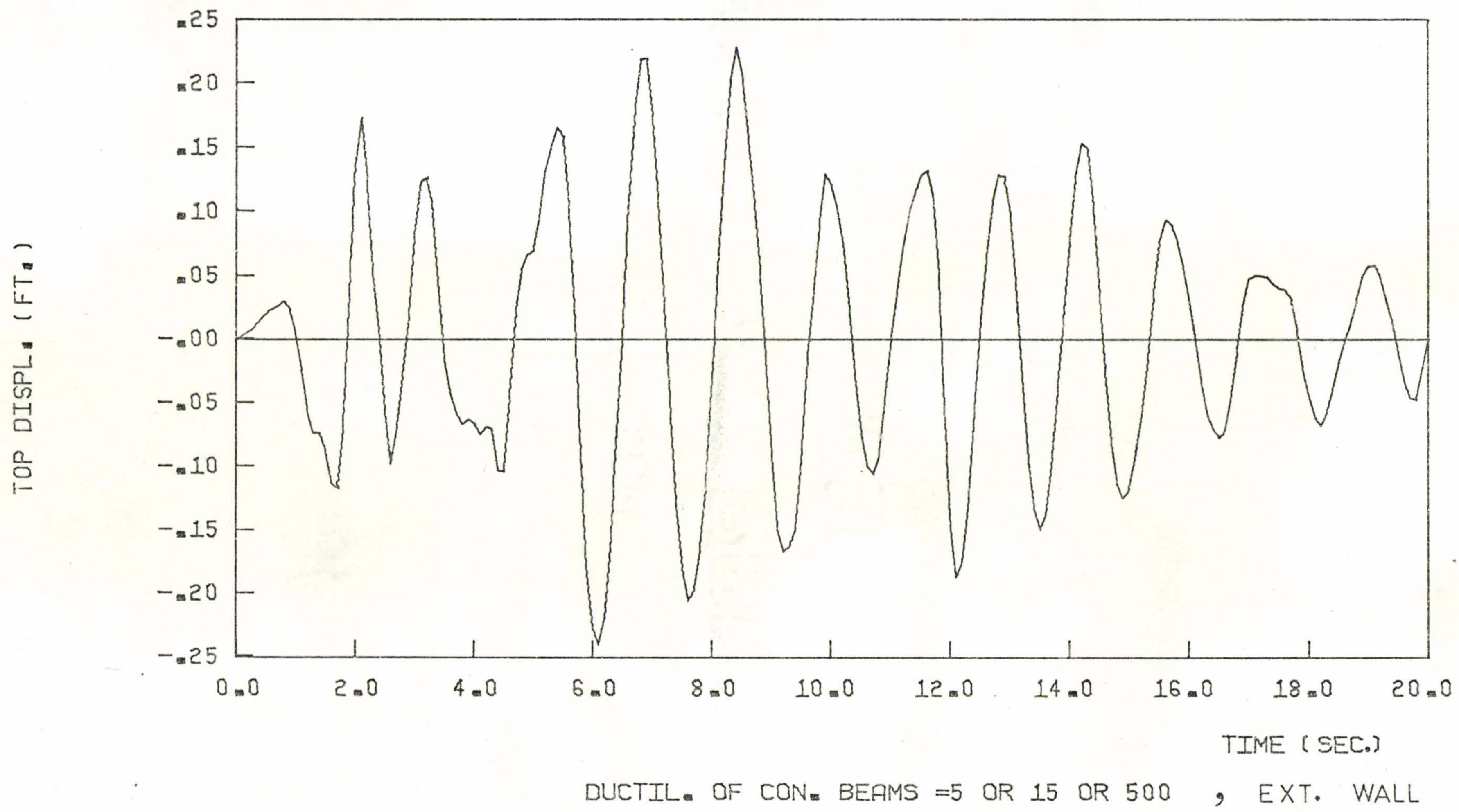

FIG. 4_33 TOP DISPL., ELCENTRO COMP. NORTH

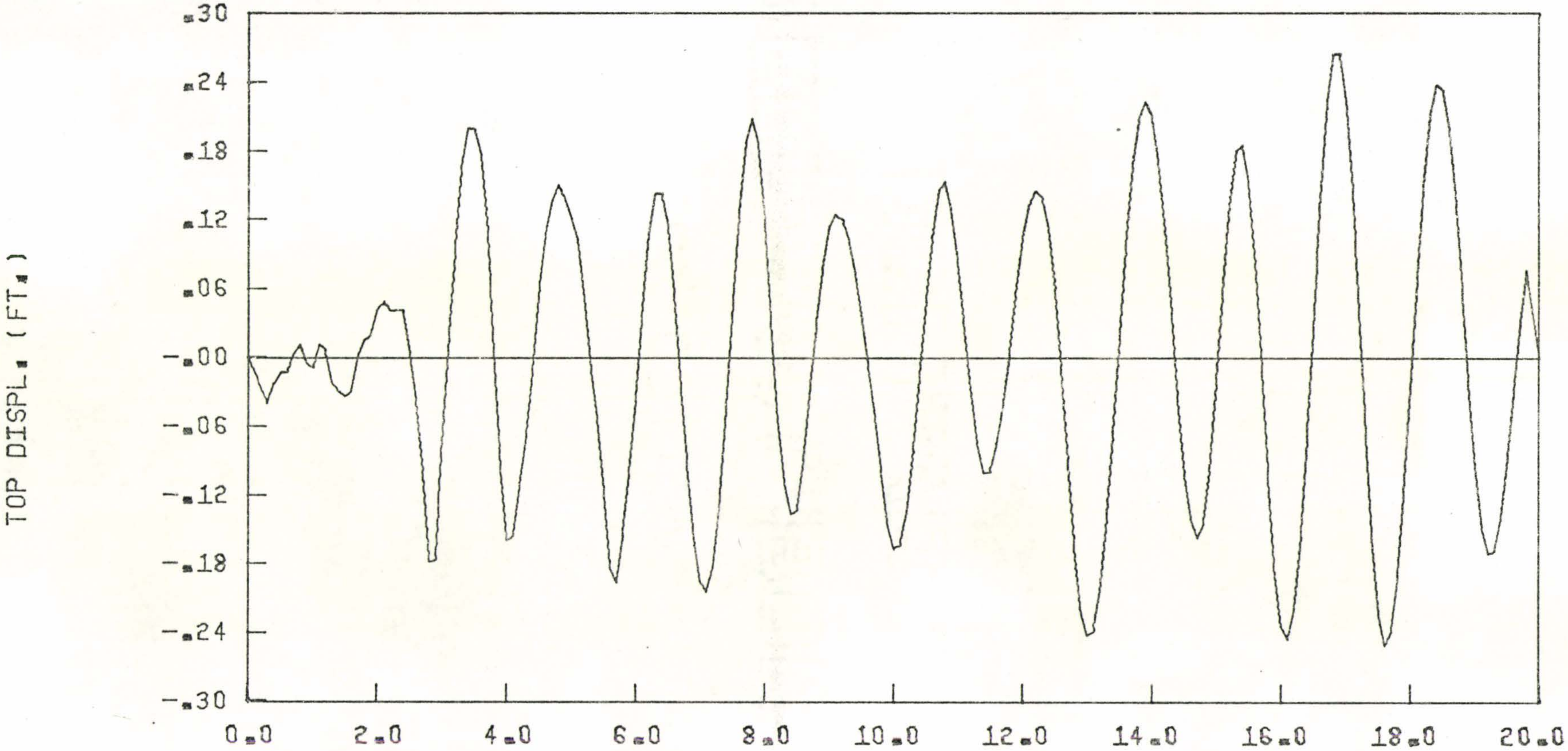

DUCTIL. OF CON. BEAMS = 15 OR 500 , EXTERIOR WALL

FIG. 4_34 TOP DISPL. , SAN FERNANDO WILSHIRE BLVD. ,BASEMENT, COMP. SOUTH

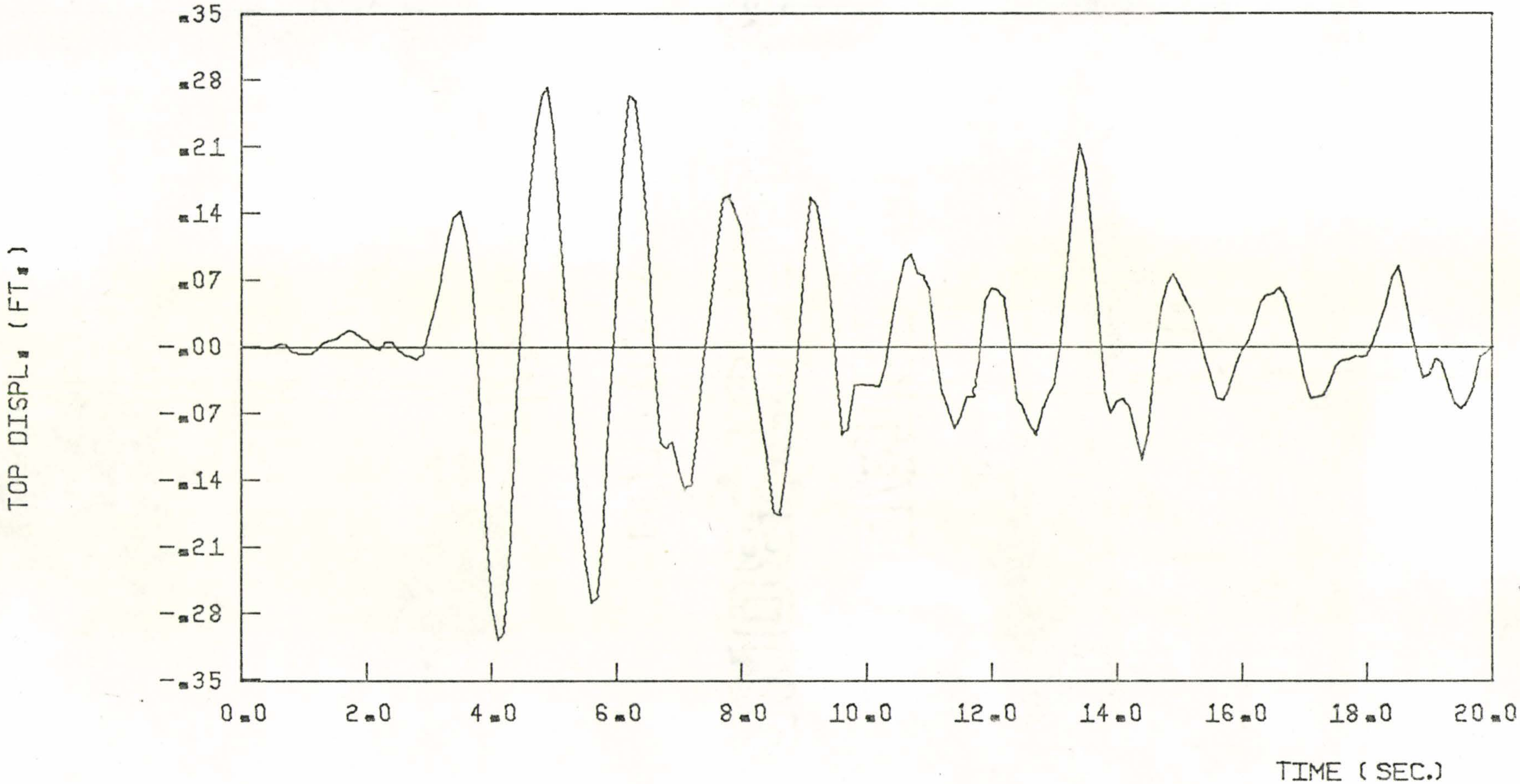

DUCTIL. OF CON. BEAMS = 15. , EXTERIOR WALL

FIG.4_35 TOP DISPL. ,TAFT E.Q. COMP N21E excitation. Shown in Figure (4-35) is the top deflection response for μ=15, which can be taken as a moderate beam ductility value.

(ii) Base Moment for Piers

The time-history responses for the moment in the base of the piers are shown in Figures (4-36), (4-37) and (4-38). Responding to the ElCentro and San Fernando records, the structure behaves essentially elastically after some elasto-plastic deformation in the connecting beams in the first few seconds. The structure in these two cases is said to be shaken down. This is due to the residual shearing force $\bar{q}_j$ which satisfies at every connecting beam j the conditions

$$\bar{q}_j + q_{j_{max}} \leq q_{pj} \tag{4-1}$$

$$\bar{q}_j + q_{j_{min}} \geq -q_{pj} \tag{4-2}$$

and which is statically admissible [10a]. The residual shears existing in the connecting beams after the structure has shaken down will not necessarily be the distribution $\bar{q}_j$, see Figures (4-42) to (4-46). The base moment in the above discussed two cases never exceeds the ultimate capacity of the wall cross section which equals to ±43400 Ft Kip.

For the response to the normalized Taft record, the bending moment, as given by Figure (4-38), is larger than

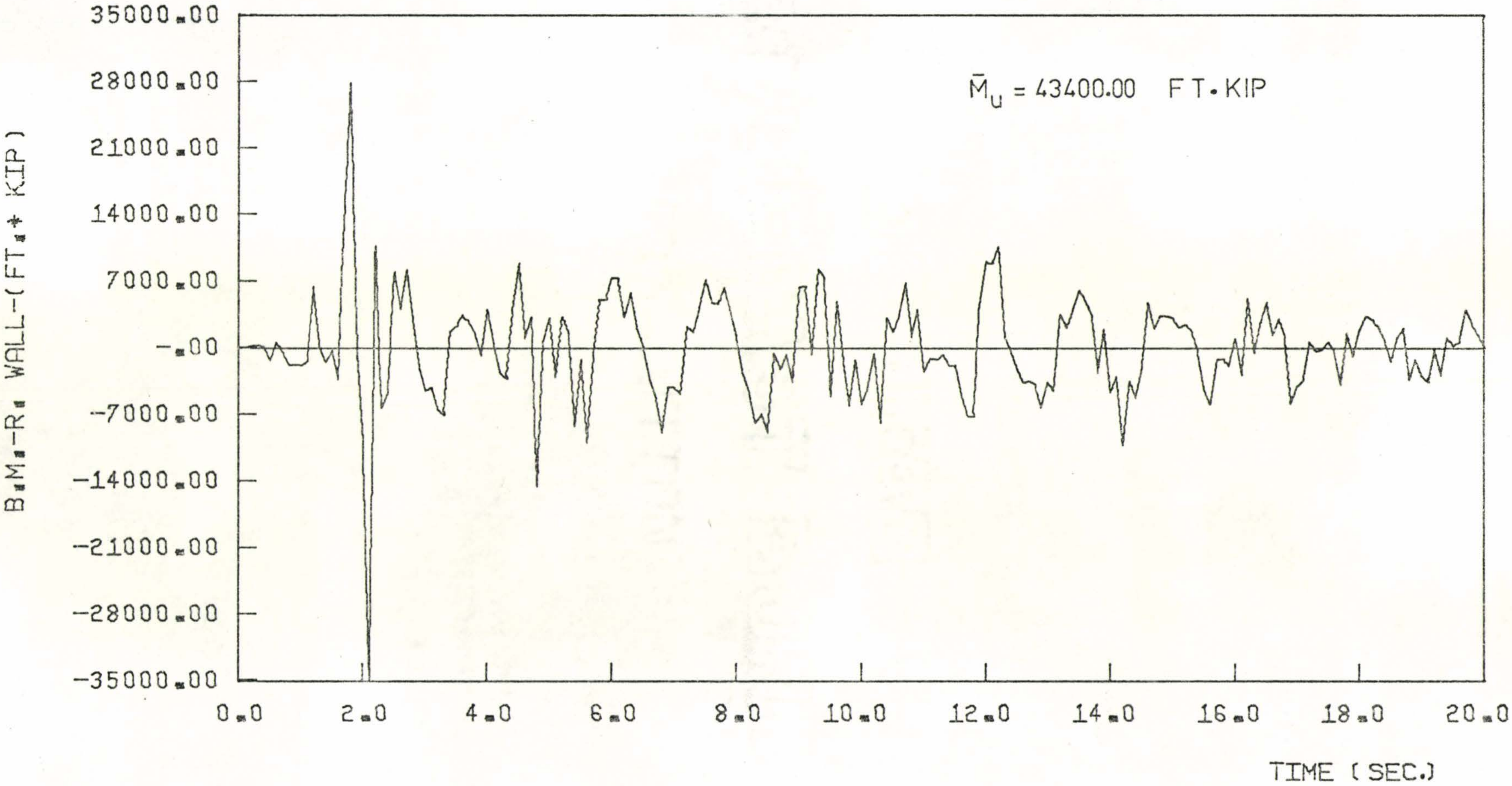

DUCTIL. OF CON. BEAMS =5 OR 15 OR 500 , EXT. WALL

FIG. 4_36 B.M.R. WALL , ELCENTRO COMP. NORTH

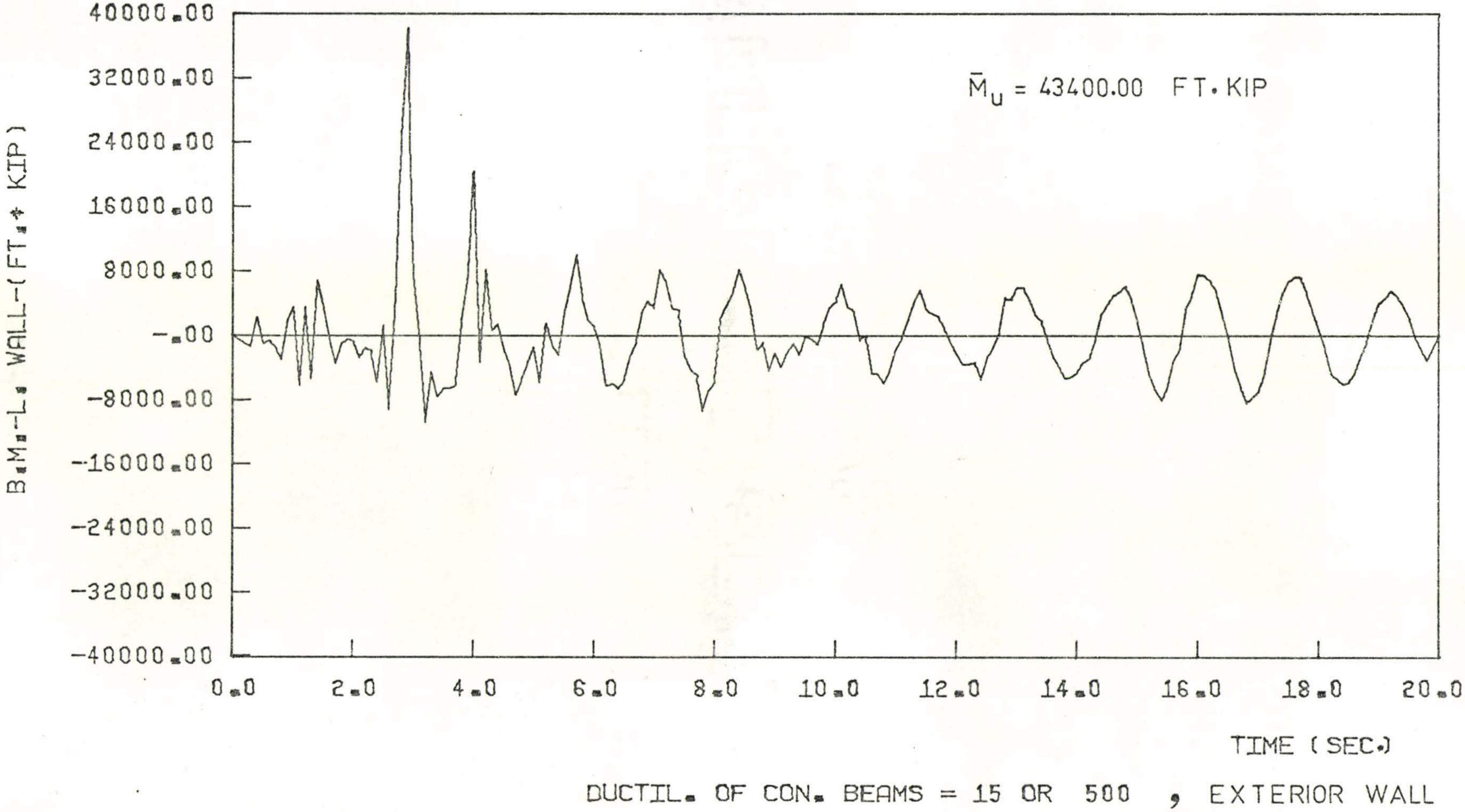

FIG. 4_37 B.M.L.WALL, SAN FERNANDO WILSHIRE BLVD. ,BASEMENT, COMP. SOUTH

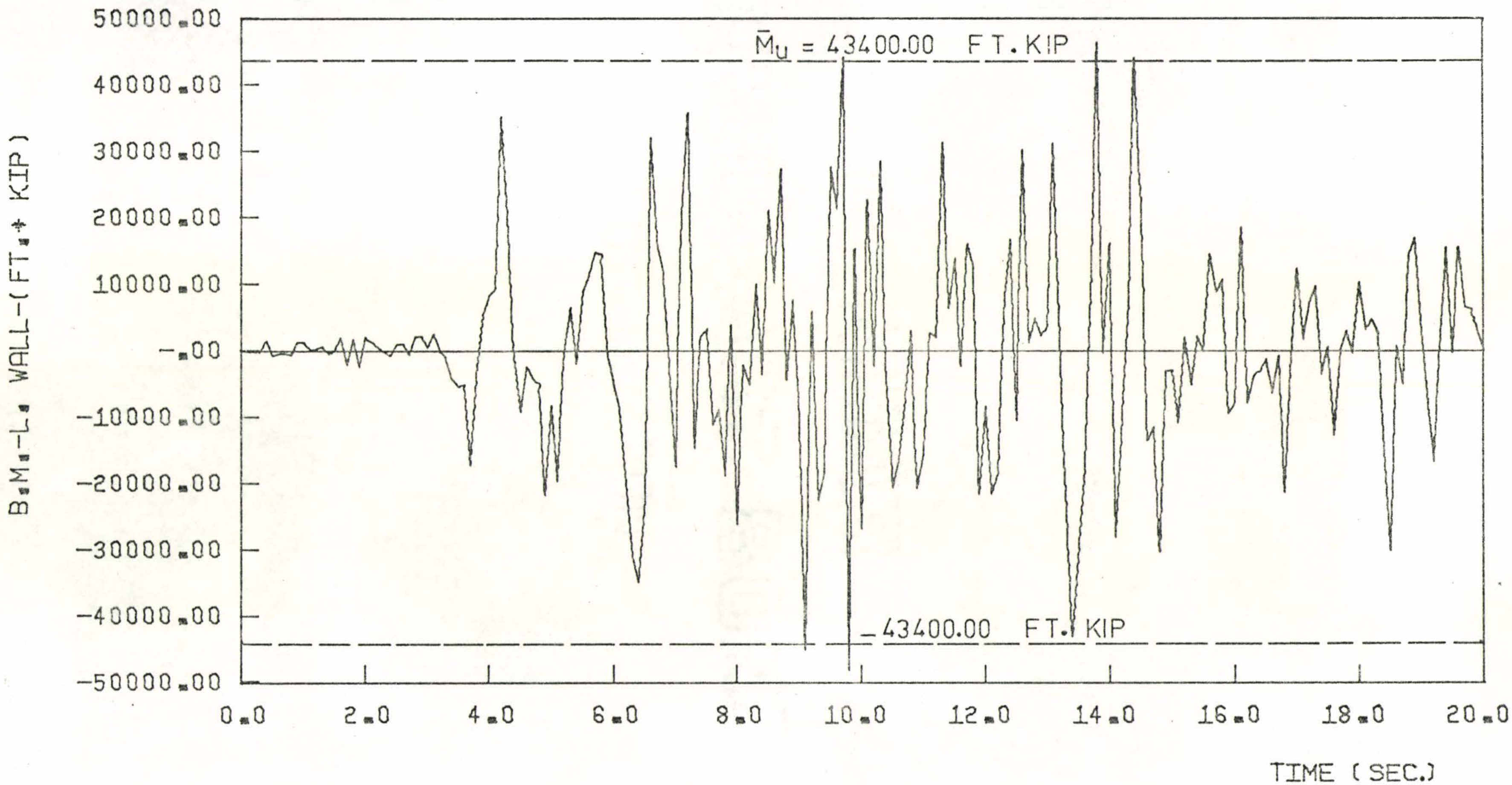

DUCTIL. OF CON. BEAMS = 15. , EXTERIOR WALL

FIG.4_38 B.M.L.WALL , TAFT E.Q. COMP N21E the ultimate capacity of the cross section in some instances. These high values are a result of the formation of real hinges in 60% of the connecting beams. Therefore, an increasing of the rotational ductility factor of the connecting beams will improve the performance of the wall substantially in this case.

(iii) Axial Forces at Base

The time-history responses are shown in Figures (4-39), (4-40) and (4-41). These Figures show that the piers may be subjected to tensile forces even after including the dead load. This is because the connecting beams have high capacity to transmit axial forces between the two walls, while the tributary area carried by the end shear wall is small compared to the interior shear wall.

To decrease the tensile forces in the piers, it is useful to arrange the walls in such a way to keep the tributary floor areas proportional to the wall stiffnesses.

4.7.2.2 Exterior Wall Subjected to Strong Earthquake Excitation

In this case, we consider the response of a wall designed for a 8% g seismic load and being subjected to the ElCentro ground excitations of 16% g. The top displacement time-history records are shown in Figures (4-52) and (4-53)

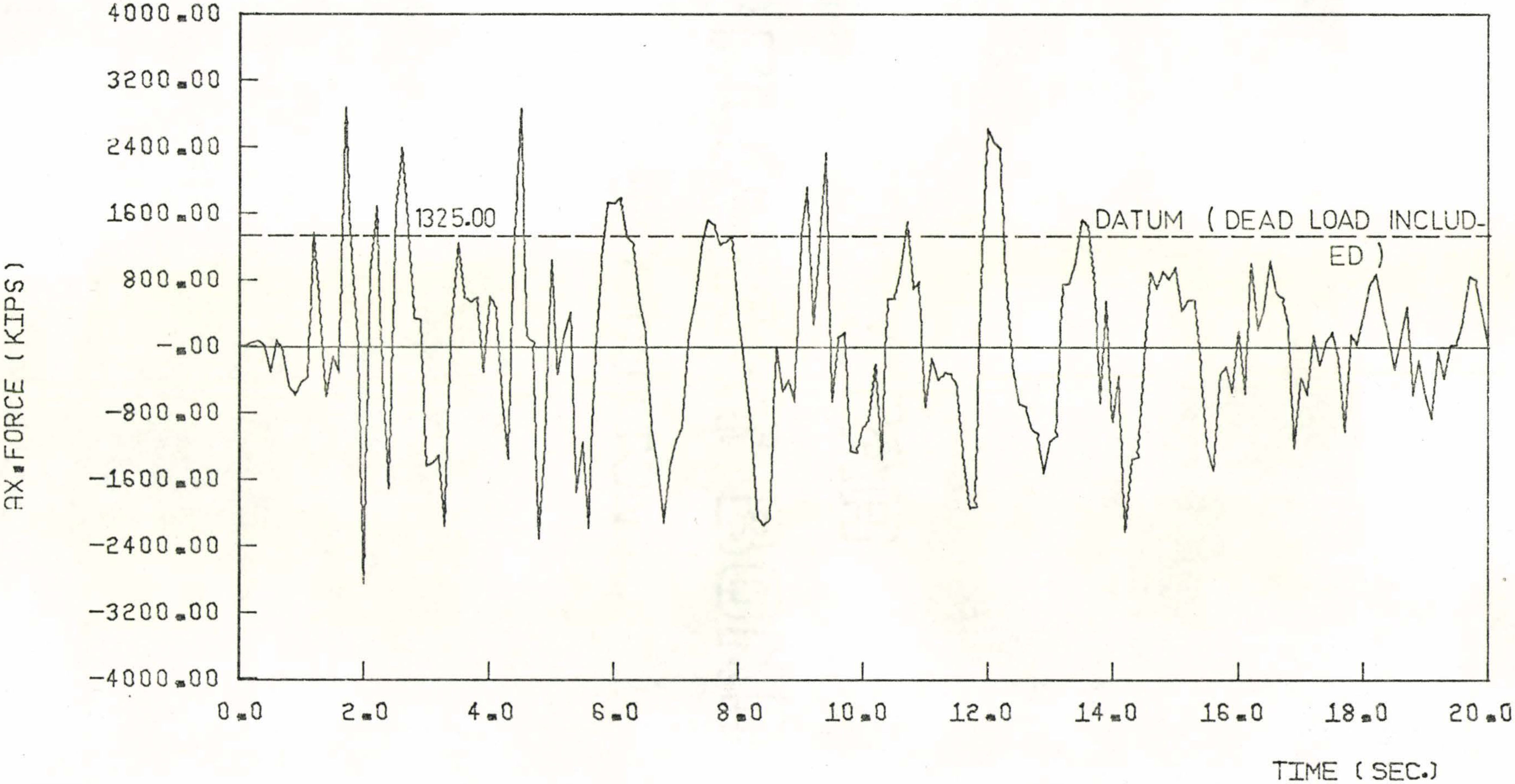

DUCTIL. OF CON. BEAMS =5 OR 15 OR 500 , EXT. WALL

FIG. 4_39 AX. FORCE , ELCENTRO COMP. NORTH

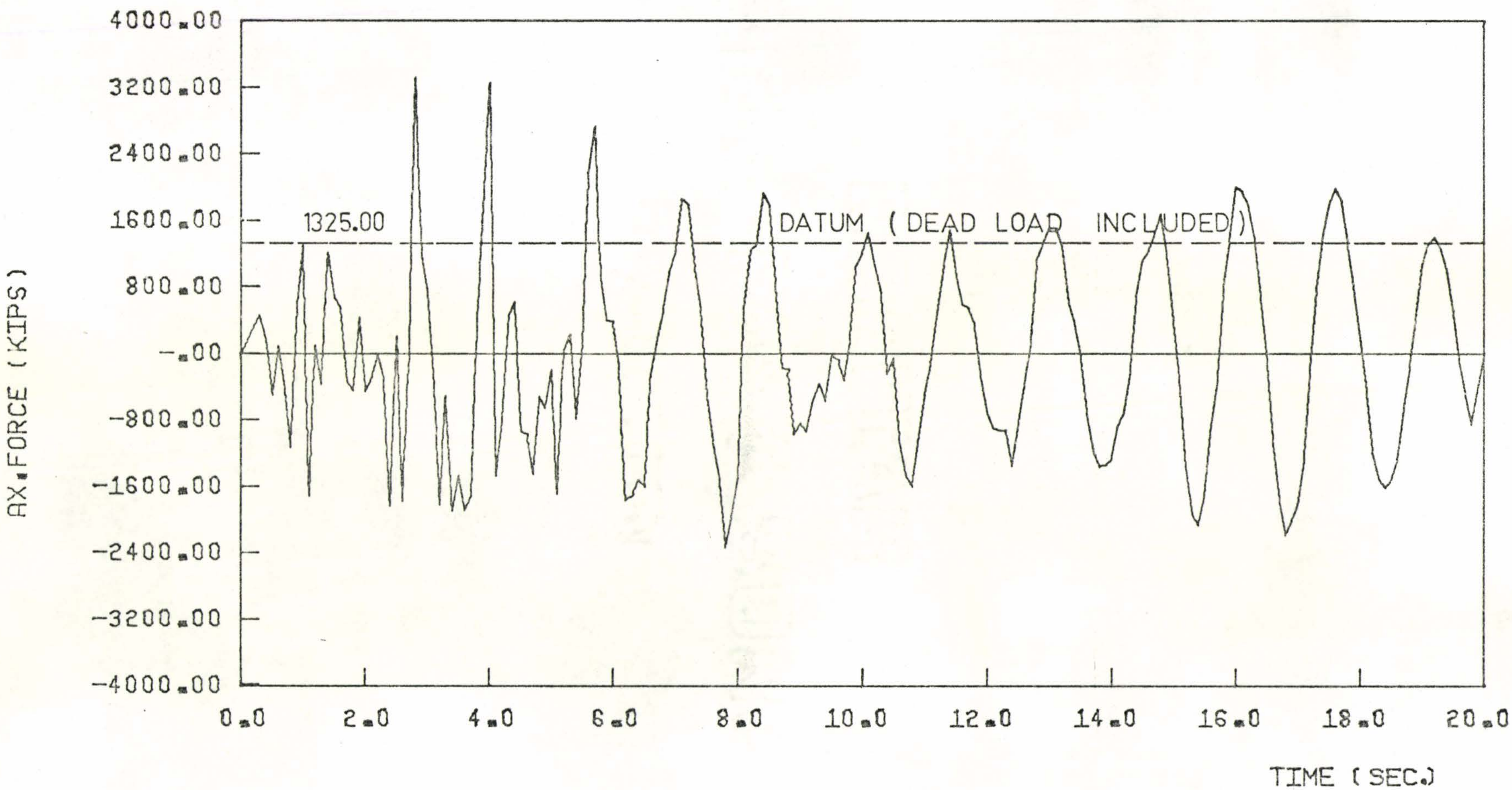

DUCTIL. OF CON. BEAMS = 15 OR 500 , EXTERIOR WALL

FIG. 4_40 AX. FORCE , SAN FERNANDO WILSHIRE BLVD. ,BASEMENT, COMP. SOUTH

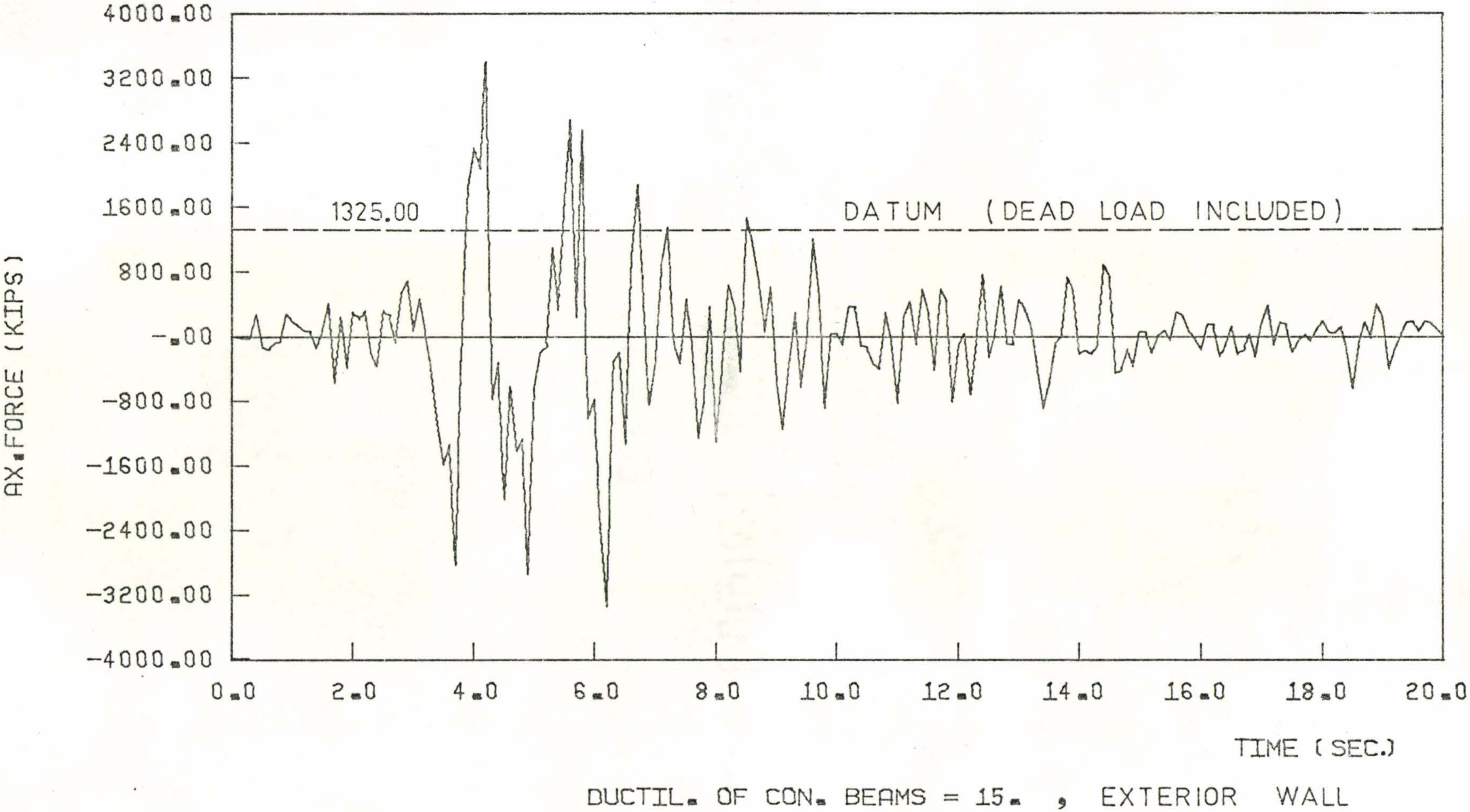

FIG.4_41 AX. FORCE , TAFT E.Q. COMP N21E

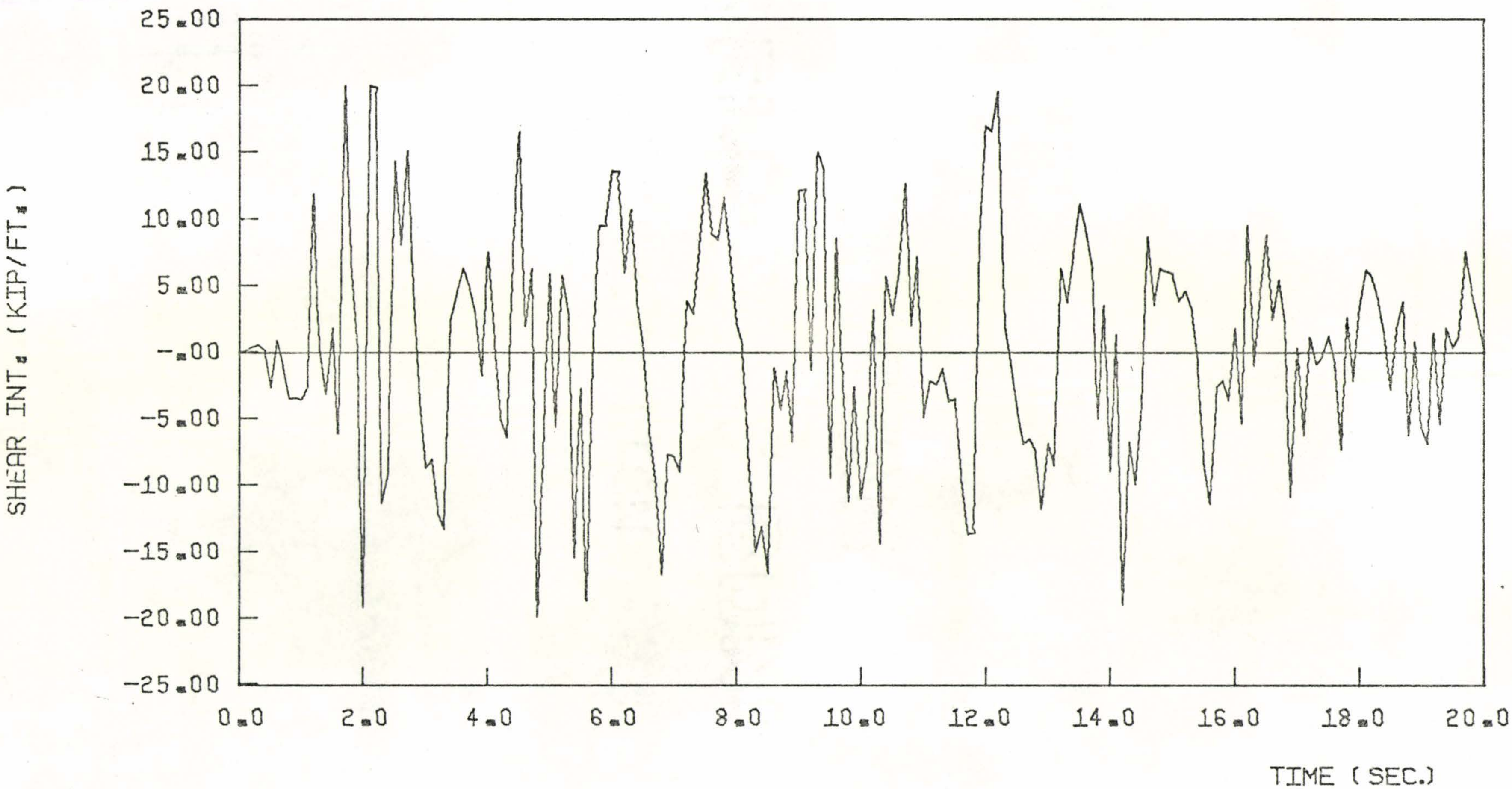

(SEGMENT NO. 1) DUCTIL. OF CON. BEAMS =5 OR 15 OR 500 , EXT. WALL

FIG. 4_42 SHEAR INT., ELCENTRO COMP. NORTH

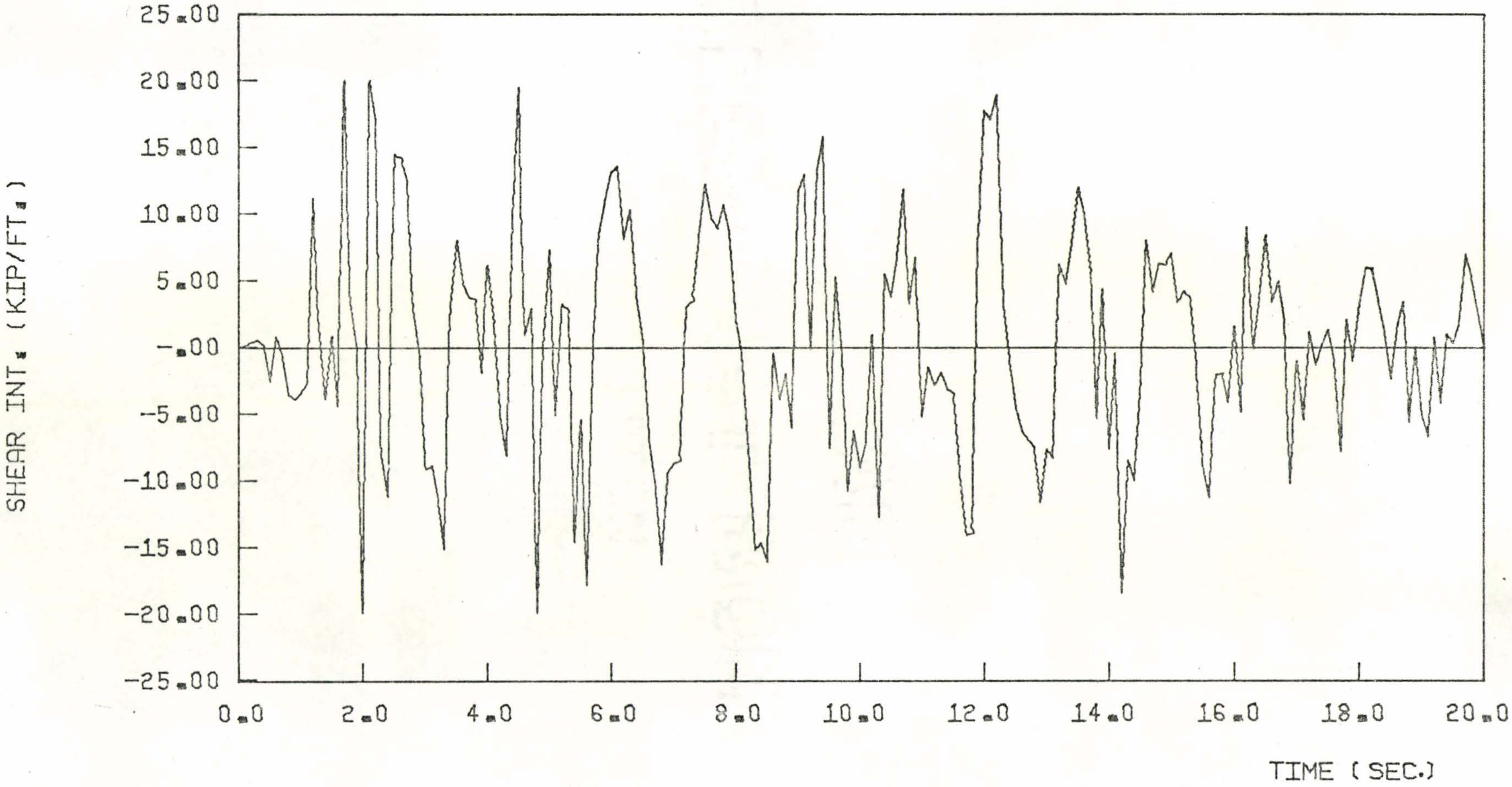

(SEGMENT NO. 2) DUCTIL. OF CON. BEAMS =5 OR 15 OR 500 , EXT. WALL

FIG. 4_43 SHEAR INT., ELCENTRO COMP. NORTH

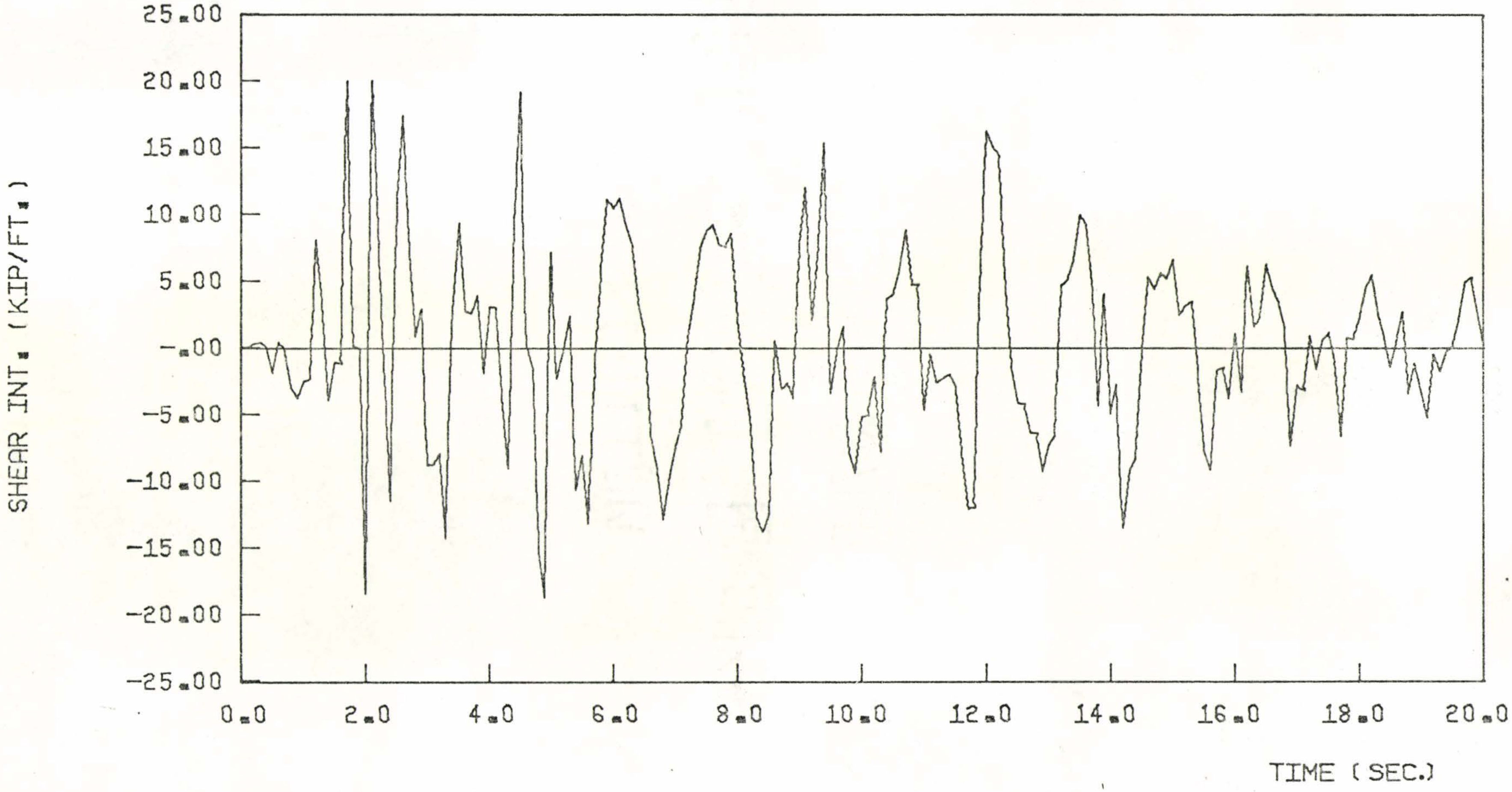

(SEGMENT NO. 3)   DUCTIL. OF CON. BEAMS =5 OR 15 OR 500 , EXT. WALL

FIG. 4_44 SHEAR INT., ELCENTRO COMP. NORTH

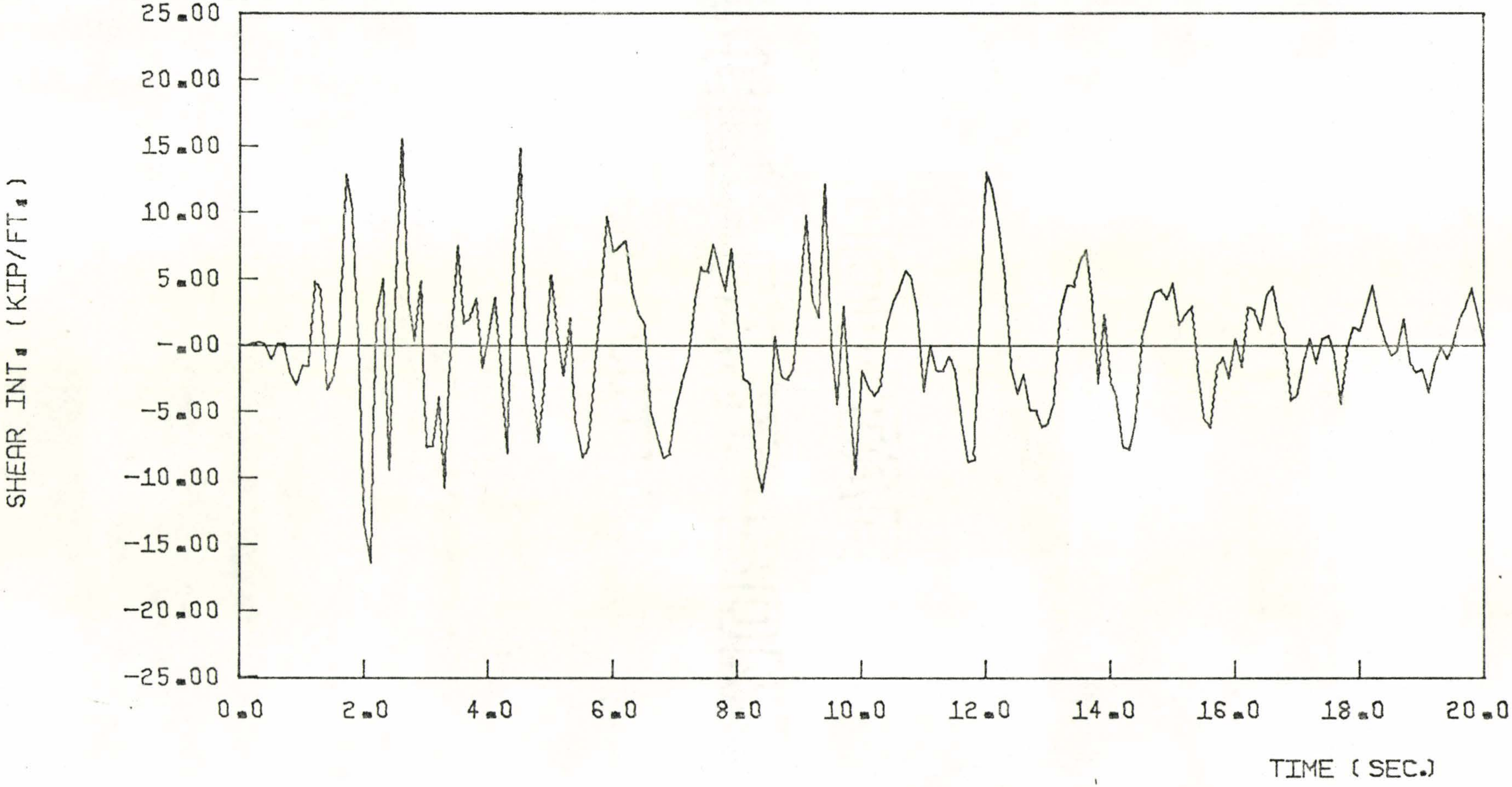

(SEGMENT NO. 4) DUCTIL. OF CON. BEAMS =5 OR 15 OR 500 , EXT. WALL

FIG. 4_45 SHEAR INT., ELCENTRO COMP. NORTH

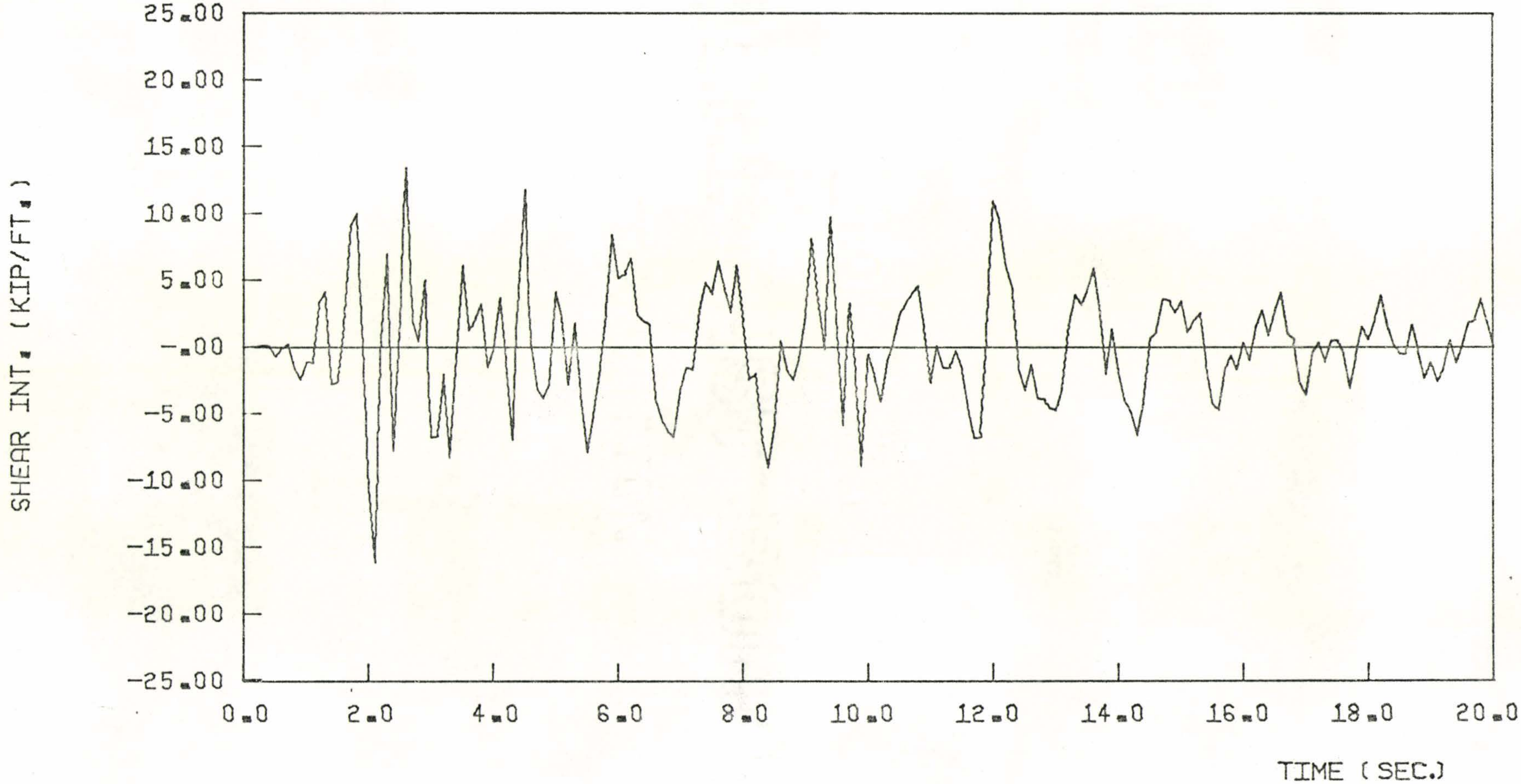

(SEGMENT NO. 5) DUCTIL. OF CON. BEAMS =5 OR 15 OR 500 , EXT. WALL

FIG. 4_46 SHEAR INT., ELCENTRO COMP. NORTH

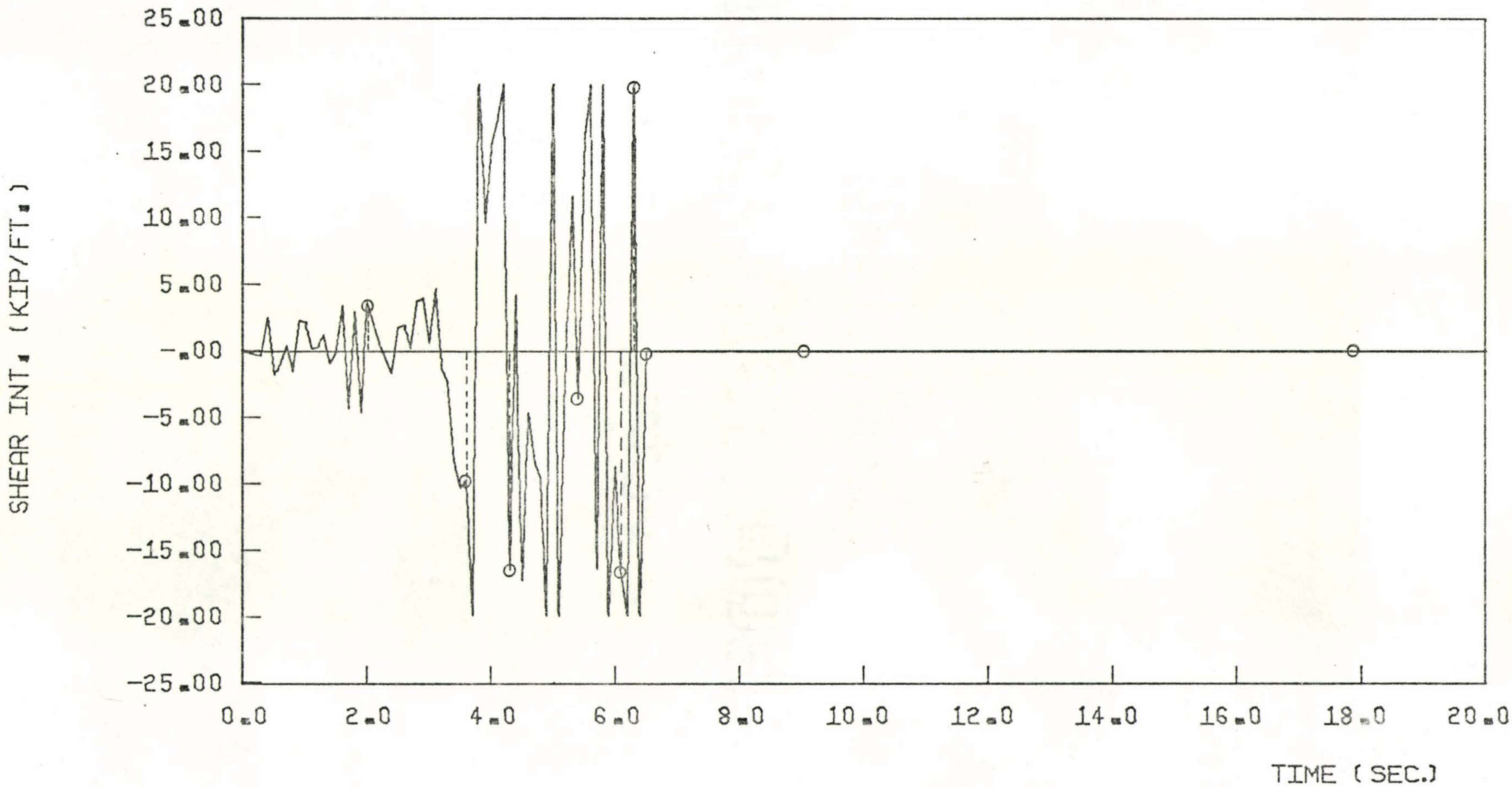

(SEGMENT NO. 1) DUCTIL. OF CON. BEAMS = 15. , EXTERIOR WALL

FIG. 4_47 SHEAR INT., TAFT E.Q. COMP N21E

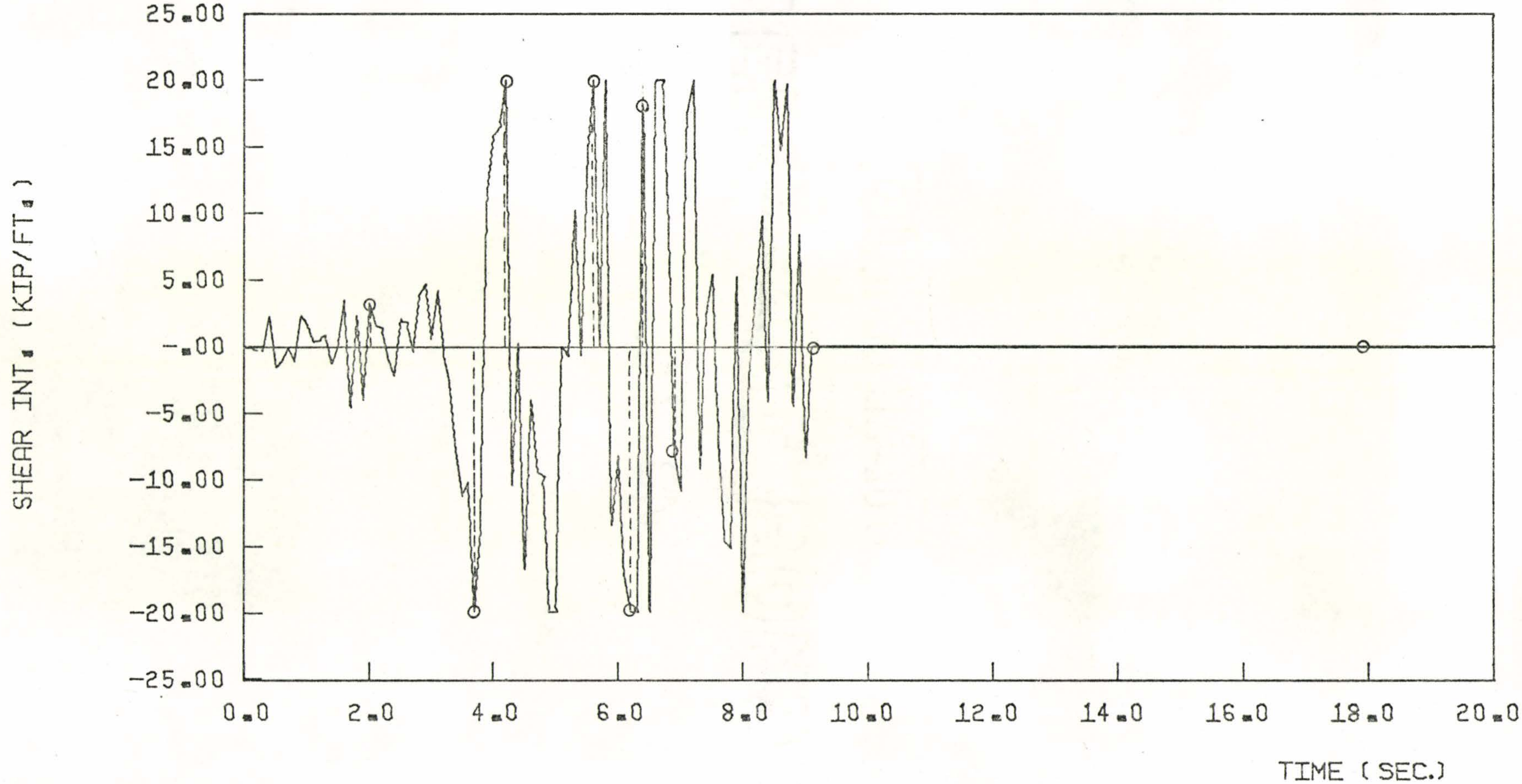

(SEGMENT NO. 2) DUCTIL. OF CON. BEAMS = 15. , EXTERIOR WALL

FIG.4_48 SHEAR INT. , TAFT E.Q. COMP N21E

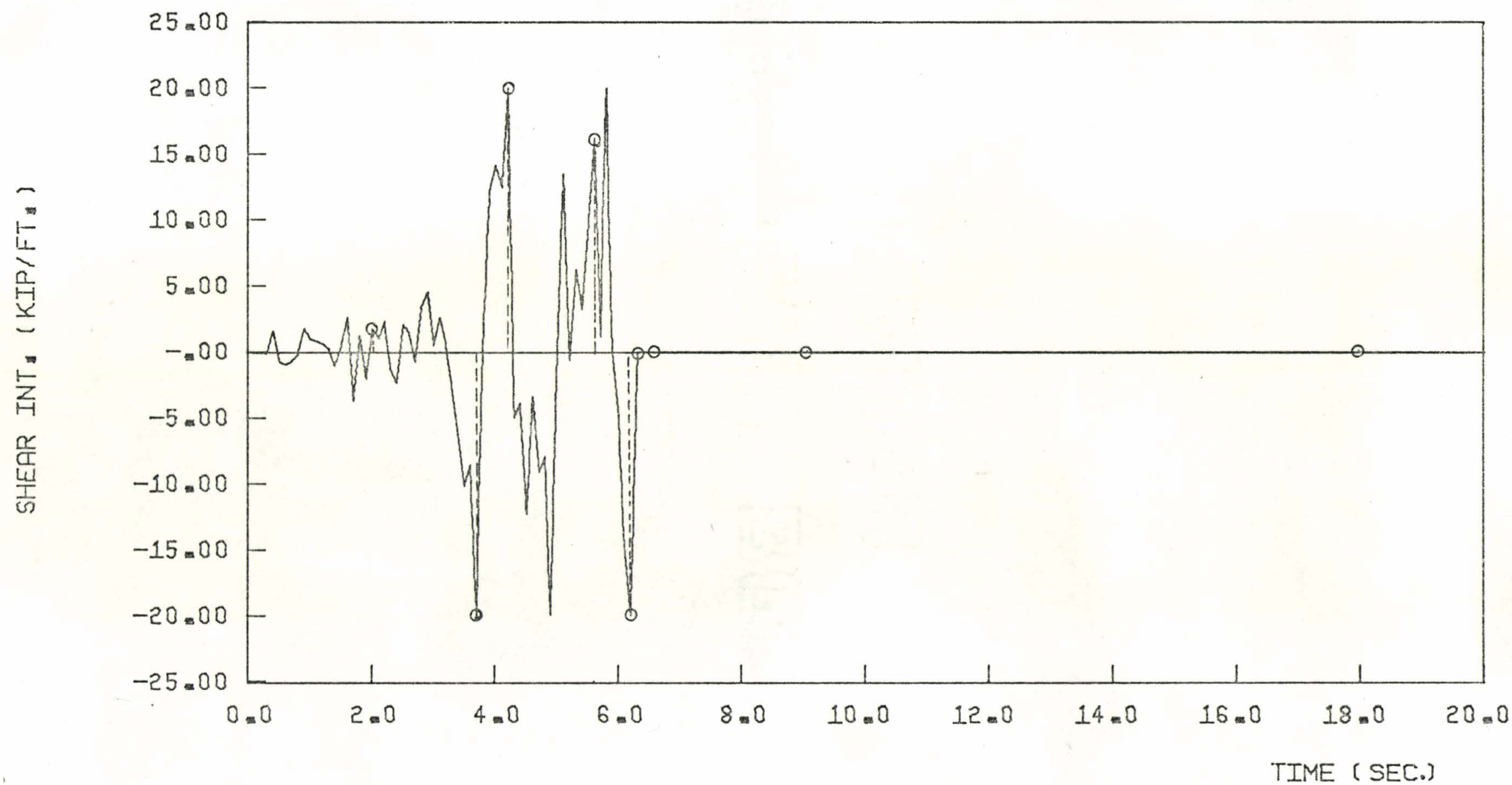

(SEGMENT NO. 3) DUCTIL. OF CON. BEAMS = 15. , EXTERIOR WALL

FIG. 4_49 SHEAR INT. , TAFT E.Q. COMP N21E

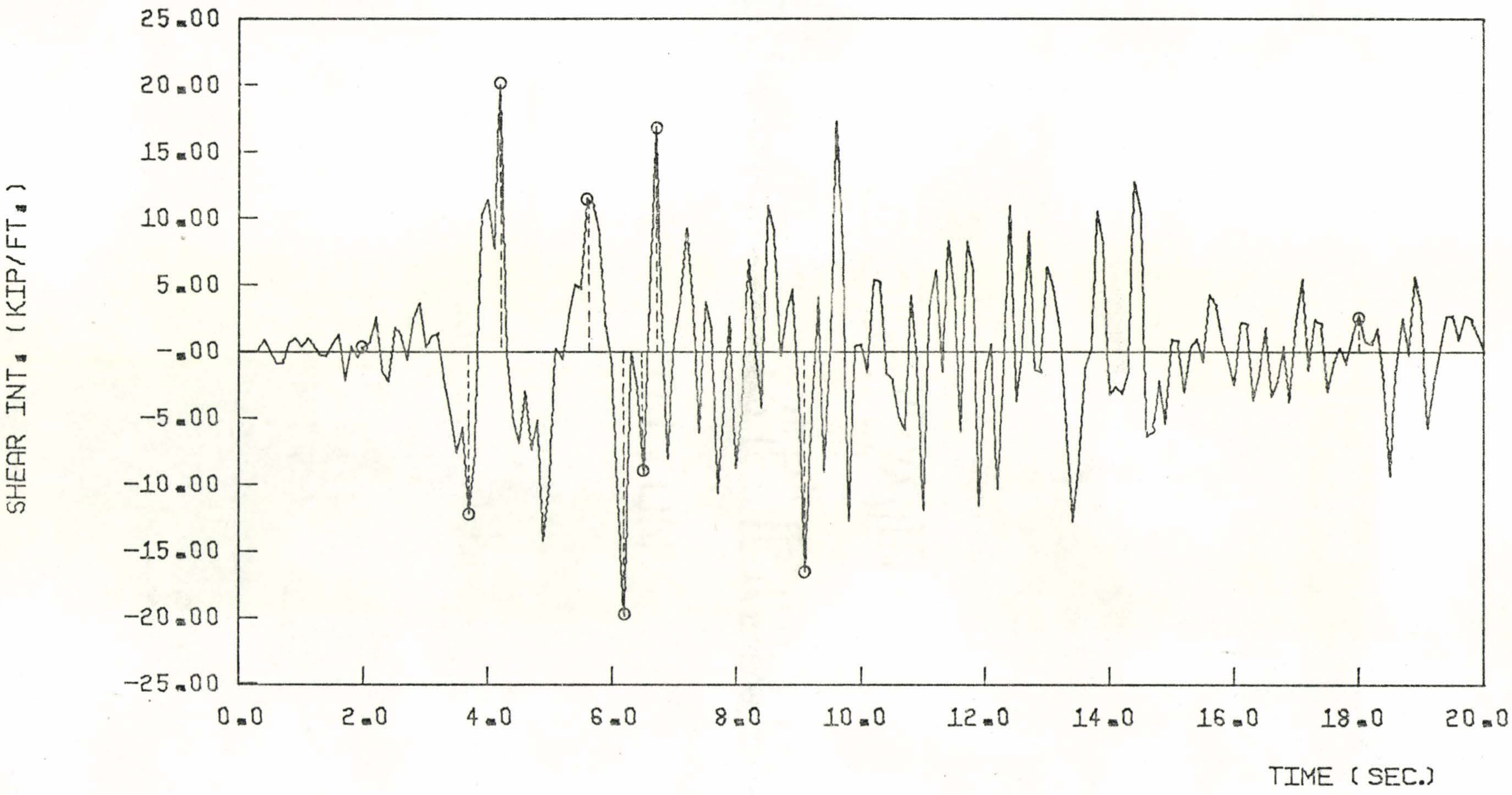

(SEGMENT NO. 4) DUCTIL. OF CON. BEAMS = 15. , EXTERIOR WALL

FIG. 4_50 SHEAR INT., TAFT E.Q. COMP N21E

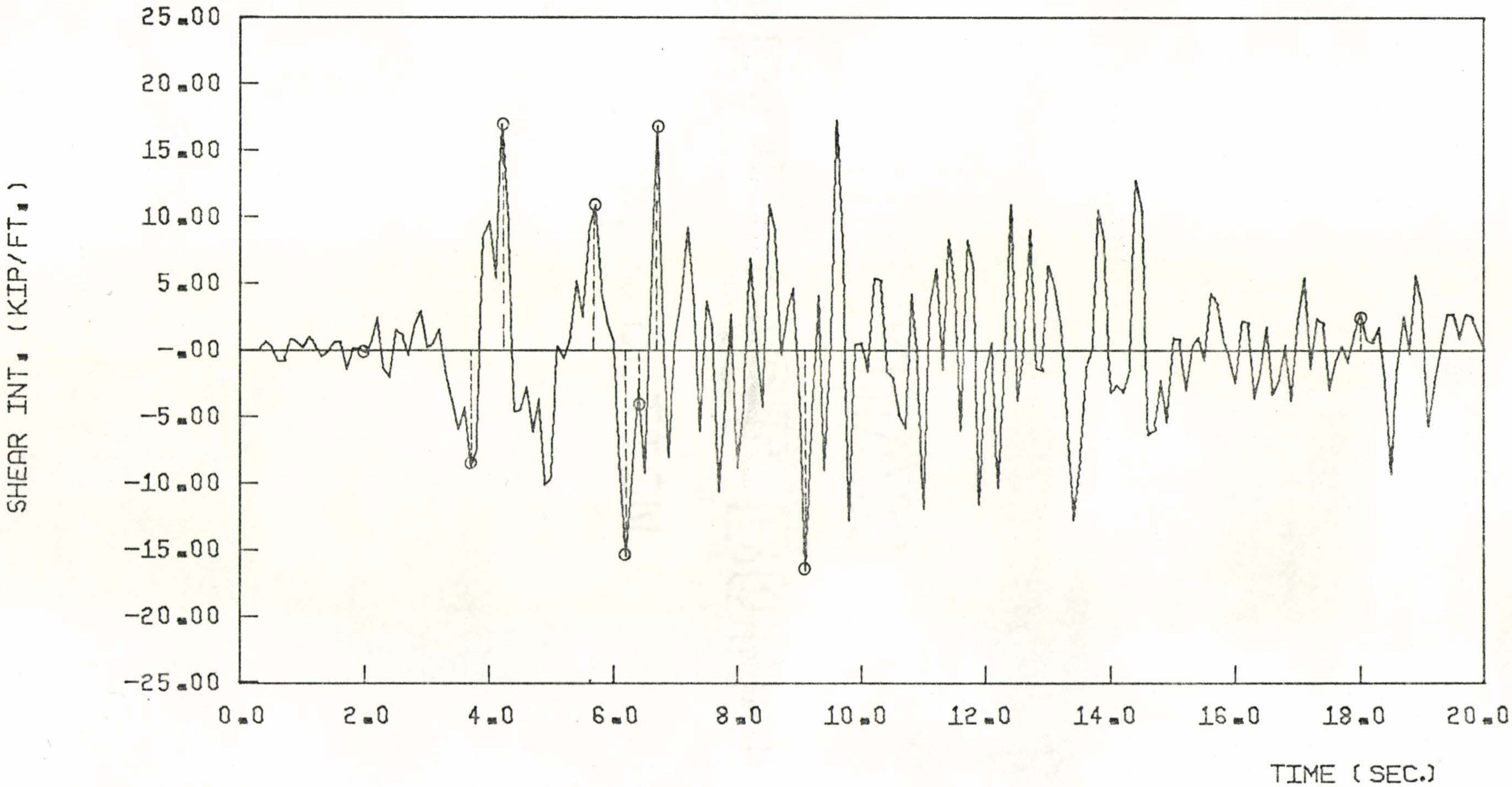

(SEGMENT NO. 5) DUCTIL. OF CON. BEAMS = 15. , EXTERIOR WALL

FIG. 4_51 SHEAR INT., TAFT E.Q. COMP N21E

for rotational ductility factors of the connecting beams equal to 15 and 500 respectively. There is little difference between the two figures. However, the response presented is larger than that for the exterior wall designed for a seismic load of 16% g.

The base moment time-history records are shown in Figures (4-54) and (4-55). For a ductility μ equals to 15, the base moment exceeds the ultimate capacity of the piers six times. This is due to the formation of real hinges in 40% of the connecting beams. For a ductility μ equals to 500, the base moment exceeds the ultimate capacity only twice. Therefore, the need for high rotational ductility factor for the connecting beams is evident if only moderate damage is expected under strong ground shaking.

The axial force time-history is shown in Figures (4-56) and (4-57). In the case where $\mu=15$, the formation of real hinges in 40% of the connecting beams reduces the axial force as shown in Figure (4-56). On the other hand, the piers are subjected to large tensile axial forces in the case of high ductility connecting beams, as shown in Figure (4-57).

Listed below are the maximum values of the parameters of interest discussed above for the exterior wall.

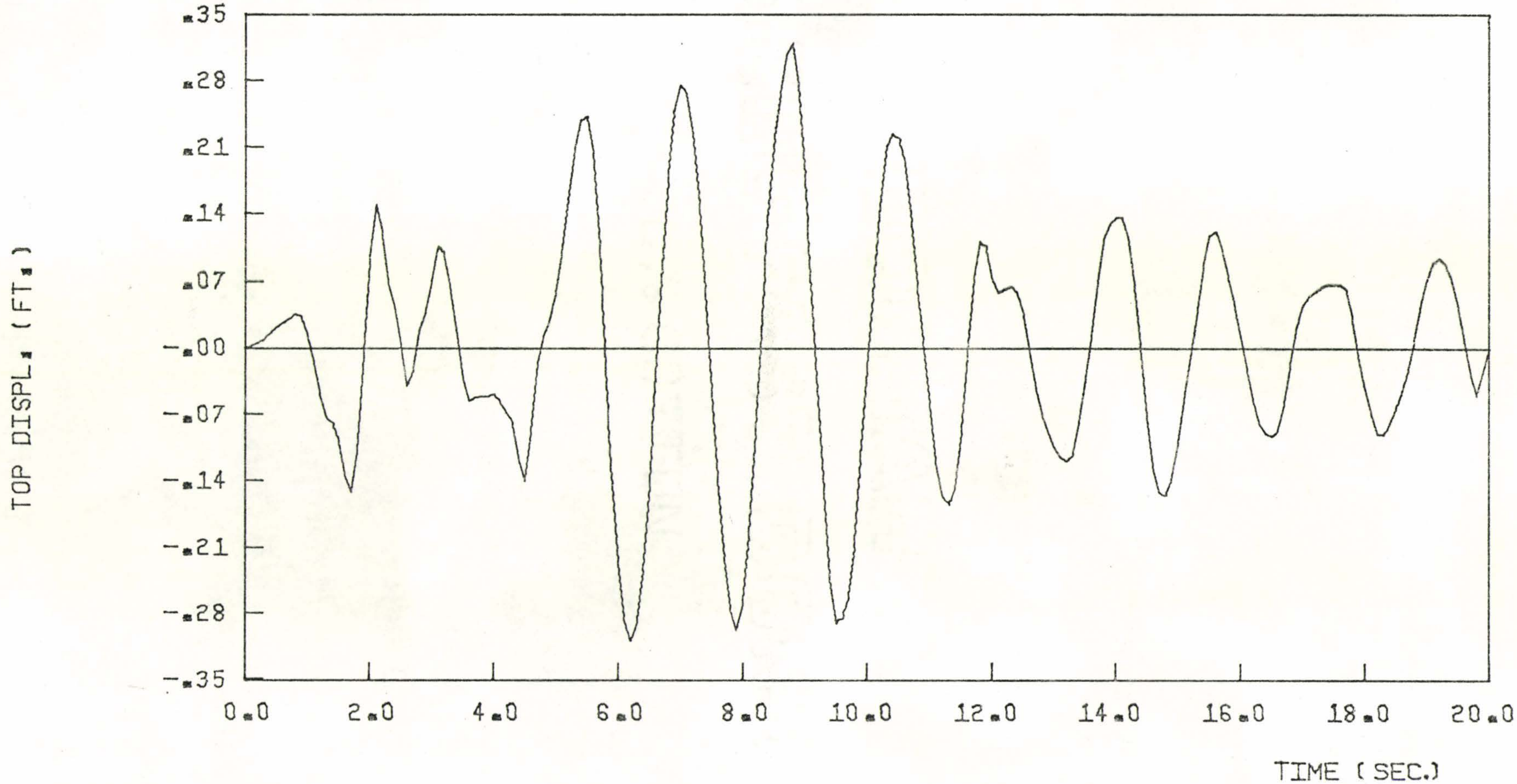

DUCTIL. OF CON. BEAMS = 15. , EXTERIOR WALL (8% g)

FIG. 4_52 TOP DISPL. , ELCENTRO COMP. NORTH

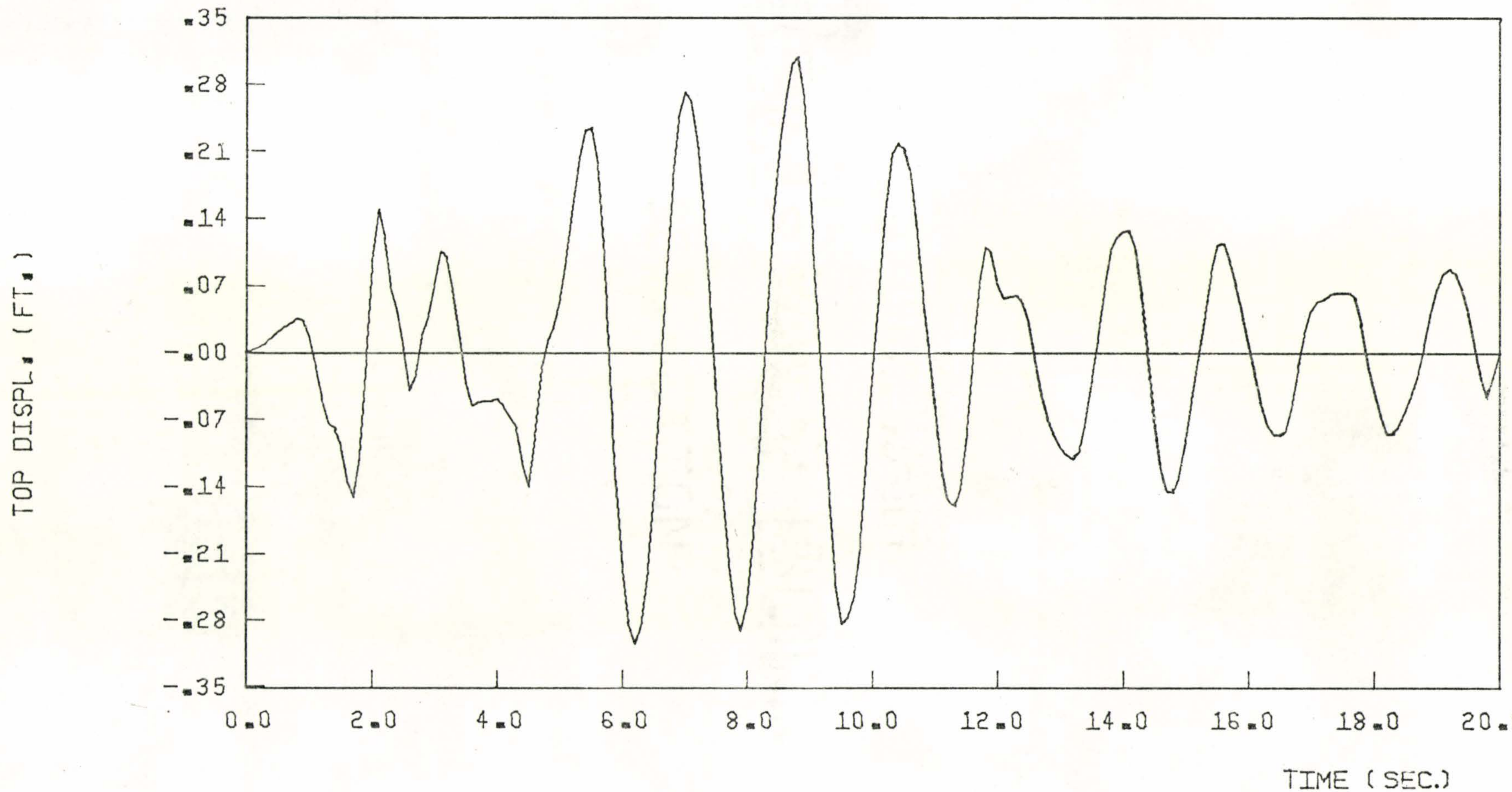

DUCTIL. OF CON. BEAMS = 500. , EXTERIOR WALL (8% g)

FIG. 4_53 TOP DISPL., ELCENTRO COMP. NORTH

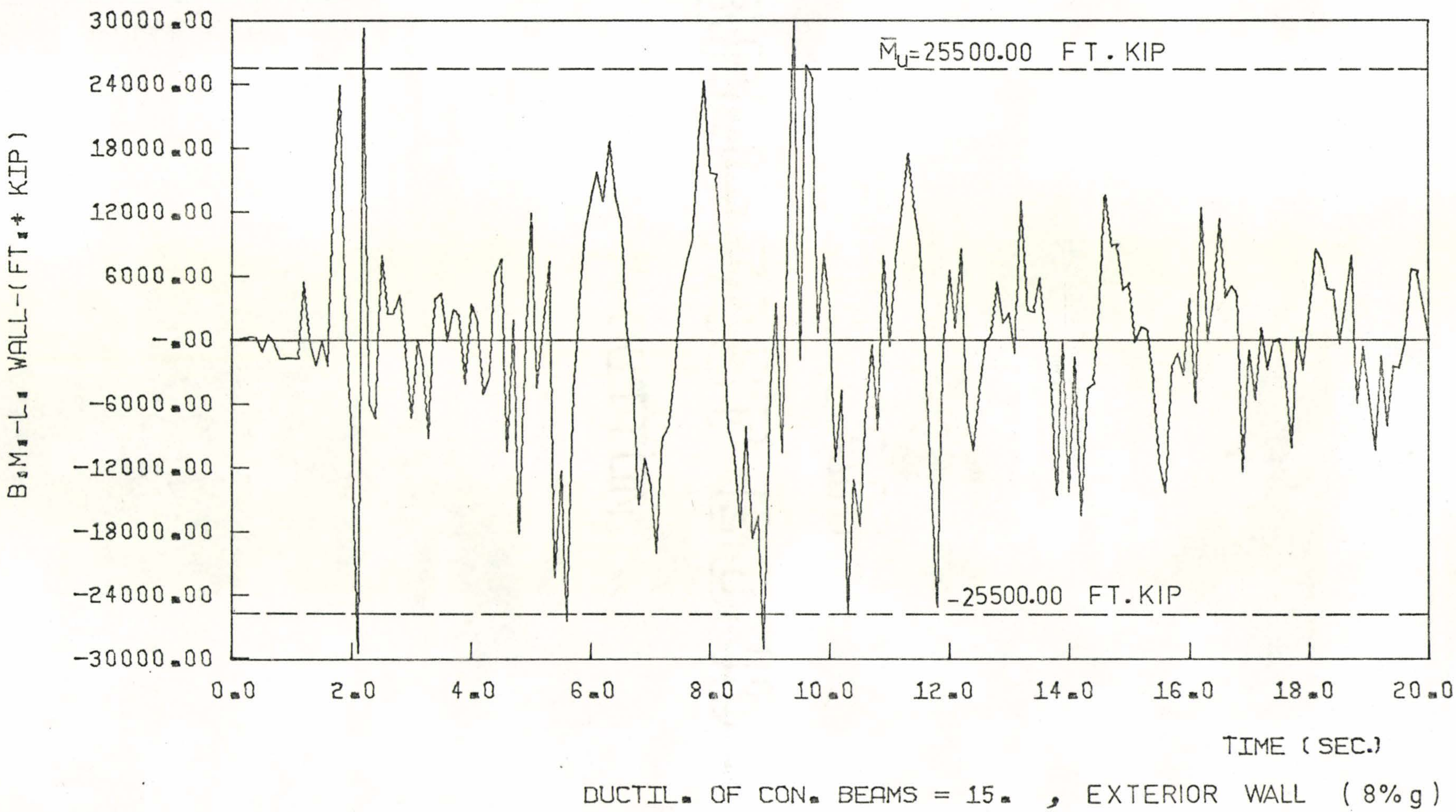

FIG. 4_54 B.M.L.WALL, ELCENTRO COMP. NORTH

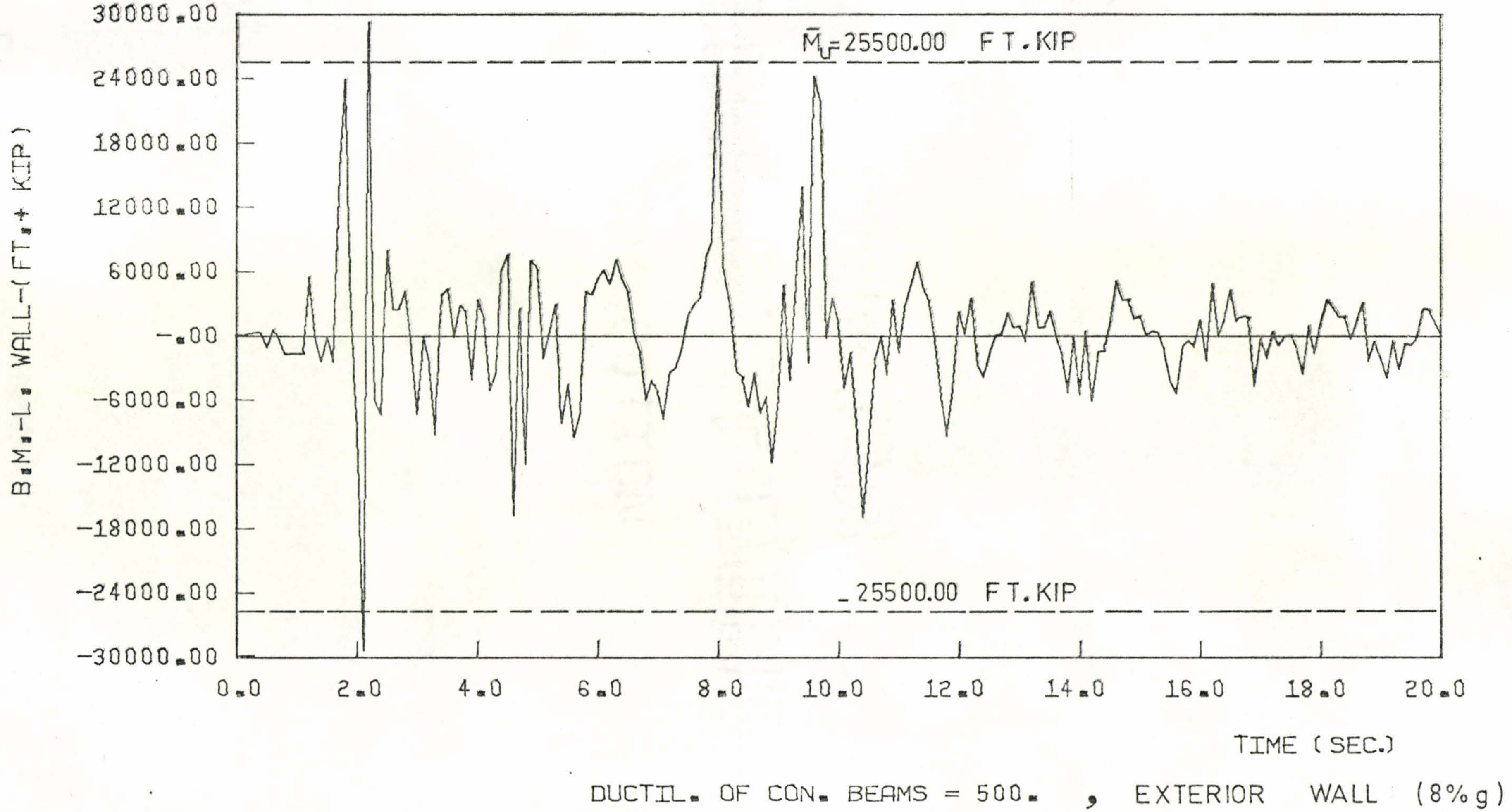

FIG. 4_55 B.M.L.WALL, ELCENTRO COMP. NORTH

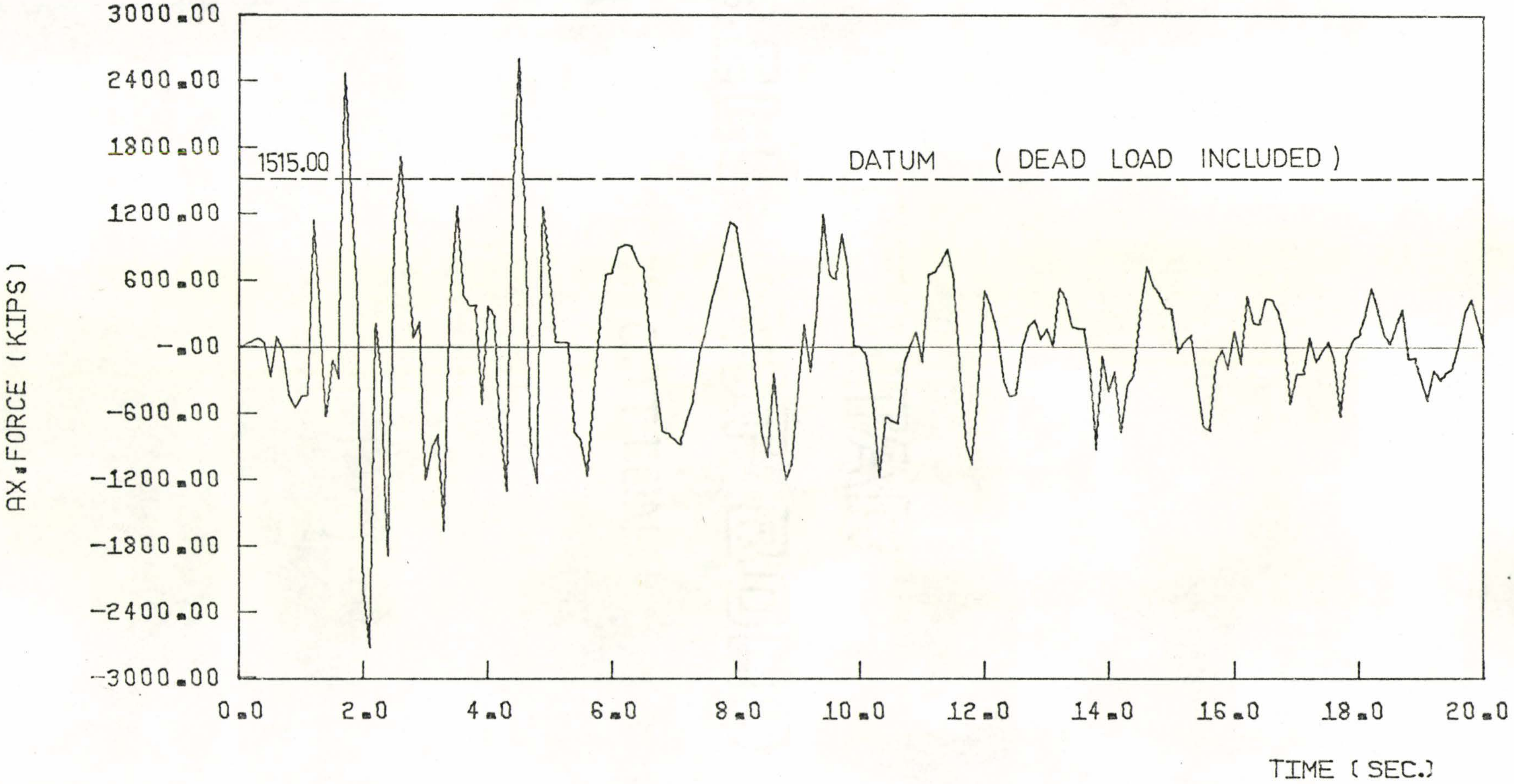

DUCTIL. OF CON. BEAMS = 15. , EXTERIOR WALL (8%g)

FIG. 4_56 AX. FORCE , ELCENTRO COMP. NORTH

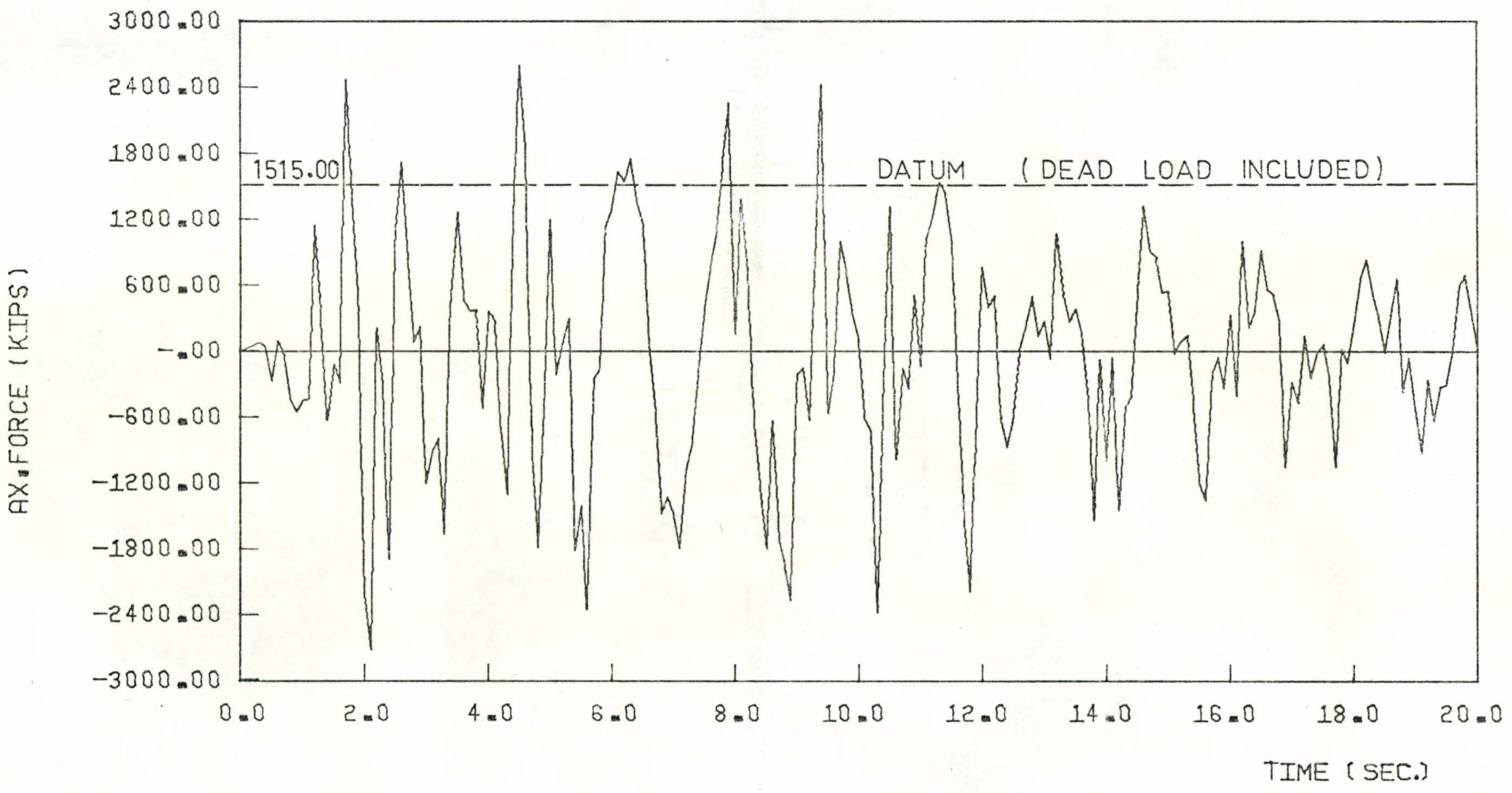

DUCTIL. OF CON. BEAMS = 500. , EXTERIOR WALL (8% g)

FIG. 4_57 AX. FORCE , ELCENTRO COMP. NORTH

Ground Acceleration (Duration = 20 sec.)	Ductility of Connecting Beams (μ)		
	5	15	500
ELCENTRO, COMP. N.S. (1940)	0.241 Ft	0.241 Ft	0.241 Ft
SAN FERNANDO, Wilshire Blvd., Basement, COMP. N.S.	0.280 Ft	0.266 Ft	0.266 Ft
TAFT, COMP. N21E (1952)	0.309 Ft	0.309 Ft	0.309 Ft

Table (4-10) Maximum Top Displacement, Exterior Wall Designed for 16% g

Ground Acceleration (Duration =20 sec.)	Ductility of Connecting Beams (μ)		
	5	15	500
ELCENTRO, COMP. N.S. (1940)	34.7×10^3 K.ft	34.7×10^3 K.ft	34.7×10^3 K.ft
SAN FERNANDO, Wilshire Blvd., Basement, COMP. N.S.	34.3×10^3 K.ft	38.3×10^3 K.ft	38.3×10^3 K.ft
TAFT, COMP. N21E (1952)	45.2×10^3 K.ft	45.2×10^3 K.ft	38.2×10^3 K.ft

Table (4-11) Maximum Base Moment (Left and Right Piers) Exterior Wall Designed for 16% g

Ground Acceleration (Duration = 20 sec.)	Ductility of Connecting Beams (μ)					
	5		15		500	
	Tension	Comp.	Tension	Comp.	Tension	Comp.
ELCENTRO, COMP. N.S. (1940)	1.55×10^3 K	4.1×10^3 K	1.55×10^3 K	4.1×10^3 K	1.55×10^3 K	4.1×10^3 K
SAN FERNANDO, Wilshire, Basement, COMP. N.S.	2.03×10^3 K	4.68×10^3 K	2.03×10^3 K	4.68×10^3 K	2.03×10^3 K	4.68×10^3 K
TAFT, COMP. N.S. (1952)	2.01×10^3 K	4.66×10^3 K	2.07×10^3 K	4.72×10^3 K	2.07×10^3 K	4.72×10^3 K

Table (4-12) Maximum Axial Force at the Base of the Piers, Exterior Wall Designed for 16% g

Ductility of Connecting Beams μ	Max Top Displacement (Ft.)	Max Base Moment (Ft.Kip)	Max Axial Force at Base (Kip)	
			Tension	Compression
5	0.34	48.3×10^3	1.3×10^3	4.31×10^3
15	0.32	30.0×10^3	1.3×10^3	4.31×10^3
500	0.31	30.0×10^3	1.1×10^3	4.13×10^3

Table (4-13) Exterior Wall Designed to resist Maximum Horizontal Acceleration of 8%g, ElCentro Comp. N.S. Normalized to 16% g

The effect of the ductility of connecting beams is significant when the coupled shearwall is subjected to earthquake of intensity higher than that used in designing the wall. Although the maximum values presented in Table (4-13) for the two cases of μ equals to 15 and 500 seemed to be the same, the repetition of the maximum values exceeding the ultimate capacity in case of μ equals 15, as shown in Figure (4-54), is of great significance to the ultimate survival of the structure.

4.8 Overall Behaviour

This section studies the relation between the overall ductility demand of the studied coupled shear walls μ overall and the connecting beam rotational ductility factor μ. The formation of the real and plastic hinges at the connecting beams and the corresponding time of the maximum number of these hinges are also presented in this section.

The overall ductility for a ductile shear wall has a value ranged from 4.0 to 5.0. The overall ductility demand is defined by

$$\mu_{overall} = \frac{\Delta u}{\Delta y} \qquad (4\text{-}3)$$

where Δu = maximum top displacement response.

Δy = top displacement at the time in which the segments first change from elastic to inelastic, due to triangular static load.

Table (4-15) indicates that the connecting beams ductility factor μ is of minor influence when we use the definition of Δu as the maximum top displacement. It should be noted that the maximum value may occur after the formation of the real hinges in the connecting beams when the structure becomes more flexible. In general, for low connecting beam ductility, the overall ductility demand will be larger than that for high connecting beams ductility.

WALL	Ground Acceleration (Duration=20sec.) ft/sec^2	Ductility of Connecting Beams (μ)		
		5	15	500
Exterior wall	ELCENTRO, COMP. N.S. (1940)	1.63	1.63	1.63
	SAN FERNANDO, Wilshire Blvd., Basement, COMP. N.S.	1.91	1.81	1.81
	TAFT, COMP. N21E (1952)	2.11	2.11	2.11
Interior wall	ELCENTRO, COMP. N.S.	2.38	2.40	2.40
	SAN FERNANDO, Wilshire Blvd. Basement, COMP. N.S.	3.95	2.89	2.89

Table (4-14) Overall Ductility Demand of the Exterior and Interior Walls of the 20 Storey Building (Max. G. Acc.=16%g)

The damage happened in the walls of the 20 storey building due to the earthquakes loads is studied through the number of segments which are changed to the real hinged state and the maximum number of segments changed to the plastic hinged state. The maximum number of segments which are changed to real hinged segments is presented in Table (4-15) for the different connecting beams ductility factors. Only the cases associated with the TAFT record gave a heavy damage in the exterior walls designed to resist lateral seismic loads of 16%g maximum acceleration. This is because the repetition of the peaks in the TAFT record as shown in Figure (4-13). For the interior walls, the damage is heavier than that for the exterior walls when the ductility of the connecting beams is low.

The maximum number of segments which are changed to plastic hinged segments and the first time at which such number occurs is tabulated in Table (4-16). The number of occurrance of such number is given in Table (4-16) as well. It can be seen from Table (4-16) that the interior walls will suffer more than the exterior walls (16%g), although the later share more than the former in resisting the lateral seismic loads. This is due to the low bending capacity of the connecting slabs in the interior walls.

The exterior walls designed to resist lateral seismic loads of 8%g suffer heavy damage when the ductility of the connecting beams is moderate or low, while the damage is slight for very high value of connecting beams ductility. Therefore, the rotational ductility factor μ has more influence in improving the coupled shear wall behaviour when subjected to earthquakes having intensities higher than the design intensity.

A segments state time-history is shown in Figure (4-58) for the exterior wall designed to 16%g maximum horizontal ground acceleration under the Taft earthquake record. The rotational ductility factor μ is taken as 15.0. The six peaks shown in Figure (4-13) occur at the following times: 3.7, 4.2, 6.2, 6.4, 6.6, and 9.1 seconds. The damage pattern is shown in Figure (4-58) at the corresponding time stations. The first three peaks cause only plastic hinges, while the other peaks cause the real hinges to form. This is because the last three peaks are accompanied with high ground velocities. After the last change in segments state happened at 9.1 seconds, the structure behaves elastically to the end of the analysis. This is due to the flexibility resulted from the lower three segments which are changed to real hinged segments.

WALL	Ground Acceleration (Duration=20 sec.)	Ductility of Connecting Beams (μ)					
		5		15		500	
		Number	Time*	Number	Time*	Number	Time*
Ext.Wall (8%g)	ELCENTRO, COMP. N.S. (1940)	2	4.6	2	5.00	0	-
Exterior Wall (16%g)	ELCENTRO, COMP. N.S. (1940)	0	-	0	-	0	-
	SAN FERNANDO, Wilshire Blvd., Basement, COMP. N.S.	1	4.10	0	-	0	-
	TAFT, COM. N21E (1952)	3	6.40	3	9.10	0	-
Interior wall	ELCENTRO, COMP. N.S. (1940)	3	4.70	0	-	0	-
	SAN FERNANDO, Wilshire Blvd., Basement, COMP. N.S.	4	7.90	0	-	0	-

* Time at which that number occurs (seconds)

Table (4-15) Max. No. of Segments which are changed to Real Hinged Segments

20 Storey Building

WALL	Ground Acceleration (Duration=20 sec.)	Ductility of Connecting Beams (μ)								
		5			15			500		
		Np*	Time‡	N_R·	N_P	Time	N_R	N_P	Time	N_R
Ext.Wall (8%g)	ELCENTRO, COMP.N.S. (1940)	3	2.10	1	3	2.10	1	3	2.10	1
Exterior Wall (16%g)	ELCENTRO, COMP.N.S. (1940)	2	1.70	1	2	1.70	1	2	1.70	1
	SAN FERNANDO, Wilshire Blvd., Basement, COMP. N.S.	3	2.80	2	3	2.80	2	3	2.80	2
	TAFT, COMP. N21E (1952)	3	4.20	2	3	4.20	2	3	4.20	3
Interior Wall	ELCENTRO, COMP.N.S. (1940)	4	1.70	1	5	8.40	4	5	8.40	4
	SAN FERNANDO, Wilshire Blvd., Basement, COMP. N.S.	5	6.30	1	5	6.30	4	5	6.30	4

*N_P = Maximum Number of plastic hinges

‡Time at first change to such number

.N_R = Number of occurrance

Table (4-16) Max. No. of Segments which are Changed to Plastic Hinged Segments 20 Storey Building

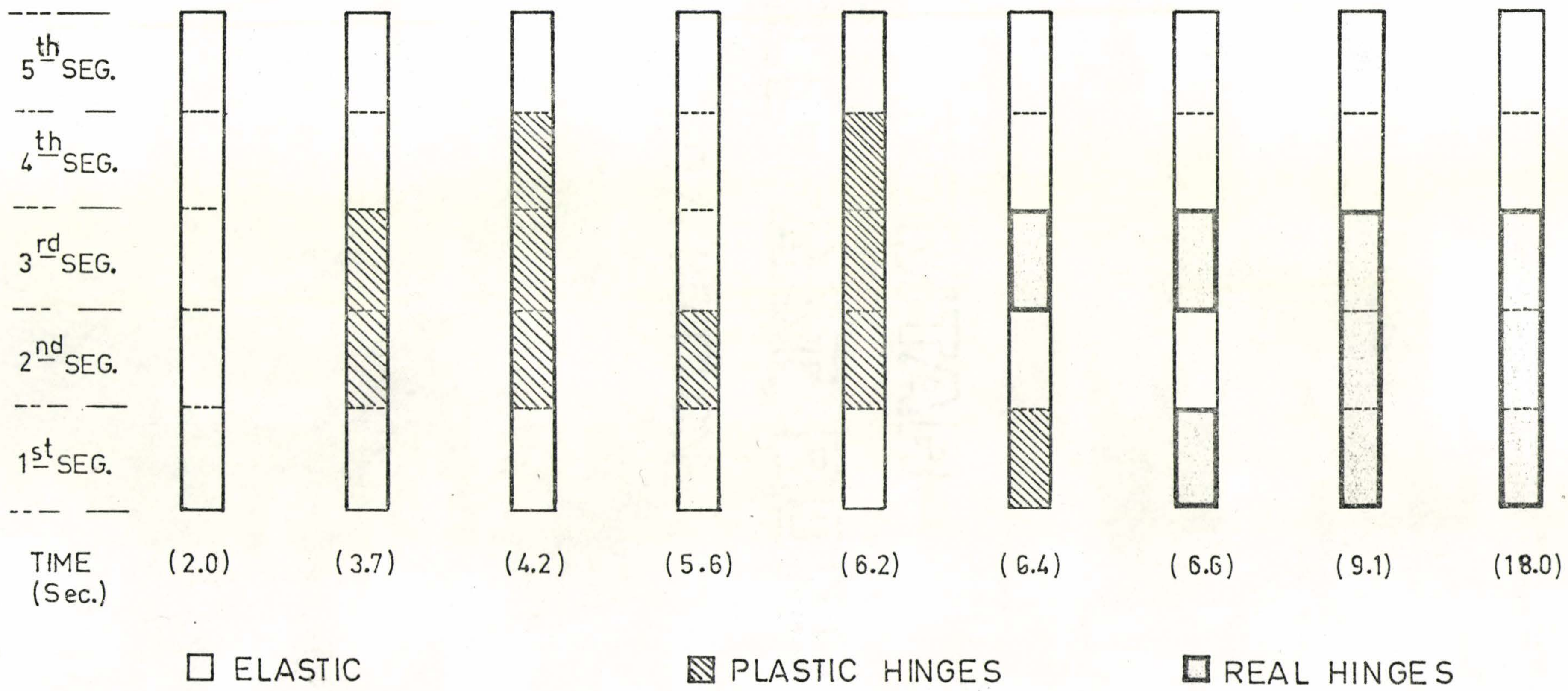

FIG. 4_58 SEGMENTS STATE TIME_HISTORY FOR THE EXTERIOR WALL, $\mu = 15.0$
(TAFT, COMP. N 21 E)

CHAPTER 5

CONCLUSIONS AND RECOMMENDATIONS

5.1 Conclusions

The following conclusions are drawn based on the work presented above.

(1) The continuum approach in combination with the transfer matrix technique can provide an efficient means to obtain a full time-history response to ground motions. The proposed method is capable of handling plane non-uniform coupled shear wall structures subjected to any ground acceleration. The effect of flexible foundation can be incorporated in the analysis. Complexity in the structural configuration and/or the inelastic regions are conveniently handled by dividing the structure into a series of segments where each segment has uniform structural properties within itself. Independent of the number of storeys of the structure or the number of segments into which the walls are to be divided, the resulting transfer matrices are six by six matrices. Therefore, computers with limited memory capacity can be used to analyze high rise buildings using the proposed method.

(2) The P-Δ Effect appears to have a minor influence in the coupled shear walls stiffness. This is due to the piers

are assumed to remain elastic throughout the analysis. With possible plastic deformations in the walls, the P-Δ Effect may be important. This aspect requires further investigation.

(3) For a twenty storey building, five lumped mass dynamic model is shown to be adequate. The response of the five mass system is found to be very close to the response of ten mass system, while the computation costs for the former is only one quarter the computation costs for the later.

(4) For a uniform building with walls of different stiffness, if the masses of the building are to be distributed uniformly throughout the height in accordance with the wall stiffnesses, only the fundamental periods of the walls will be the same. The periods of the other modes will be different. To obtain identical periods for all modes in the walls, it becomes necessary to distribute the masses non-uniformly along the height of each wall, even though the building as a whole is a uniform building.

(5) For the same building, under the same ground motions, the walls coupled by floor slabs (flexible connection) suffer more damage than those coupled by stiff connecting beams, although the latter share more in resisting the lateral earthquake loads.

(6) Due to the high shearing force transmitting capacity of the connecting beams, the axial force in the piers due to

lateral load may exceed the dead load carried by each pier. In such a case a tensile force will occur at the base of the pier. This situation is particularly serious for end walls where the coupling deep beam is stiff and yet the tributary area for gravity load is small.

(7) Based on the present limited study, it shows that the model structure will suffer light damage if it is exposed to earthquake having the same intensity as that used in designing the coupled shear wall according to the NBCC [10] and the ACI Code [1]. On the other hand, if the wall is exposed to earthquake having a higher intensity compared with the design earthquake, a heavy damage may occur even in the piers for rotational ductility factor μ equals to 15.

(8) The improvement gained in the coupled shear wall behaviour by increasing the rotational ductility factor of the connecting beams is noticeable when the wall is exposed to strong earthquakes, while this improvement is limited when the wall is exposed to moderate earthquakes.

5.2 Recommendations

The following points require further investigations.

(1) Detailed modeling techniques such as the use of cracked sections, strain hardening as exhibited by steel, deteriorate stiffness due to the cyclic loading of concrete members are useful to incorporate into the analysis to

obtain more realistic results.

(2) To avoid any tensile forces to be existing in the piers, it is necessary to increase the dead load carried by the piers when the coupling beams have stiff connecting beams. This can be done by arranging the walls in such a way keeps the tributary area proportional to the wall stiffness for all the walls.

APPENDIX A

DESIGN CALCULATION FOR EXTERIOR AND INTERIOR WALLS IN EXAMPLE BUILDINGS

For the multi-storey building shown in Figure (4-1), the straining actions at the base of the piers are to be calculated according to National Building Code of Canada for 16% g and for 8% g seismic loading. The two coupled shear walls given in Chapter 4 are considered in this Appendix, the first will be designed to 16% g, while the second example will be designed twice, once for 16% g and the other for 8% g seismic loading.

The two walls are designed to resist the dead load, live load and earthquake loads. The critical design sections for each wall are the connecting beams cross section, and the piers cross section at base.

As the earthquake loads are to be distributed according to the walls stiffnesses, it is necessary to estimate from the beginning the stiffnesses of these walls. The overall stiffness of the wall is affected by the stiffness of the connecting beams which can be represented by the factor α, where

$$\alpha^2 = \frac{12 I_p}{h c^3} \left[\frac{\ell^2}{I} + \frac{A}{A_1 A_2}\right] \qquad \text{(A-1)}$$

where

$$I = I_1 + I_2$$

$$A = A_1 + A_2$$

$$h = \text{Storey height}$$

and I_p = Moment of inertia of connecting beams.

A-1 Stiffness of the Connecting Beams

a- Exterior Wall

Let us consider the connecting beams are doibly reinforced concrete cross section. Taking

$$E_s = 29x10^3 \text{ Ksi} \ , \ E_c = 3.5x10^3 \text{ Ksi}$$

$$, \ f'_c = 4 \text{ Ksi and } f_y = 60 \text{ Ksi}$$

We have $A_s - A'_s = 0$

So neglect A_s' in getting $\bar{M}_u$

$$A_{s_b} = A_c[0.85x\frac{f'_c}{f_y}xKx\frac{87000}{87000+f_y}] \quad \text{(A-2)}$$

$$= 2.85\% \ A_c$$

Trying 4#9 (A_s = 4 in^2)

$$\therefore A_s/A_{s_b} = 70\% \text{ .. O.K.}$$

$$A_s\text{-}A_c = 2\%$$

To obtain the Comp. zone, Figure (A-1)

$$a = \frac{A_s\ f_y}{0.85 f'_c . b} = 7.8 \text{ in}$$

<u>Ultimate Bending Moment Capacity</u>

$$\bar{M}_u = A_s\ f_y\ (d - a/z)$$

$$= 4 \times 60000 \times 18.1 = 43.45 \times 10^5 \text{ in.lb}$$

$$= \underline{362.0 \text{ ft.Kip}}$$

$$,\quad q_p = 2\bar{M}_u/(c.h) = 2 \times 362/(5 \times 8.75) = \underline{16.0 \text{ Kip/ft}}.$$

<u>I Cracked</u>

$$e = \frac{7.8 \times 9 \times 8.1}{22 \times 9 \left(\frac{7.8}{22} + \frac{2.0 \times 2}{100} \times \frac{29}{3.5}\right)} = 4.1''$$

$$I_{cr} = \frac{7.8^{3} \times 9}{12} + 9 \times 7.8 \times \frac{2}{4.0} + \frac{29}{3.5} \times 4 \left[\frac{2}{5.9} + \frac{2}{14.1}\right]$$

$$= \underline{0.4575 \text{ ft}^4}$$

<u>Check for Tension Steel</u>

$$\varepsilon_s = 0.003 \times [22 - (7.8/0.85)]/(7.8/0.85) = 0.00425$$

$$f_s = 0.00425 \times 29000000 = 129000 \; p_{si}$$

$$= 129 \; K_{si} > f_y$$

$\therefore$ Steel yields.

Check for Comp. Force

C = 7.8 x 9 x 0.85 x 4 = 240 Kip #

T = 4 x 6000 = 240 Kip # O.K.

Factor α H_T

$$\alpha^2 = \frac{12x0.4575}{8.75x(5)^3}\left[\frac{\overline{22.5}^2}{670} + \frac{26.25}{(13.125)^2}\right] = 0.00455 \; ft^{-2}$$

$\therefore$ αH_T = 0.0675 x 87.5 = 5.9 (moderately coupled wall)

b - Interior Wall

From [7] , with the following dimensions

$L = 5'$, $\frac{L}{X} = 0.125$ and $Y/X = 0.5$

, see Figure (A-2).

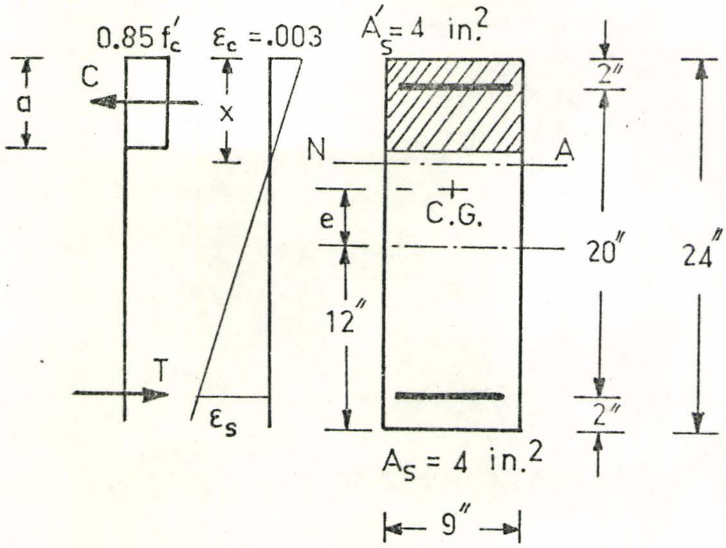

FIG. A_1 STRESS_STRAIN DISTRIBUTION FOR CONNECTING BEAMS OF THE EXTERIOR WALL

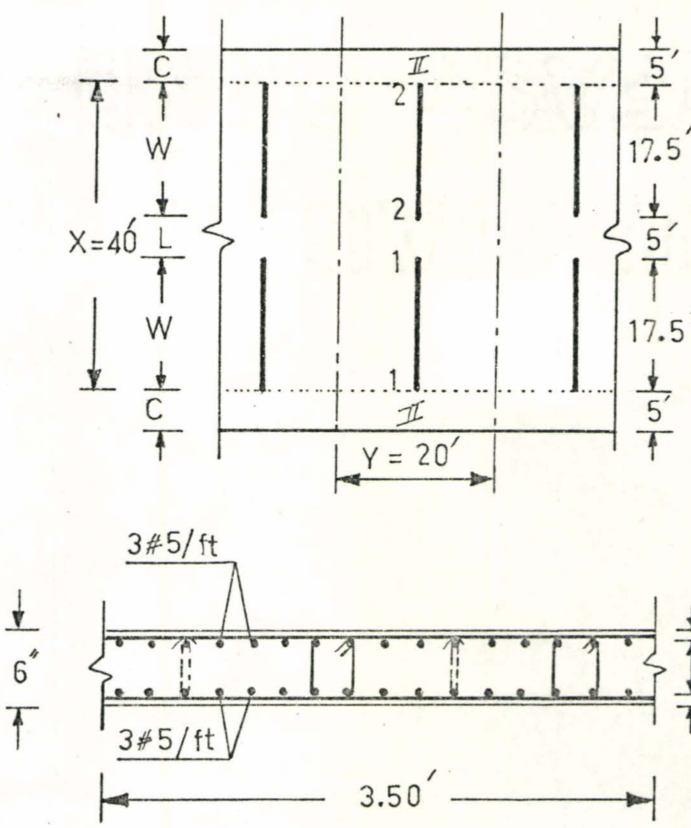

FIG. A_2 CONNECTING SLABS OF INTERIOR WALLS

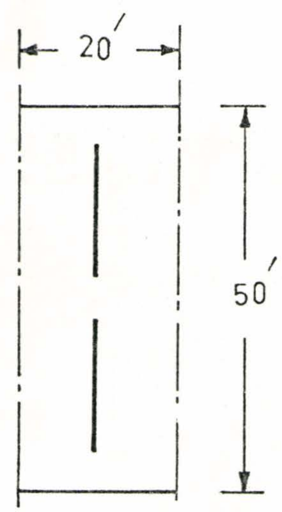

FIG. A_3

TRIBUTARY AREA FOR INTERIOR WALLS

$\therefore \quad Y_e/Y = 0.175$

$\therefore \quad Y_e = 0.175 \times 20$

$= 3.5$ ft.

$A_{s_b} = 2.85\% \; A_c$

Take $\quad A_s \simeq 0.5 \; A_{s_b}$

$\simeq 15\% \; A_c$

$= 3.15 \text{ in}^2$

Take $\quad 3\#5/ft' = 3.2 \text{ in}^2$

$\therefore \quad \frac{A_s}{A_c} = 1.525\%$

$a = 1.34$ in

$\therefore \quad \bar{M}_u = 58.5$ K.ft.

$\therefore \quad q_p = \underline{2.68 \text{ K/ft.}}$

I Cracked

$e = 1.2$ in

$I_{cr} = \underline{0.0235 \text{ ft}^4}$

Check for Tension Steel

$$\varepsilon_s = 0.00652$$

$$f_s = 189\ K_{si} > f_y \qquad \text{O.K. yielded}$$

Check for Comp. Force

$$C = 1.34 \times 42 \times 0.85 \times 4 = 192 \text{ Kips \#}$$

$$T = 3.2 \times 60 = 192 \text{ K9ps \#}$$

Factor αH_T

$$\alpha^2 = \frac{12\text{x}0.0235}{8.75\text{x}(5)^3} \left[\frac{\overline{22.5}^2}{670} + \frac{26.25}{(13.125)^2}\right] = 0.000234 \text{ ft}^{-2}$$

$$\therefore \alpha H_T = 0.0153 \times 87.5 = \underline{1.34} \qquad \text{(Flexible coupled Wall)}$$

A.2 Limit States Design

The factored load combinations shall be equalled to

$$\gamma[\alpha_D D + \psi(\alpha_L L + \alpha_Q Q + \alpha_T T)] \qquad \text{(A-3)}$$

where

* α_D = 1.25 or in case of over turning, uplift and stress reversal 0.85 ,

α_L = 1.5 ,

α_Q = 1.5 , and

α_T = 1.25

* ψ = 1.0 when only 1 of the loads L, Q and T acts,

  ψ = 0.7 when 2 of the loads L, Q and T act, and

  ψ = 0.6 when all the loads L, Q and T act.

* γ = 1.0 for all buildings, except as provided in Clause (b) - 4.1.4.2 (5), N.B.C. (1975).

<u>Coupled Shear Wall II - II</u>

<u>Dead Loads</u>

- <u>Own Wt.</u>

$$0.75 \times 17.5 \times 2 \times 0.150 = 3.92 \text{ K/ft}$$

- <u>Slabs</u> :- Figure (A-3)

  Cover = 30 lb/ft^2

  Slabs wt. = 0.5 x 150 = 75 lb/ft^2

$\therefore$ Reaction of slab on the coupled shear wall = (0.03+0.075) x50x20

= 105 Kip/Storey

- <u>Partitions</u>

Assume the total wt. of the partitions ≃ total wt. of walls

$\therefore$ Total D.L./storey = 105+3.92x2x8.75 = 105+68.5

= <u>173.5 Kips</u>

$\therefore$ Total D.L. at G.L. = <u>1735 Kips</u>

Live Loads

* As the coupled shear wall supports an area of floor and roof > 900 ft^2

  ∴ Multiplied factor equals to $0.5+15/\sqrt{A} = 0.975$

* For Residental Areas

  40 psf in the min. design load for apartments, hotels...

  20 psf in the min. design load for roofs.

  20 psf in the min. design load for snow for roofs with a slope of 30 deg. or less.

∴ L.L. (1st floor → 9th floor) = (.040x20x40+0.100x20x10) 0.975

= 50.7 Kips

& L.L. (10th floor - roof) = (.040x20x50)0.975

= 39.0 Kips

∴ Total L.L. at G.L. = 50.7x9+39 = 495 Kips

& Max. O.T.M. at G.L. = (5x20x0.1x22.5x9+20x20x0.04x10x9 +25x20x0.04x12.5)x0.975

= 3625 K.ft

Coupled Shear Wall I-I

Dead Loads

- Own Wt. 3.92 K/ft.
- Slabs 52.5 K/storey
- Partitions ≃ 3.92 K/ft.

Total D.L./storey = 52.5+3.92x2x8.75 = 121 Kips

Total D.L. at G.L. = 1210 Kips.

Live Loads

Total L.L. at G.L. = 254 Kips.

Max. O.T.M. at G.L. = 1855 K.ft.

Whole Building

Effect of Earthquakes

The base shear Q can be determined from the following equations

$$Q = A.S.K.I.F.W$$

where

A = percentage of the gravity acceleration g 0.16 as upper limited in Vancouver area with probability of annual exceedance equals to 0.005, NBC commentary J [10].

, S = Seismic Response factor $(0.5/3\sqrt{T})$ (A-4)

, T = Period of the structure $(0.05h_n/\sqrt{D})$ (A-5)

$= 0.05 \text{x} 87.5/ 40 = \underline{0.69 \text{ sec.}}$

$\therefore$ S $= 0.5/\sqrt[3]{0.69} = \underline{0.565}$

, K = Structural factor (1.0 for ductile shear wall)

, I = Important factor (1.0 for ordinary structures)

, F = Foundation factor (1.3 for dense sand)

And W = Weight of the structure + Snow for roofs

$= (7x1735+3.92x8.75x10+50x140x0.02)$ = <u>12627 Kips.</u>

$\therefore$ $Q = 0.16x0.565x1.0x1.0x1.3x12627$ = <u>1465 Kips.</u>

As $h_n/D_s < 3$ $\therefore$ No concentrated force at top.

As the storey height is constnat with the height and the masses at slab levels are equal

$$\therefore F_x = (Qh_x / \sum_{i=1}^{n} h_i)$$

$$\sum_{i=1}^{n} h_i = (1+2+3+4+5+6+7+8+9+10)8.75 = 55x8.75 \text{ ft.}$$

$\therefore$ $F_1 = 1465 \text{ x } \frac{1}{55} = \underline{26.6K}$

, $F_2 = \underline{53.5K}$, $F_3 = \underline{79.9K}$, $F_4 = \underline{106.6K}$, $F_5 = \underline{133.2K}$

, $F_6 = \underline{159.8K}$, $F_7 = \underline{186.4K}$, $F_8 = \underline{213.2K}$, $F_9 = \underline{239.8K}$

And $F_{10} = \underline{266.4K.}$

As $T = 0.69$ sec. $(0.5<T\leqslant1.5)$ $\therefore$ $J = 1.1-0.2+0.69$

$= \underline{0.962}$

The reduced overturning moment and the shearing force diagrams are given by Figure (A-4)

* As $\alpha H_{T_{I-I}} \approx 4.5\ \alpha H_{T_{II-II}}$

$\therefore$ The stiffness of wall I-I is much bigger than the stiffness of wall II-II. So, assume the stiffness of wall I-I equals to three times the stiffness of wall II-II.

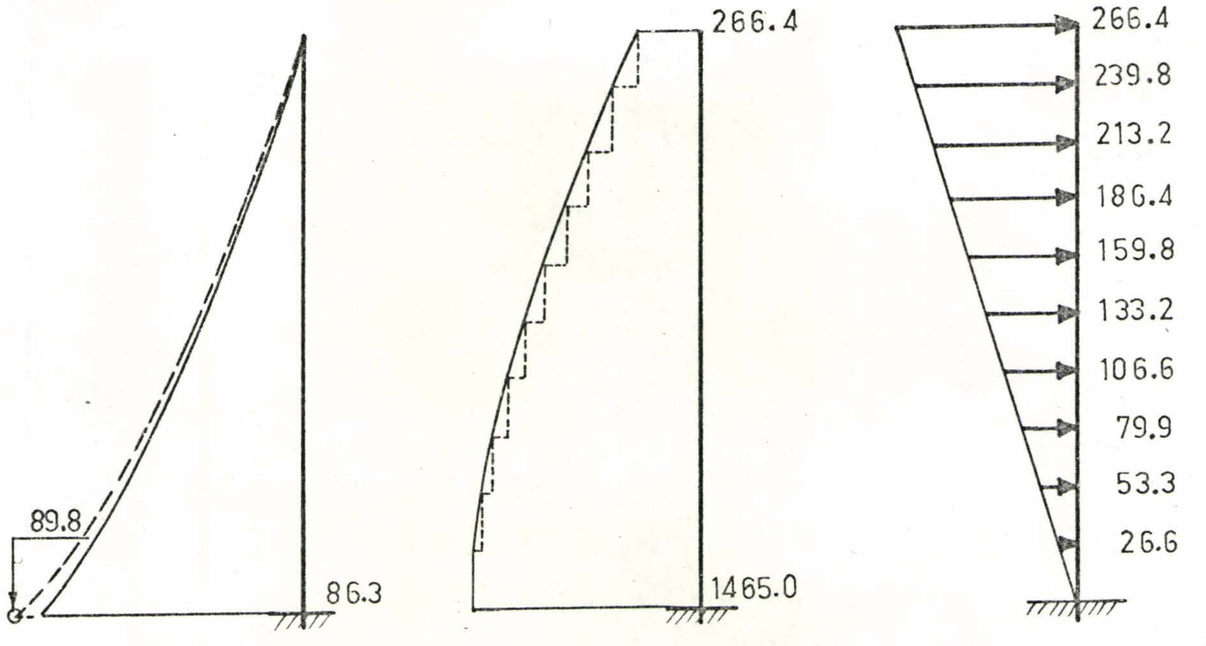

FIG. A_4 LOADING AND STRAINING ACTIONS (EARTHQUAKE EFFECT)

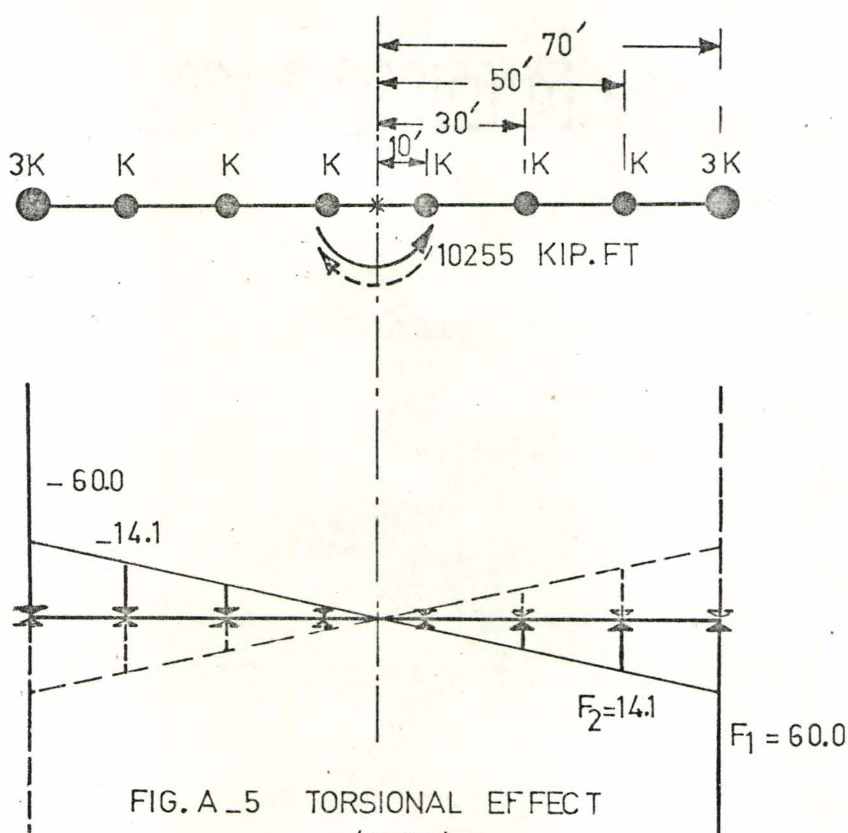

FIG. A_5 TORSIONAL EFFECT
(KIPS)

$\therefore$ The effect of Earthquake on wall I-I $= \frac{3}{(2x3+7)}[86300]$

$= \underline{1995 \text{ K.ft}}$

And the effect of earthquake on wall II-II

$$= \frac{1}{13}[86300] = \underline{665 \text{ K.ft}}$$

Effect of Torsion

For symmetrical plan as given by Figure (A-5) the accidental torsion must be considered. Equation (A-6) gives the accidental torsion moment.

$$M_T = e_x V$$

where V = Base shear

= 1465 Kip.

$e_x = 0.05B$

= 7.0 ft.

$$\therefore M_T = 7x1465 = \underline{10255 \text{ Kip.ft.}}$$

From Figure (A-5)

$$\sum nx^2 = (6*7^2+2*5^2+2*3^2+2*1^2)x100$$

$$= (294+50+18+2)100$$

$$= 36400 \text{ ft}^2$$

$$\therefore \quad F_1 = \frac{\pm 10255 \times 3 \times 70}{36400}$$

$$= \underline{\pm 60 \text{ Kip.}} \text{ (at base)}$$

$$F_2 = \frac{\pm 10255 \times 50}{36400}$$

$$= \underline{\pm 14.1 \text{ Kip.}}$$

$$\therefore \; M_{II_{Total}} = 1995*(1+\frac{13 \times 60}{3 \times 1465}) = 23500 \text{ Kip. ft.} \quad \text{(17\% increase)}$$

$$M_{II\ II_{Total}} = 665*(1+\frac{13 \times 14.1}{1465}) = 7450 \text{ Kip.ft.} \quad \text{(12.4\% increase)}$$

<u>Thermal Effect:</u> Neglected

<u>Design Tables</u>

$$\gamma = 1.0 \quad , \; \alpha_L = \alpha_Q = 1.5$$

Wall	I-I (Exterior)							II-II (Interior)						
Load Combination	D	D+L		D+Q		D+L+Q		D	D+L		D+Q		D+L+Q	
ψ	1.0	1.0		1.0		0.7		1.0	1.0		1.0		0.7	
α_D	1.25	1.25	0.85	1.25	0.85	1.25	0.85	1.25	1.25	0.85	1.25	0.85	1.25	0.85
Axial Force Kip	-1510	-1890	-1440	*-1510	**-1060	-1776	-1326	-2170	-2902	-2207	-2170	-1475**	*-2684	-1989
Shearing F. Kip	0	0	0	600	600	420	420	0	0	0	210	210	147	147
O.T.M. Kip.ft.	0	2785	2785	35250	35250	26600	26600	0	5440	5440	11200	11200	11650	11650

Table (A-1) Straining Actions at the Base, 10 Storey Building

* Critical for Over Stressing

** Critical for Over Turning

Walls Constants

$$^2 = \frac{\mu^2}{EI} \quad , \quad ^2 = \frac{\alpha^2 EI}{a+(I/A.a)} \quad , \quad I = I_1+I_2$$

and $\frac{1}{A} = \frac{1}{A_1} + \frac{1}{A_2}$

For both $A = 6.5625$ ft^2 , $I = 670$ ft^4

, $a = 22.5$ ft and $E = 3500$ K_{si}

Wall	αH_T	α^2	μ^2	γ^2	γ^2/α^2	Mov. st.	Mov. T	Tov. st.	Tov. T.
I-I	5.9	0.00455	394	0.000168	0.0370	35250	35250	±1305	±1305
II-II	1.34	0.000234	20.4	0.0000087	0.0370	11650	11200	±430*	±415*

* Bigger than T_{max}.

Table (A-2) Walls Constants and Axial Forces due to the O.T.M. at Base, 10 Storey Building

At base $T = \frac{\gamma^2}{\alpha^2} M_{(x=0)}$ $\quad |T| \ngtr |T_{max}|$ (A-6)

$T_{max} = \pm H_T * q_p$

Wall I-I: $T_{max} = \pm 87.5*16 = \pm 1400$ Kip.

Wall II-II: $T_{max} = \pm 87.5*2.68 = \pm 234.5$ Kip.

So from table (A-2) $T_{over\ stressing}$ and $T_{over\ turning}$ are bigger than T_{max} for wall II-II.

$$\therefore \quad T_{ov.st} = T_{ov.T} = \pm 234.5 \text{ Kip.}$$

For $I_1 = I_2$, $M_1 = M_2 = \frac{M - T.a}{2}$

Wall	Over stressing				Over turning			
	M_{max} K'	N_c K	M_c K'	N_{max} K	M_{max} K'	N_c K	M_c K'	N_{max} K
Wall I-I	2925	+550	1 2925	1 -2060	2 2925	2 +775	2925	-1835
Wall II-II	3185	-1107.5	3 3185	3 -1576.5	2735	-498.0	2735	-967.0

Table (A-3) Design Values, 10 Storey Building

1 & 3 - Check for Comp. in Concrete

2 - Check for A_s.

For the two walls the same cross section and reinforcement will be considered.

For the material properties chosen for the connecting beams

$$A_{s_b} = 2.85\% \ A_c$$

Choose $A_s = 0.3A_{s_b} = 0.854\%\ A_c$

$$= \frac{0.854x9x12x17.0}{100} = \underline{15.65\ in^2} \quad (12\#10)$$

The wall cross section is shown in Figure (A-8a)

$$A_{s_{act}} = 14.7\ in^2 \quad (0.285\ A_{s_b})\ \&\ (0.8\%\ A_c)$$

<u>Check</u>

$$A_{s_{Total}} = P_t.b.t \qquad \therefore\ P_t = \frac{1.6}{100} = \underline{0.016}$$

$$d/t = \frac{17.0}{17.5} = \underline{0.975}\ \&\ \frac{2}{t} = (\bar{M}/P)t = (M/P)/17.5$$

For the above three values we can use the interaction diagrams [24]

$$m = f_y/(0.85\ f_c') = \underline{17.65}$$

Wall	Pt.m	$\frac{e}{t}$	K	$P_u' = K.b.t.f_c'$	$M_u' = P_u'.e$	$\frac{\bar{P}_u}{P}$	$\frac{M_u'}{M}$	Comments
I-I (1)	0.2825	0.0815	0.860	6500	9250	3.15	3.15	F.O.S. =3.15
I-I (2)	-	-	-	-	-	-	-	P is a Tension Force
II-II(3)	0.2825	0.1160	0.835	6250	12600	3.98	3.98	F.O.S. =3.98

Table (A-4) Check for the Assumed Section, 10 Storey Building

For the Case (2) Wall I-I

$$P = +775 \quad , M = 2925$$

$$\therefore \; e = 3.78' \quad < \quad \frac{d-d'}{2}$$

$\therefore$ P acting inside the reinforced steel.

$\therefore$ Neglect the concrete, Figure (A-6)

To get the ultimate values, $\bar{P}_u$ and $\bar{M}_u$, we have the following equations

$$\bar{N}_u = 2A_s \, f_{s_1} = 29.4 \times f_{s_1} \qquad (i)$$

$$\bar{M}_u = A_s(d-d').f_{s_2} = 242.5 \, f_{s_2} \qquad (ii)$$

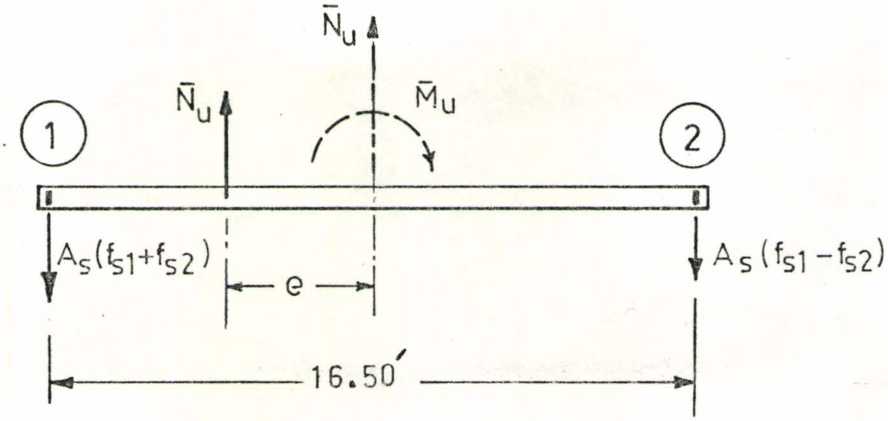

FIG. A_6 STEEL SECTION

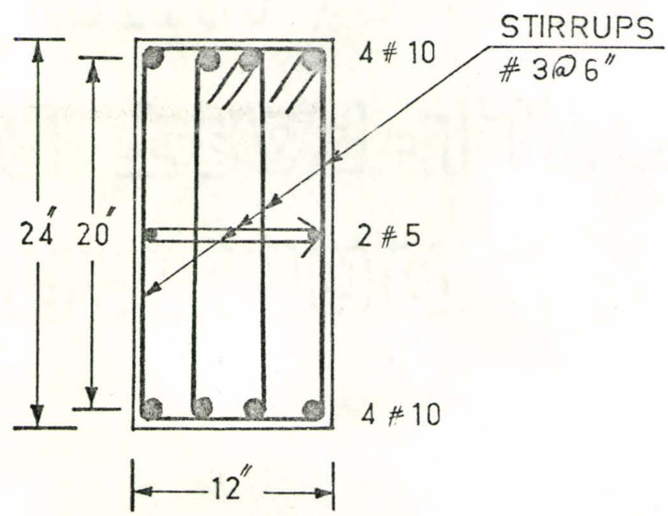

FIG. A_7 CONNECTING BEAMS CROSS SECTION, EXTERIOR WALL (20 STORY BUILDING , 16 %g)

$$f_{s_1} + f_{s_2} = f_y = 60 \qquad \text{(iii)}$$

$$\therefore \quad f_{s_1} = 60 - f_{s_2}$$

$$\bar{M}_u = \bar{N}_u . e = 3.78\ \bar{N}_u \qquad \text{(iv)}$$

$$\therefore \quad 3.78\bar{N}_u = 242.5\ f_{s_2}$$

$$\bar{N}_u = 29.4(60-f_{s_2}) = 1765 - 29.4\ f_{s_2}$$

$$= 1765-29.4\text{x}0.0156\ \bar{N}_u$$

$$\therefore \quad \bar{N}_u = \frac{1765}{1.46} = 1210$$

$$\text{F.O.S.} = \frac{\bar{N}_u}{P} = \frac{1210}{775} = \underline{1.57}$$

* Additional safety can be gained by introducing the long steel.

For all connecting beams are real hinges (Wall I-I).

P = -755 K. (constant)

To get the ultimate B.M. assume large eccentrisity

<u>Check</u>

$$\therefore \ K = 0.10 \quad \therefore \ \frac{e_u}{t} = 1.5 \quad \therefore \ e_u = 26.25 \text{ ft.}$$

$$\therefore \bar{M}_u = 26.25 * P = \underline{19.8\text{x}10^3 \text{ K.ft.}}$$

A-3 Case of 20 Stories: [16%g, ground acceleration]

Take $b = 12''$ ($T = 1.38$ sec.)

Wall I-I (Exterior)

$H_T = \underline{11.4}$ and $q_p = \underline{20 \text{ Kip/ft}}$

Wall II-II (Interior)

$H_T = \underline{2.33}$ and $q_p = \underline{2.68 \text{ Kip/ft}}$

Design Tables

Wall	I-I (Exterior)							II-II (Interior)						
Load Combination	D	D+L		D+Q		D+L+Q		D	D+L		D+Q		D+L+Q	
ψ	1.0	1.0		1.0		0.7		1.0	1.0		1.0		0.7	
α_D	1.25	1.25	0.85	1.25	0.85	1.25	0.85	1.25	1.25	0.85	1.25	0.85	1.25	0.85
Axial Force Kip	-3310	-4065	-3005	-3310*	-2250**	-3840	-2780	-4630	-6142	-4662	-4630	-3150**	-5690*	-4210
Shearing F. Kip	0	0	0	1050	1050	735	735	0	0	0	390	390	245	245
O.T.M. 1000 K.ft.	0	5.9	5.9	109.0	109.0	80.5	80.5	0	11.8	11.8	35.0	35.0	32.7	32.7

Table (A-5) Straining Actions at the Base, 20 Storey Building (16% g)

- * Over Stressing

** Over Turning

For Both : $A = 8.825\ ft^2$, $I = 895\ ft^4$, $a = 22.5$ ft and $E = 3500\ K_{si}$

$$A_{s_b} = 2.85\%\ A_c$$

Take $A_s \simeq 0.4\ A_{s_b} \simeq 1.15\%\ A_c \simeq 29\ in^2$

Choose 18#11 (26.5 in^2) , 0.366 A_{s_b} and 1.04% A_c

The wall cross section is shown in Figure (A-8)

Check

$$P_t = \frac{2.08}{100} \quad , \quad m = 17.65 \quad \therefore \quad P_t.m = \underline{0.367}$$

$$d/t = \frac{16.875}{17.500} = \underline{0.967}$$

Wall	$P_t.m$	$\frac{e}{t}$	K	$\bar{P}_u = K.b.t.f'_c$	$\bar{M}_u = \bar{P}_u.e$	$\frac{\bar{P}_u}{P}$	$\frac{\bar{M}_u}{M}$	F.O.S.
(1) I-I	0.367	0.170	0.800	8000	23700	1.55	1.55	1.55
(2) I-I	-	0.370	-	-	-	0.84	0.84	Unsafe*
(3) II-II	0.367	0.191	0.770	7700	25600	2.32	2.32	2.32

Table (A-8) Check for the Assumed Section, 20 Storey Building (16% g)

* $\therefore$ Increase the area of steel by using 22#11 (32.2 in^2)

$\therefore$ F.O.S. = 1.04 (Wall I-I only).

$$\frac{A_s}{A_{s_b}} = 0.445 \ \& \ A_s = 1.28\%\ A_c$$

* For all connecting beams real hinges (wall I-I) $P = -1655$ K.

$\therefore\ K = 0.165 \qquad \therefore\ \frac{e_u}{t} = 1.50 \qquad \therefore\ e_u = \underline{26.25 \text{ ft.}}$

$\therefore\ \bar{M}_u = \underline{43400 \text{ K.ft.}}$

A-4 Case of 20 Stories: [8%g, ground acceleration]

Taking $b = 0.75'$ (g'') , $(T = 1.38$ sec.)

The connecting beam cross section will take as given by Figure (A-1).

Exterior Wall (I-I)

$\alpha H_T = 11.8$ and $q_p = 16$ K/ft

Interior Wall (II-II)

$\alpha H_T = 2.33$ and $q_p = 2.68$ K/ft.

Design Tables

Wall	Exterior (I-I)							Interior (II-II)						
Load Combination	D	D+L		D+Q		D+L+Q		D	D+L		D+Q		D+L+Q	
ψ	1.0	1.0		1.0		0.7		1.0	1.0		1.0		0.7	
α_D	1.25	1.25	0.85	1.25	0.85	1.25	0.85	1.25	1.25	0.85	1.25	0.85	1.25	0.85
Axial force Kip	-3030	-3785	-2810	-3030*	-2055**	-3560	-2585	-4350	-5862	-4467	-4350	-2955**	-5410*	-4015
Shearing force Kip	0	0	0	480	480	336	336	0	0	0	183	183	128	128
O.T.M. 1000 Kip.ft	0	5.9	5.9	50.0	50.0	39.2	39.2	0	11.8	11.8	16.5	16.5	20.0	20.0

* Over stressing

** Over turning

Table (A-9) Straining Actions at the Base , 20 Storey Building (8% g)

For both: $A = 6.5625\ ft^2$, $I = 670\ ft^4$, $a = 22.5\ ft$ and $E = 3500\ K_{si}$

WALL	γ^2/α^2	K.ft $M_{ov.st.}$	K.ft $M_{ov.t.}$	K.ft $T_{ov.st.}$	K $T_{ov.t}$
Exterior (I-I)	0.0370	50000	50000	±1850	±1850
Interior (II-II)	0.0370	20000	16500	±740*	±610*

* Bigger than T_{max}.

Table (A-10) Axial Force due to the O.T.M. at Base, 20 Storey

$T_{max_{I-I}}$ = ±16x175 = ±2800 Kip.

$T_{max_{II-II}}$ = ±2.68x175 = ±469 Kip.

	Over Stressing				Over Turning			
WALL	K.ft. M_{max}	K N_c	K.ft. M_c	K N_{max}	K.ft. M_{max}	K N_c	K.ft. M_c	K N_{max}
Exterior (I-I)	4250	+335	(1) 4250	-3365	(2) 4250	+822	4250	-2878
Interior(II-II)	4750	-2236	(3) 4750	-3174	3000	-1008	3000	-1946

1 & 3 check for Comp. in concrete.

2 check for A_s.

Table (A-11) Design Values, 20 Storey Building (8%g)

Trying the wall cross section shown in Figure (A-8a).

Check

$d/t = 0.975$, $\frac{e}{t} = (\frac{M}{P})/17.5$ and $mP_t = 0.2825$

Table (A-12) gives the facyor of safety with the three cases of loading given by Table (A-11).

WALL	$P_t.m$	$\frac{e}{t}$	K	$\bar{P}_u=K.B.t.f'_c$	$\bar{M}_u=\bar{P}_u.e$	$\bar{P}_u/P$	$\bar{M}_u/M$	F.O.S.
(1) Exterior (I-I)	0.2825	0.072	0.860	6500	8200	1.94	1.94	1.94
(2) Exterior (I-I)	-	0.297	-	-	-	1.333	1.333	1.333
(3) Interior(II-II)	0.2825	0.086	0.880	6500	9800	2.05	2.05	2.05

Table (A-12) Check for the Assumed Section, 20 Storey Building (8% g)

For all connecting beams real hinges (wall I-I) P = -1515 Kip.

$\therefore$ K = 0.200 $\quad \therefore \frac{e_u}{t} = 0.96 \quad \therefore e_u = 16.8$ ft.

$\therefore \bar{M}_u$ = 25500 ft.Kip.

In table (A-13) a summary of the actual design with $\bar{M}_u$ value for ezample 2 with the two cases considered, namely: design for 0.16g, and design for 0.08g.

WALL	Max.G. Acceleration=16%g					Max. G. Acceleration=8%g				
	Wall Width	A_{s_b}	A_{s_w}	q_p	$\bar{M}_{u_w}$	Wall Width	A_{s_b}	A_{s_w}	q_p	$\bar{M}_{u_w}$
Exterior	12"	4#10	22#11	20 K/ft	43400 K'	9"	4#9	12#10	16 K/ft	25500K'
Interior	12"	3#5/ft*	18#11	2.68K/ft	37700K'	9"	3#5/ft*	12#10	2.68K/ft	25500K'

* Connecting slab width = 3.5 ft.

Table (A-13) Summary of Actual Design, 20 Storey Building

Note:

The dimensions and reinforcements in the case of 8%g not exactly one half those for the case of 16%g due to the minimum requirements recommended by the code, also due to the live and dead loads effect.

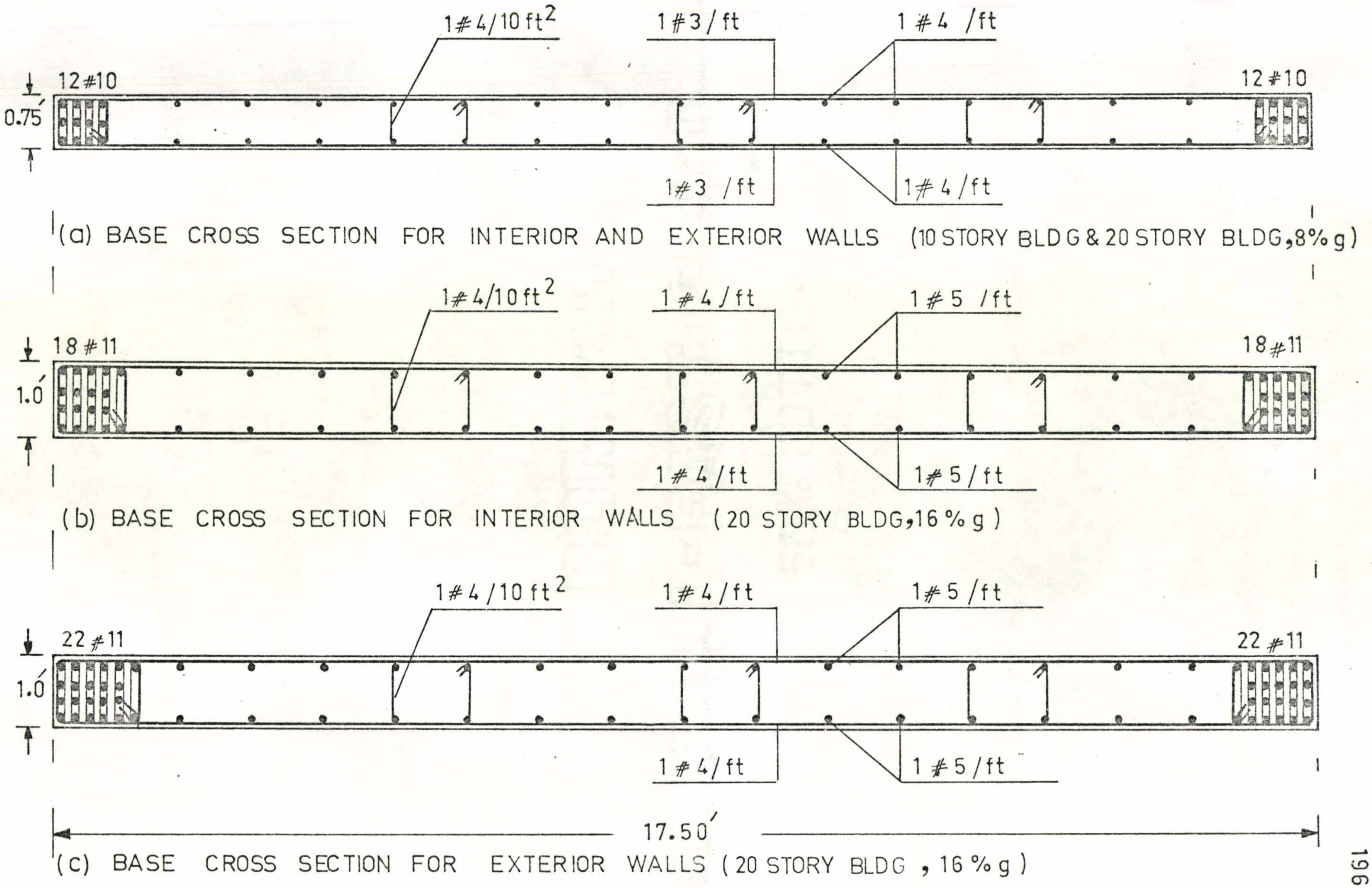

FIG. A_8 DETAILING OF BASE CROSS SECTIONS

REFERENCES

1. ACI Standard 318-71, Building Code Requirements for Reinforced Concrete.

2. Bathe, K.J. and Wilson, E.L., "Stability and Accuracy of direct integration methods", Int. J. Earthquake Engineering and Structural Dynamics, Vol.1, 283-291 (1973).

3. Biggs, J.M., "Introduction to structural dynamics", McGrow-Hill (1964).

4. Clough, R.W. and Penzien, J., "Dynamics of Structures", McGrow-Hill (1975).

5. Coull, A. and Choudury, J.R., "Stresses and deflections in coupled shear walls", ACI Journal, Proceedings V.64, No.2, Feb. 1967, pp.65-72.

6. Coull, A. and Choudury, J.R., "Analysis of coupled shear walls", ACI Journal, September 1967, pp.587-593.

7. Coull, A. and El Hag, A.A., "Effective coupling of shear walls by floor slabs", Supplement to Journal of American Concrete Institute, August (1975).

8. Gluck, J. "Elasto-plastic analysis of coupled shear walls", Journal of the Structural Division, ASCE, Vol.99, ST8, August 1973, pp.1743-1760.

9. Jennings, P.C. and Skattum, K.S., "Dynamic properties of planar, coupled shear walls", Earthquake Engineering and Structural Dynamics, Vol.1, 387-405 (1973).

10. National Building Code of Canad (1975)

10a. Neal, B.G., "The plastic method of structural analysis", Science Paperbacks.

✗11. Newmark, N.M., "A method of computation for structural dynamics", Proc. Am. Soc. Civ. Engs., 85, EM3, 67-94 (1959).

12. Poulay, T., "Design aspects of shear walls for seismic areas", Second Canadian Conference on Earthquake Engineering, Paper 14, June 1975.

13. Paulay, T., "An elasto-plastic analysis of coupled shear wall" ACI Journal, November 1970, pp.915-922.

14. Paulay, T, "Simulated seismic loading of spandrel beams", Journal of Structural Division, ASCE 97, ST9, Sept. 1971, pp.2407-2419.

15. Portland Cement Association, Sperial Publication, April 1971.

16. Smith, S., "Modified beam method for analyzing symmetrical Interconnected shear walls", ACI Journal, Nov. 1970, pp. 977-980.

17. Saul, W.E., "Damping in structures with rigid body displacement components", Second Canadian Conference on Earthquake Engineering, Paper 10, June 1975.

18. Tso, W.K. and Chan, P.C.K., "Static analysis of stepped coupled walls by transfer matrix method", Build. Sci. Vol.8, Perganon Press 1973, pp.167-177.

19. Tso, W.K. and Chan, H., "Dynamic analysis of plane coupled shear walls", J. Engineering Mech. Div., ASCE, 97, No.EMI, Proc. Paper 7899, 33-48 (1971).

20, Tso, W.K. and Chan, P.C.K., "Flexible foundation effect on coupled shear walls", ACI Journal, November 1972, pp. 678-683.

*21. Wiegel, "Earthquake engineering", Prentice-Hall, Inc., Englewood Cliffs, N.J. (1970).

22. Wilson, E.L. and Farhood and Bathe, K.J., "Non-linear dynamic analysis of complex structures", Int. J. Earthquake Engineering and Structural Dynamics, Vol. 1, 241-252 (1973).

23. Winokur, A. and Gluck, J., "Ultimate strength analysis of coupled shear walls", ACI Journal, Proceedings V.65, No.12, Dec. 1968, pp. 1029-1036.

24. Winter, G., "Design of concrete structures", McGrow-Hill (1964).